Role of the precentral cortex in adapting behavior to different mechanical environments

by

Andrew Garmory Richardson

B.S., Biomedical Engineering
Case Western Reserve University, 2000

S.M., Mechanical Engineering
Massachusetts Institute of Technology, 2003

Submitted to the Harvard-MIT Division of Health Sciences and Technology
in partial fulfillment of the requirements for the degree of

Doctor of Philosophy in Biomedical Engineering

at the

MASSACHUSETTS INSTITUTE OF TECHNOLOGY

June 2007

Signature of Author..……..
Harvard-MIT Division of Health Sciences and Technology
May 11, 2007

Certified by……..
Emilio Bizzi, M.D.
Institute Professor
Thesis Supervisor

Accepted by ……
Martha L. Gray, Ph.D.
Edward Hood Taplin Professor of Medical and Electrical Engineering
Director, Harvard-MIT Division of Health Sciences and Technology

Role of the precentral cortex in adapting behavior to different mechanical environments

by

Andrew Garmory Richardson

Submitted to the Harvard-MIT Division of Health Sciences and Technology on May 11, 2007 in partial fulfillment of the requirements for the degree of Doctor of Philosophy in Biomedical Engineering

Abstract

We routinely produce movements under different mechanical contexts. All interactions with the physical environment, such as swinging a hammer or lifting a carton of milk, alter the forces experienced during movement. With repeated experience, sensorimotor maps are adapted to maintain a high level of movement performance regardless of the mechanical environment. This dissertation explored the contribution of the precentral cortex to this process of motor adaptation. In the first experiment, we recorded precentral neural activity in rhesus monkeys that were trained to perform visually-cued reaching movements while holding on to a robotic manipulandum capable of changing the forces experienced during the task. Preparation and control of the reaching movements were correlated with single cell activity throughout the precentral cortex, including the primary motor cortex and five different premotor areas. Precentral field potential activity was also modulated during the reaching behavior, particularly in the beta and high gamma frequency bands. When novel forces were introduced, single cell activity changed in a manner that specifically compensated for the applied forces and mirrored the time course of behavioral adaptation. Force-related changes were present in the field potential activity as well. Some of these changes were maintained following removal of the forces. Control data and simulations revealed that these residual changes were well described by a model of noisy adaptation in a redundant cortical network. In the second experiment, human subjects performed the same reaching paradigm after receiving transcranial magnetic stimulation to transiently inhibit cortical activity. Initial learning of the novel force environment was normal but recall of the field 24 hours later was impaired relative to controls. Taken together, the results suggest that distributed areas within the precentral cortex are involved in recalibrating sensorimotor maps to fit the present mechanical context and in initiating a memory trace of newly-experienced environments.

Thesis Supervisor: Emilio Bizzi, M.D.
Title: Institute Professor

Thesis Chair: Ann M. Graybiel, Ph.D.
Title: Walter A. Rosenblith Professor of Neuroscience

Thesis Reader: Christopher I. Moore, Ph.D.
Title: Mitsui CD Chair, Assistant Professor of Neuroscience

Acknowledgments

Emilio Bizzi, my advisor throughout graduate school, provided me with a great deal of support while allowing me the independence to follow my intellectual curiosity. I am very thankful for the time I have had to learn from him. I have seen firsthand his unmatched ability to reinvent his laboratory to lead, rather than follow, new developments in the field.

I am also grateful to the other members of my thesis committee, Ann Graybiel and Chris Moore. Both Ann and Chris asked exactly the right questions, pushing me toward a better understanding of my data. I only regret that I did not form my committee sooner so as to take more advantage of the fantastic advice they provided me.

Matt Tresch guided me through the first half of my graduate career and I could not have had a better role model during my early years. My approach to scientific research is largely modeled after his.

Margo Cantor has been a constant help with the ever-mischievous monkeys as well as with most other aspects of daily life in the lab. Charlotte Potak also has been crucial in helping me navigate the many procedural and financial aspects of graduate school.

I am very thankful for the collaborations I have had over the years with Simon Overduin, Dan Press, Toni Valero-Cabre, Camillo Padoa-Schioppa, Glenda Lassi Tucci, Russ Tedrake, Uri Rokni, Ram Srinivasan, and Caterina Stamoulis. Simon, in particular, has been an enormous help in almost every project I have undertaken in the Bizzi Lab. Camillo collected all of the SMA data and part of the cingulate data analyzed in this thesis. Glenda also collected some of the cingulate data. Uri was the driving force behind the work in Chapter 5. Simon, Dan, Toni, and Camillo all were involved in the project described in Chapter 6.

A number of undergraduates have also taken time out of their busy schedules to make valuable contributions to my research, including Jeff Moore, Roger Li, Courtney Lane, Christi Winiarz, and Martin Ramos Rizo-Patron.

Finally I would also like to thank the following members of the Bizzi Lab, both past and present, for thoughtful advice, the occasional poker night, and a constant willingness to listen: Robert Ajemian, Chris Bae, Max Bernike, Vincent Cheung, Alessandro d'Ausilio, Andrea d'Avella, Timothee Doutriaux, Maureen Holden, Silvestro Micera, Jinsook Roh, and Philippe Saltiel.

Contents

Foreword

We routinely produce movements under different mechanical contexts. Behaviors such as swinging a hammer, opening a door, and lifting a carton of milk all involve forces acting on the moving arm that are not present when the arm is moving freely. Indeed, all interactions with the physical environment alter the forces experienced during a movement. Behavioral studies show that subjects quickly adapt to and proactively compensate for these forces in order to maintain a high level of movement performance regardless of the mechanical environment. The motor system generally provides proactive compensation by developing some estimate of the relationship between forces and motions of the body. This relationship is governed by the laws of classical mechanics and is referred to as a system's equations of motion, or movement dynamics. The neural transformation that estimates this relationship is often referred to as an "internal model" of the dynamics. This dissertation explores the motor cortical contribution to adapting and storing this transformation.

Maintaining good performance in a changing environment generally involves not only adaptive estimates of the dynamics of movement, but also adaptive estimates of the kinematics of movement (Atkeson, 1989). The latter provide mappings between kinematic variables in different coordinate frames, which are a function of the possibly changing geometry of the elements involved (e.g. size and orientation of tools). The study of internal models of movement kinematics has a long history compared to the relatively recent study of dynamics models (Held and Freedman, 1963). The degree to which kinematics and dynamics mappings are adapted and stored independently is uncertain (Krakauer et al., 1999; Tong et al., 2002). Furthermore, the robotics literature provides examples of unified adaptive controllers that deal with both kinematic and dynamic uncertainties in parallel (Cheah et al., 2006). Nevertheless, for practical reasons, this thesis focuses exclusively on internal models of dynamics with the acknowledgement that it is just one component of adaptive movement control.

In addition, recalibration of an internal model to the relevant mechanical context is just one type of motor learning. Other types include learning the sequence of movements involved in a new motor skill and learning a mapping between a sensory stimulus and a motor response (Sanes and Donoghue, 2000). Internal models of movement dynamics differ from the latter type of learning in that the learned transformation is governed by the physical laws of motion rather than arbitrary "man-made" laws (e.g. a green light maps to pressing the car accelerator). Finally, the

general concept of internal models, in which neural networks mimic the input-output properties of physical systems, has relevance to many other functions of the brain, including perception and cognition (Wolpert et al., 2003; Davidson and Wolpert, 2005). Thus, while this thesis has a narrow focus with respect to motor system function, it is also germane to the study of internal models across systems neuroscience.

The work presented in this thesis focuses exclusively on adaptation during arm reaching behaviors in the primate. As such, Chapter 1 is devoted to characterizing the psychophysics of reaching in familiar and novel mechanical environments. Chapters 2 and 3 quantify motor cortical activity during the familiar reaching task. These chapters provide a reference with which to judge changes in activity associated with motor learning. Chapters 4 and 5 quantify changes in motor cortical activity that are correlated with adaptation to novel environments. Finally, in Chapter 6 we present a study which tested the causal link between motor cortex and adaptation, to complement the correlational analyses of the previous chapters.

1 Psychophysics of reaching in familiar and novel environments

1.1 Introduction

Through interaction with the physical environment, even familiar movements can experience novel, perturbing forces. For example, simply holding a mass in your hand can change the position-, velocity-, and acceleration-dependence of shoulder and elbow torques during whole-arm reaching. Without proper recalibration of the motor controller, these changes in the dynamics can degrade performance. Psychophysical experiments can give insight into how this recalibration occurs. We begin this chapter with a review of the psychophysics of adaptive control in humans. Then the remainder of the chapter explores the psychophysics of adaptive control in monkeys. This will provide the behavioral background for interpreting the monkey neurophysiological data presented in later chapters.

Human psychophysics

Many psychophysical studies have been conducted over the past 12 years to address how humans adapt to changes in dynamics (Shadmehr and Wise, 2005). The initial studies altered the dynamics of reaching movements with novel velocity-dependent forces. Lackner and DiZio (1994) used velocity-dependent inertial forces (Coriolis forces), created by rotating the room in which the subjects performed the task. Shadmehr and Mussa-Ivaldi (1994) used velocity-dependent mechanical forces (curl force field) generated by a robotic arm held by the subject. Subsequent studies have used many other methods to alter the movement dynamics during reaching (Flanagan and Wing, 1997; Sainburg et al., 1999; Dingwell et al., 2002; Lai et al., 2003; Mah and Mussa-Ivaldi, 2003). These methods differ not only in how they perturbed the movement dynamics, but also in what type of sensory information the nervous system receives regarding the novel forces (e.g. cutaneous feedback is available in mechanical but not inertial perturbations). Typically, these studies analyze movement kinematics (e.g. arm position and velocity) before, during, and after the perturbation. A robust finding across these studies is that subjects adapt to the altered dynamics such that their kinematics is indistinguishable from what it was under control (i.e. normal dynamics) conditions.

Adaptation to novel movement dynamics can be achieved by both dynamics-specific and dynamics-nonspecific mechanisms. The former can be referred to as model-based control, where an internal model of the specific altered dynamical environment is acquired by the nervous system and used to generate feed-forward motor commands. The latter can be achieved by simply co-contracting antagonistic muscles indiscriminately to increased overall arm stiffness in order to minimize the effect of perturbations. The theoretical utility of these mechanism for adaptive control has been demonstrated in the engineering literature (Tin and Poon, 2005). To dissociate these mechanisms, control trials of normal dynamics can be used, either randomly interspersed during adaptation ("catch trials") or in a block following adaptation. If a mirror pattern of errors is seen in these control trials (i.e. equal but oppositely directed errors to that of the early adaptation trials), it indicates a feed-forward strategy is being used consistent with model-based control. Such dynamics-specific errors are referred to as "aftereffects". If no errors are seen, then the adaptation is likely nonspecific (although, see next paragraph). In the studies mentioned above, subjects exhibited aftereffects after adaptation to the altered dynamics. Thus, these studies provide evidence that human reaching movements are controlled using adaptive estimates of the movement dynamics.

There are two types of dynamics-specific mechanisms for adaptation: a proactive mechanism (i.e. internal model-based control) (Kawato, 1999) and a reactive mechanism (i.e. impedance control) (Hogan, 1985). Internal model-based control is proactive in the sense that the controller produces a compensatory response for a predicted perturbation without regard for whether the perturbation actually occurs. This is why aftereffects occur on catch trials. On the contrary, the perturbation must occur for an impedance controller to generate a compensatory response. What differentiates impedance control from a nonspecific co-contraction strategy is the characteristics of the response it generates; impedance controllers adapt the reactive response to optimally counteract the predicted perturbation. Hence, impedance control is specific to the dynamics since it relies on a prediction of the mechanical environment. However, impedance controllers do not produce aftereffects as defined above. Rather, to dissociate an impedance controller from nonspecific co-contraction, one must show that the constitutive mechanical properties of the arm (i.e., stiffness, viscosity, inertia) are specifically adapted to the environment. Specific adaptation of arm stiffness has been shown to occur when subjects make reaching movements in a divergent, position-dependent force field (Burdet et al., 2001). This study shows that in such

unstable dynamics, subjects actually cannot form internal models of the pattern of forces and thus resort to a reactive control strategy. Therefore, whether a proactive or reactive mechanism is employed by the motor system depends on how the movement dynamics is altered. In fact, both mechanisms may be used simultaneously when some components of the movement dynamics are amenable to internal model-based control and others are not (Franklin et al., 2003; Osu et al., 2003).

An important issue regarding dynamics-specific adaptation is whether the nervous system learns a mapping from the mechanical states (i.e. positions, velocities, and accelerations) of the arm to the novel forces or whether it just memorizes a temporal sequence of forces for each trajectory it experiences in the altered dynamics. Conditt and colleagues found that adaptation to velocity-dependent forces generalized across different movements that visited the same mechanical states (Conditt et al., 1997). Furthermore, the human motor system tends to represent forces as a function of mechanical state even when those forces are purely a function of time (Conditt and Mussa-Ivaldi, 1999). Therefore, the computations underlying control of reaching movements include an adaptable neural transformation between limb motions and forces. This transformation is not likely solving the equations of motion explicitly. Rather, acquisition of internal models may result from a relatively simple adaptation law driven implicitly by performance errors that ultimately leads to a neural transformation that approximates the movement dynamics. Several formulations of how this may occur have been proposed (Atkeson, 1989; Sanner and Kosha, 1999; Gribble and Ostry, 2000; Thoroughman and Shadmehr, 2000). The implicit nature of the adaptation process has recently been demonstrated. When velocity-dependent curl forces were applied with incrementally increasing amplitude across trials, memory of the novel dynamics was the same as when the forces were applied at full magnitude on every trial (Klassen et al., 2005). This result suggests large errors are not needed to recalibrate an internal model and the recalibration can occur without conscious awareness.

A related, but different, question is to what degree the learned map of the movement dynamics generalizes to mechanical states that were not experienced during learning. If the map was the exact equations of motion, it would generalize to all states. At the other extreme, if the map was a “look-up table” between motions and forces previously experienced, it would not generalize at all. Biologically, this map must be generated by combination of basis elements, or nodes in a neural network. Accordingly, generalization is partially a function of how broadly

tuned these basis elements are to the mechanical states of the limb. Studies indicate that the basis elements have broad position tuning (Shadmehr and Moussavi, 2000), more narrow velocity and directional tuning (Gandolfo et al., 1996; Thoroughman and Shadmehr, 2000; Donchin et al., 2003), and weak acceleration tuning (Hwang et al., 2006). The network supporting motor adaptation may also rapidly select or adapt the tuning of basis elements based on the spatial complexity of the dynamical environment (Thoroughman and Taylor, 2005). The psychophysics of generalization has also revealed the coordinate frame of internal model computations. In particular, the network represents motions and forces in an intrinsic (i.e. muscle or joint) rather than an extrinsic (i.e. hand) coordinate frame (Shadmehr and Mussa-Ivaldi, 1994; Gandolfo et al., 1996; Shadmehr and Moussavi, 2000; Malfait et al., 2002; Malfait et al., 2005).

Next, we consider the controller architecture—that is, how an internal model of movement dynamics is used to generate predictive motor commands. Many different model-based controller architectures can, in theory, produce similar system behavior. One architecture is to use the model of the plant dynamics to predict the current motion of the limb from past motor commands and delayed sensory feedback, and to generate new commands based on the difference between predicted and desired motion. When an internal model is used with this causality, it is often called a "forward" model (Jordan and Rumelhart, 1992; Miall and Wolpert, 1996). Alternatively, when an internal model is used to predict the motor commands required to produce a desired motion, it is called an "inverse" model (Atkeson, 1989). Both controllers are viable in theory, as is an architecture that uses forward and inverse models of the plant dynamics to both compute commands needed to produce desired movements and anticipate the consequences of motor commands (Wolpert and Kawato, 1998; Bhushan and Shadmehr, 1999; Wang et al., 2001; Flanagan et al., 2003). The actual architecture almost certainly involves an inverse model (Bhushan and Shadmehr, 1999) and likely also includes a forward model, although the evidence (Wolpert et al., 1995; Ariff et al., 2002; Nanayakkara and Shadmehr, 2003) has been rather non-specific (Mehta and Schaal, 2002). As any of these control architectures could, at least theoretically, be responsible for the behavioral results summarized above, I describe the neural transformation used for adaptive reaching control only as a map between arm motions and forces, without assigning a causality to the relationship.

Finally, several studies have explored how internal models of movement dynamics are stored in memory. To date, all the work on this topic has specifically looked at whether newly acquired

internal models go through a process of consolidation, where consolidation is defined as a time-dependent stabilization (i.e. resistance to interference) of the memory (McGaugh, 2000). Brashers-Krug et al. (1996) used an "ABA" paradigm in which subjects adapted to novel dynamics (A1) and then, after a variable wait, had to learn a different dynamics (B), and finally were brought back the next day to perform the first dynamics (A2) to test for retention of learning. They found that retention only occurred if session B occurred more than 4 hours after session A1. This evidence supports the consolidation hypothesis, suggesting that memories of novel movement dynamics are initially labile and easily overwritten, but by about 4 hours after acquisition they have become resistant to interference from new learning. While a subsequent study confirmed this result (Shadmehr and Brashers-Krug, 1997), a more recent study failed to find any interval between A1 and B (up to 1 week) which allowed retention of learning, suggesting memories of movement dynamics are always overwritten (Caithness et al., 2004). This discrepancy has been reconciled by a study that showed intermittent practice of the dynamics due to the presence of catch trials (which were used by the Brashers-Krug studies but not by Caithness et al.) is critical to memory stabilization (Overduin et al., 2006).

We should note that some people have challenged the notion that we acquire internal models of the dynamics of movement, arguing both that the evidence cited above is not specific and that theoretically the use of such internal models to control movement is physiologically implausible (Ostry and Feldman, 2003). We believe these arguments are in general well reasoned, but only when very narrow definitions are used for what an internal model is and how it can be used. Here, we broadly equate the existence of an internal model of movement dynamics with the ability to control the dynamics of movement in an anticipatory manner (Kalaska et al., 1997). Under this definition, the existence of internal models is practically a truism. The presence of adaptation aftereffects is a hallmark of anticipatory control and, therefore, of internal models. Regarding physiological implausibility, Ostry and Feldman (2003) argue that controlling muscle force is implausible (preferring muscle length instead) and therefore the use of an inverse internal model, which maps desired motions into appropriate forces, is implausible. However, this logic is easily circumvented by broadening the definition of how an internal model could be used. In particular, the model's output need not be the ultimate motor command if, for example, the internal model is embedded in a hierarchical motor controller architecture that may ultimately map desire motion to muscle length or to some other control variable.

In summary, humans adaptively control reaching movements to meet the mechanical demands of each task. Underlying proactive forms of adaptive control is a plastic neural transformation, or internal model, that approximates the physical relationship between the motions and forces involved in the task. The internal model can be used to predict appropriate motor commands from desired limb motions and predict the motion consequences of past motor commands.

Monkey psychophysics

With the human psychophysics of dynamic motor adaptation well described, the next step is to determine what neural structures are responsible for this type of learning. Work has begun in this direction by drawing upon neuropathological populations (Maschke et al., 2004; Smith and Shadmehr, 2005; Chen et al., 2006), as well as by using non-invasive techniques such as functional imaging (Diedrichsen et al., 2005) and transcranial magnetic stimulation (Richardson et al., 2006) in neurologically-intact individuals. Complementary to this work is the use of invasive neural recordings in non-human primates. A series of papers have explored how the cortical motor areas of rhesus monkeys are involved in adapting reaching movements to novel environments (Gandolfo et al., 2000; Li et al., 2001; Padoa-Schioppa et al., 2002, 2004; Xiao et al., 2006). The psychophysics of adaptation in the monkey has been described in these papers, but not in the same detail or rigor as the human studies. In this chapter, we more rigorously quantify the monkey psychophysics in order to have a better understanding of the behavior prior to looking for its neural correlates.

1.2 Methods

Paradigm

We studied the behavior of five rhesus macaques (*Macaca mulatta*), four males and one female, trained to perform a visuomotor reaching task. Preliminary analyses of the behavior of three of the animals (F, C, R) have been reported previously (Padoa-Schioppa et al., 2002, 2004; Xiao et al., 2006). Data from the other two animals (K, T) were newly obtained for this thesis.

The monkeys were trained to sit in a chair and hold on to a handle at the end of a two-link, planar robotic manipulandum with their right hand (Fig. 1-1A). On each trial, they moved the

handle in the horizontal plane between two targets located 6 cm (monkey R), 8 cm (monkeys F, C, and K), or 10 cm (monkey T) apart. The targets (1.5-1.7 cm white squares) and current position of the handle (a 0.3 cm white square) read from potentiometers on the robotic arm were indicated on a monitor with a black background placed approximately 75 cm in front of the monkey and slightly below eye level. The movements involve primarily right shoulder and elbow extension and flexion. However, note that neither the wrist flexion-extension nor shoulder abduction-adduction angles were experimentally regulated.

Each trial began with a 1 s hold time at the center target, followed by the presentation of a pseudorandomly chosen peripheral target (i.e. the cue). The peripheral target was in one of eight locations, spaced uniformly 45º apart in a circle around the center target. The center target remained on for a variable 0.5 to 1.5 s (monkeys F, C, K, and T) or 1.1 to 1.9 s (monkey R) after the cue to indicate the instructed delay time. Upon disappearance of the center target (i.e. the go signal), the monkey made a reaching movement to place the cursor in the peripheral target, where it had to remain for 1 s to receive a juice reward (Fig. 1-1B). Movement duration had to be less than 3 s and movements had to remain at all times within a region ±60º about a line connecting the center and peripheral targets. Any error resulted in abortion of the trial without reward. The hand trajectory (position and velocity) on each trial was recorded at 100 Hz.

In control sessions, the monkeys performed at least 480 correct trials with no external forces (i.e. a null force field). In learning sessions, the monkeys performed ~160 correct trials with no external forces (baseline epoch), followed immediately by another ~160 correct trials during which the robotic manipulandum applied forces on the hand that were proportional and perpendicular to its velocity vector (force-field epoch), and finally another ~160 correct trials with no external forces (washout epoch). The magnitude of the velocity-dependent curl force field was 6 Ns/m (monkeys F, C, K, T) or 7 Ns/m (monkey R). For Monkey T, 8% of all trials (both correct and aborted) during the force-field epoch of each learning session were catch trials, where the force field was suddenly and unpredictable turned off in order to measure the time course of internal model formation. In the learning sessions, the force field could be either clockwise or counterclockwise. Thus overall, the monkeys performed reaching movements in three types of force fields: null field, clockwise curl field, or counterclockwise curl field. Only one type of field was used per daily session.

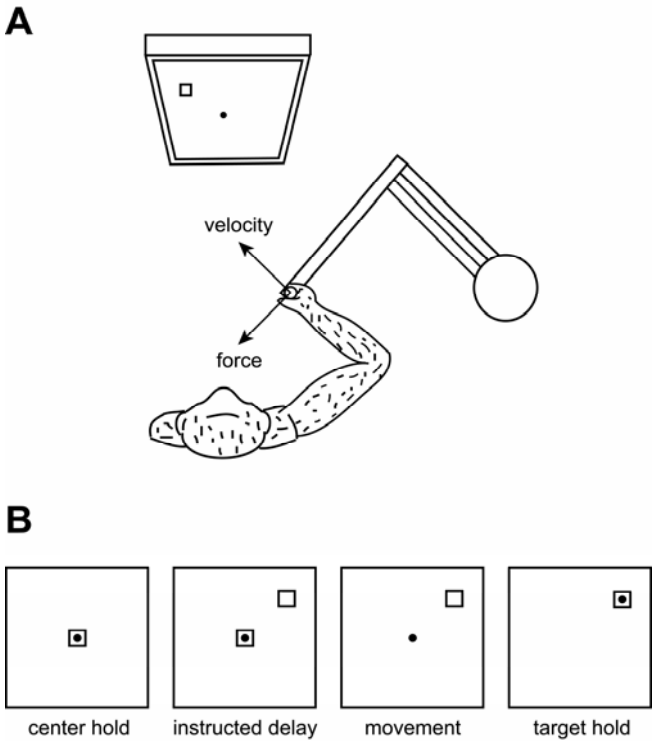

Figure 1-1. Behavioral paradigm. **A**, Schematic of the approximate relative orientation of the monkey, robotic manipulandum, and monitor. Forces applied to the arm were proportional and perpendicular to the hand velocity vector. **B**, Schematic of the cursor (circle) and targets (squares) on the monitor during the four phases of each trial.

Analysis

Performance was quantified on each successful trial by the signed deviation area between the hand path and the line connecting the beginning and end positions (Richardson et al., 2006). To assess robustness of our results we also computed two other performance metrics: the peak perpendicular displacement of the hand path from a straight line (Shadmehr and Moussavi, 2000) and the perpendicular displacement of the hand path 250 ms after movement onset from a straight line (Thoroughman and Shadmehr, 2000). All three performance metrics yielded very similar results; for brevity we report the results using the deviation area measure only. We also looked at the trial success rate, but it did not generally capture the performance as well as the trajectory-based measures. All aborted trials were excluded from the analysis.

Force field-related changes in performance were tested with five planned comparisons (t-tests) for each session: an adaptation test (trials 161-200, ii in Fig. 1-2, versus 281-320, iii), an

aftereffect test (trials 121-160, i, versus 321-360, iv), a deadaptation test (trials 321-360, iv, versus 441-480, v), a completeness of adaptation test (trials 121-160, i, versus 281-320, iii), and a completeness of deadaptation test (trials 121-160, i, versus 441-480, v). Any catch trials that fell within the force-field epoch blocks (ii and iii) were excluded. A per comparison error rate ($p < 0.05$) was used to judge significance since only the overall percentage of significant tests across sessions was of interest (conservatively assuming up to 5% were type I errors).

In addition to the above comparisons, which lumped together trials in all eight target directions, we assessed whether performance changes due to the perturbation (early force field, trials 161-200, ii) or due to aftereffects (early washout, trials 321-360, iv) were directionally tuned. We took the absolute value of the performance to capture both changes in the mean and variance. Changes were defined relative to the mean late baseline (i) performance in the corresponding directions. For each monkey, performance changes were compiled across all learning sessions, separating clockwise from counterclockwise. The four data sets (perturbation or aftereffect changes due to clockwise or counterclockwise force fields) were subjected to Rayleigh tests for uniformity across directions with a unimodal alternative and with a bimodal alternative (Fisher, 1993), using Moore's modification for weighted directional data (Moore, 1980).

We quantified trends in mean performance across sessions using linear regression. Also, correlations between across-session performance in the five blocks of trials (i, ii, iii, iv, v) were assessed by computing the rank correlation coefficient, with statistical significance judged by a permutation test.

Finally, we looked at two additional behavioral measures: reaction time (RT) and movement time (MT). RT was defined as the time interval from the go signal (i.e. disappearance of the center target) to movement onset. Movement onset was defined as the last time at which hand speed crossed a 4 cm/s threshold prior to the time of peak speed. MT was defined as the time interval from movement onset to the time at which the cursor reached the peripheral target. To exclude from the analysis trials in which the monkey anticipated the go signal or was inattentive to the task, we place loose bounds on RT and MT (0.1 to 0.7 s and 0.3 to 1.2 s, respectively). On average across the five monkeys, this excluded 8.9% of successful trials from the RT analyses and 3.4% of successful trials from the MT analyses.

1.3 Results

Adaptation, aftereffect, and deadaptation

Each monkey was over-trained on the null-field (i.e. control) reaching task for several months prior to experiencing any forces. Typical behavior during a control session is shown in Figure 1-2A. Despite the loose regulation of hand path (see Methods), the paths from the center target to each of the eight peripheral targets were quite straight. To quantify the straightness, on each trial we computed the signed area between the hand path and a straight line connecting the center and peripheral targets (deviation area). The mean deviation area was generally near zero throughout all 480 trials of the control session (Fig. 1-2C).

In learning sessions, the monkeys initially performed 160 null-field trials (baseline epoch). Then for the next 160 trials, they were exposed to forces that were proportional and perpendicular (either counterclockwise or clockwise) to the hand velocity vector (force-field

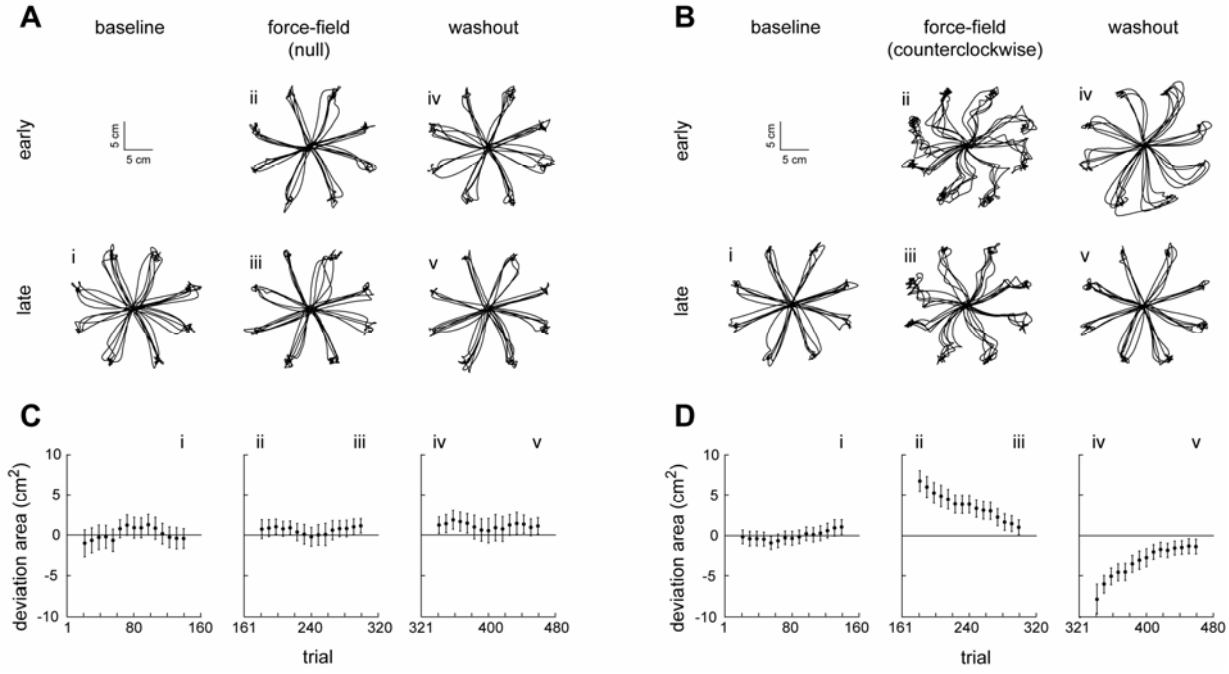

Figure 1-2. Example behavior of monkey K in a control session (null field) and a learning session (counterclockwise curl field). **A**, Hand trajectories from a control session. Each movement began at the center and ended at one of the eight peripheral targets. **B**, Hand trajectories from a learning session. **C**, Performance during the control session in A, quantified by the area between the trajectory and a straight line path (40 trial moving average shown with 95% student-t confidence intervals). Roman numerals indicate which paths in A correspond with which trials in C. **D**, Performance during the learning session in B. Note that the trajectory perturbation (change from i to ii), adaptation (ii to iii), aftereffect (i to iv), and deadaptation (iv to v) are well captured by the signed deviation area measure.

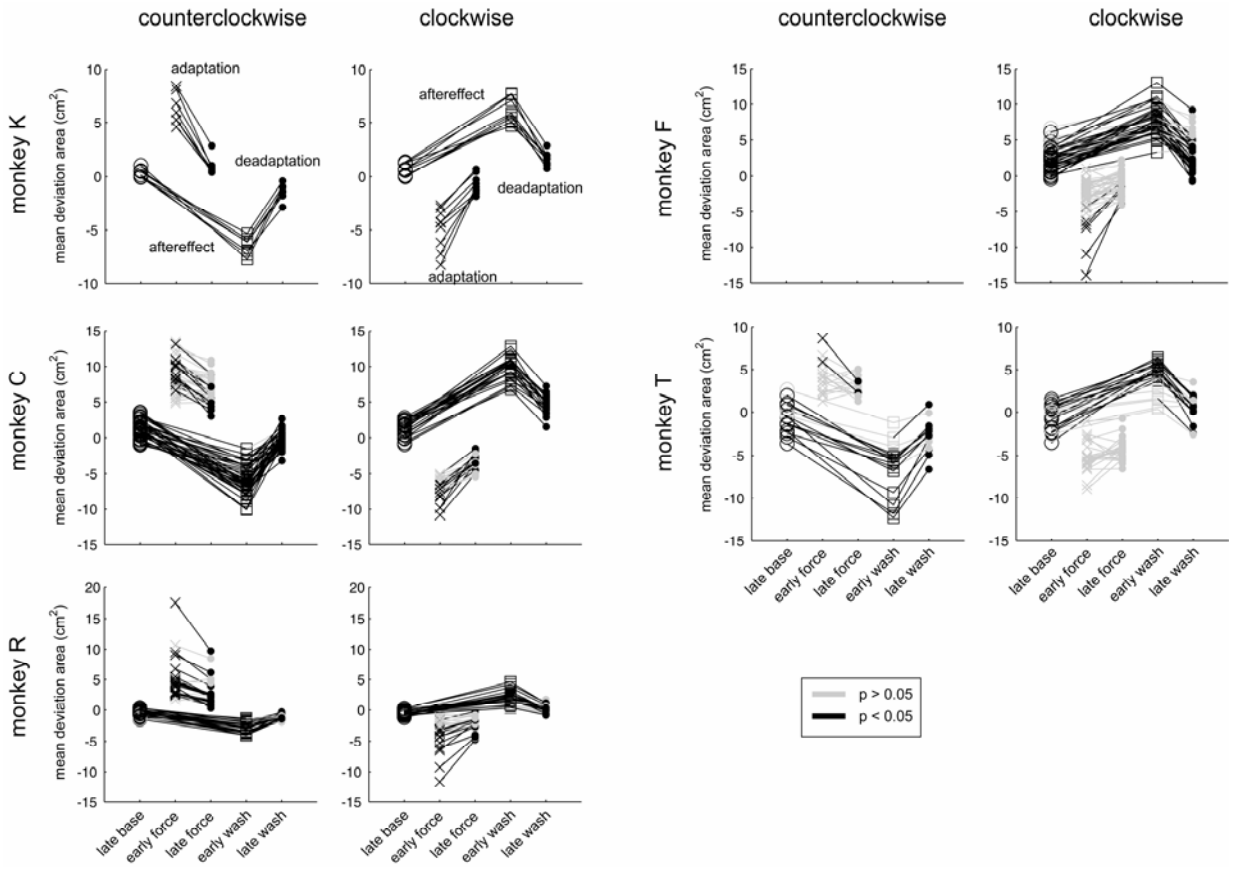

Figure 1-3. Significance of adaptation, aftereffect, and deadaptation in each learning session for all five monkeys. Each marker indicates the mean performance (deviation area) over a 40 trial block in one session. The lines between the markers represent a statistical comparison of two blocks (t-test). Black lines indicate the test was significant ($p < 0.05$); gray lines indicate the test was insignificant ($p > 0.05$). Sessions are divided according to the applied force field: counter-clockwise (left column) and clockwise (right column).

epoch). These perturbing forces caused the hand paths to become curved (Fig. 1-2B, ii). With experience making movements in the force field the paths became straighter, indicating the monkeys adapted to the forces (Fig. 1-2B, iii). Next, the forces were abruptly turned off and the monkey performed a final 160 null-field trials (washout epoch). Turning off the force field caused the hand paths to be curved again, but this time in the direction opposite to that seen in the early force-field epoch (Fig. 1-2B, iv). This phenomenon is called the aftereffect of adaptation. Finally, the hand paths once again became straight by the end of the washout indicating the monkeys had deadapted back to null-field conditions (Fig. 1-2B, v).

The adaptation, aftereffect, and deadaptation can be seen clearly in the time course of deviation area changes (Fig. 1-2D, ii to iii, i to iv, and iv to v, respectively). We tested whether

these changes were statistically significant in each session. Across all five monkeys there were 206 learning sessions. Out of 618 tests (i.e. tests of adaptation, aftereffect, and deadaptation in each session), 375 (60.7%) were significant (t-test, 5% level). To emphasize that these changes were related to the force fields, we performed the same tests for the 56 control sessions. Only 7 of the 168 tests (4.2%) were significant, which is below the level of chance. The results of these tests for each monkey are shown in Figure 1-3. Each line represents a statistical test and its color indicates whether the test was significant (black) or insignificant (gray). There were differences between monkeys in the number of significant tests. In monkey K, all learning-session tests were significant (Fig. 1-3, first row). Monkeys C had a smaller percentage of learning sessions with significant adaptation, but almost every learning session was still significant for aftereffects and deadaptation (Fig. 1-3, second row). Monkey T had even fewer sessions with significant adaptation and had some sessions without significant aftereffects or deadaptation either (Fig. 1-3, fifth row). The percent of learning sessions with significant adaptation, aftereffects, or deadaptation for each monkey is summarized in Figure 1-4 (black bars).

Next, we tested the completeness of adaptation and deadaptation. In learning sessions with significant adaptation or deadaptation, we compared the performance in the late baseline epoch

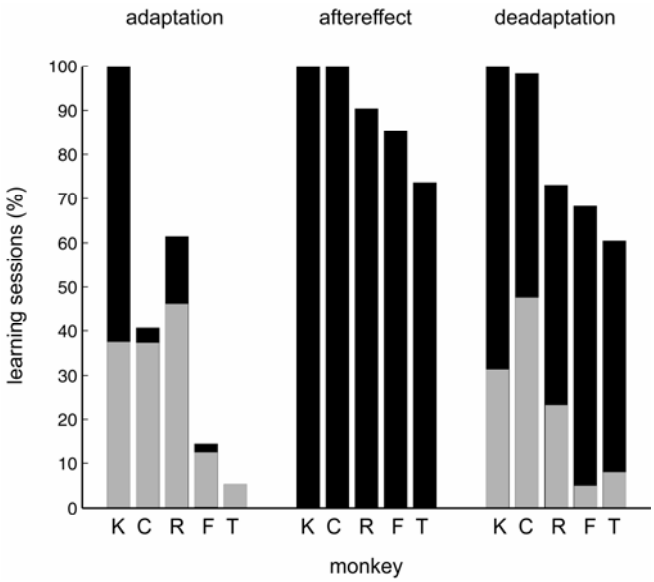

Figure 1-4. Summary of significance of adaptation, aftereffect, and deadaptation for all five monkeys (K, C, R, F, and T). Black bars indicate the percent of all learning sessions (i.e. sessions that applied either counterclockwise or clockwise force fields) that had a significant adaptation (left), aftereffect (middle), or deadaptation (right). Gray bars indicate the percent of all learning sessions with significant, but incomplete adaptation or deadaptation. Control sessions are excluded.

with that of the late force-field or washout epoch. The results for each monkey are summarized in Figure 1-4 (gray bars). Overall, 59 of 80 sessions (73.8%) with significant adaptation had significant differences between late baseline and late force-field epoch performance (t-test, 5% level). In all cases the differences were due to under-compensation, not over-compensation, of the force field. Also, 50 of 163 sessions (30.7%) with significant deadaptation had significant differences between late baseline and late washout epoch performance (t-test, 5% level).

Force-field related changes in performance were generally not uniform across the eight reaching directions, due possibly to mechanical anisotropies of the limb. For example, in monkey K, trajectory perturbations in early force field trials due to clockwise forces were much more pronounced in the 113º and 293º target directions than the 23º and 203º directions, thus forming a bimodal distribution of error across target direction (Fig. 1-5A, top left). This bimodal tuning was significant (Rayleigh test, $p < 0.001$), as indicated in the figure by a red line along the major

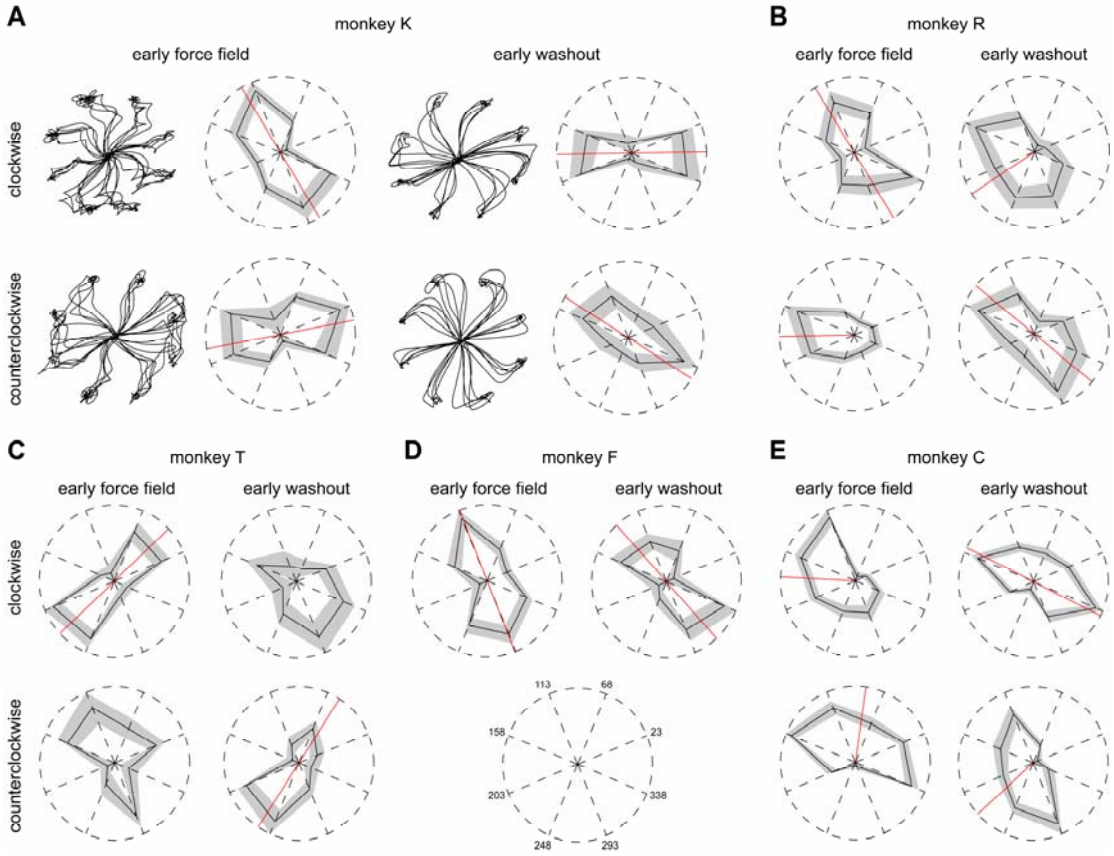

Figure 1-5. Directional tuning of performance in early force field trials and early washout trials. **A**, Hand trajectories are shown along with polar plots of the mean absolute change in performance, relative to late baseline, in each direction for monkey K. Gray regions indicate 95% confidence intervals on the mean. Red lines indicate significant unimodal (radial line) or bimodal (axial line) tuning based on Rayleigh tests ($p < 0.01$). **B-E**, same as in A but for the other four monkeys.

axis of the distribution. The trajectory perturbations due to counterclockwise forces were distributed bimodally as well, however the distribution was oriented differently (Fig. 1-5A, bottom left). Therefore, the directional dependency of trajectory errors was force-field specific. This directional tuning and force-field specificity could also be seen in the early washout trials, where trajectory perturbations were due to adaptation aftereffects instead of applied forces (Fig. 1-5A, right). There was a correspondence in directional tuning between clockwise-deviated trajectories and counterclockwise-deviated trajectories regardless of the source of the deviation (direct perturbation from applied forces or aftereffects of learned forces). These observations were generally seen in the other four monkeys as well (Fig. 1-5B,C,D,E). However, while some commonalities existed, the specific distribution of errors across directions often differed between monkeys, possibly reflecting inter-monkey differences in the use of redundant degrees of freedom of the limb (e.g. at the wrist and shoulder). The directional tuning of performance in the early force field and washout trials was clearly related to the forces, since no such tuning was found in late baseline trials of learning sessions or in early force field or washout trials of control sessions (Rayleigh tests, $p > 0.01$; data not shown). Lastly, nearly the same directional tuning was seen in adaptation and deadaptation changes (data not shown). Thus adaptation and deadaptation was most evident in movements that incurred the largest initial deviations.

The presence of adaptation aftereffects indicates that the monkeys used a proactive control

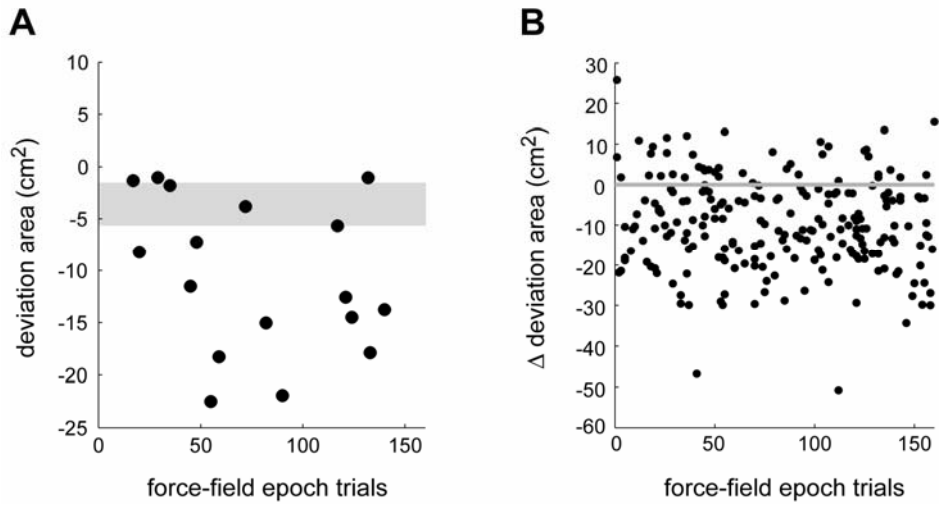

Figure 1-6. Catch trial performance of monkey T. **A**, Performance on null-field trials during the force-field epoch (i.e. catch trials) of the first session with a counterclockwise force field. The gray band indicates the 95% confidence interval on the mean performance during the baseline epoch. **B**, All catch trials performed by monkey T during counterclockwise force-field sessions. Performance is relative to the mean baseline epoch performance in each session.

strategy that specifically took into account the nature of the change in dynamics (i.e. the addition of a velocity-dependent force). The time course of internal model formation was investigated in one monkey (T) by suddenly removing the forces on random trials (catch trials) during the force-field epoch. Figure 1-6A shows the catch trial performance on the monkey's first session with counterclockwise forces. While early catch trial performance looked very similar to baseline performance, aftereffects were frequently seen after about 50 force-field trials. This time course was not, however, a consistent feature of subsequent sessions with the counterclockwise forces. When the catch trials from all such learning sessions were plotted (Fig. 1-6B), no clear trend was seen. The same was true of the clockwise force-field sessions (data not shown). In 33 of 38 learning sessions (86.8%), the mean catch trial performance was significantly different from the mean baseline performance (t-test, 5% level), indicating that on average catch trials produced adaptation aftereffects. However, the lack of any consistent trend across force-field epoch trials may indicate that the monkey was able to recall his initial experience with the forces and in subsequent sessions use a proactive control strategy throughout the force-field epoch, even on early trials. Evidence for retention of force-field learning is presented in the next section.

In summary, the monkeys adaptively controlled movements, though incompletely, using a proactive internal-model based approach to maintain good performance despite changes in movement dynamics. However, one seemingly contradictory result evident in Figures 1-3 and 1-4 is that in many cases the monkeys had significant aftereffects and deadaptation without significant adaptation. How can one deadapt or have adaptation aftereffects without first adapting? The answer may be related to the fact that, as mentioned in the Introduction, there is more than one mechanism for adaptation. In addition to acquiring an internal model of the force field, one may effectively compensate for perturbing forces through modulating the impedance of the limb. This latter mechanism may mask the presence of the former when both are operating simultaneously (see Discussion).

Across-session performance

Figure 1-3 shows that the mean performance in each of the five blocks of trials was variable across sessions. We were interested in whether the performance variability in any two blocks of trials was correlated. Essentially this analysis could tell us how the performance in one block of trials is related to the performance in another block of trials. We computed the rank correlation

between the mean performance in learning sessions for each pair of trial blocks, for a total of 10 comparisons per monkey. The results of this analysis are summarized in Table 1-1. For all five monkeys, their performance in the late baseline epoch was not significantly related to their performance in the force field or washout epochs (Table 1-1, comparisons 1, 2, 3, and 4). In contrast, in all but one case, their performance in early force-field trials and early washout trials was positively correlated with their performance in late force-field trials and late washout trials, respectively (Table 1-1, comparisons 5 and 10). These relationships can also be seen in the relative ordering of the lines showing adaptation and deadaptation in Figure 1-3. Finally, with the exception of monkey F, the performance in the force-field epoch was negatively correlated with the performance in the washout epoch (Table 1-1, comparisons 6, 7, 8, and 9). Taking into account the difference in sign of the deviation area in these two epochs, this relationship indicates that relatively good (bad) performance in the force field epoch occurred in sessions that also had relatively good (bad) performance in the washout epoch.

Table 1-1. Correlation between the mean performance in different blocks of trials. For each monkey and pair of trial blocks given in the first two columns, Spearman's rank correlation coefficient was computed to indicate the monotonic relationship between the mean performance in those blocks across all learning sessions. An asterisk (*) next to the rank correlation coefficient indicates that the correlation was statistically significant ($p < 0.001$), as judged by a permutation test. Null field sessions are excluded.

			K		C		R		F		T	
1.	late base (i)	Early force (ii)	-0.54		0.24		0.03		-0.07		-0.12	
2.	late base (i)	late force (iii)	-0.45		0.15		0.01		-0.05		0.14	
3.	late base (i)	Early wash (iv)	0.38		0.07		0.09		0.34		0.24	
4.	late base (i)	late wash (v)	0.56		0.07		0.06		0.42		0.36	
5.	early force (ii)	late force (iii)	0.85	*	0.87	*	0.95	*	0.58	*	0.76	*
6.	early force (ii)	Early wash (iv)	-0.87	*	-0.77	*	-0.86	*	-0.14		-0.83	*
7.	early force (ii)	late wash (v)	-0.83	*	-0.72	*	-0.76	*	-0.26		-0.63	*
8.	late force (iii)	Early wash (iv)	-0.84	*	-0.77	*	-0.84	*	0.05		-0.68	*
9.	late force (iii)	late wash (v)	-0.79	*	-0.72	*	-0.73	*	-0.02		-0.54	*
10.	early wash (iv)	late wash (v)	0.84	*	0.79	*	0.86	*	0.41		0.81	*

Next, we studied the how the performance changed from one daily session to the next. The sequence of force fields presented across sessions was different for each monkey. However, for each monkey, there were a series of sessions in which the same force field was applied. We looked at how the mean performance in the late baseline epoch, early force field epoch, and early washout epoch changed across sessions after repeated exposure to the same force field. Significant trends in performance, as judged by a fitted linear regression line to the data with

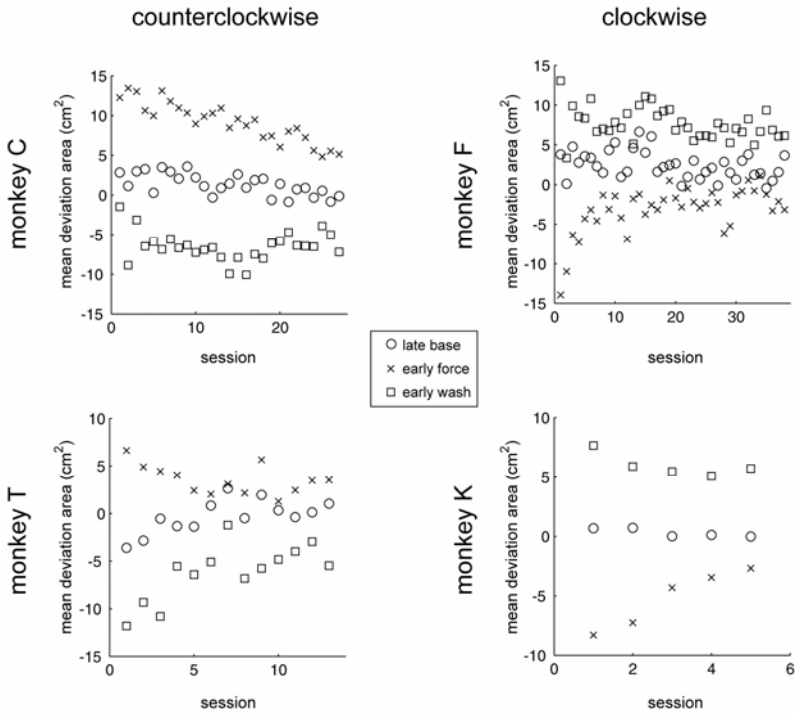

Figure 1-7. Behavioral evidence of long-term learning of the curl force fields. The mean performance in the last 40 trials of the baseline epoch (circle), first 40 trials of the force-field epoch (x), and first 40 trials of the washout epoch (square) are plotted for a series of daily sessions in which the monkey experienced the same force field each day.

non-zero slope ($p < 0.05$), were seen in all monkeys except monkey R. In Figure 1-7, we show one series of sessions for each of the other four monkeys to illustrate the types of trends observed. For monkey T, the mean performance in the late baseline epoch showed a significant trend across sessions, whereas this was not the case for the other three monkeys (Fig. 1-7). In particular, the baseline performance moved in the direction of the force field perturbations (i.e. more positive). This unique baseline trend across days has also been seen in human subjects performing this task and seems to be related to the presence of catch trials (Donchin and Shadmehr, 2004), which monkey T experienced but the others did not. In the force-field epoch, all four monkeys showed a progressive improvement in mean performance (i.e. absolute value of the deviation area got smaller) across sessions (Fig. 1-7). The early washout performance often also improved with experience in the same force field, although not for monkey C (Fig. 1-7).

The results shown in Figure 1-7 suggest that the monkeys retain some memory of their experiences moving in the altered dynamical environment and that this impacts their

performance on subsequent days. Taken together with the correlation analysis between trial blocks, we can say that the initial movement perturbation due to the force field (early force-field epoch performance) and the initial movement perturbation due to adaptation aftereffects (early washout performance) were correlated and tended to decrease after multiple sessions with the same force field.

Reaction time and movement time

In addition to the foregoing analysis of force field-related performance, we looked at two more general behavioral measures: reaction time (RT) and movement time (MT). RT was the time from the go signal to movement onset and MT was the time from movement onset to the movement end (see Methods). First, we asked whether RT and MT changed as a function of the duration of the instructed delay time (DT). The DT (i.e. time from the cue signal to the go signal) was randomly varied on each trial, with a uniform probability distribution. The information provided during the DT was the spatial target to which the upcoming movement should be directed (Fig. 1-1). As the only uncertainty during the DT is the time at which the go signal is given, the paradigm is a simple (as opposed to choice) reaction time task. Psychological studies in humans have long shown that in simple reaction time tasks, there is an inverse relationship between the DT and RT (Niemi and Naatanen, 1981) although there is generally no relationship

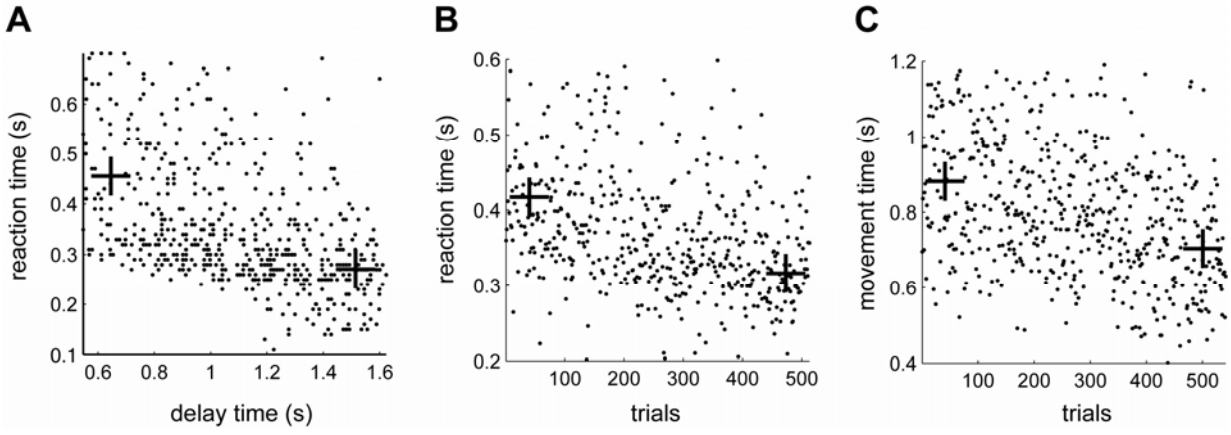

Figure 1-8. Examples of significant reaction time (RT) and movement time (MT) relationships. **A**, RT as a function of the instructed delay time for one session by monkey F. Crosses indicate the mean RT for trials with the shortest and longest delay times (0.2 s bins). **B**, RT as a function of trials for one session by monkey T. Crosses indicate the mean RT for first and last 80 trials of the session. **C**, MT as a function of trials for one session by monkey T. Crosses indicate the mean MT for first and last 80 trials of the session.

between the DT and MT. We found this to be the case for the monkeys. We compared the RTs or MTs between trials with the shortest DTs (DT = 0.5 to 0.7 s for monkeys F, C, K, and T or DT = 1.1 to 1.3 s for monkey R) and trials with the longest DTs (DT = 1.3 to 1.5 s for monkeys F, C, K, and T or DT = 1.7 to 1.9 s for monkey R). In 98.3% of sessions across all monkeys, the mean RT in trials with the shortest DTs was longer than the mean RT in trials with the longest DTs (one-tailed t-test, 1% level). An example of this inverse relationship is shown in Figure 1-8A. However, in only 4.2% of sessions across all monkeys was the mean MT different between trials with the shortest and longest DTs (t-test, 1% level).

Second, we asked whether the RT and MT were stationary as a function of trial number. We compared the RTs or MTs between the first 80 trials and last 80 trials of each session. Across monkeys R, F, C, and K, 16.7% of sessions were significant for a change in RT and 17.4% of sessions were significant for a change in MT (t-test, 1% level). Of those changes, there was nearly an equal likelihood that the RT or MT would increase as decrease throughout the session. The behavior of monkey T was, however, significantly less stationary than the other four monkeys. 60% of monkey T's sessions had a significant change in RT and 80% had a significant change in MT (t-test, 1% level). In all cases, the RT and MT decreased throughout the session (see Fig. 1-8B,C for examples).

1.4 Discussion

In this chapter, we have analyzed the psychophysics of five monkeys trained to perform reaching movements in null-field and curl force-field environments. First, the monkeys generally adapted their movements from the null-field to the force-field and deadapted from the force-field back to the null field. Second, adaptation aftereffects were prominent, indicating that the adaptation mechanism was proactive. Third, consistent changes in performance were seen across sessions with the same force field indicating there was some long-term learning or memory component of this task. All three of these findings have been reported previously (Gandolfo et al., 2000; Li et al., 2001; Padoa-Schioppa et al., 2002, 2004; Xiao et al., 2006). However, there are a number of details to these, and other, findings that were discovered by our analysis. Below we discuss these details in the context of interpreting neuronal data.

Deadaptation without adaptation

In many cases, we found that an aftereffect and deadaptation occurred in a session without significant prior adaptation (Fig. 1-3). There are several possible explanations for this. First, significant co-contraction of arm muscles at the beginning of the force-field epoch could mask adaptation as we define it (i.e. performance improvement from the early to late force-field epoch). Indeed, work in humans suggests that the initial phase of learning novel environments is dominated by an increase in arm stiffness, which eventually subsides once an internal model of the environment is formed (Thoroughman and Shadmehr, 1999; Osu et al., 2002; Franklin et al., 2003; Osu et al., 2003). Impedance control early in the force-field epoch and internal model-based control late in the force-field epoch could result in a nearly constant level of error throughout the epoch despite gradual acquisition of the internal model. However the improvements in early force-field epoch performance, and the corresponding lack of significant adaptation, occurred only after several daily sessions with the same force field (Fig. 1-6). It is somewhat counterintuitive that experience with a stable force field would lead to increased arm stiffness when encountering the force field again. It seems reasonable that the factors (e.g. metabolic efficiency) driving the transition from impedance control to internal model-based control when adapting to an environment would also prefer using an already acquired internal model when experiencing that environment again. Thus as a second possibility, immediate recall or faster acquisition (in << 40 trials) of an internal model of the force field could also improve performance at the beginning of the force-field epoch such that no adaptation is observed by our analysis. This explanation makes more intuitive sense with the across-session performance results, inter-epoch correlation analysis, and catch trial results. However, we did not measure arm impedance in these experiments and therefore we cannot rule out the first scenario.

Our results suggest that the large variation in degree of behavioral adaptation across sessions should be taken into account when analyzing the neural data. Correlates of adaptation (or memory recall) may be best captured by looking for co-variations with these across-session differences.

Incomplete adaptation and deadaptation

We found that force-field epoch performance did not return to the baseline level in nearly 74% of learning sessions with significant adaptation. This incomplete adaptation has important implications regarding interpretation of neuronal data. The previous non-human primate studies

using this task were largely devoted to dissociating cortical motor activity associated with movement kinematics and movement dynamics (Gandolfo et al., 2000; Li et al., 2001; Padoa-Schioppa et al., 2002, 2004; Xiao et al., 2006). The question of whether motor cortex encodes kinematics (i.e. relatively high-level motor commands) or dynamics (i.e. relatively low-level motor commands) has dominated motor cortex physiology for 40 years (Evarts, 1968). The null-field "center-out" reaching task that we employ, as first developed by Georgopoulos and colleagues (Georgopoulos et al., 1982), has highly correlated kinematic and dynamic variables and thus, on its own, is a poor paradigm for dissociating the cortical representation of these variables (Chan and Moran, 2006). However, much in the same manner as Evarts' original work on this question, Gandolfo and colleagues applied forces during the center-out reaching task and analyzed the neural data before and after adaptation to these forces (Gandolfo et al., 2000). A dissociation between kinematics and dynamics was then achieved, provided that the monkey's kinematics before and after adaptation was the same. However, in the monkeys we analyzed, 74% of the time the adaptation was not complete and the kinematics before and after adaptation were not the same. Based on this behavioral result, we cannot, by any analysis, make strong claims as to whether kinematics or dynamics are represented in motor cortex. Rather, our goal in analyzing the neuronal data will be to look for learning-related activity, which does not rely on the completeness of the learning.

We also found that washout epoch performance did not return to the baseline level in nearly 31% of learning sessions with significant deadaptation. Compared to 74% in the case of adaptation, we can say that the monkeys tended to completely deadapt back to null field conditions much more than they completely adapted to the force fields. This is despite there being an equal number of trials (160) in the force-field and washout epochs. The discrepancy may be due to a difference in the rates of adaptation and deadaptation. It has been shown in humans that adaptation to a novel force field is generally much slower than deadaptation back to a null field (Shadmehr et al., 1998; Davidson and Wolpert, 2004; Smith et al., 2006). We could not more directly assess this possibility since the variance of the performance measure was generally too large to estimate the learning rate with reasonable confidence. Another possibility is that adaptation and deadaptation processes have the same rate but there is a limit to how straight the monkey can make its trajectories in the force field, perhaps due to tradeoffs between performance and stability.

Changes in reaction time and movement time

Finally, we found that reaction time (RT) and movement time (MT) changed from the beginning to the end of a session. This was most prominent in monkey T, where RT changed in 60% of the sessions and MT changed in 80% of the sessions. This result is also important to interpreting neuronal activity. Several of the previous studies found there to be a difference in the activity of many cells from the baseline epoch to the washout epoch and interpreted this change to be indicative of a memory of the force field (Gandolfo et al., 2000; Li et al., 2001). This interpretation is invalid if the neural changes are correlated with behavioral changes from the baseline to washout epoch. Thus changes in RT and MT should be considered, along with performance changes due to incomplete deadaptation as described in the last section, when validating putative memory-related neuronal activity.

2 Cortical motor activity during reaching: I. time-domain analysis

2.1 Introduction

In recent years, anatomical studies have identified at least six distinct premotor areas in the primate frontal lobe (Dum and Strick, 2002). Understanding the differential contribution of these areas to the preparation and execution of reaching movements is a matter of ongoing research (Kalaska and Crammond, 1992; Kalaska et al., 1997). This is particularly true of the three cingulate motor areas, located within the cingulate sulcus on the medial wall of the cerebral hemisphere, whose physiology has only recently been studied (Cadoret and Smith, 1995, 1997; Shima and Tanji, 1998; Backus et al., 2001; Akkal et al., 2002; Russo et al., 2002; Crutcher et al., 2004; Hoshi et al., 2005).

Through a series of investigations into cortical correlates of movement dynamics, we have accumulated a relatively large database of cells recorded in a reaching paradigm involving both familiar and novel dynamical environments (Gandolfo et al., 2000; Li et al., 2001; Padoa-Schioppa et al., 2002, 2004; Xiao et al., 2006). This database includes cells from primary motor cortex (M1), dorsal premotor cortex (PMd), the supplementary motor area (SMA), and the dorsal, ventral, and rostral cingulate motor areas (CMAd, CMAv, and CMAr). Here we compared how each of the areas is involved in a well-rehearsed reaching task (i.e. in the familiar environment). Previous studies have compared neuronal activity between one or two cingulate areas and another motor area (usually SMA), but never have all three cingulate areas been compared to each other or to M1, SMA, and PMd. The unprecedented breadth of our study, therefore, provides a more global view of cortical motor activity during reaching.

Our analysis focused on timing of neuronal activity relative to behavioral events. The behavioral paradigm included an instructed delay between target presentation and response initiation and between response completion and reward. Thus the task allowed the dissociation of activity associated with movement preparation, movement execution, and reward anticipation. We quantified the relative proportion of cells associated with each of these stages of the task. The paradigm also involved movements in eight different directions. So at each task stage the activity was also classified based on its tuning to movement direction. To provide additional perspective on the neuronal activity, we also analyzed the task-relatedness and directional-

selectivity of activity at two other levels of the motor system: at the level of muscles, as reflected in the electromyogram, and at the level of cortical networks, as reflected in the local field potential.

2.2 Methods

Five rhesus macaques (*Macaca mulatta*) were used in this study (referred to as monkeys K, C, R, F, and T). The behavioral paradigm has been described previously (Chapter 1). Also, experimental procedures and initial results have been reported previously for monkeys C, R, and F (Padoa-Schioppa et al., 2002, 2004; Xiao et al., 2006). Here we reanalyzed those data along with newly obtained recordings from two other monkeys (K and T). Experimental procedures adhered to National Institutes of Health guidelines on the use of animals and were approved by the Massachusetts Institute of Technology Committee for Animal Care.

Surgery

All surgeries were performed using sterile techniques with the monkey under general anesthesia. After sufficiently training on the task, a stainless steel head restraining device was fixed to the skull near lambda. The monkey was then re-trained to perform the task under head-fixed conditions. Then a circular craniotomy was performed, leaving the dura mater intact, and a stainless steel recording well was fixed to the skull around this site. Relative to the interaural line (rostral zero) and midline (lateral zero; left cerebral hemisphere), the center of the craniotomy was 23 mm rostral and 0 mm lateral in K, 22 mm rostral and 0 mm lateral in C, 20 mm rostral and 15 mm lateral in T, 18 mm rostral and 0 mm lateral in F, and 16 mm rostral and 15 mm lateral in R. The diameter of the craniotomy was 28 mm in monkeys K, C, and T, 19 mm in monkey F, and 18 mm in monkey R. Systemic antibiotics and analgesics were given following the surgeries and the monkeys were allowed several days of rest to recover from each procedure. The exposed dura mater was treated with topical antibiotics and anti-inflammatories daily. Periodically (once every ~2-3 weeks), scarring that would accumulate over the dura mater was mechanically removed.

In one monkey (T), we also implanted 11 chronic intramuscular electrodes in the right arm. Each electrode was made of two Teflon-coated 50-μm stainless steel wires knotted together at one end. The knot was covered by a wax ball that insulated the two cut ends and anchored the

electrode under the muscle belly. A 1-3 mm segment of insulation was stripped from both wires at a distance from the wax ball such that the exposed segments would lie approximately in the middle of the muscle belly. The orientation of the intramuscular electrodes was approximately parallel to the muscle fibers. The following muscles were implanted: rhomboid, trapezius (2 electrodes), infraspinatus, supraspinatus, pectoralis major, deltoid (2 electrodes), biceps brachii (2 electrodes), and triceps brachii. Six additional muscles were implanted, but due to poor signal quality their recordings were excluded. After electrode implantation, the wires were tunneled subcutaneously and attached to a cranially-mounted connector.

Electrophysiology

Intracortical microstimulation (ICMS) was used to map the arm representations of the cortical motor areas. ICMS consisted of 50 ms trains of biphasic pulses at 330 Hz, with 0.2 ms pulse duration and 10-120 μA pulse amplitude. Stimulus-evoked muscle twitches were observed and mapped to the cortical location of the stimulus (Fig. 2-1B).

After locating the arm representations, extracellular recordings were made from these locations during each session that the monkeys performed the task. For the recordings, we used epoxylite-insulated tungsten microelectrodes, with 1-3 MΩ impedance and 250 μm diameter shaft tapered down to a 3 μm diameter tip (FHC). The electrodes were lowered transdurally using a custom-made manual microdrive with a depth resolution of approximately 30 μm. Due to dimpling of the cortex upon penetration and limitations in depth resolution, the laminar location of the recorded cortical cells was generally not known. Up to eight electrodes were used in each recording session. The analog electrical signals from the electrodes were passed first to a preamplifying headstage (AI 401, Axon Instruments or HS-27, Neuralynx) located about 5 cm from the electrodes, then to an amplifier (Cyberamp 380, Axon Instruments or Lynx-8, Neuralynx) where they were amplified (10000 gain) and filtered (300 Hz to 10 kHz passband) to obtain multiunit activity, and finally to an A/D board (DT3010, Data Translation) where they were digitized (12 bit resolution at 32 kHz/channel). The multiunit activity was not recorded continuously, but rather action potentials (i.e. spikes) were detected online by a manually-determined threshold crossing and only the spike times, along with behavioral task event times, were recorded to file with 0.1-ms resolution. Spike waveforms (i.e. 1.00 or 1.75 ms of the continuous signal around the spike time) were also saved for subsequent offline spike sorting.

Spike sorting was done manually, with the aid of software packages (Autocut 3, DataWave Technologies; MClust 3.3, A. David Redish, University of Minnesota), by detecting clusters in spike waveform feature space. Clusters of spikes were assumed to come from one neuron if they were: (1) reasonably separated from other clusters and noise spikes in feature space, (2) had temporally continuous, if not constant, waveform features, and (3) exhibited at least a 1 ms refractory period. Spike clusters meeting these criteria were classified as single unit activity.

In monkey T, the preamplified signals were amplified and filtered in two different ways in order to extract both multiunit activity (as above) and local field potentials. For the latter, the analog signal was filtered with a passband of 10 Hz (1^{st}-order Butterworth) to 400 Hz (4^{th}-order Bessel), amplified by 5000, digitized (12 bit resolution at 2 kHz/channel), and recorded continuously to file.

Electromyographic (EMG) data was recorded in monkey T for seven days following the completion of the cortical recording sessions. The EMG signals were amplified (5000 gain), filtered (10 Hz to 1000 Hz passband, 60 Hz notch filter), digitized (12 bit resolution at 2 kHz/channel), and recorded continuously to file.

Anatomy and histology

At the end of the recording sessions, the boundaries of the recording sites were marked with electrolytic lesions (cathodal current, 20 μA, 2 min). Then the monkeys were given an overdose of pentobarbital sodium and perfused transcardially with heparinized saline followed by buffered formalin. India ink was used to mark the surface of the cortex at selected coordinates near the recording sites. The brains were then removed from the skull and photographed to record anatomical landmarks (e.g. sulci) relative to the recording sites. In monkey F, the brain was sectioned and stained with cresyl violet for histological analysis. Monkey T died from bloat prior to applying electrolytic lesions, but the relative anatomical location of the recording sites was confirmed through gross anatomy.

Analysis

In this chapter, we restricted the analysis to the baseline epoch in order to focus on characterizing cortical motor activity during reaching in a familiar environment. In particular, we analyzed neural activity recorded during the last 120 trials (15 trials to each of the 8 targets) of

the baseline epoch of each session. The first 40 baseline trials were excluded due to the potential for behavioral instability, from the monkey readjusting to the experimental conditions, and recording instability, from rebounding movement of the neural tissue relative to the electrode, during this time.

The reaching task consisted of five behavioral intervals (center hold, CH; delay time, DT; reaction time, RT; movement time, MT; target hold, TH) divided by four events (peripheral target on, cue; center target off, go; movement onset, mo; movement end, me). Definitions of these intervals and events have been stated previously (Figure 1-1, Chapter 1). The goals of our analysis were to quantify the average neural activity changes relative to these events (i.e. quantify event-related activity) and characterize differences in event-related activity between the cortical motor areas.

SUA. Event-related single unit activity was studied using two complementary analyses. First, we explored the activity in a continuous, holistic fashion using the whole trial. This permitted at least a qualitative comparison between the firing rates at any two times, without bias from subjectively focusing on only certain parts of the trial. Second, we compared the firing rate in several trial windows, identified from the first analysis, to provide more quantitative results.

For the whole-trial analysis, we aligned each trial on all four behavioral events, despite the inter-trial differences in duration of the DT, RT, and MT (CH and TH were always 1 s each). DT activity was aligned on the cue rather than the go signal, as this is most appropriate for identifying cue-related and preparatory-related activity, and padded out to the longest DT duration to make it of constant length. We analyzed DT activity only up to the time at which half the trials (60 trials) had yet to encounter the go signal (first 1 s of DT in monkeys K, C, T, F; first 1.5 s of DT in monkey R), as beyond this point the analysis would be based on too few trials. We then resampled the DT activity of monkey R to have the same length as that of the other monkeys. RT and MT activity were aligned on both bordering events (go to mo and mo to me, respectively) by temporally rescaling the data to have a duration of 300 ms and 600 ms (approximately the mean RT and MT durations across all monkeys), respectively. The final result of these procedures was a whole trial record of constant length (rescaled duration of 3.9 s) with both pre- and post-alignment on the cue, mo, and me events and post-alignment on the go event. Due to the temporal rescaling, the RT and MT activity in all monkeys was not in absolute time, but rather in time relative to the duration of the interval (i.e. a spike at 150 ms after the go

signal in the rescaled data occurred half way between the go and mo events in the unscaled data). Also the DT activity in monkey R, while in absolute time, was not in the same time units as the DT activity from the other monkeys. These two time-scale manipulations effectively normalized the behavior in time across trials and monkeys.

After aligning the data, we computed the instantaneous firing rate within each interval on each trial by convolving the spike train with a Gaussian window (50 ms standard deviation). Using the instantaneous firing rate in the 15 trials to each target direction, we computed the significance of directional tuning at each instant in time. Significance of tuning was based on a one-tailed permutation test on the resultant vector magnitude (rvm) of the directional data. The distribution of the rvm under the null hypothesis (i.e. no tuning, uniform or antipodal symmetric distribution of firing rates across target directions) was obtained by shuffling the relationship between trial and direction, computing the rvm for this shuffled data, and repeating these two steps 1000 times. If less than 10 values from this distribution were greater that the actual rvm, the tuning was considered to be significant ($p < 0.01$). When the directional tuning was significant, we also computed the preferred direction of the tuning curve (i.e. the direction of the resultant vector). We summarized the activity of each cell using these three quantities: mean instantaneous firing rate, instantaneous tuning significance, and instantaneous preferred direction. For the mean instantaneous firing rate, we averaged over trials in all eight directions when the tuning was not significant and over trials in the four directions closest to the preferred direction (i.e. the preferred hemifield) when the tuning was significant.

Next, we excluded from the whole-trial analysis cells whose activity was not significantly modulated during the task. We defined a statistic, the modulation index, which quantified changes in the mean instantaneous firing rate for each cell based on 95% student-t confidence intervals on this mean (cim). The modulation index was defined as the fraction of time (out the 3.9-s rescaled trial duration) that the lower cim was greater than the median firing rate (i.e. excitation) and the upper cim was less than the median firing rate (i.e. inhibition). The modulation index could range from 0 (no modulation) to 1 (continuous modulation). To estimate the distribution of this statistic under the null hypothesis (i.e. no modulation, constant firing rate), we generated surrogate data by simulating stationary Poisson point processes. In particular, we computed the modulation index for 1000 surrogate "cells", each with 120 Poisson spike trains of 3.9-s duration that were convolved with the same Gaussian window used for the real data. As the

modulation index is sensitive only to modulation duration, not amplitude, the simulated modulation index distribution was largely independent of the chosen firing rate of the Poisson spike trains. Nevertheless, we chose the across-cell distribution of firing rates to correspond to that of the real data (exponential distribution, $P(r) = \exp(-r/8)/8$ where r is the firing rate in Hz and $r \geq 0.3$ Hz, see below). The 99^{th} percentile of the generated modulation index distribution (0.16) was used as the critical value for rejecting the null hypothesis. The simulations, as well as observation of the real data, indicated that cells with very low but relatively constant firing rates were not always detected by the above procedure. Thus we also removed from the analysis cells with average firing rate less than 0.3 Hz.

For the population whole-trial analysis, we z-score transformed the mean instantaneous firing rate for each cell (i.e. subtracted the mean and divided by the standard deviation). This allowed us to focus only on the modulation timing with respect to behavioral events. Then we identified subpopulations using the k-means clustering algorithm, which iteratively defined clusters of whole-trial activity patterns by minimizing the within-cluster sum of distances from the cluster centroids. Two different types of activity patterns were used to define the subpopulations: the instantaneous firing rate and the instantaneous tuning significance. The latter was a binary vector where zero indicated no tuning and one indicated tuning. Distance in the 390-dimensional space (i.e. the length of each rescaled trial) was defined to be squared Euclidean distance for the instantaneous firing rate and Hamming distance (i.e. percentage of differing bits between binary vectors) for the instantaneous tuning significance. Other distance measures produced very similar results. To compensate for the potential convergence of the algorithm to local minima, the clustering procedure was repeated 100 times with randomly-selected initial centroid locations. The repetition with the least error was chosen. The number of clusters, k, was chosen subjectively, however the major results of the analysis were evident across many values of k. To compare across the cortical areas, the clustering was done on all areas simultaneously. Then we used a two-way contingency table test, Pearson's chi-squared, to determine whether there was a relationship between the activity pattern clusters and the cortical areas.

In addition to the whole-trial analysis, we performed a second, more conventional analysis of event-related single unit activity without aligning the data on multiple events. We analyzed the mean firing rate within four, 400-ms perievent windows to quantify cue-related activity (post-cue window, cue + 50 ms to cue + 450 ms), preparatory-, or set-, related activity (delay-time

window, cue + 500 ms to cue + 900 ms, for monkeys T, C, F, K, or cue + 1000 ms to cue + 1400 ms, for monkey R), movement-related activity (movement-time window, mo – 100 ms to mo + 300 ms) and reward-related activity (target-hold window, me + 600 ms to me + 1000 ms). We compared the activity in each of these four windows to control activity (center-hold window, cue – 700 ms to cue – 300 ms) using a two-way, repeated-measures ANOVA with window and target direction as factors. We reported only the main effects of window and interaction effects of window x direction. Main effects of direction were redundant since control activity was not directionally tuned and, therefore, they were almost entirely due to window x direction interactions. A main effect of window in this test could reflect either phasic event-related activity or tonic activity associated with a previous event. Therefore we also compared the mean activity in the delay-time, movement-time, and target-hold windows with the mean activity in the 400-ms preceding each window using a second two-way, repeated-measures ANOVA. A significant main or interaction effect was indicative of phasic event-related activity or directional tuning, respectively. Note, the interaction effect in this test could reflect onset of tuning or a change in tuning; we did not distinguish between these two possibilities. Thus, for each cell we performed seven tests: one to determine cue-related activity (which, being the first event in the trial, was always defined to be phasic), and two tests each to determine the tonic and phasic components of set-related, movement-related, and reward-related activity. In each test we also noted the sign of the difference in means to classify the changes as either excitatory or inhibitory. For consistency, we only included in this analysis cells which were significantly modulated according to the whole-trial test described above.

LFP. We also studied event-related local field potential activity. The LFPs were first preprocessed with both frequency- and time-domain filters to remove two sources of noise. Power-line noise was attenuated with a stopband filterbank, with stopbands centered on each 60 Hz harmonic from 60 Hz to 480 Hz and of width 3 Hz (for centers <= 150 Hz) or 6 Hz (for center > 150 Hz). We used elliptical filters (40 dB attenuation in the stopbands, 0.5 dB ripple in the passbands) run in both forward and reverse directions to prevent phase distortion. Brief noise (< 40 ms duration) at the time of each behavioral event was present in many of the early LFP recordings due to electrical crosstalk in the acquisition system. We removed this noise and replace it with a reflection of the signal occurring immediately before the noise. Finally, the LFPs were low-pass filtered with a zero-phase, 2^{nd} order Butterworth filter with 100 Hz nominal

cutoff frequency.

After preprocessing, we aligned the LFPs to each of the four behavioral events individually and averaged over the 120 trials. By visual inspection, there appeared to be two relatively consistent event-related potential (ERP) complexes with three peaks each: a negative (cN1)-positive (cP1)-negative (cN2) complex occurring after the cue and a positive (mP1)-negative (mN1)-positive (mP2) complex occurring around movement onset. The latter could often also be seen when aligning trials on the go signal rather than movement onset. We identify these nine peaks (i.e. cN1-cP1-cN2, aligning on the cue, and both sets of mP1-mN1-mP2, aligning on the go or mo), and their duration, in each trial-averaged LFP. The duration was defined by the first zero crossing on either side of the peak.

Next, we determined the significance of the peaks. The strength of a peak was defined to be the square root of the integral of the square of the signal over the identified peak duration (rms). We calculate the rms for all peaks (i.e. between every two consecutive zero-crossings) in a 1.75 s window around the relevant event (cue, go, or mo). The result was an approximately exponential distribution of rms values. If the putative ERP peak had a rms that was greater than 3 times the mean of this distribution (approximately 95^{th} percentile assuming an exponential distribution) and had a duration greater than 50 ms, it was considered significant. The latter criterion was to ensure the peak was not due to residual noise, which was typically of short duration. LFPs that had at least one significant peak were defined as being modulated (Table 2-1).

As a measure of the contribution of each trial to an ERP, we projected the signal in each trial onto the trial-averaged signal over the duration of the peak. The projection captured the similarity in phase between each trial signal and the mean signal, weighted by the trial signal's amplitude. This measure was appropriate given that, in agreement with recent EEG literature, the ERPs appeared to result more from phase resetting of ongoing field potential oscillations rather than from addition of a high-amplitude signal to background field potential activity (Makeig et al., 2002; Jansen et al., 2003; Klimesch et al., 2004; Gruber et al., 2005). Using this measure, we looked for relationships between ERPs and behavior that have been identified recently. We tested the relationship between ERP strength and movement direction (Cardoso de Oliveira et al., 2001; Mehring et al., 2003a; Rickert et al., 2005) and between ERP strength and both instructed delay duration and reaction time (Roux et al., 2006). The significance of each relationship was assessed using a permutation test.

EMG. Finally, we examined the event-related modulation of electromyographic (EMG) signals. Preprocessing the EMG involved removal of occasional brief, high amplitude artifacts using a time-domain filter similar to that used in the LFPs. Then the EMG amplitude envelope on each trial was estimated by rectifying and lowpass filtering (zero-phase, 2^{nd}-order Butterworth filter with 10 Hz cutoff frequency) the signal. To facilitate comparison with the single-cell data, the EMG amplitude was aligned on multiple events and the instantaneous preferred direction was computed in the same manner as the SUA whole-trial analysis described above.

2.3 Results

Neural database

We recorded cortical motor activity in five rhesus macaques while they performed a visuomotor reaching task. As the task involved movement of the right arm, we targeted our recordings to the arm representation of motor areas in the left cerebral hemisphere (Fig. 2-1A, region inside the dashed lines). There are at least seven anatomically distinct motor areas in the monkey cerebral cortex: primary motor cortex (M1) and six premotor areas (Dum and Strick, 2002). The premotor areas (dorsal premotor, PMd; ventral premotor, PMv; supplementary motor area, SMA; rostral cingulate motor area, CMAr; dorsal cingulate motor area, CMAd; and ventral cingulate motor area, CMAv) are operational defined as cortical regions that project directly to M1 and to the spinal cord, both cervical and lumbar segments (Dum and Strick, 1991). The corticospinal neurons in most of these areas are topographically organized such that there are spatially-distinct arm (cervical-projecting) and leg (lumbar-projecting) representations (He et al., 1993, 1995). We used intracortical microstimulation (ICMS) to distinguish between different motor areas and to locate the arm representation within each area (Mitz and Wise, 1987; Luppino et al., 1991). Specifically, we mapped the lateral motor areas (M1, PMd, and PMv) in monkeys T and R and the medial motor areas (SMA, CMAr, CMAd, CMAv) in monkeys C and K.

The ICMS maps were quite consistent between monkeys. Figure 2-1B shows the composite ICMS map of both lateral motor areas (from monkey T) and medial motor areas (from monkey C), generated by aligning the map from each monkey rostrocaudally on the genu of the arcuate sulcus and mediolateral on the midline. Just rostral of the central sulcus, the threshold stimulus intensity was lowest and the somatic representations had a mediolateral distribution: face (lateral) to arm to leg (medial). These are characteristic features of M1. The threshold stimulus

intensity increased as we moved rostrally toward the arcuate sulcus, indicating a transition from M1 to PMv (lateral to spur of the arcuate sulcus) and PMd (medial to spur of the arcuate sulcus). Near the midline was the caudal leg representation and rostral arm representation of SMA. The arm representation continued rostrally past the level of the genu of the arcuate sulcus into the preSMA, an area we do not consider premotor since it does not send direct projections to the spinal cord (He et al., 1995). Moving down the medial wall (i.e. ventrally) from preSMA is CMAr, which had an arm representation that extended over both dorsal and ventral banks of the cingulate sulcus and possibly a leg representation as well. More caudally in the dorsal bank of the cingulate sulcus were two interleaved leg and arm representations of CMAd. Finally, on the caudal part of the ventral bank of the cingulate sulcus was the arm representation, and possibly

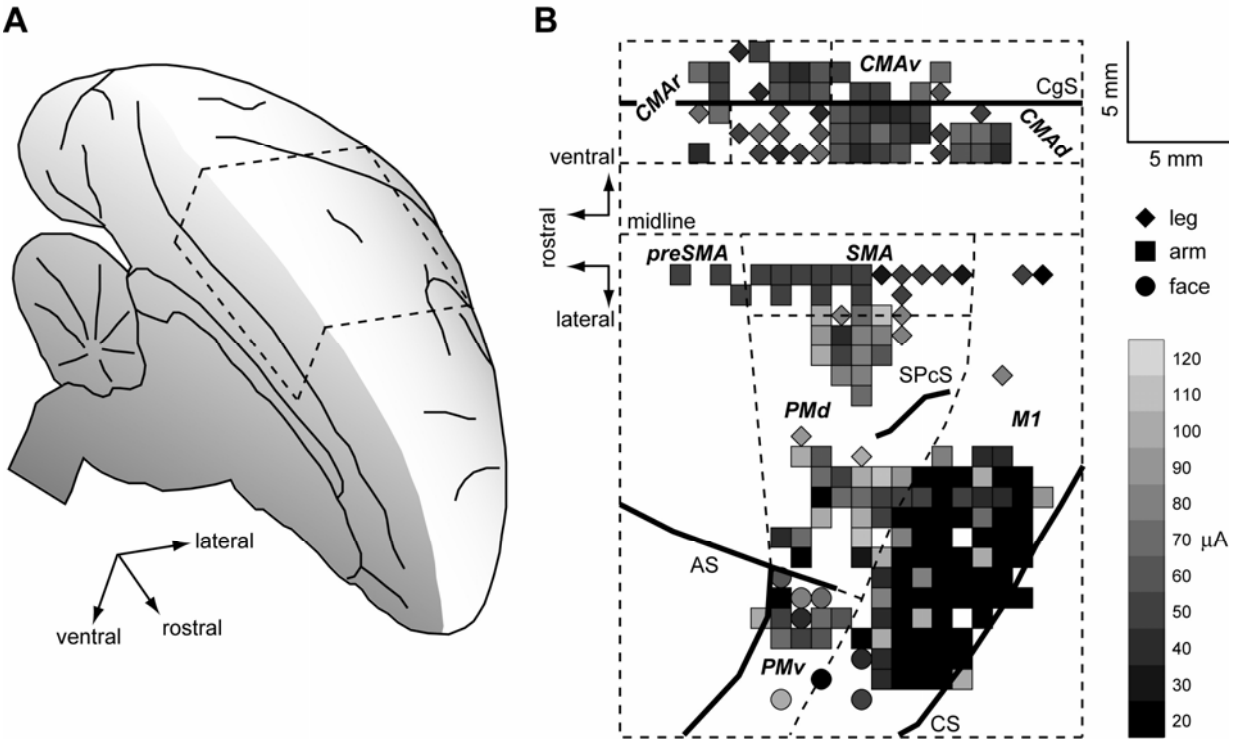

Figure 2-1. Intracortical microstimulation (ICMS) results. **A**, Schematic of the left hemisphere of a rhesus macaque brain. The dashed lines indicate the approximate area of the cerebral cortex shown in B and in Figure 2-2A,B. **B**, Composite ICMS map from monkeys T and C. Diamonds, squares, and circles indicate where the leg, arm, and face are represented in the cortex, respectively. The color indicates the minimum stimulus intensity required to elicit a response. Solid thick lines show the relative location of sulci (CS, central sulcus; AS, arcuate sulcus; SPcS, superior precentral sulcus; CgS, cingulate sulcus). Dashed thin lines are the putative borders between different cortical motor areas (M1, primary motor; PMv and PMd, ventral and dorsal premotor; SMA and preSMA, supplementary and pre-supplementary motor areas; CMAr, CMAv, and CMAd, rostral, ventral, and dorsal cingulate motor areas).

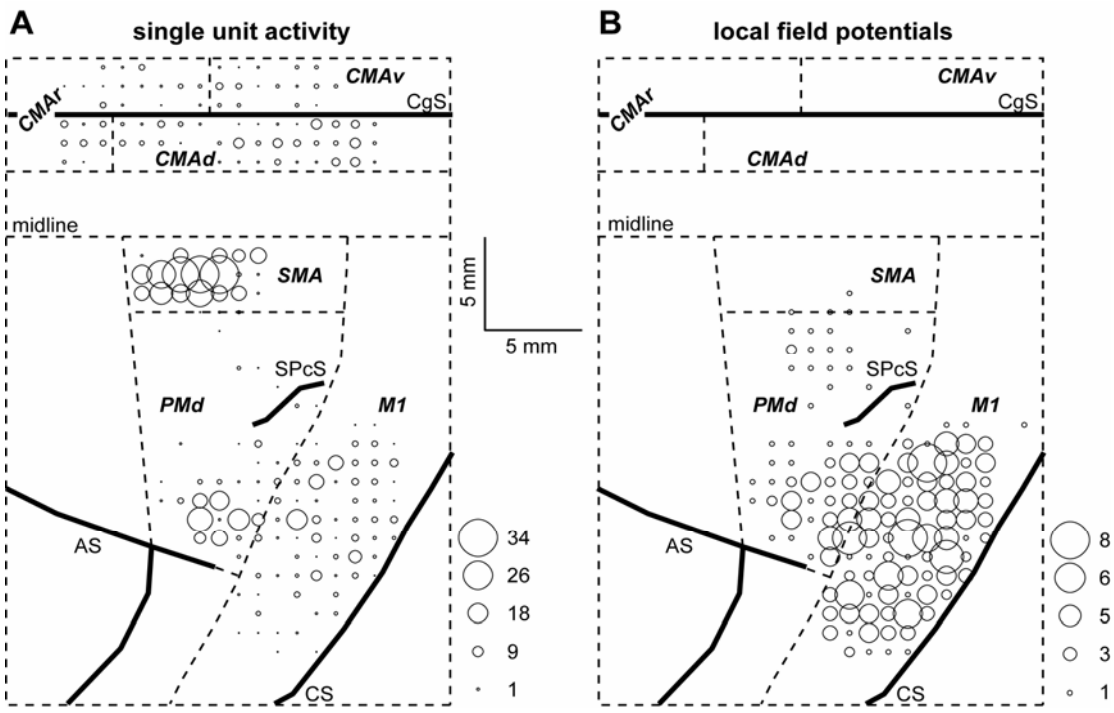

Figure 2-2. Neural recording locations. **A**, Location of single unit activity recorded from all five monkeys. The size of the circle indicates the number of cells recorded at each location (see scale on the lower right). **B**, Location of local field potentials recorded from monkey T. Sulci are indicated by solid thick lines and area borders are indicated by dashed thin lines, as in Fig. 2-1B.

even more caudal leg representation, of CMAv. This map is largely congruent with maps from anatomical studies (c.f. Fig. 17 in He et al. (1993), lateral motor areas; Fig. 8 in He et al. (1995), medial motor areas). Note that the composite ICMS map in Figure 2-1B is just for illustrative purposes; the assignment of recording locations to different cortical motor area was based on the anatomy and physiology (i.e. ICMS results) of each monkey individually. Also, in monkey F, the SMA recording locations were verified by histological analysis rather than ICMS (Padoa-Schioppa et al., 2004).

From the identified arm representations, we recorded single unit activity (SUA) and local field potentials (LFPs) while the monkeys performed the reaching task. A summary of the recording locations from all monkeys is given in Figure 2-2 (cortical anatomy aligned across monkeys as in Figure 2-1B). Overall, we recorded from 981 single cells in six cortical motor areas and 339 LFPs in two cortical motor areas (Table 2-1). From those totals, 261 cells and 129 LFPs were recorded in control sessions. The remaining neural activity was recorded in learning sessions in which either a counterclockwise or a clockwise curl force field was applied.

However, below we describe only the activity preceding the application of forces (i.e. activity recorded during the baseline epoch of each session).

Table 2-1. Neural database. Single unit activity (SUA) and local field potentials (LFP) recorded in each cortical area (M1, PMd, SMA, CMAr, CMAd, CMAv) for each monkey (T, R, F, C, K). The last row indicates the number of cells and LFPs that were significantly modulated during the task.

		SUA						LFP	
		M1	PMd	SMA	CMAr	CMAd	CMAv	M1	PMd
monkeys	T	198	63					239	100
	R	47	112						
	F			59					
	C			245	47	93	31		
	K				19	50	17		
total		245	175	304	66	143	48	239	100
mod		220	164	293	43	100	37	229	86

Event-related neuronal activity

Of the 981 recorded cells, 857 were significantly modulated during the baseline epoch (Table 2-1, last row; see Methods). There were a variety of modulation patterns in relation to the four behavioral events of the task (cue signal, go signal, movement onset, movement end). Several examples are shown in Figure 2-3. In Figure 2-3A, we show raster plots for one SMA cell both before (top) and after (bottom) aligning the activity to all four events. This alignment procedure temporally normalized the behavior across trials, which allowed us to examine average event-related activity continuously along the trial duration (see Methods). The neuronal activity gradually increased between the cue and go signals (i.e. during the instructed delay time), rapidly decreased after the go signal, and finally increased again following movement end, as captured by the instantaneous firing rate (Figure 2-3A, middle). The cell was not directionally tuned at any point along the trial. In contrast, the cells shown in Figures 2-3B (PMd cell) and 2-3C (CMAd cell) were tuned to the target direction. When tuning was significant, as determined by a permutation test, the mean instantaneous firing rate was based on the activity in the four directions closest to the preferred direction (i.e. the preferred hemifield; thick line in top plots of Fig. 2-3B,C) rather than the activity in all eight directions (thin line in top plots of Fig. 2-3B,C). Some cells became directionally tuned during the instructed delay time, soon after the target

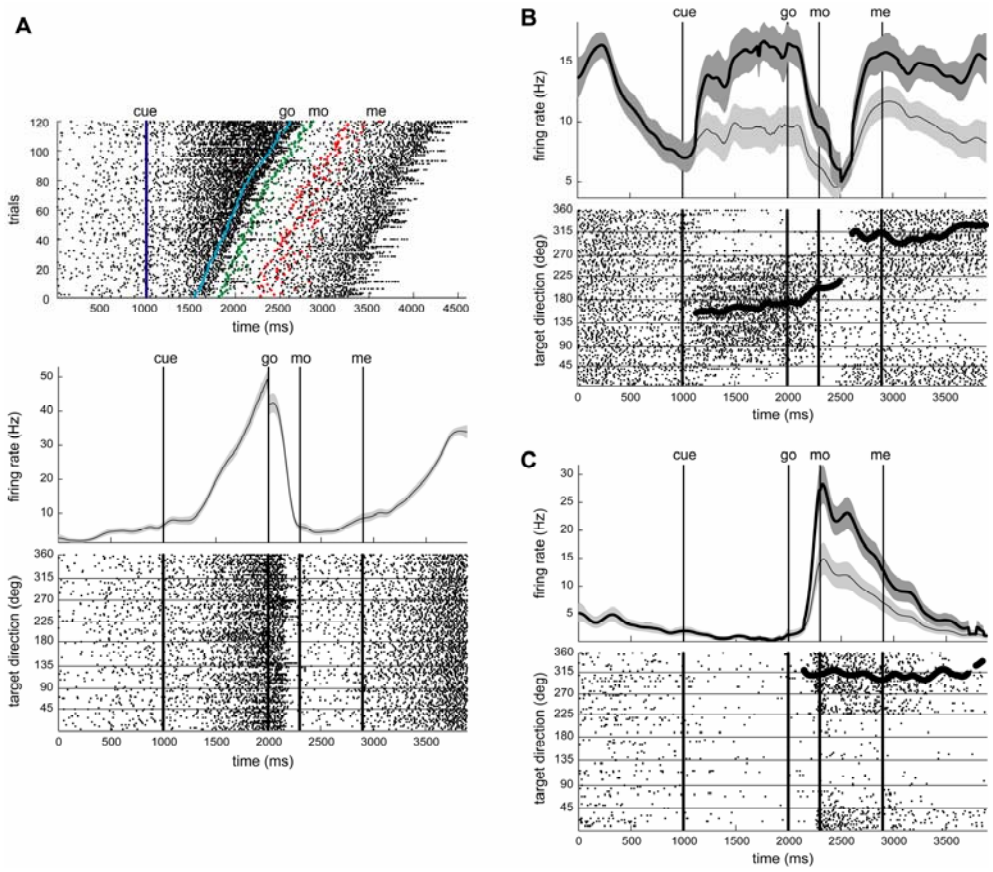

Figure 2-3. Examples of single unit activity. **A**, SMA cell. Raster plot of activity prior to alignment procedure, with trials ordered by delay time (top). Mean instantaneous firing rate of aligned activity with 95% confidence intervals in gray (middle). Raster plot of aligned activity, with trials ordered by target direction (bottom). **B**, PMd cell. Thick lines indicate mean instantaneous firing rate of the preferred hemifield (top) and instantaneous preferred direction (bottom). Absence of a thick line indicates insignificant tuning. **C**, CMAd cell.

presentation (cue), as seen in Figure 2-3B. We characterized the tuning curve at each point in time with a single parameter: the preferred direction (PD; thick line, bottom plots of Fig. 2-3B,C). The PD was often not constant. For the cell in Figure 2-3B, the change in PD from the delay time to the target hold time was about 140 degrees. Finally, the most typical modulation was an increase in directionally-tuned activity during the reaction time just prior to movement, as in Figure 2-3C.

The average activity across the population of significantly modulated cells in each cortical motor area is shown in Figure 2-4. All areas had a phasic, excitatory response around movement onset, as was expected of motor areas (Fig. 2-4, top row). PMd also had an excitatory population response after the cue, suggesting this area was involved in the visuomotor transformation. SMA had maintained excitation in the post-movement period in contrast to PMd, where the post-movement response was largely inhibitory. Directional tuning was most prominent during

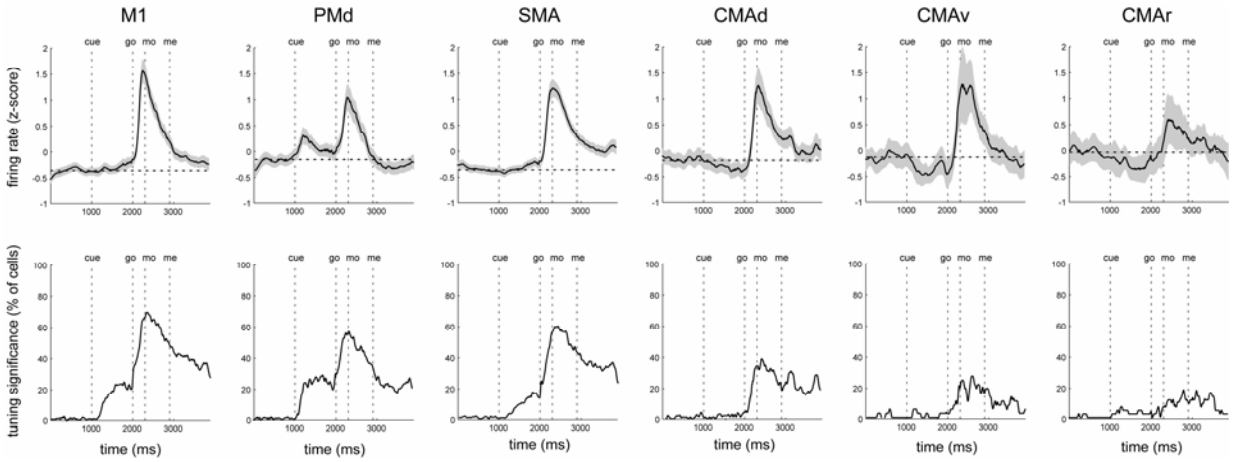

Figure 2-4. Population average single unit activity for six cortical motor areas. Top row, the population mean of the z-score transformed instantaneous firing rates. Gray regions indicate 95% student-t confidence intervals on the mean. Dotted horizontal line is at the level of the average center-hold activity. Bottom row, the percent of all cells that were significantly directionally tuned at each point in time.

movement (Fig. 2-4, bottom row). M1 had the highest percent of cells with significant tuning, reaching nearly 70% at movement onset. M1, PMd, and to a lesser extent SMA, showed directional tuning in the delay time, starting approximately 100 ms after the cue. Tuning persisted after movement during the target hold time. Directional tuning was less frequent in the cingulate motor areas, particularly in CMAr.

The distribution of PDs for each area is shown in Figure 2-5 (CMAr and CMAv were omitted due to the paucity of tuning in these areas). Since we observed that the instantaneous PD of any given cell could change over the course of the trial (e.g. Fig. 2-3B), we chose to look at the PD distribution as a function to time as well. The distribution of mean PDs in each non-overlapping, 150-ms window was tested for uniformity with a unimodal alternative and a bimodal alternative (Rayleigh tests, familywise error rate, $p < 0.05$). The PD distribution of M1 was mostly uniform, except for broad unimodal tuning (red crosses in Fig. 2-5) at movement onset and bimodal tuning (red circles in Fig. 2-5) just prior to the reward. PMd also had a unimodal PD distribution during movement, as well as during the early instructed delay time. Finally, both SMA and CMAd had significant bimodal tuning throughout parts of the reaction time, movement time, and target hold time. Interestingly, the major axes of the bimodal distributions were nearly identical in SMA and CMAd (approximately 150º-330º axis). Also the preferred directions of the unimodal distributions during the movement time in M1 and PMd

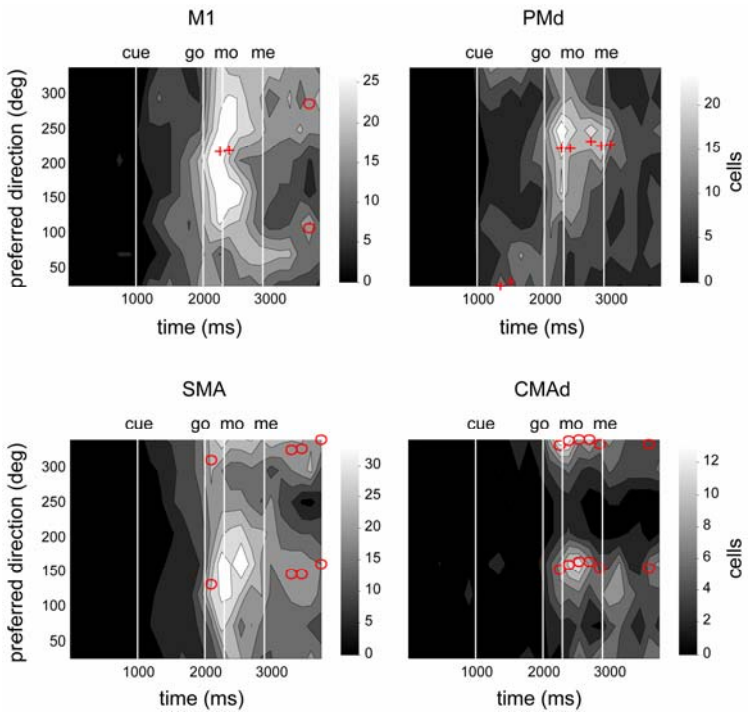

Figure 2-5. Population preferred direction distributions across time. Contour plots are two-dimensional histograms of the number of cells with a particular preferred direction at a particular time. Red crosses indicate the preferred direction of the distribution when it was significantly unimodal (Rayleigh test, $p < 0.025$). Red circles indicate the major axis of the distribution when it was significantly bimodal (Rayleigh test with bimodal alternative, $p < 0.025$).

were very similar (approximately 230º) and nearly orthogonal to the bimodal axis of SMA and CMAd.

Next, we explored the variability about the mean population responses and, in particular, whether distinct subpopulations could be defined. Towards this goal, we used the k-mean clustering algorithm to define groups of cells with similar event-related activity (see Methods). Clustering was done both on the instantaneous firing rate and the instantaneous tuning significance of each cell. For simplicity of presentation, we included only the four areas from which we had collected the most cells (M1, PMd, SMA, and CMAd). The results of the cluster analysis are shown in Figure 2-6. For the instantaneous firing rate, we show six clusters (Fig. 2-6, top row) although there was no clear correct number of clusters. An objective measure of cluster quality, silhouette analysis, indicated that the clusters were not particularly well separated (average silhouette value of 0.23, out of a possible 1, when extracting between 2 and 12 clusters). Thus the firing rate patterns form more of a continuum. Nevertheless, the cluster analysis served to highlight different dimensions of this continuum. Furthermore, several distinguishing features between the cortical areas were evident regardless of the number of clusters extracted. Below we

highlight three of these features.

First, there was a predominance of PMd cell activity in the post-cue, instructed delay time. This can be seen in cluster 2 (Fig. 2-6, top row), which consisted of cells that had a ramp-like increase in firing rate during the instructed delay. We formed a two-way contingency table of the number of cells in each cortical area that were either in the cluster or not in the cluster (4 x 2 table). We found that the two categorical variables (cortical area and cluster inclusion) were not independent ($\chi^2(3) = 23.08$, $p < 0.0001$). Indeed, over 20% of PMd cells were included in cluster 2 while the same was true of less than 10% of cells from any other area (Fig. 2-6, top right). Second, tonic movement-related activity was more prevalent in the medial motor areas (SMA and CMAd) than the lateral motor areas (M1 and PMd), as can be seen in cluster 4 ($\chi^2(3) = 36.43$, $p < 0.0001$). PMd, in particular, had relatively little activity extending into the target hold time. Third, phasic movement-related activity was more prevalent in the lateral motor areas than the medial motor areas, as can be seen in cluster 5 ($\chi^2(3) = 24.62$, $p < 0.0001$).

There were six basic patterns of directional tuning significance along the trials (Fig. 2-6, bottom row). Cells in cluster 1 were significantly tuned during the delay time and reaction time and then became untuned during the movement time. PMd had the highest proportion of cells in

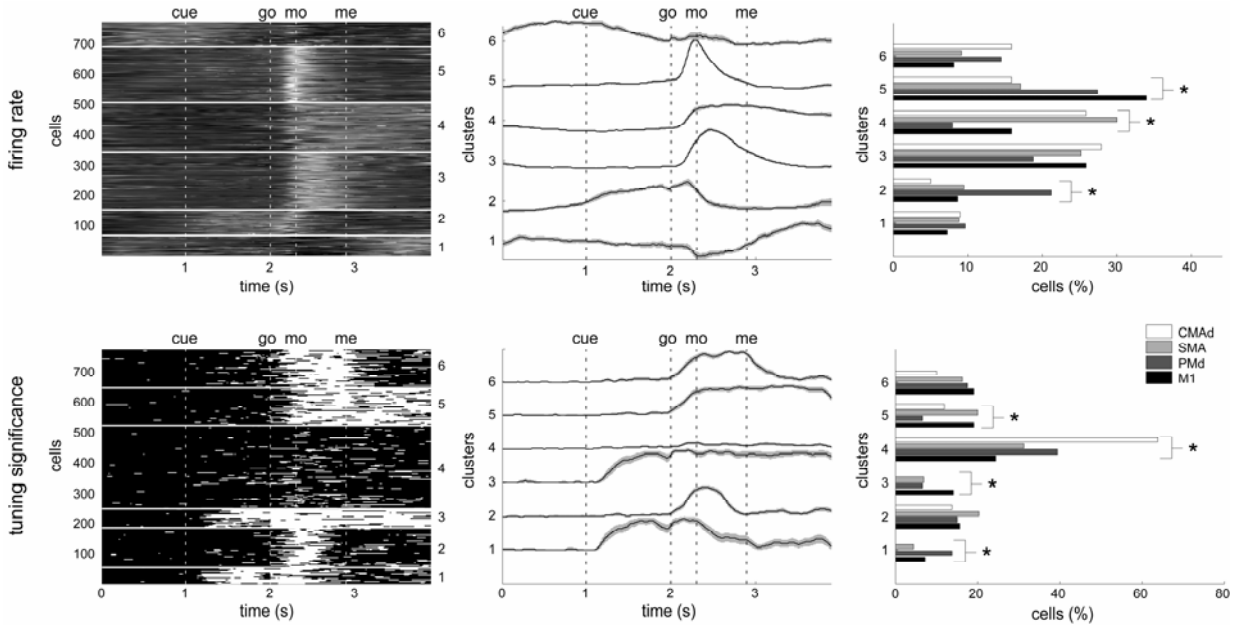

Figure 2-6. Subpopulations of event-related activity defined by cluster analysis. Left, clustered instantaneous firing rate (top) and instantaneous tuning significance (bottom) profiles. Middle, average profile of each cluster. 95% confidence intervals on the mean shown in gray. Right, percent of cells from each cortical area that are in each cluster. An asterisk indicates a significant difference in the proportion of cells from each area in the cluster (χ^2 test, $p < 0.05$).

this group while CMAd had no cells in this group ($\chi^2(3) = 21.92$, $p = 0.0001$). Cluster 2 was composed of a roughly equal proportion of cells from each area that were tuned briefly around movement onset ($\chi^2(3) = 3.49$, $p = 0.3223$). Cells in cluster 3 were tuned continuously from the delay time through the target hold time. M1 had the highest proportion of cells in this group and, again, CMAd had no cells in this group ($\chi^2(3) = 19.59$, $p = 0.0002$). Conversely, cluster 4, which had relatively high number of CMAd cells and low number of M1 cells, had no consistent tuning at any time ($\chi^2(3) = 52.90$, $p < 0.0001$). Cells in cluster 5 were tuned in the movement time and target hold time but not the delay time. M1 and SMA had the highest proportion of cells in this cluster ($\chi^2(3) = 14.16$, $p = 0.0027$). Finally, cluster 6 was composed of a similar proportion of cells from each area that were tuned throughout the movement time ($\chi^2(3) = 4.17$, $p = 0.2438$). This analysis shows that CMAd had no appreciable delay time directional tuning (clusters 1 and 3), CMAd had relatively less tuning overall than the other areas (cluster 4), and PMd had relatively little tuning during the target hold time compared to M1 and SMA (clusters 5). It also demonstrates that, as expected, the cue signal (clusters 1 and 3) and go signal (clusters 2, 5, and 6) were the primary events that triggered the onset of directional tuning.

To further quantify event-related neuronal activity, independent from the preceding whole-trial analysis, we analyzed the average firing rate in four, 400-ms perievent windows to identify cue-related, set-related, movement-related, and reward-related activity (see Methods). We performed two, two-way ANOVAs (factors: window, target direction) in order to compare the activity in these windows both to control activity during the center hold (to identify total, tonic + phasic, changes) and to activity in a 400-ms window preceding each of these windows (to identify only phasic changes). The proportion of significant main effects of window ($p < 0.05$) for each cortical area is shown in the Figure 2-7A, separated by whether the change was excitatory or inhibitory. The colored and uncolored portions of the bars indicate the proportion of phasic and tonic activity changes, respectively. When grouping the results shown in Figure 2-7A across all cortical areas, there were two striking features. First, a greater proportion of mean firing rate changes were excitatory in the movement window (75.8%) relative to the other three windows (46.5%, 45.8%, and 50.5%; $\chi^2(3) = 155.15$, $p < 0.0001$). Second, out of all significant changes in mean firing rate, a much greater proportion were tonic in the set (38.0%) and reward (29.5%) windows than in the movement window (6.4%) ($\chi^2(2) = 189.00$, $p < 0.0001$; the cue window was by definition always phasic, see Methods). This latter result suggests (1) that cue-

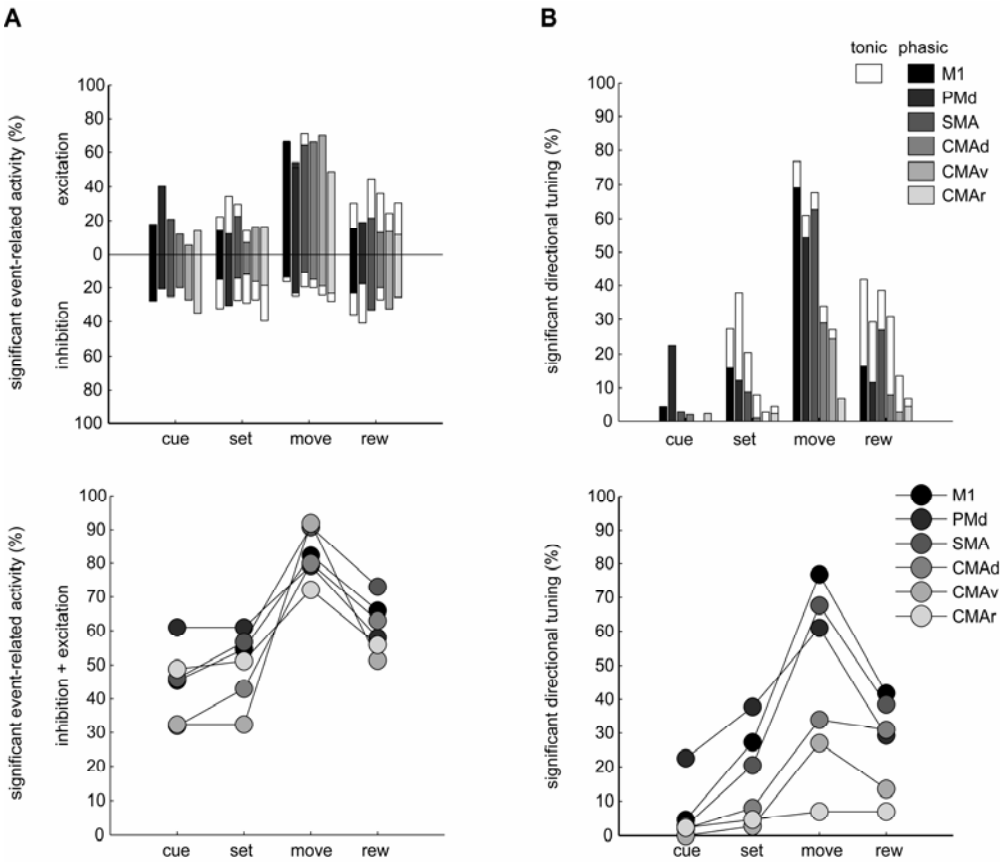

Figure 2-7. Proportion of event-related changes in mean firing rate and directional tuning. **A**, Percent of cells classified as cue-, set-, movement-, or reward-related based on significant changes in mean firing rate. Top: colored portions of the bars indicate proportion of phasic event-related changes relative to the activity just preceding the event (main effect of window in 1st two-way ANOVA, $p < 0.05$). Full bars, both colored (phasic) and uncolored (tonic) portions, indicate proportion of event-related changes relative to control activity during the center hold (main effect of window in 2nd two-way ANOVA, $p < 0.05$). The relative proportion of excitatory and inhibitory changes is indicated by the direction (upward or downward, respectively) of the bars. Bottom: Proportion of changes relative to control activity (i.e. phasic + tonic), combining both excitatory and inhibitory. **B**, Same as in A but for significant directional tuning (window x direction interaction in 1st and 2nd two-way ANOVAs, $p < 0.05$).

and movement-related activity were often tonic, extending into the set and reward windows, respectively and (2) the duration of set-related activity did not often extend past movement onset. All of these features can be readily observed in the firing rate profiles (Figs. 2-3 and 2-6).

When comparing the results shown in Figure 2-7A between the cortical areas, there were also several significant features. First, PMd had proportionally more cue-related activity (60.1%) than the other areas ($\chi^2(5) = 25.40$, $p = 0.0001$), as observed in the population and subpopulation whole-trial analyses above. Second, as we also observed in the previous analyses (e.g. Fig. 2-4), total excitatory set-related activity was more prominent in M1, PMd, and SMA (28.2%, grouped) than the cingulate areas (11.7%, grouped; $\chi^2(1) = 20.91$, $p < 0.0001$). Third, the proportion of

phasic movement-related activity was similarly large in each area (ranging from 72.1% to 89.1%; $\chi^2(5) = 5.20$, $p = 0.3922$). Fourth, the tonic reward-related activity was mostly excitatory in the four medial motor areas, mostly inhibitory in PMd, and equally excitatory and inhibitory in M1. These reward-related features are also apparent in the population activity profiles in Figure 2-4, particularly for PMd and SMA.

The proportion of significant window x direction interactions ($p < 0.05$) for each cortical area is shown in the Figure 2-7B. These results largely mirror the whole-trial directional tuning analysis presented in Figure 2-4 (bottom row) and Figure 2-6 (bottom row), despite the difference in tuning significance criteria. Directional tuning in the post-cue window was proportional much higher in PMd (23%) than the other areas (< 5%; $\chi^2(5) = 81.75$, $p < 0.0001$). Tuning during the set window was also most prominent in PMd, however it was more related to tonic activity from the cue (26%) than from phasic set-related activity (12%). The cingulate motor areas had very little tuning overall. However, the caudal cingulate areas had much more directional tuning during movement (32.1%, grouped) compared to CMAr (7%; $\chi^2(1) = 10.72$, $p = 0.0011$). Lastly, SMA had a notably high proportion of phasic reward-related tuning (27%) compared to all other areas (< 16%; $\chi^2(5) = 39.98$, $p < 0.0001$).

Finally, we examined the extent to which instructed delay-time activity, tentatively called preparatory or set activity above, truly reflected movement preparation. In particular, we asked whether there was a correlation between single unit delay-time activity and a measure of motor preparedness—the reaction time (RT) (Kubota and Hamada, 1979; Lecas et al., 1986; Riehle and Requin, 1993). In the behavioral RT analysis (Chapter 1), we found that in almost all sessions there was a significant negative correlation between duration of the instructed delay and the RT. Ramp-like single unit activity during the delay (e.g. cluster 2 in Fig. 2-6, top row) would therefore imply a correlation between unit activity and the RT. Here we sought to quantify that relationship explicitly. For each session, we performed a trial-by-trial correlation between the RT and the average firing rate in the 400 ms preceding the go signal. Unlike the previous analyses, we used all trials within a session (i.e. baseline, force field, and washout epoch trials) to maximize statistical power and to be consistent with the behavioral RT analysis. For robustness, we both excluded trials with extreme RT values (less than 100 ms or more than 600 ms) and used a rank correlation coefficient (Kendall's τ). The results, listed in Table 2-2, are sorted according to whether the delay-time activity was greater than, less than, or the same as the center-hold

Table 2-2. Incidence (and %) of significant correlations between the reaction time and the average firing rate in the last 400 ms of the delay time (Kendall's τ, $p < 0.05$ as judged by a permutation test). The values are divided according to both the sign of the correlation and whether the delay-time activity was excitatory, inhibitory, or the same relative to the center-hold activity (two, one-tailed t-tests, $p < 0.05$).

	M1			PMd			SMA		
	N	$\tau > 0$	$\tau < 0$	N	$\tau > 0$	$\tau < 0$	N	$\tau > 0$	$\tau < 0$
excit.	34	1 (3)	14 (41)	72	0 (0)	34 (47)	63	1 (2)	16 (25)
inhib.	86	14 (16)	7 (8)	41	5 (12)	3 (7)	92	15 (16)	4 (4)
same	125	6 (5)	33 (26)	62	1 (2)	14 (23)	149	17 (11)	15 (10)
	CMAd			CMAv			CMAr		
	N	$\tau > 0$	$\tau < 0$	N	$\tau > 0$	$\tau < 0$	N	$\tau > 0$	$\tau < 0$
excit.	6	0 (0)	1 (17)	2	0 (0)	0 (0)	5	0 (0)	1 (20)
inhib.	36	2 (6)	1 (3)	16	3 (19)	0 (0)	19	2 (11)	0 (0)
same	101	1 (1)	9 (9)	30	0 (0)	0 (0)	42	4 (10)	1 (2)

activity (as judged by two, one-tailed t-tests; $p < 0.05$). Overall the correlations were fairly weak ($\tau < \pm 0.3$ for all cells). However, the sign of a statistically significant correlation was generally appropriate for the sign of the change in activity during the delay, suggesting that the test results were not spurious. For example in SMA, negative correlations with RT were observed in 25% of cells with excitatory delay-time activity and only 4% of cells with inhibitory delay-time activity. Conversely, positive correlations with RT were observed in 16% of cells with inhibitory delay-time activity and only 2% of cells with excitatory delay-time activity. Thus, as implied by the previous analyses, changes in delay-time activity were often correlated with movement preparation.

In summary, all cortical motor areas had a high proportion of cells that were engaged in the reaching task. Each area had a phasic, excitatory population response around movement onset with a corresponding increase in proportion of directionally tuned cells. However, there were several differences between the cortical areas, which were most apparent either in the delay-time before movement or the target hold-time after movement. PMd activity began and ended earlier in the trial compared to the other areas. Significant cue-related activity was most prominent in PMd. The three cingulate motor areas were unique in their relative lack of excitatory set-related activity and directional tuning. Within the cingulate, CMAr had less directional tuning than the caudal cingulate areas. M1 and SMA activity was very similar, although the latter tended to have more tonic movement-related activity and reward-related tuning. Finally, there was a striking similarity in the bimodal PD distributions of the SMA and CMAd and the unimodal PD

distributions of M1 and PMd. Interestingly, the PD distributions of the medial areas and lateral areas were nearly orthogonal to one another.

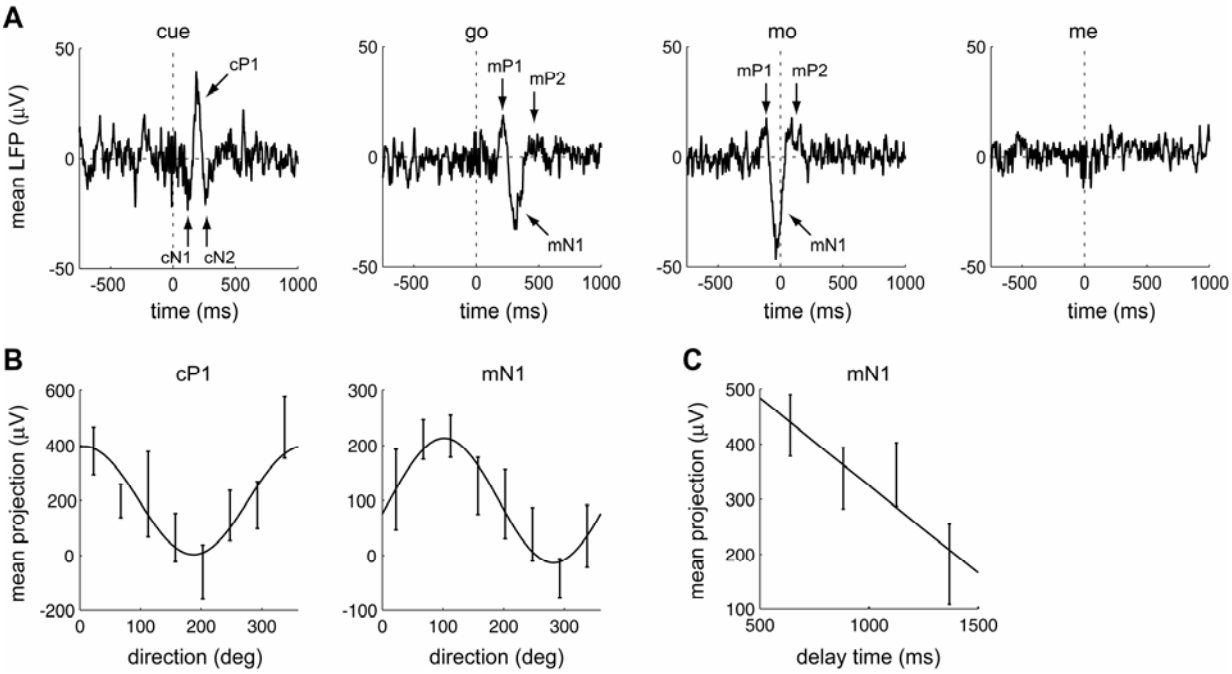

Figure 2-8. Example of event-related potentials in a trial-averaged LFP. **A**, Average LFP aligned on each of the four behavioral events (cue, go, mo, me). Arrows point to each component of the cue-related potentials (cN1, cP1, cN2) and movement-related potentials (mP1, mN1, mP2). The movement-related potentials can be seen both by aligning on the go signal and on movement onset. **B**, The cP1 component and mN1 component were tuned to the direction of movement. Vertical lines are mean ± sem of the projection of each trial in a given direction along the trial-averaged LFP component. The cosine fit to these values is also shown. **C**, The strength of the mN1 component was inversely proportional to the duration of the instructed delay.

Event-related LFP activity

There were two prominent event-related potentials in the trial-averaged LFPs: a cue-evoked potential (cEP) and a movement-evoked potential (mEP). An example is shown in Figure 2-8. In this example, the cEP had three components, or peaks: a negative peak (cN1), a positive peak (cP1), and a second negative peak (cN2). The mEP also had three components, but with the reverse polarity: a positive peak (mP1), a negative peak (mN1), and a second positive peak (mP2). The mEP was also evident when aligning on the go signal, although mN1 and mP2 were less pronounced than in the movement onset alignment (Fig. 2-8A). There were no evoked potentials associated with the end of movement.

Table 2-3. Statistics on event-related potentials (ERPs). 'mod' is the incidence (and %) of significant ERP peaks. 'peak' is the time of the ERP peak relative to the event (ms; mean ± sd). 'rms' is the strength of the ERP peak (μV•s; mean ± sd). 'dir' is the incidence (and %) of directional tuning of significant ERP peaks. 'delay' and 'rt' are the incidence (and %) of a correlation with the delay and reaction time of significant ERPs, respectively.

	M1								
	cue			go			mo		
	cN1	cP1	cN2	mP1	mN1	mP2	mP1	mN1	mP2
mod	53 (22)	110 (46)	19 (8)	54 (23)	188 (79)	177 (74)	77 (32)	199 (83)	210 (88)
peak	121 ± 14	209 ± 19	298 ± 25	213 ± 18	301 ± 42	442 ± 52	-124 ± 23	-41 ± 20	83 ± 51
rms	3.5 ± 1.0	3.2 ± 0.9	2.4 ± 0.8	2.7 ± 1.1	5.2 ± 2.2	3.1 ± 1.4	2.7 ± 1.3	6.7 ± 3.0	4.2 ± 1.7
dir	6 (11)	22 (20)	1 (5)	9 (17)	13 (7)	35 (20)	12 (16)	44 (22)	58 (28)
delay	4 (8)	7 (6)	2 (10)	3 (5)	63 (34)	16 (9)	2 (3)	89 (45)	39 (19)
rt	0 (0)	4 (4)	3 (16)	11 (20)	120 (64)	100 (56)	6 (8)	89 (45)	45 (21)
	PMd								
	cue			go			mo		
	cN1	cP1	cN2	mP1	mN1	mP2	mP1	mN1	mP2
mod	27 (27)	50 (50)	9 (9)	10 (10)	55 (55)	54 (54)	19 (19)	62 (62)	73 (73)
peak	122 ± 12	207 ± 27	276 ± 24	217 ± 38	313 ± 82	447 ± 60	-148 ± 35	-49 ± 20	88 ± 48
rms	3.3 ± 1.4	3.1 ± 1.0	2.2 ± 0.5	2.2 ± 0.6	3.8 ± 1.7	2.8 ± 1.2	2.0 ± 0.8	4.5 ± 2.2	3.3 ± 1.6
dir	4 (14)	13 (26)	3 (33)	2 (20)	6 (11)	5 (9)	0 (0)	14 (23)	18 (25)
delay	2 (7)	4 (8)	1 (11)	2 (20)	10 (18)	1 (2)	2 (11)	18 (29)	8 (11)
rt	0 (0)	3 (6)	0 (0)	0 (0)	20 (36)	24 (44)	2 (11)	17 (27)	7 (10)

315 out of the 339 recorded LFPs had at least one ERP component that was significant (Table 2-1, last row; see Methods). mEPs were more frequent than cEPs in both M1 and PMd (Table 2-3). The most frequent evoked-potential component in both cortical areas was mP2, which was significant in 88% of M1 LFPs and 73% of PMd LFPs. The latency of the first cue-related peak, cN1, was about 120 ms in both areas. The latency of the first movement-related peak after the go signal, mP1, was about 215 ms in both areas. The incidence and strength of mEPs in PMd were less than in M1, although the cEPs were in all respects similar in both areas (Table 2-3).

A substantial fraction of event-related potentials were broadly, unimodally tuned to the direction of movement. In the example LFP in Figure 2-8A, both the cP1 peak and the mN1 peak had significant directional tuning (Fig. 2-8B; permutation test on the resultant vector magnitude statistic, $p < 0.05$). The cP1 peak was directionally tuned in 20% of M1 LFPs and 26% of PMd LFPs that had a significant cP1 peak (Table 2-3). For the mN1 peak, these percentages were 22% and 23%, respectively. As seen in Figure 2-8C, the preferred directions of tuning in the cEP and mEP generally differed. Over the 34 M1 LFPs with at least one tuned peak in both the cEP and mEP, the average difference in preferred direction was 63 deg. Another example of tuning, this time where both the mN1 and mP2 peaks are significantly tuned, is shown in Figure 2-9A. In the

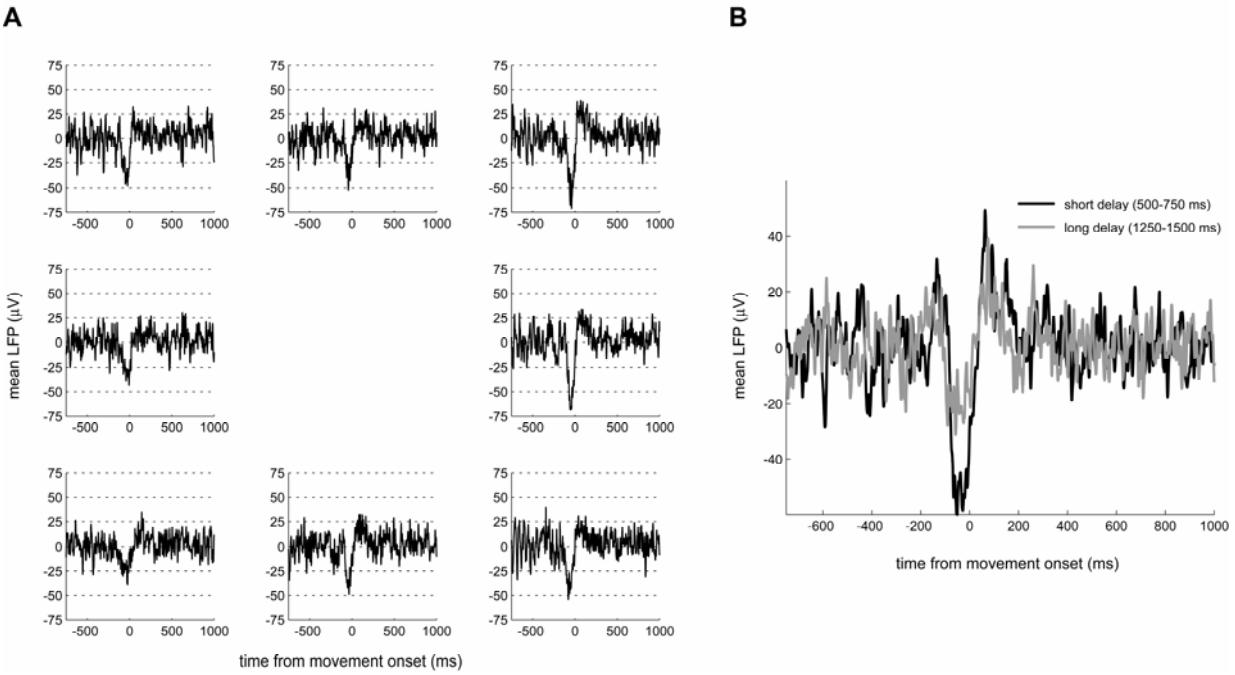

Figure 2-9. Examples of relationship between movement-evoked potentials (mEPs) and behavior. **A**, Trial-averaged LFP aligned on movement onset and sorted by movement direction. The mEP shows broad, unimodal tuning to movement direction. **B**, Trial-averaged LFP aligned on movement onset and sorted by duration of the instructed delay. The negative peak of the mEP is largest when delay times are short.

mEP, tuning was more frequent in later peaks (mN1 and mP2) than in mP1 (Table 2-3). Over the population, the distribution of preferred directions was significantly nonuniform (Rayleigh tests, $p < 0.025$). The preferred directions of the cP1 peaks were unimodally distributed with a mean direction of 48º (M1) and 50º (PMd). The preferred directions of the mP2 peaks were unimodally distributed with a mean direction of 104º (M1) and 103º (PMd).

Finally, some components of the mEP were modulated by the duration of the instructed delay period. For example, in Figure 2-8C and Figure 2-9B, the strength of the mN1 peak was negatively correlated with the delay time (permutation test on Kendall's τ statistic, $p < 0.05$). In fact, component mN1 was negatively correlated with the delay time in 45% of M1 LFPs with significant mN1 peaks (Table 2-3). The same was true for the mP2 component in 19% of M1 LFPs. These percentages were lower in PMd (29% and 11%, respectively). The correlations were generally weak (e.g. $\tau = -0.20 \pm 0.06$ for the mN1 peaks in M1), but consistently negative. The incidence of significant correlations for the other peaks (mP1 and the cEP peaks) was near chance levels (assuming 5% type I errors) or inconclusive due to an inadequate number of

significant peaks. Since the reaction time (RT) was correlated with the delay duration (Chapter 1), it is not surprising that the mEP was also correlated with the RT. In fact, the mEP-RT correlations were often even more pronounced, particularly for the go-aligned mEP (Table 2-3).

In summary, evoked-potentials were present following the cue and go signals, further demonstrating the saliency of these events. The relationship of the evoked potentials to both movement direction and delay duration suggests that, like the neuronal activity described above, they reflect cortical processing of movement preparation and execution. The cEP was in all respects essentially the same in both cortical areas, but the mEP was more prominent and more often related to the delay duration and reaction time in M1 than in PMd.

Event-related EMG activity

EMGs were recorded from 11 intramuscular electrodes implanted in eight proximal arm muscles in monkey T for seven sessions following completion of the cortical recordings. These data were obtained to provide insight into how the neural activity described above resembled or

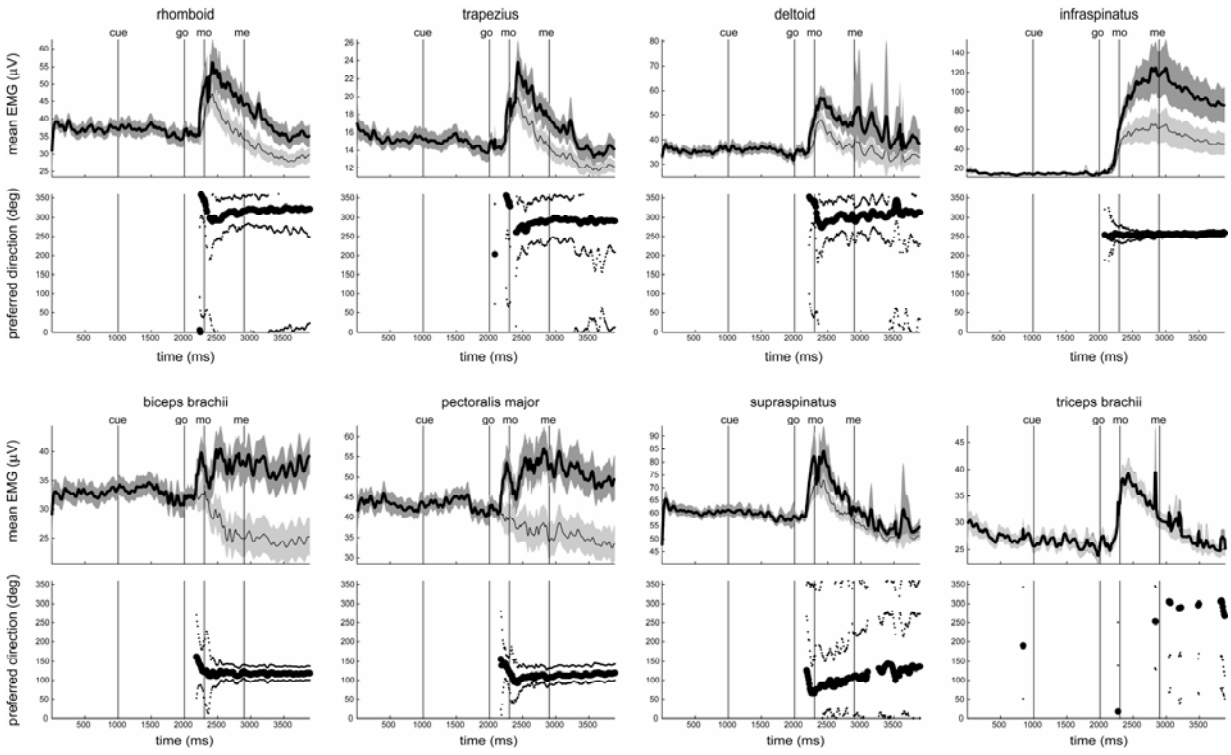

Figure 2-10. Event-related electromyographic (EMG) activity of proximal arm muscles. For each of the eight muscles, the mean EMG (top; all directions, thin line; preferred hemifield, thick line) and instantaneous preferred direction of activity (bottom) is shown, along with 95% confidence intervals.

differed from the muscular activity required to make the reaching movements. In Figure 2-10 we show the mean activity, and its instantaneous preferred direction, for the eight muscles. Trapezius, deltoid, and biceps were implanted with two electrodes each, but the activity was very similar on each pair and thus not shown separately. Furthermore, the mean activity and preferred direction of activity was very similar for each muscle across sessions. Thus Figure 2-10 just shows the activity of each muscle in one representative session.

Four features of the EMG activity stood out. First, the activity profiles were composed of phasic (rhomboid, trapezius, deltoid, supraspinatus, triceps) or tonic (infraspinatus, biceps, pectoralis) movement-related activity with no cue-related or set-related activity. Second, the activity was tuned to movement direction in most muscles (all but triceps), with tuning onset occurring in the reaction time and continuing throughout the movement and target-hold times. Third, the preferred direction did not change much over the course of the trial. Fourth, the preferred directions of these proximal muscles were clustered around 250-300 degrees (rhomboid, trapezius, deltoid, infraspinatus) and 100-150 degrees (biceps, pectoralis, supraspinatus). These preferred directions for the most part agree with the known mechanical actions of the muscles, except for supraspinatus which was, however, only weakly tuned.

Comparison of PD distributions

As described above, nonuniform PD distributions were a notable feature of the population analysis at all three physiological levels (SUA, LFP, and EMG). We more directly compared these distributions in Figure 2-11. Across all levels, the nonuniformities tended to lie along one of two approximately orthogonal axes. The proximal muscle activity, mEP, movement activity of CMAd, and target hold activity of M1, SMA, and CMAd all had a disproportionate number of PDs along the ~150º-330º axis. The cEP, delay activity of PMd, and movement activity of M1 and PMd all had a disproportionate number of PDs along the ~50º-230º axis. Below we discuss several interpretations of this arrangement of directional representations.

2.4 Discussion

This chapter examined how six cortical motor areas in the rhesus macaque are involved in planning and executing well-rehearsed reaching movements. Many features of the neural activity for each area have been reported previously, as we discuss below. However, the strength and

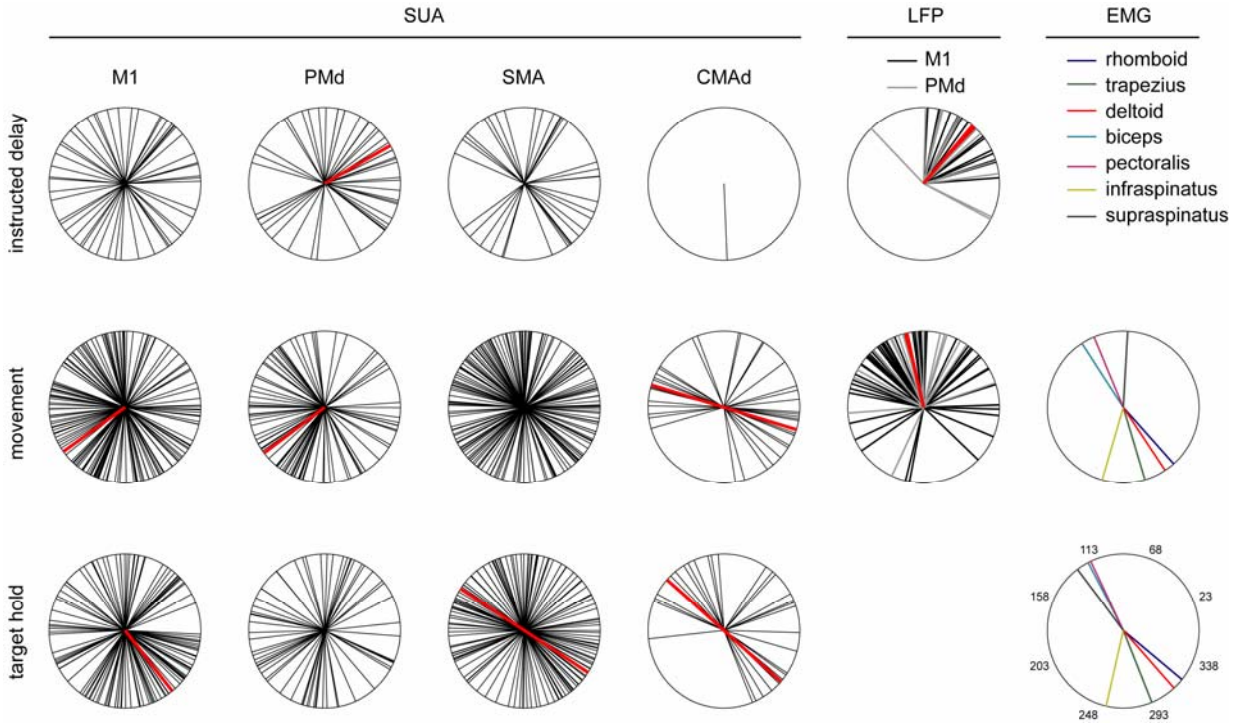

Figure 2-11. Preferred direction (PD) distributions of SUA, LFP, and EMG activity. The SUA and EMG distributions are of the average PDs during the last 500 ms of the instructed delay (top row), the interval -100 ms to +400 ms around movement onset (middle row), and the last 500 ms of the target hold period (bottom row). The LFP distributions are for the cP1 peak of the cue-evoked potential (top row) and the mP2 peak of the movement-evoked potential (middle row). Thick red lines indicate significant unimodal (radial line) or bimodal (axial line) distributions based on Rayleigh tests ($p < 0.025$).

uniqueness of the current study was in comparing the relative prominence of these features across so many different areas and different levels (muscles, single cells, networks) of the motor system.

Distributed network for movement preparation and control

Our results emphasize the distributed nature of motor processing in the frontal lobe (Kalaska and Crammond, 1992). Activity in the five premotor areas was proportionally very similar to that of M1 during movement initiation. Anatomical studies have shown that each of these premotor areas projects to the spinal cord and M1 (Dum and Strick, 2002). The strong premotor area responses suggest that these parallel motor pathways are indeed used to recruit muscles involved in reaching.

Likewise, several different areas contributed to movement preparation. During the instructed delay prior to movement, M1, SMA, and PMd had sustained, excitatory neuronal responses that were typically directionally tuned (Tanji and Evarts, 1976; Tanji et al., 1980; Weinrich and Wise, 1982). This set-related activity was often correlated with the reaction time, indicating that it truly reflected the preparation for movement (Kubota and Hamada, 1979; Lecas et al., 1986; Riehle and Requin, 1993). PMd was unique in that it had the highest proportion of cells with phasic responses to the visual cue (Weinrich and Wise, 1982). This is consistent with more specific evidence linking this area to a prominent role in visuomotor transformations (di Pellegrino and Wise, 1993; Crammond and Kalaska, 1994; Shen and Alexander, 1997; Cisek and Kalaska, 2004).

The preparatory responses in the cingulate motor areas, however, were comparatively more inhibitory and untuned. In fact, CMAr was uniquely untuned to movement direction throughout the task (Hoshi et al., 2005). A prominent feature of the cingulate areas, as well as SMA, was tonic, excitatory movement-related activity lasting throughout the post-movement hold time and up until the reward (Akkal et al., 2002). This is in contrast to PMd activity, which was more phasic and inhibitory following movement. Post-movement, reward-related activity has been previously documented in the CMAr (Shima and Tanji, 1998; Akkal et al., 2002; Hoshi et al., 2005), although not, to our knowledge, in the caudal cingulate motor areas.

Nonuniform neuronal PD distributions

The analysis of event-related neuronal changes, as summarized above, suggested that all the cortical motor areas were similarly engaged during movement and differentially engaged before and after movement. However, even during movement there was some indication of heterogeneity of function. In particular, we found that both during and after movement the PD distributions of SMA and CMAd were quite different from the PD distributions of M1 and PMd and all distributions were often significantly nonuniform.

Nonuniform PD distributions have been reported previously in M1 (Georgopoulos et al., 1982; Scott and Kalaska, 1997; Scott et al., 2001; Mitsuda and Onorati, 2002; Kurtzer et al., 2006; Naselaris et al., 2006a). However, many other reports of PD distributions, including the initial report on the SMA data analyzed here (Padoa-Schioppa et al., 2004) and the only such report on the caudal cingulate (Russo et al., 2002), concluded that the distributions were uniform.

There are at least two reasons for this discrepancy. First, nonuniform PD distributions are correlated with anisotropic mechanical properties of the limb (Scott et al., 2001). Task differences in limb configuration change the degree of mechanical anisotropy and, correspondingly, the distribution of PDs (Scott and Kalaska, 1997). This does not explain, however, different conclusions reached from the same data set (Padoa-Schioppa et al., 2004). For this, it is important to note that many of the nonuniform PD distributions found by us and others were bimodal, just as the mechanical properties (e.g. endpoint inertia) are bimodal. Thus a second reason for a discrepancy in inference on the shape of a PD distribution is the specific hypothesis test used to make the inference. Padoa-Schioppa et al. (2004) and Russo et al. (2002) used the standard Rayleigh test, whose null and alternative hypotheses are uniformity and unimodality, respectively (Fisher, 1993). Bimodal distributions will generally fail to show significance in this test. Indeed, notwithstanding differences in task and analysis details, the SMA and CMAd PD distributions reported in these papers (Fig. 6, target-hold, in Padoa-Schioppa et al., 2004; Fig. 11, movement, in Russo et al., 2002) actually appear to agree quite closely with our results.

The functional significance of the nonuniform neuronal PD distributions and of differences in nonuniformity between lateral and medial cortical areas cannot be conclusively determined from the present data. PD distributions play a central role in the population vector theory of representation in the motor cortex (Georgopoulos et al., 1986; Georgopoulos et al., 1988). We did not include an analysis of the population vectors in this chapter, as it provided no additional insight into the physiology (Mussa-Ivaldi, 1988; Sanger, 1994). Essentially, the population vectors deviated from the direction of movement in a way that simply reflected the specific nonuniformity of the PD distribution (Scott et al., 2001).

Some insight into the functional significance of the nonuniform PD distributions can, however, be made by considering the results of the EMG analysis. The proximal musculature was most active in movements away from or toward the body. The PD distributions of CMAd, both in movement and target hold, and of M1 and SMA during the target hold were oriented approximately along this same axis. Thus one interpretation is that CMAd was involved mostly in controlling proximal muscles and that most of the neuronal target hold activity was also associated with controlling proximal muscles. Several other reports have also shown that the nonuniformity in neuronal PD distributions is due to an overrepresentation of movements away

from and toward the body (Scott et al., 2001; Kurtzer et al., 2006; Naselaris et al., 2006a). This could reflect either the need for greater overall muscular effort in these directions (Scott et al., 2001) or that statistically the monkey, in its everyday life, tends to make more reaches in these directions (Naselaris et al., 2006a).

While we did not record from distal arm muscles, we can deduce from the lack of proximal arm activity that distal muscles were more involved in reaching along the orthogonal axis (to the left and toward the body and to the right and away from the body). Anecdotally, there appeared to be greater changes in wrist angle along these directions, thus implicating forearm muscles, although we did not specifically measure the joint kinematics. Therefore a tentative interpretation is that the unimodal PD distributions in M1 and PMd during movement reflect control of the more distal musculature.

Evoked potentials in the precentral cortex

The LFPs in both M1 and PMd were found to have two major event-related potentials: one occurring about 120 ms after the cue signal (cEP) and another occurring about 215 ms after the go signal (mEP). The mEP has been described in many primate electrophysiological studies (Gemba and Sasaki, 1984; Cardoso de Oliveira et al., 2001; Donchin et al., 2001; Mehring et al., 2003a; Rickert et al., 2005; Roux et al., 2006). The cEP has received less attention in this literature, however it is likely distinct from the mEP only when an instructed delay period is present. Indeed, one recent study that did include an instructed delay period found an evoked potential with similar latency from the instructional cue as that found here (O'Leary and Hatsopoulos, 2006). The cEP and mEP were only evident in the trial-averaged LFP, rather than individual trials, and thus seemed to reflect phase-locking, rather than amplitude modulation, of the LFP (Makeig et al., 2002; Jansen et al., 2003; Klimesch et al., 2004; Gruber et al., 2005). O'Leary and Hatsopoulos (2006), using frequency-domain rather than time-domain techniques, showed explicitly that M1 and PMd LFP oscillations in three different frequency bands are indeed phase-locked at a latency of about 120 ms following visual cue presentation.

LFPs are thought to reflect synchronized postsynaptic currents in a relatively large population of neurons in the vicinity of the recording electrode (Klee et al., 1965; Mitzdorf, 1985). The cEP and mEP therefore indicate that, not surprisingly, the cue and go events trigger a large amount of coincident activity in motor and premotor cortices. The cEP and mEP were

found to have consistently opposite polarity, likely due to the electric dipoles created by active neurons (Johnston and Wu, 1995). In particular, excitatory synaptic inputs associated with visual input to the network (cEP) cause the soma to act as a current source and the dendrites as a current sink whereas somatic action potentials associated with motor outputs of the network (mEP) cause the soma to be a sink and dendrites to be a source. Since our technique for isolating single cells likely resulted in electrode locations closer to the soma (i.e. in deeper cortical layers), these dipole orientations will result in the observed large positive peak for the cEP and large negative peak for the mEP.

Directional tuning of evoked potentials has been observed previously for both the cEP (O'Leary and Hatsopoulos, 2006) and mEP (Cardoso de Oliveira et al., 2001; Mehring et al., 2003a; Rickert et al., 2005; O'Leary and Hatsopoulos, 2006). Here we found directional tuning in approximately a quarter of the significant evoked potentials. It is somewhat surprising that M1 and PMd LFPs, which as mentioned above are the sum of activity from a large number (~thousands) of neurons, are directionally tuned. If one assumes a simple model that cortical neurons control a muscle, or group of muscles with similar action, and the neural tuning simply reflects the muscular tuning, then one would not expect tuning of the LFPs given that muscle representations in motor cortex are known to be quite distributed (Rathelot and Strick, 2006). However, there is some physiological evidence of small-scale spatial ordering of directional tuning in the motor cortex (Amirikian and Georgopoulos, 2003; Ben-Shaul et al., 2003; Naselaris et al., 2006b). In fact, the mere presence of LFP directional tuning might itself be evidence of this spatial ordering (Mehring et al., 2003b).

The PD distributions of both the cEP and mEP were significantly nonuniform (O'Leary and Hatsopoulos, 2006). The mean direction of the mEP PD distribution was oriented away from the body and aligned closely with the axis of preferred directions of proximal muscles. This relationship might indicate that the increased mEP amplitude in this direction reflects a biomechanical requirement for greater muscular effort and thus more coincident, motor output-related activity. This interpretation implies that tuning of evoked-potentials may not be due to any spatial order of directional representation in motor cortex and, in fact, not due to the directional tuning of motor cortical neurons at all. Rather, assuming the LFP reflects a sufficiently large number of cortical cells, the mEP tuning may simple be a result of the need for more cortical motor output in some movement directions than others. The cEP had even sharper

unimodal tuning, both in M1 and PMd. The mean direction was similar to that of the delay-time PD distribution of PMd cells, suggesting a link between the single cell and network levels of delay-time activity.

Surprisingly, the strength of the mEP was modulated by the duration of the instructed delay and correlated with the reaction time. Roux et al. (2006) observed a similar effect, although emphasized that the modulation primarily occurred during the mP1 peak. Here the modulation was more prevalent in the mN1 and, to a lesser extent, mP2 peaks. It is not clear exactly why the level of movement preparedness should impact the mEP. The EEG literature has documented a potential, called the contingent negative variation (CNV), which occurs during an instructed delay over large regions of the scalp and whose amplitude is related to level of expectance or preparedness of movement (Walter et al., 1964; Brunia, 1999). However, the absolute amplitude of the CNV is positively, not negatively, correlated with expectancy (Trillenberg et al., 2000). Thus the CNV is more closely related to the ramp-like increase in set-related activity that we and others have observed in PMd, M1, and SMA neurons as well as in the basal ganglia (Alexander and Crutcher, 1990). This latter area is thought to be the source of the CNV (Ikeda et al., 1997; Brunia, 1999). Here we did not observe the CNV, probably since we high-pass filtered the LFP recordings in line with other non-human primate field potential studies.

One hypothesis for the negative correlation of the mEP amplitude and delay duration is that a function of movement preparation is to prime downstream circuits (e.g. bring spinal neurons closer to threshold). With downstream circuits sufficiently primed, presumably less cortical output would be need to drive the movement and therefore the mEP would be of lower amplitude. With short delays, and the priming function not completed, presumably more cortical output would be need to drive the movement and the result would be a higher amplitude mEP. Spinal interneurons are indeed primed during an instructed delay prior to movement (Prut and Fetz, 1999). Furthermore, motor preparedness has been shown to be correlated with the strength of gamma-band coherence between motor cortex and spinal neurons (Schoffelen et al., 2005). Finally, a recent human TMS study has found corticospinal excitability is modulated by the level of expectance and that spinal, rather than cortical, mechanisms are likely responsible for these changes (van Elswijk et al., 2007).

Interpretational limitations

The "center-out" reaching task employed in this study has several limitations with regard to interpretation of neural data. First, we cannot dissociate whether cue-related activity, both in SUA and LFPs, is a visual response to the target or a movement planning response (Shen and Alexander, 1997). Second, although we often referred to post-movement, target-hold activity as related to the reward, we can not rule out the possibility that the activity is related to planning the unregulated, post-reward movement back to the center target to start the next trial. Third, the baseline, center-out reaching task is not designed to dissociate between different cortical representations, either in terms of the variable represented or the coordinate frame of the representation (Paninski et al., 2004; Chan and Moran, 2006). Thus, our emphasis on quantifying tuning of neural activity to the direction of movement should not be interpreted as advocating any particular encoding scheme in motor cortex. Rather, directional tuning is simply a very prominent feature of the activity which could reflect encoding of movement kinematics or kinetics in a variety of coordinate frames.

Three other limitations are related not to the task, but to the dataset. First, the contrasts highlighted above between lateral and medial motor areas, including post-movement activity and PD distributions, could not be observed in a single animal with the current data set. The data from the lateral areas and medial areas were collected in different animals. A second limitation was the relatively small number of cells collected in CMAr and CMAv. Due to this fact, we did not emphasize the cell classification proportions in these areas. A third limitation was that the LFP data were recorded from only one monkey. Preliminary data (44 LFPs from M1 and PMd) from a second monkey had similar evoked potentials following the cue and movement onset as those reported in this chapter. However, the second monkey's data also indicated that setting the high-pass cutoff frequency of the analog LFP filter to 1 Hz, instead of 10 Hz (see Methods), caused there to be more low frequency peaks associated with each evoked potential. For example, for the mEP there was a second negative peak as described by Rickert et al. (2005).

Conclusions

Control of the visuomotor reaching behavior was distributed across many cortical motor areas. PMd was most involved in responding to the visual cue and, with M1 and SMA, in the visuomotor transformation required to plan the upcoming movement. Network activity in these areas suggested that part of the movement planning may have involved priming downstream

circuits. All areas were similarly involved in executing the movement, though possibly with some specialization regarding the control of proximal (SMA, CMAd) versus distal (M1, PMd) muscles. M1, SMA, and CMAd all participated in the post-movement target hold, where the activity was mostly restricted to movement directions involving proximal muscles.

3 Cortical motor activity during reaching: II. time-frequency analysis

3.1 Introduction

Oscillatory neural activity is pervasive in the motor system, as in other brain systems (MacKay, 1997; Farmer, 1998; Schnitzler and Gross, 2005). In the motor areas of the precentral cortex, field potentials oscillate at several frequencies contingent on behavioral context. Beta band (~15-35 Hz) precentral oscillations have greatest amplitude during movement preparation (Sanes and Donoghue, 1993; Donoghue et al., 1998; Rubino et al., 2006), maintained posture (Baker et al., 1997; Baker et al., 1999), and exploratory movements (Murthy and Fetz, 1992, 1996a; Donoghue et al., 1998), but generally attenuate during well-rehearsed movements (Sanes and Donoghue, 1993; Donoghue et al., 1998; Pfurtscheller et al., 2003; Rickert et al., 2005). High gamma band (~60-100 Hz) precentral oscillations, on the other hand, generally have increased amplitude during well-rehearsed movements (Pfurtscheller et al., 2003) and are modulated by movement parameters such as direction and speed (Rickert et al., 2005; Heldman et al., 2006).

Field potential oscillations likely play a role in cortical motor processing as they modulate single cell activity. In particular, field potential oscillations are associated with synchronous (i.e. phase-locked) oscillatory discharge of precentral cortical neurons (Murthy and Fetz, 1996b; MacKay, 1997). Several hypotheses have been advanced regarding the functional role of these synchronous oscillations. First, synchronous oscillatory activity of precentral neurons may allow more efficient communication with other neuronal populations (Salinas and Sejnowski, 2001) and more efficient recruitment of muscular activity (Baker et al., 1999). Second, synchronized neuronal oscillations, or correlated neuronal activity in general, may in fact encode motor information such as desired movement direction (Hatsopoulos et al., 1998; Maynard et al., 1999; Oram et al., 2001). Third, oscillatory neuronal activity may promote learning through spike-timing-dependent plasticity by naturally correlating pre- and post-synaptic activity (Sejnowski and Paulsen, 2006). However, to date there has been little evidence linking oscillatory activity with motor learning.

Here, we investigated the role of oscillatory neural activity in a particular type of motor learning: adaptation to altered mechanical environments. In this chapter, we begin with a

thorough characterization of precentral neural oscillations during reaching in a familiar environment. In the next chapter, we explore how features of the oscillations change when adapting to a novel environment.

3.2 Methods

The behavioral (Chapter 1) and electrophysiological (Chapter 2) methods have been described previously. The neural database analyzed in this chapter was the same as in Chapter 2.

Analysis

We restricted the analysis to the last 120 trials of the baseline epoch to focus only on the oscillatory activity that occurred during reaching in the familiar environment.

The recorded local field potential (LFP) activity was filtered to remove noise, as in Chapter 2. Recordings with very low amplitude signal or with excessive spectral noise peaks not removed by the filtering were excluded from the analysis. The remaining LFPs (79%, 268 of 339 across all cortical areas) were subjected to the following analyses.

Power spectrograms were computed from the filtered LFPs using the short-time discrete Fourier transform with a sliding Hamming window of 200 ms width, stepped every 20 ms. This time-frequency analysis allowed us to characterize what oscillations where present, and at what time, during the baseline reaching task. Frequencies between 1 Hz and 95 Hz were analyzed in four, 1100 ms time epochs around the cue signal, go signal, movement onset (mo), and movement end (me) events. The noise filtering removed or significantly degraded any signal between 55 Hz and 65 Hz and therefore this band was removed from the spectrograms. Power at frequencies higher than 95 Hz was not analyzed since it was likely related to spiking neuronal activity, which was analyzed previously (Chapter 2).

Two frequency bands, the 12-27 Hz band (i.e. beta band) and the 70-95 Hz band (i.e. gamma band), were subjected to a time-resolved directional tuning analysis using the same sliding windows as for the spectrograms. For this analysis, average intra-band power was calculated on each trial. Then a permutation test was used, as in Chapter 2, to determine whether the power varied significantly with target direction. The standard permutation test described in Chapter 2 assessed whether directional tuning was unimodal. However, bimodal tuning also appeared to be

a prominent feature of the LFP activity (see Results). Therefore we performed two permutation tests, one with a unimodal alternative and one with a bimodal alternative (achieved by doubling the angles at each direction, modulo 360 deg), each with a significance level of $p = 0.025$ for a familywise error rate of $p = 0.05$. If the p-value of both tests was less than 0.025, then the tuning curve was classified based on the test with the lowest p-value. At each instance of significant tuning, the preferred direction (unimodal) or major axis (bimodal) of the tuning curve was computed through vector summation.

We also examined the relationship between neuronal activity and beta or gamma LFP oscillations. First, the LFP was bandpass filtered to isolate the beta or gamma oscillations using a 2^{nd}-order Butterworth filter run in both forward and reverse directions to prevent phase distortion. Then we estimated the instantaneous amplitude and phase of the oscillations. This can be done using either a complex wavelet or the Hilbert transform (Le Van Quyen et al., 2001), of which we chose the latter. Then we compiled the LFP amplitude and phase corresponding to each spike time. A Rayleigh test was used to determine whether the distribution of phases corresponding to all the spike times of a cell was significantly nonuniform.

To compare directional tuning curves, Pearson's correlation coefficient was computed for the mean tuning curves of each pair of LFP and single cell recordings on the same electrode and each pair of simultaneously recorded LFPs. A significant relationship between tuning curves was assessed at the population level by determining, with a t-test, if the mean of the distribution of correlation coefficients was significantly nonzero.

3.3 Results

LFP oscillations and behavior

Local field potentials (LFPs) recorded in the precentral cortex exhibited oscillatory activity during distinct phases of the reaching task. Figure 3-1A shows a spectrogram computed from the activity of one LFP. First, at the lowest frequencies (< 12 Hz) power occurred predominantly at the time of the cue and movement onset (mo). Power at these low frequencies was another manifestation of the cue- and movement-evoked potentials characterized previously using a time-domain analysis (see Chapter 2). Second, the highest power in the spectrum was concentrated in a band around 20 Hz, which we refer to as the beta (β) band (12-27 Hz). Beta-

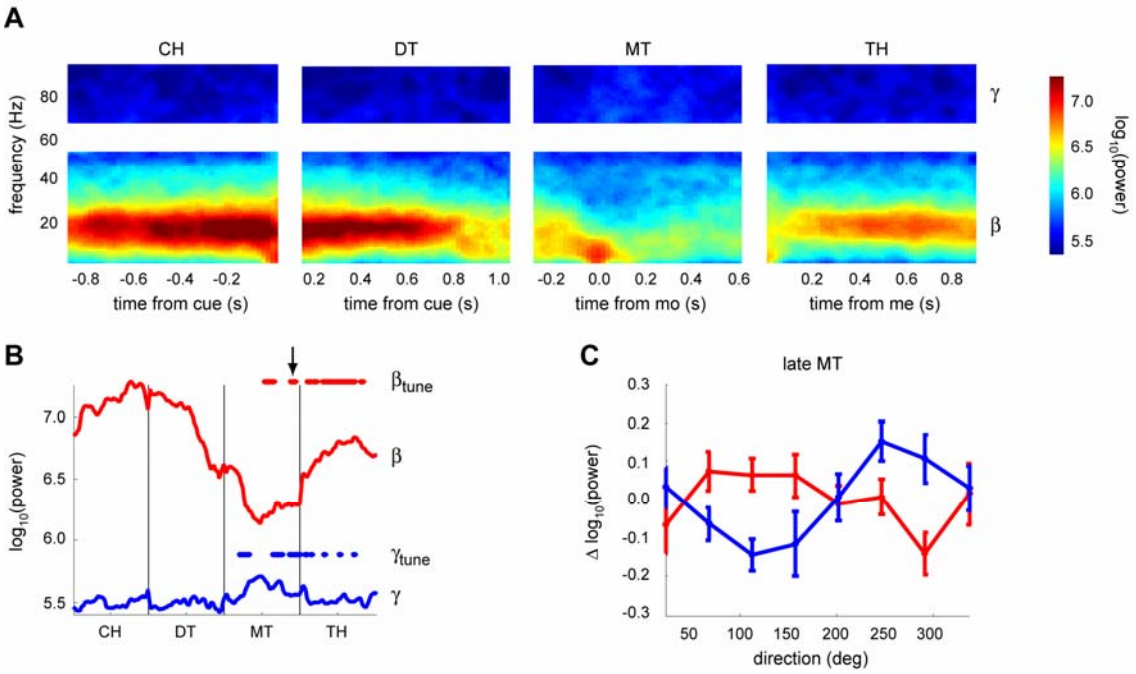

Figure 3-1. Oscillatory activity of an example LFP recorded in M1. **A**, Power spectrogram of LFP activity, averaged across the last 120 trials of the baseline epoch. CH = center hold; DT = delay time; MT = movement time; TH = target hold; mo = movement onset; me = movement end. **B**, Average power in the 12-27 Hz band (β-band, red) and the 70-95 Hz band (γ-band, blue) as a function of time. Times at which the power was significantly tuned to target direction are indicated above each trace. **C**, Tuning curves (mean ± sem) of average β (blue) and γ (red) power in a 200-ms window at the end of the MT (arrow in B). Power is relative to the all-trial mean power in each band.

band oscillations gradually increased in amplitude during the center hold (CH), gradually decreased throughout the instructed delay time (DT) and movement time (MT), and finally increased at the end of movement (me) and throughout the target hold time (TH). Thus maintained posture was associated with high-amplitude, beta-band oscillations while movement (including the movement back to the center just prior to the start of the CH) caused a decrease in oscillation amplitude at these frequencies. Third, higher-frequency oscillations around 70-95 Hz, which we refer to as the gamma (γ) band, were present during movement and not during the other phases of the task. Gamma band power was about 10-fold less than beta-band power, but showed clear modulation with movement, as can be seen in the temporal profile of average power in Figure 3-1B. Fourth, the task-relatedness of oscillations with frequencies between the beta and gamma bands (~35-70 Hz) was less consistent and at least partially unobservable due to power-line noise (white-out segment in Fig. 3-1A). These four observations held true at the population level as well (Fig. 3-3A,B). There were no consistent differences between the

amplitude of LFP oscillations in M1 and PMd. Thus for Figure 3-3, as well as the rest of the chapter, the M1 and PMd LFPs were combined into a single data set.

In addition to these event-related modulations, power in both the beta and gamma bands systematically varied with the direction of movement. A time-resolved analysis of spectral directional tuning for the example LFP shown in Figure 3-1 found that both beta- and gamma-band power were tuned at various times during the MT and the TH (Fig. 3-1B). The tuning curves at the end of the MT (arrow in Fig. 3-1B) were broadly unimodal, similar to the cosine tuning of single cell activity, and the preferred directions (PDs) of the beta- and gamma-band tuning curves were almost 180º apart (Fig. 3-1C). However, we also observed that beta oscillations were often bimodally, rather than unimodally, tuned to direction. An example is show in Figure 3-2A. During the TH, this LFP had relatively high beta-band power in the

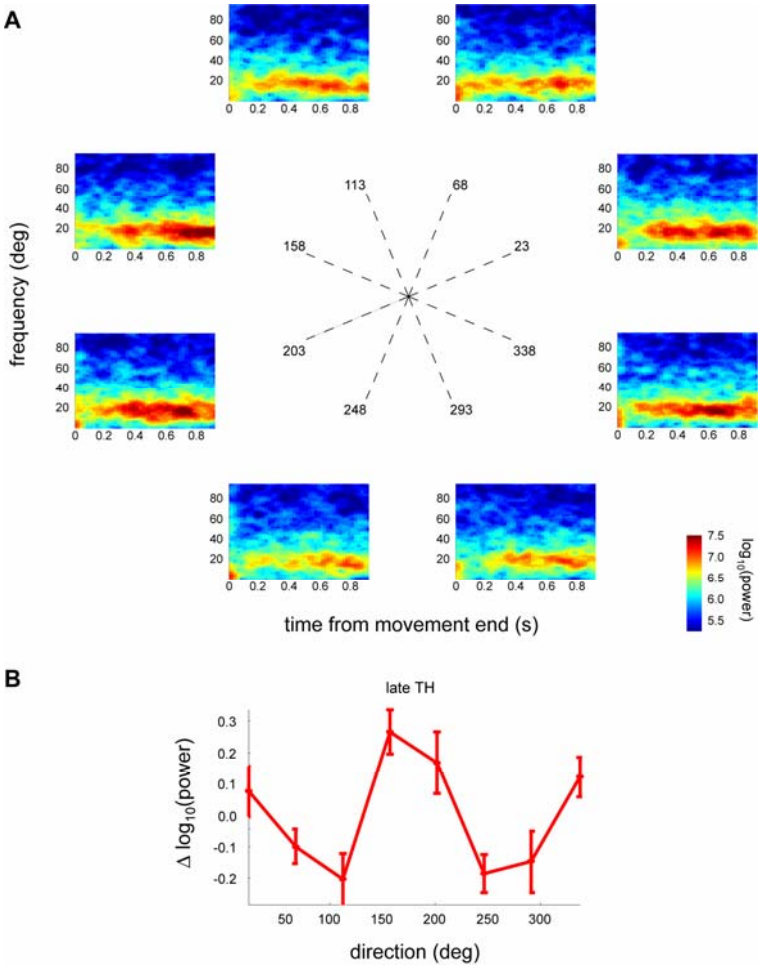

Figure 3-2. Bimodal directional tuning of beta oscillations. **A**, Spectrograms of target hold LFP activity in each of the eight movement directions for the example LFP. **B**, Tuning curve of β-band power for the example in A.

rightward and leftward directions and relatively low beta-band power in the forward and backward directions. Thus the tuning curve was bimodal (Fig. 3-2B). Across the population, spectral tuning in the beta band occurred primarily in the early DT (several 100 ms after cue presentation) and during the TH following movement (Fig. 3-3C, red). This tuning was unimodal in the DT (solid red line in Fig. 3-3C) and both unimodal and bimodal (dashed red line in Fig. 3-3C) in the TH. In contrast, spectral tuning in the gamma band was only prominent during movement and was largely unimodal (Fig. 3-3C, blue).

The orientation of the spectral tuning curves was relatively consistent across recordings and

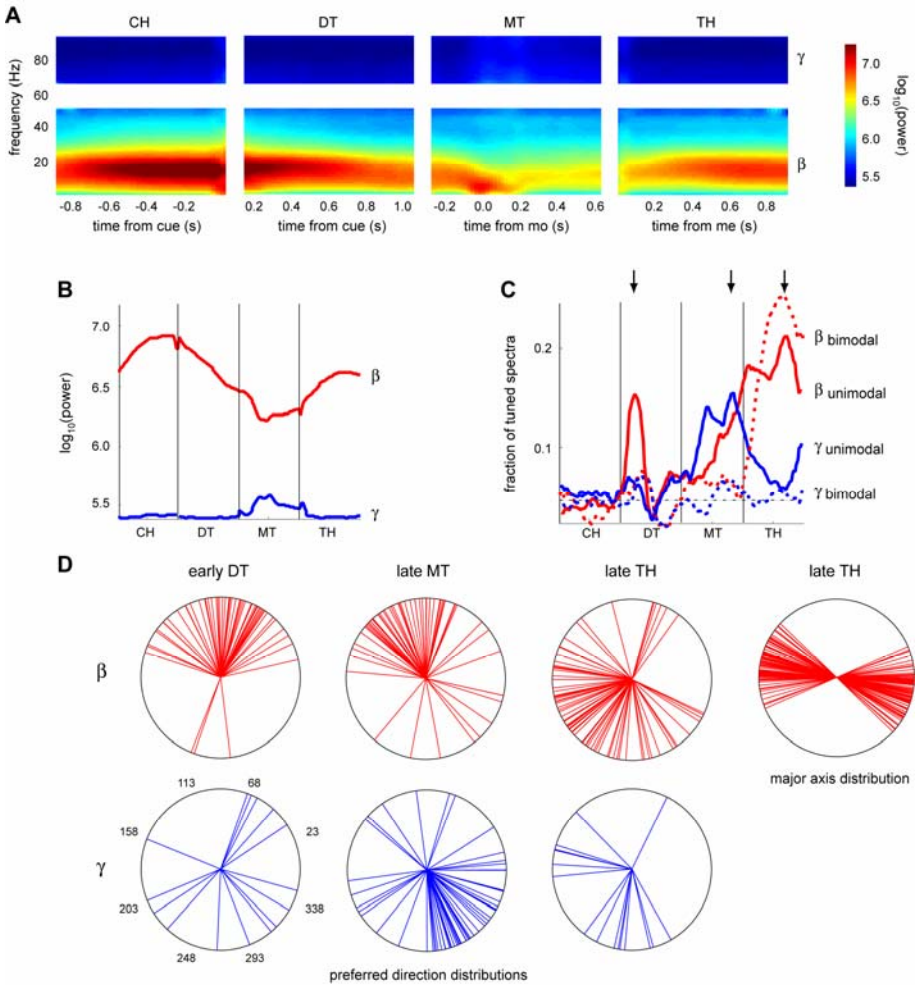

Figure 3-3. Population spectrogram and spectral tuning analysis. **A**, Mean spectrogram averaged across all LFPs. **B**, Average power in the β-band (red) and γ-band (blue) as a function of time. **C**, Fraction of LFPs with tuned β-band (red) or γ-band (blue) power at each time point. Solid and dashed lines indicate unimodal and bimodal tuning, respectively. **D**, Preferred direction distributions (unimodal) and major axis distribution (bimodal) of the tuned activity in each band at the times indicated by the arrows in C.

quite specific to both frequency band and time epoch. The distribution of preferred directions (unimodal tuning curve orientation) and major axes (bimodal tuning curve orientation) for three specific 200-ms time windows (early DT, late MT, late TH; arrows in Fig. 3-3C) are shown in Figure 3-3D. The beta-band PD distributions in the early DT, late MT, and late TH windows were unimodal (Rayleigh test, $p < 0.001$) with mean directions of 83º, 105º, and 215º, respectively. The major axes of the beta-band bimodal tuning curves of the late TH window were also highly clustered with a mean along the 168º-348º axis. For the gamma-band, the PD distribution of the late MT window was significantly unimodal (Rayleigh test, $p < 0.001$), with a mean direction of 304º. Interestingly, during the MT the beta- and gamma-band PD distributions were nearly 180º apart, as in the example in Figure 3-1. The consistency of tuning orientation across the population is further demonstrated by and partially attributable to the high correlation between tuning curves of simultaneously-recorded LFPs (Fig. 3-4A). For the 168 pairs of LFPs that were recorded simultaneously, the distribution of correlation coefficients (black bars in Fig. 3-4A) was much different than the distribution expected if the tuning curves were completely uncorrelated (gray lines in Fig. 3-4A; derived from 10,000 pairs of shuffled cosine tuning curves matched to the experimental spatial sampling frequency). This was true both of beta-band tuning (Fig. 3-4A, top row) and gamma-band tuning (Fig. 3-4A, bottom row) in all three time windows. The mean of the correlation coefficient distribution was always significantly positive (t-test, $p < 0.001$) and was the highest for beta-band tuning curves in the late TH window (mean correlation = 0.71). Note that these correlations across simultaneously-recorded LFPs were true despite fairly large inter-electrode distances, which ranged from 1 mm to 15 mm and averaged about 4 mm.

Finally, power in the beta-band was often significantly correlated with reaction time (RT). This relationship can be seen implicitly in the spectrograms of Figures 3-1 and 3-3. Beta-band power gradually decreased throughout the DT. Since we previously found that the instructed DT duration (0.5 to 1.5 s, uniformly distributed) was negatively correlated with the RT (see Chapter 1), this means that beta-band power was likely also correlated with the RT. As we did for the single cell activity in Chapter 2, we more explicitly analyzed this relationship by computing the trial-by-trial correlation between the DT or RT and the average beta-band power in the 400 ms preceding the go signal. Like that previous analysis, we both included trials in all three epochs to maximize statistical power and, for robustness, excluded trials with extreme RT values (less than

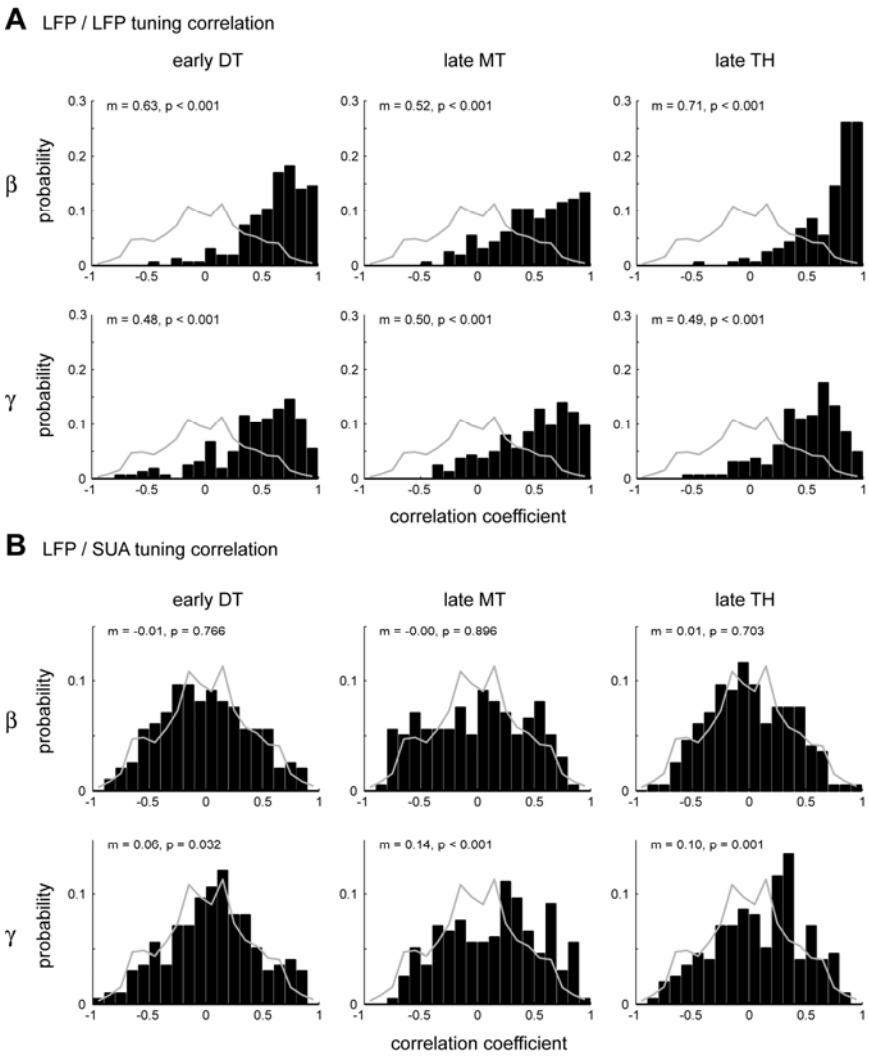

Figure 3-4. Directional tuning curve correlations for beta- and gamma-band LFP activity in three time windows (early DT, late MT, and late TH). **A**, Correlation between mean tuning curves of pairs of simultaneously recorded LFPs. The correlation coefficient distribution is shown (black) along with the distribution expected if the tuning curves were uncorrelated (gray). m = mean of distribution; p = p-value of t-test. **B**, Same as A but for paired LFP and SUA recordings made simultaneously on the same electrode.

100 ms or more than 600 ms). Example relationships are shown in Figure 3-5. Beta-band power was significantly negatively correlated with the instructed DT in 94% of the LFPs (permutation test, $p < 0.05$; rank correlation coefficient, $r = -0.22 \pm 0.12$, mean ± std). Beta-band power was weakly positively correlated with the RT in 67% of the LFPs (permutation test, $p < 0.05$; rank correlation coefficient, $r = 0.08 \pm 0.07$, mean ± std). The correlation with RT was often due to the tails of the RT distribution, as seen in the example in Figure 3-5. Very short or long RTs were seen only with low or high beta band power, respectively. But the majority of the RTs around the middle of the distribution had very little relationship with beta-band power.

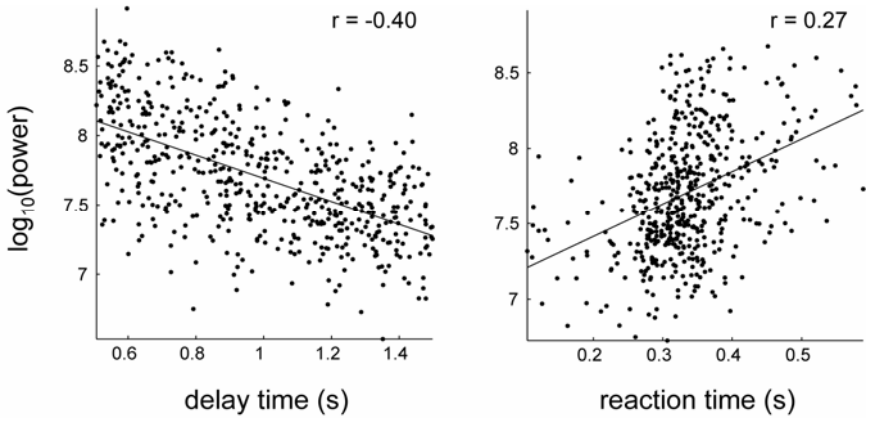

Figure 3-5. Example of correlations between beta-band power and the delay time and reaction time. For both plots, power is the average power in the 400 ms prior to the go signal on each trial from one LFP. Linear regression lines are shown along with the rank correlation coefficient (r).

Significant correlations between gamma-band power and the DT and RT were only present in 13% and 16% of the LFPs, respectively.

In summary, precentral LFP oscillations were very reliably related to several features of the reaching behavior. High-amplitude oscillations in the 12-27 Hz (beta) range were present both before and after but not during the reaching movements. Likewise, these beta oscillations were directionally tuned mostly in the pre-movement delay time, where they were unimodally tuned, or post-movement hold time, where they were bimodally tuned. The pre-movement beta oscillations were also correlated with the level of movement preparedness, as quantified by the RT. High-amplitude oscillations in the 70-95 Hz (gamma) range were present only during movement, were only directionally tuned during movement, and exhibited very little involvement in movement preparation.

LFP oscillations and single cell activity

In addition to these behavioral correlates, LFP oscillations were closely associated with the timing of spiking activity in precentral cortical neurons. In particular, single cell activity was often phase-locked to oscillations in both the beta band and the gamma band. An example of the relationship between beta-band LFP oscillations and single cell activity is shown in Figure 3-6. Beta oscillations in one trial are shown along with the spike times (in red) of a cell recorded on the same electrode (Fig. 3-6, top left). Below this trace are estimates of the instantaneous amplitude and instantaneous phase of the oscillations, derived from the Hilbert transform of the

signal (see Methods). As shown in the previous section, the beta-band oscillations are of highest amplitude before and after movement. Focusing only on the high amplitude portion before movement (box in left column), it is clear that the spikes occurred at relatively consistent times relative to the beta oscillation: at phases between -50º and -100º, which correspond to the up-slope of the oscillation about midway from trough to peak (Fig. 3-6, right column). A similar example, only for gamma-band oscillations, is shown in Figure 3-7. Again as described in the last section, the gamma oscillations have highest amplitude during movement (Fig. 3-7, left column). Focusing on a narrow window just after movement onset (box in left column), we again saw phase-locking of the spikes (Fig. 3-7, right column). In this case, however, the spikes occurred closer to the trough of the oscillation.

To quantify these effects across trials, for each cell recorded simultaneously with an LFP we compiled the phase and amplitude of the beta and gamma oscillations at each spike time. Then

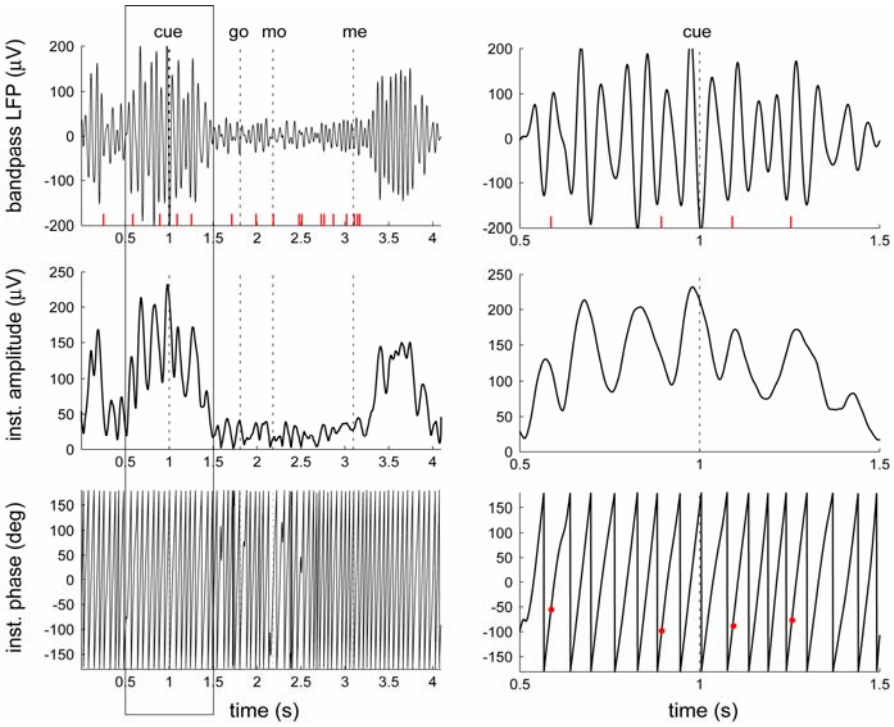

Figure 3-6. Example of relationship between beta-band LFP oscillations and single cell activity. The 12-27 Hz bandpass LFP for one trial is shown in the top row. The red tick marks indicate spike times of one cell recorded on the same electrode as the LFP. The instantaneous amplitude and phase of the LFP beta oscillations, derived from the Hilbert transform of the signal, are shown in the middle and bottom row, respectively. A phase of -180 and 180 corresponds to the oscillation trough and a phase of 0 corresponds to the oscillation peak. Red dots in the bottom right plot mark the phase of the oscillation at each spike time. The box in the left column indicates the portion of the trial that is shown in the right column.

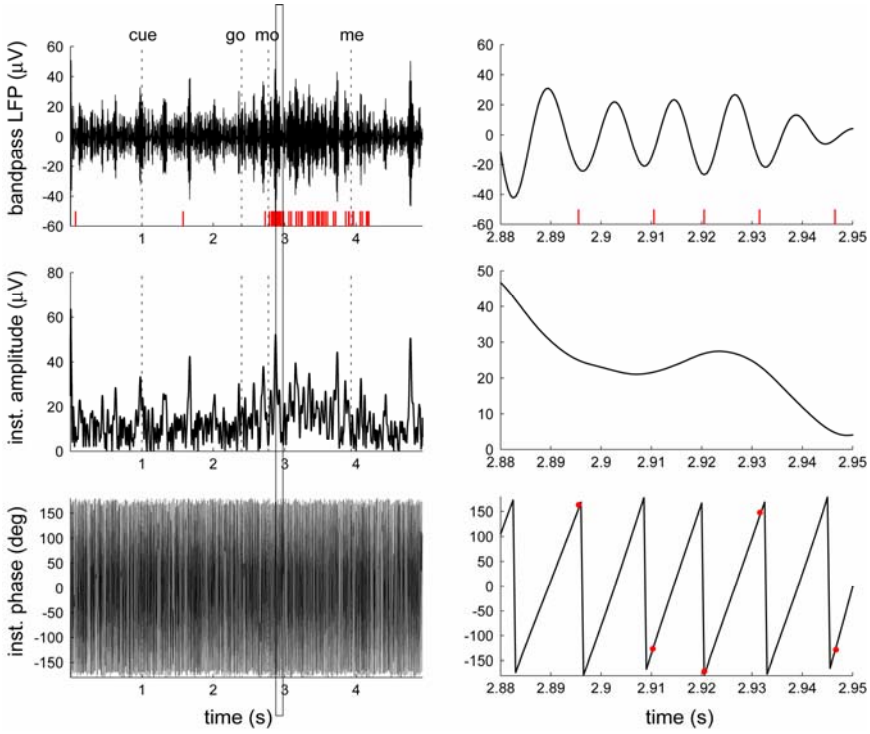

Figure 3-7. Example of relationship between gamma-band LFP oscillations and single cell activity. The 70-95 Hz bandpass LFP for one trial is shown in the top row. The red tick marks indicate spike times of one cell recorded on the same electrode as the LFP. The instantaneous amplitude and phase of the LFP beta oscillations, derived from the Hilbert transform of the signal, are shown in the middle and bottom row, respectively. Red dots in the bottom right plot mark the phase of the oscillation at each spike time. Note that -180 and 180 are the same phase (the trough). The box in the left column indicates the portion of the trial that is shown in the right column.

we used the Rayleigh test to determine whether the distribution of phases for each cell was uniform, indicating no phase-locking, or nonuniform, indicating phase-locking. Since the degree of phase-locking was likely contingent on the amplitude of the oscillation, for each cell we divided the spikes, and their associated phases, into two groups: those occurring when the oscillation amplitude was greater than or less than the median amplitude. An example of the results of this analysis for one cell is shown in Figure 3-8A. The distributions of phases were nonuniform (Rayleigh tests, $p < 10^{-6}$) indicating that spikes of this cell were phase-locked to both beta and gamma oscillations. This effect was more pronounced for high-amplitude oscillations (Fig. 3-8A, bottom row) than low-amplitude oscillations (Fig. 3-8A, top row). The mean phase of the beta phase and gamma phase distributions differed. Like the example trials in Figures 3-6 and 3-7, spikes tended to occur on the upslope from trough to peak of beta oscillations and at the trough of gamma oscillations.

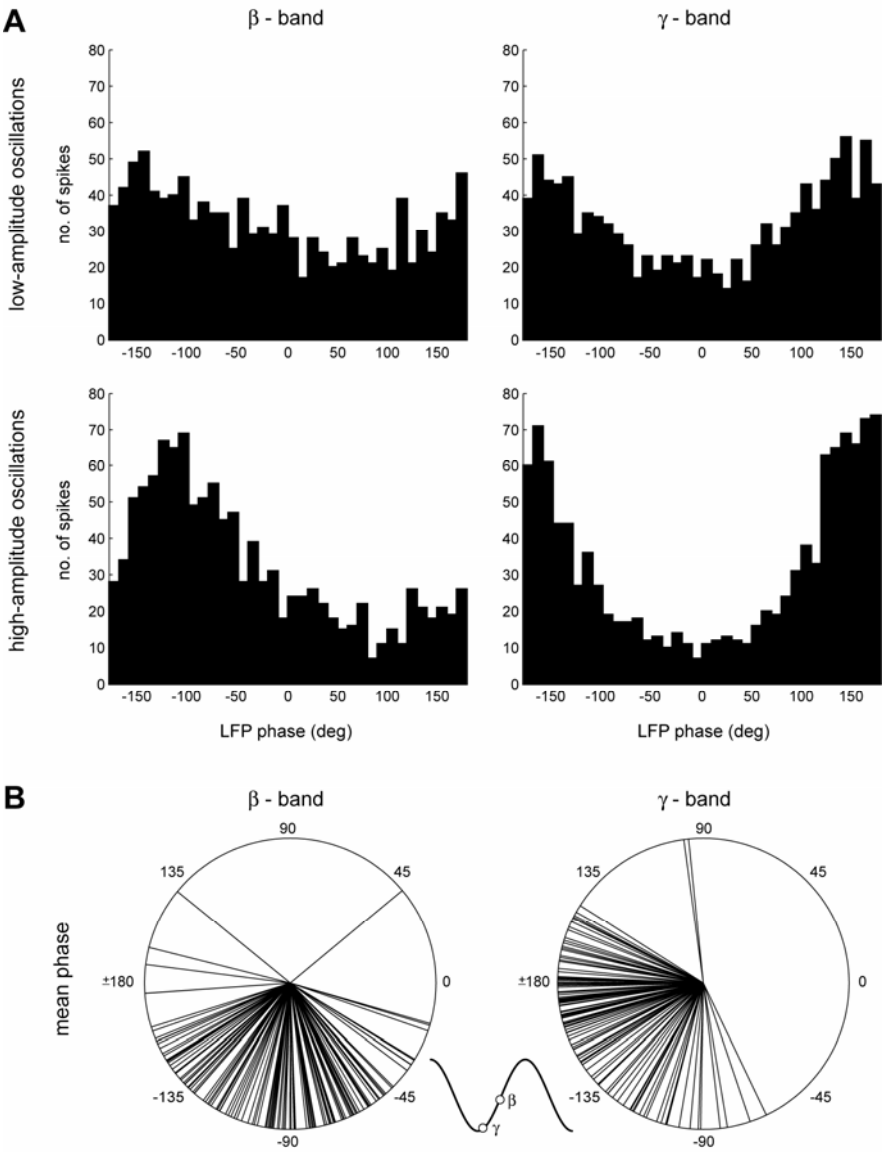

Figure 3-8. Phase-locked single cell activity to beta and gamma LFP oscillations. **A**, Distribution of oscillation phase at each spike time for one example cell, separated by whether the spike occurred during a period of high (above median) or low (below median) oscillation amplitude. **B**, Distribution of mean phase for all cells with significant phase-locking (Rayleigh test, $p < 10^{-6}$). Inset shows grand mean phase across all cells relative to peak and trough of oscillation.

The phase-locking of single cell activity seen in the example in Figure 3-8A was very typical of the population. Of the 198 cells recorded simultaneously with LFPs, 63% had activity that was phase-locked to high-amplitude beta oscillations and 57% had activity that was phase-locked to high-amplitude gamma oscillations (Rayleigh test, $p < 10^{-6}$). For low-amplitude oscillations, the percentages were 13% and 28%, respectively, indicating that phase-locking was often a function of oscillation amplitude. The mean phase for each of the cells significantly phase-locked to the

high-amplitude oscillations is shown in Figure 3-8B. The distribution of mean phases for both the beta-band and gamma-band was strongly unimodal, suggesting that the relationship between single cell activity and LFP oscillations was relatively consistent across precentral neurons. The inset of Figure 3-8B indicates the grand mean phase, which was -98º for the beta oscillations and -160º for the gamma oscillations.

A second relationship between single cell activity and LFP activity involved the similarity of directional tuning curves. For each of the 198 cells recorded simultaneously with LFP activity, we computed the correlation between the mean tuning curves of single cell firing rate and LFP power in the beta or gamma band. This comparison was made for three separate time windows, early DT, late MT, and late TH, as we did for the LFP-LFP comparison described above. The distribution of correlation coefficients for each of the six comparisons (three windows x two frequency bands) was broad, ranging nearly from -1 to 1, due to the low spatial sampling frequency (45º) of the tuning curves (Fig. 3-4B). The distributions were quite similar to the simulated distribution of uncorrelated tuning curves (gray lines in Fig. 3-4B). However, for the comparisons between gamma-band tuning and spike-rate tuning the means of the distributions were significantly positive. The significance was marginal for the DT window (t-test, mean correlation = 0.06, $p = 0.032$) and high for the MT and TH windows (t-tests, mean correlation = 0.14, $p < 0.001$ and mean correlation = 0.10, $p < 0.001$, respectively). Thus, across the population there was a slight tendency for the gamma-band LFP directional tuning to be related to the tuning of local cells. On the contrary, beta-band tuning and spike-rate tuning were not related in the DT, MT, or TH windows.

In summary, the timing of activity in the majority of precentral neurons was influenced by both beta and gamma LFP oscillations. Phase-locked activity was more likely to occur with higher amplitude oscillations. Cells were biased towards discharging at the trough of gamma oscillations and on the upslope between trough and peak of beta oscillations. Furthermore, across the population, the directional tuning of gamma oscillations were slightly positively correlated with local neuronal tuning while tuning of beta oscillations was essential independent of local neuronal tuning.

3.4 Discussion

In this chapter, we characterized oscillatory field potential activity in the precentral cortex both in terms of its relation to behavior and its relation to single cell activity. We focused on oscillations in two different bands, the beta (12-27 Hz) and high gamma (70-95 Hz) bands, which had relatively homogeneous intra-band features. Each band had unique relationships with behavior and neuronal activity which we discuss below.

Beta oscillations in precentral cortex

Beta oscillations are the prevailing rhythm in the precentral cortex. We found that they had greatest amplitude during non-movement periods and were largely absent during movement (Sanes and Donoghue, 1993; Pfurtscheller et al., 2003). The 'antikinetic' nature of beta oscillations in precentral cortex has long been observed (Jasper and Penfield, 1949) and is one of several examples of event-related desynchronization (ERD) in the brain (Brunia, 1999). As also reported by the original Jasper and Penfield study, the decrease in beta oscillation amplitude actually occurred during movement preparation such that the desynchronizing event was the signal cueing the upcoming movement rather than the signal initiating the movement. We further demonstrated the relationship between beta desynchronization and movement preparation by showing that beta oscillation amplitude was often positively correlated with reaction time. A similar correlation has been described in the beta-band field potential activity of the subthalamic nucleus in Parkinson's patients (Williams et al., 2005). In fact, the prominence of beta oscillations in the basal ganglia of Parkinson's patients, who suffer from akinesia, is causal evidence that beta desynchronization is necessary for movement initiation (Hutchison et al., 2004). However, beta desynchronization does not have to occur globally to allow movement to occur. It has recently been shown that in the normal monkey, beta oscillations in the striatum are prevalent during rest and only decrease at focal sites during a simple motor task—sites that were specifically engaged in the task (Courtemanche et al., 2003). A similar result in motor cortex was reported much earlier, again by Jasper and Penfield, who noted that decreased beta activity during movement preparation was often restricted to local cortical areas that were specifically involved in the upcoming movement (Penfield and Jasper, 1956). The desynchronizing mechanism involves inhibition of cortical inhibitory interneurons thought to drive the beta rhythm (Hasenstaub et al., 2005) throughout the precentral cortex, basal ganglia, and cerebellum (Courtemanche et al., 2002).

An additional component of the behavior-dependent modulation of beta oscillation amplitude was the dependence on target direction. Directionally tuned beta-band activity occurred transiently in response to the cue signal and in a more sustained fashion during the hold period following movement but was not present during movement. The lack of beta-band tuning during the movement time is consistent with previous observations (Donoghue et al., 1998; Rickert et al., 2005). Transient cue-related tuning of beta oscillations has only recently been described (O'Leary and Hatsopoulos, 2006). Like this previous study, we found that the preferred directions of the tuning curves were clustered, at least in part due to the strong correlations between tuning curves of simultaneously recorded LFPs. Directional-tuned beta oscillations during movement preparation have also been observed at the single cell level in PMd, though only in a relatively small minority of neurons (Lebedev and Wise, 2000).

The tuning of beta oscillations during the target hold is a novel finding. This finding is even more intriguing given that the majority of the activity was bimodally tuned—a tuning shape not generally seen in either LFP or neuronal activity in the precentral cortex. One interpretation of this result is that it arises due to anisotropic demands on the motor controller during the target hold. Several studies have shown that beta oscillations are intimately related to isometric motor output. In particular, corticomuscular coherence at beta-band frequencies is task specific, being present only during periods of steady muscle contraction (e.g. during maintained posture as in the target hold period) (Conway et al., 1995; Baker et al., 1997; Baker et al., 1999; Omlor et al., 2007). Furthermore, cortical neuronal activity is often synchronous with beta oscillations during these hold periods and synchrony between cells is contingent on the similarity of their relationship to muscle activity (Baker et al., 2001; Jackson et al., 2003). Given this close connection between beta oscillations and motor output during hold periods, if certain targets required more active maintenance of posture while others could be achieved more passively then the cortical beta oscillations could reasonably be tuned to target direction. In addition, this mechanism could certainly result in bimodal tuning as long as the motor demands were bimodal (e.g. differential amount of muscular effort needed to hold at forward and backward targets compared to leftward and rightward targets). However, at present, we do not have direct evidence to support this interpretation.

Finally, we found a relatively robust relationship between beta oscillations and single cell activity. Precentral neurons tended to fire during a specific phase of the beta oscillations, about

midway from trough to peak of an oscillatory cycle, particularly during periods of high amplitude oscillation. The consistency of the phase relationship across the population of cells with known functional heterogeneity (see Chapter 2) argues against the possibility of phase-coding in the precentral cortex, or the encoding of information via the phase-spike relationship (Huxter et al., 2003; Lee et al., 2005). More generally, however, the phase-locked activity suggests that cortical neurons have synchronous oscillatory activity in the beta-band range prior to and following movement, as has been explicitly shown by cross-correlation analyses of pairs of single units (Murthy and Fetz, 1996b; Baker et al., 2001).

Gamma oscillations in precentral cortex

Gamma oscillations in the LFP were much lower amplitude than the beta oscillations, but were reliably modulated during the reaching task. In particular, the amplitude transiently increased during movement (Pfurtscheller et al., 2003; Rickert et al., 2005). The 'prokinetic' nature of gamma oscillations and their reciprocal relation to the 'antikinetic' beta oscillations has been observed both in precentral cortex and the basal ganglia (Schnitzler and Gross, 2005). The generation of gamma oscillations is, like beta oscillations, thought to involve networks of cortical inhibitory interneurons (McBain and Fisahn, 2001) and possibly classes of interneurons with intrinsic high-frequency oscillatory firing properties (Gray and McCormick, 1996; Chen and Fetz, 2005).

The LFP gamma oscillations were unimodally tuned to target direction primarily during movement (Rickert et al., 2005). In this respect the gamma-band tuning, unlike the beta-band tuning, was similar to the tuning of neurons and muscles (see Chapter 2). The correlation between gamma-band tuning and the tuning of single cells recorded on the same electrode was weak but, across the population, significant. A similarly result was found previously (Mehring et al., 2003b). The distribution of preferred directions of the tuning was nonuniform, again probably due to the positive correlations between gamma-band tuning curves of simultaneously recorded LFPs (O'Leary and Hatsopoulos, 2006).

As with the beta oscillations, single cell activity in the precentral cortex was consistently phase-locked with the gamma oscillations. The cells fired most frequently during the trough of the gamma oscillation cycle. A very recent study looking at single cell activity in humans found

phase-locking at the trough of gamma oscillations was a consistent feature across many areas of the brain, including frontal areas (Jacobs et al., 2007).

Relationship of oscillations to evoked potentials

In the previous chapter, we used a time-domain LFP analysis to identify evoked potentials in response both to the cue signal (cEP) and movement onset (mEP). Many of the properties of the evoked potentials were similar to those of the beta oscillations. Specifically, the cue-related beta-band tuning had a nearly identical distribution of preferred directions as that of the cEP. The same was true of the small amount of movement-related beta-band tuning and the mEP. Also, both mEP amplitude and beta oscillation amplitude were negatively correlated with the duration of the instructed delay and, in turn, correlated with reaction time. Thus, the evoke potentials and beta-band oscillations may be essential the same phenomenon viewed in two different ways. On the other hand, gamma oscillation features were unrelated to the properties of the evoked potentials.

We previously noted that since the cEP and mEP were not evident in individual trials, the evoked potentials likely reflect phase-locking to each event rather than amplitude modulation. This was made explicit in the work of O'Leary and Hatsopoulos (2006), who found that oscillations up to 45 Hz were transiently phase-locked several 100 ms after a cue signal. Presumably phase-locking also occurs around movement onset. Thus phase-locked beta (and lower) oscillations at the cue and movement onset likely produced the evoked potentials and were, therefore, the reason for the similarity in the properties described above.

Interpretational limitations

The data presented in this chapter were recorded from only one monkey. However, many of the same results have been observed in preliminary recordings (44 LFPs from M1 and PMd) from a second monkey. There were only two exceptions. First, in the second monkey, beta-band power was not correlated with the instructed delay time or RT. There was a transient beta desynchronization in response to the cue but the beta-band power remained fairly level after this until the movement-evoked desynchronization. Despite this difference, the cue-related directional tuning of the beta oscillations was equally as present in the second monkey. The reason for this discrepancy may be training. The first monkey had performed the instructed-delay

reaching task for approximately two years while the second monkey had only performed the task for about six months. Second, there was almost no bimodal direction tuning of beta oscillation amplitude during the target hold in the second monkey, although unimodal tuning was very similar. Assuming the interpretation given above, this may be due to a difference between animals in the postures used for the hold period. All other results, including the phase-locking of single cell activity to the LFP oscillations, were very similar between the two monkeys' data sets.

4 Cortical correlates of adaptation to a novel mechanical environment

4.1 Introduction

Motor performance is a function of experience. As the adage goes, practice makes perfect. While adaptive perceptual or cognitive processing can play a role, experience-dependent performance improvements often involve an implicit recalibration of sensorimotor transformations. As a result, sensory stimuli (e.g. trajectory of a baseball) trigger a modified motor output (e.g. greater bat speed) that leads to a better behavioral outcome (e.g. ball traveling further).

Recalibration of sensorimotor maps has been studied extensively in humans making reaching movements in altered mechanical environments (Lackner and Dizio, 1994; Shadmehr and Mussa-Ivaldi, 1994). The neural structures involved in this type of motor learning have been pursued in studies of humans with specific nervous system lesions and through functional imaging and transcranial magnetic stimulation (TMS) in neurologically-intact individuals. Adaptation is profoundly impaired in patients with global cerebellar degeneration (Maschke et al., 2004; Smith and Shadmehr, 2005) or with lesions to the cerebellar thalamus (Chen et al., 2006). However, adaptation is not impaired by striatal dysfunction, at least as manifest in Huntington's disease (Smith and Shadmehr, 2005). A recent fMRI study has confirmed that the cerebellum, but not the striatum, is involved in adaptation to novel environments (Diedrichsen et al., 2005). This imaging study also found that cerebral cortical structures, including primary motor and somatosensory cortices and posterior parietal cortex (PPC) were involved. The latter cortical area has also been investigated by Della-Maggiore et al. (2004), who found that single-pulse TMS applied over the PPC 40ms after movement onset impaired adaptation relative to controls. Therefore, the evidence from the human literature suggests that sensorimotor adaptation of reaching movements involves a cerebello-thalamo-cortical circuit.

Intracranial neural recordings in non-human primates have provided greater insight into this putative circuit. Neuronal activity correlated with the dynamics of arm movements has been found throughout motor areas of the cerebral cortex and cerebellum during behavioral tasks requiring minimal adaptation to applied loads (Evarts, 1968; Thach, 1978; Cheney and Fetz, 1980; Kalaska et al., 1989; Sergio et al., 2005). These studies suggest that kinetic parameters

(e.g. joint torque) may be represented in motor cortex and the cerebellum but they do not specifically address if and how these areas are involved in adaptive control when the dynamics of movement are altered. Thus a series of studies were conducted that recorded neuronal activity in the precentral cortex of monkeys performing a reaching task very similar to the human studies mentioned above (Gandolfo et al., 2000; Li et al., 2001; Padoa-Schioppa et al., 2002, 2004; Xiao et al., 2006). A correlate of the altered task dynamics was found in the movement-related neuronal activity of primary motor cortex (M1), premotor cortex (PM), and supplementary motor area (SMA). In particular, there were systematic shifts in the directional tuning of these neurons between the no-force and force conditions that mirrored similar shifts in tuning of muscle activity (Thoroughman and Shadmehr, 1999; Shadmehr and Moussavi, 2000). In PM and SMA, these shifts were also apparent in the preparatory period prior to movement (Padoa-Schioppa et al., 2002, 2004; Xiao et al., 2006). These studies, therefore, identified cortical single-cell activity related to the recalibration of motor commands to meet the novel mechanical demands of a task.

Here, we extended this series of studies to answer several further questions regarding the role of precentral cortex in motor adaptation. First, are the changes observed in single cell activity gradual, following the time-course of learning? Second, do the cingulate motor areas play a similar role in adaptation as M1, PM, and SMA? Finally, are correlates of adaptation also apparent at the level of precentral cortical networks, as reflected in the local field potential?

4.2 Methods

The behavioral (Chapter 1) and electrophysiological (Chapter 2) methods have been described previously. The neural database analyzed in this chapter was the same as in Chapters 2 and 3.

Analysis

We analyzed electromyographic (EMG) and neural data across the three epochs of the behavioral task: baseline epoch (forces off), force-field epoch (forces on), and washout epoch (forces off). Consistent with previous work, we looked for directional tuning changes that where correlated with adaptation (i.e. a change between the baseline and force-field epochs) and deadaptation (i.e. a change between the force-field and washout epochs). In computing the tuning curves, the first 40 trials in each epoch were omitted to focus only on post-adaptive changes (e.g.

Li et al., 2001). Based on previous studies as well as our analysis of the activity in the baseline epoch (Chapters 2 and 3), we chose two windows in which to look for tuning changes: a movement window (-100 ms to 300 ms around movement onset) and a preparatory window (-400 ms to 0 ms around the go signal). Tuning curves were computed from the average activity in each window of each trial. Significance of tuning was judged by a permutation test ($p < 0.01$; same as in Chapter 2). Changes in directional tuning between epochs were summarized by a single parameter: the shift in preferred direction. Only activity that was significantly tuned in the baseline and force-field epochs (adaptation) or the force-field and washout epochs (deadaptation) was included in this analysis.

To capture how gradual tuning changes were, we also performed a trend analysis on the activity in each individual target direction and each epoch. For this analysis, we included all trials of the force-field and washout epochs rather than omitting the first 40 trials as before. A model with just a linear component, plus an offset, often fit the activity changes well. In the examples shown (Figs. 4-1 and 4-2), a fitted line with nonzero slope is shown only when the linear component was significant (linear regression, $p < 0.01$).

Aside from direction tuning changes, we identified more general force field-related activity through a pair of one-tailed t-tests. In particular, we defined field-related activity as an increase (decrease) in activity in at least one direction between late baseline and early force-field epochs and a decrease (increase) in activity in those same directions between late force-field and early washout epochs. These tests were performed on 40 trial blocks at each instant along the time-resolved activity. Activity satisfying these tests thus followed the profile of change in applied forces across the three epochs.

4.3 Results

EMG and neuronal correlates of motor adaptation

Proximal arm muscle activity was modified in a very specific and predictable manner during force-field learning. An example, of the rhomboid muscle, is shown in Figure 4-1. During the baseline epoch, rhomboid EMG activity was highest when reaching to targets toward the body and to the right (~338º target direction; Fig. 4-1A). Subsequently, when a clockwise force field was imposed EMG activity gradually increased in all directions, with the largest increases occurring in the 293º and 248º target directions (Fig. 4-1A). Note that these directions are

clockwise relative to the baseline preferred direction (PD) and resulted in a force-field epoch directional tuning curve that was shifted relative to the baseline tuning curve (Fig. 4-1B). The constant rate of change of the EMG in these specific directions was correlated with the constant rate of performance improvement in the force-field epoch (Fig. 4-1C). In this session, there was little behavioral deadaptation during the washout epoch. Likewise, aside from a mean difference, the EMG tuning curves were very similar in the force-field and washout epochs (Fig. 4-1B). Mean differences in tuning curves across epochs may be attributed to non-specific effects such as fatigue but the PD shifts were specific to the force-field adaptation, as will be shown more conclusively in the population analysis below.

Although somewhat counterintuitive, a shift in EMG PD toward the same, rather than opposite, direction of the curl force field was the appropriate compensatory response. The curl field produced forces perpendicular to the direction of movement. Thus, forces experienced in

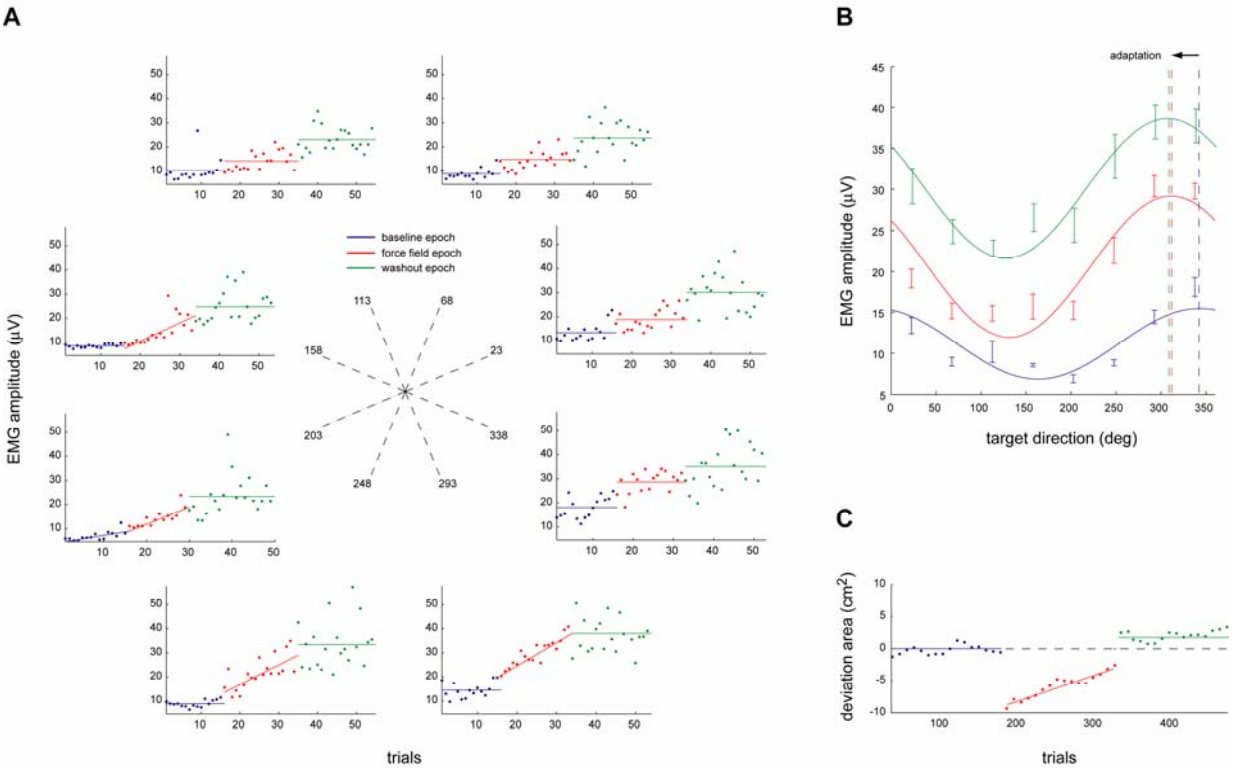

Figure 4-1. An example of changes in the directional tuning of rhomboid muscle activity during adaptation to a clockwise force field. **A**, Average EMG amplitude on each trial in a window around movement onset (-100 ms to +300 ms), sorted by target direction. Color indicates the absence (blue and green) or presence (red) of the force field. **B**, Cosine fits of the activity shown in A. Vertical dotted lines mark the preferred direction of each tuning curve. **C**, Behavioral performance in the session from which the EMG activity shown in A and B was recorded (mean deviation area over 40 trial blocks).

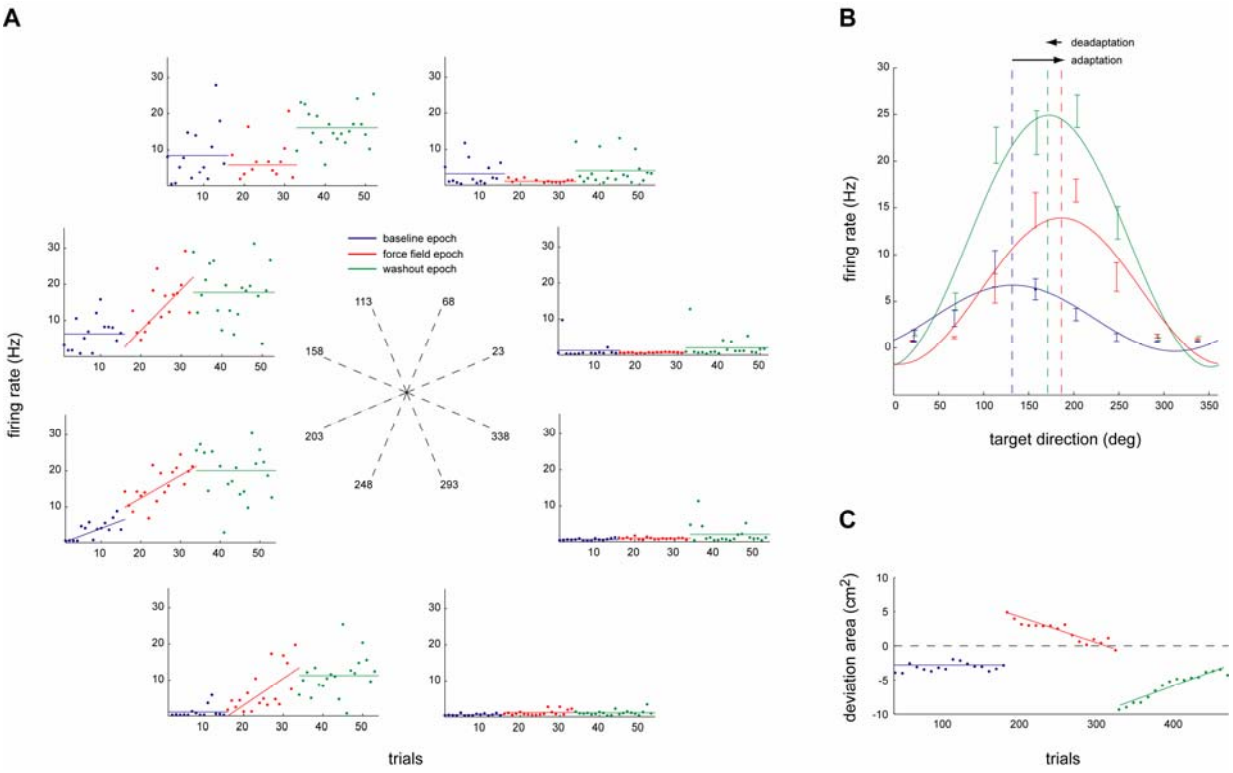

Figure 4-2. An example of changes in the directional tuning of M1 neuronal activity during adaptation to a counterclockwise force field. **A**, Average firing rate on each trial in a window around movement onset (-100 ms to +300 ms), sorted by target direction. Color indicates the absence (blue and green) or presence (red) of the force field. **B**, Cosine fits of the activity shown in A. Vertical dotted lines mark the preferred direction of each tuning curve. **C**, Behavioral performance in the session from which the neuronal activity shown in A and B was recorded (mean deviation area over 40 trial blocks).

movement directions that were perpendicular to the EMG PD were oriented along the muscle's line of action (i.e. movement direction 90º from PD ± force 90º from movement direction = force 0º or 180º from PD). A force 0º or 180º relative to the PD will shorten or lengthen the muscle, respectively. Since muscles can only pull, not push, compensatory EMG activity only developed for forces oriented 180º relative to the PD. In a clockwise or counterclockwise curl field, such force orientations occurred on movements 90º clockwise or counterclockwise from the EMG PD, respectively. Therefore, in clockwise fields compensatory activity occurred in directions clockwise to the baseline EMG PD and in counterclockwise fields compensatory activity occurred in directions counterclockwise to the baseline EMG PD, resulting in the observed PD shifts.

Similar changes in directional tuning were observed in the cortical neuronal activity. An example, of one M1 neuron, is shown in Figure 4-2. For this cell, the baseline epoch firing rate

was highest when reaching in the 113º target direction (Fig. 4-2A). The onset of a counterclockwise force field caused the firing rate to gradually increase in the 158º, 203º, and 247º target directions, but decrease in the 113º and 68º directions (Fig. 4-2A). The result was a counterclockwise shift in PD between baseline and force-field epoch tuning curves (Fig. 4-2B). Again, the gradual increase in firing rate in field-appropriate directions was correlated with the gradual performance improvement over the force-field epoch (Fig. 4-2C). Also in this session, significant deadaptation occurred during the washout epoch (Fig. 4-2C). A correlate of this deadaptation can be seen in the washout epoch tuning curve of this cell, whose PD shifted clockwise back towards the baseline PD, although not completely (Fig. 4-2B).

Field-appropriate PD shifts in EMG and neuronal activity were also present at the population level. In the top row of Figure 4-3, we show the distribution of adaptation PD shifts and deadaptation PD shifts for EMG activity recorded in clockwise, counterclockwise, or null-field (i.e. control) sessions. Only muscles in which multiple reliable recordings were obtained in all three types of force fields where included in the distributions (rhomboid, infraspinatus, biceps brachii, and pectoralis). In the counterclockwise field, the adaptation and deadaptation distributions of EMG PD shifts had significantly nonzero means of 14.2 deg and -25.1 deg, respectively (t-test, $p < 0.01$). In the clockwise field, only the adaptation distribution mean (-16.2 deg) reached significance. These population effects truly reflect the motor learning processes since the sign of the shifts were appropriate for the force field and since no significant population shift was seen for the control sessions.

The neuronal population PD shifts are shown in the middle row (preparatory activity) and bottom row (movement activity) of Figure 4-3. These distributions are derived from all M1, PMd, and SMA cells with significant directional tuning in the baseline and force-field epochs (adaptation) or force-field and washout epochs (deadaptation). The cingulate motor areas were excluded from this analysis since there was relatively little directional tuning in these areas (see Chapter 2). The combined M1, PMd, and SMA PD shift distributions for the movement window were very similar to the EMG PD shift distributions. In the counterclockwise field, the adaptation and deadaptation distributions of neuronal PD shifts had significantly nonzero means of 8.0 deg and -6.5 deg, respectively (t-test, $p < 0.01$). In the clockwise field, only the adaptation distribution mean (-10.5 deg) was significant. Again, there was no significant population PD

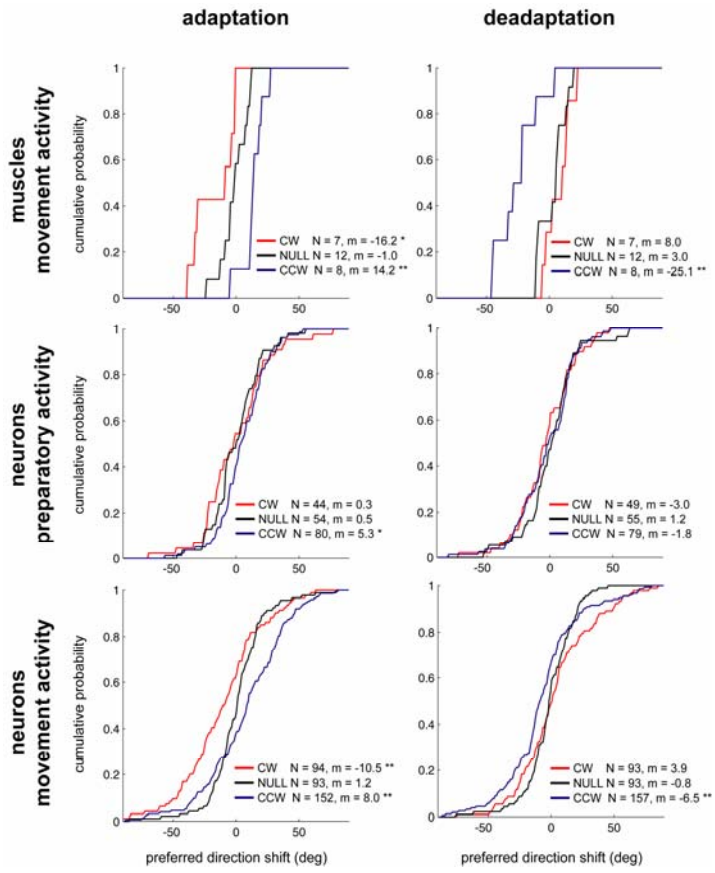

Figure 4-3. Cumulative distributions of shifts in the preferred direction (PD) of muscle (rhomboid, infraspinatus, biceps, pectoralis) and neuronal (M1, PMd, SMA) activity between baseline and force-field epochs (adaptation; first column) and between force-field and washout epochs (deadaptation; second column). The PDs were computed from average activity in a movement window (mo-100 ms to mo+300 ms) or preparatory window (go-400ms to go). CW = clockwise force field; NULL = null force field; CCW = counterclockwise force field; N = number of muscles/cells in distribution; m = mean of distribution. Asterisks indicate that the distribution mean was significantly non-zero at the $p < 0.05$ (*) or $p < 0.01$ (**) level (t-test).

shift for the null-field sessions. For the preparatory activity, only the adaptation distribution mean in the counterclockwise field (5.3 deg) was significant (Fig. 4-3, middle row).

Table 4-1 gives the mean population PD shifts considering M1, PMd, and SMA separately. The PD shifts for clockwise sessions were multiplied by -1 and then combined with the counterclockwise session PD shifts to pool the data in the "fielded" sessions. Thus, field-appropriate adaptation was a positive PD shift and field-appropriate deadaptation was a negative shift. All three areas had significant population PD shifts of movement activity for adaptation, but only PMd had a similar shift for deadaptation. SMA was the only area to have a significant population PD shift of preparatory activity. None of the control session shifts were significant.

Table 4-1. Mean population PD shifts for M1, PMd, and SMA (in degrees). P = preparatory activity mean; M = movement activity mean. Shaded boxes indicate the distribution mean was nonzero (t-test, $p < 0.05$).

		adaptation			deadaptation		
		M1	PMd	SMA	M1	PMd	SMA
P	control	1.1	0.9	-0.4	2.8	-5.4	2.5
	fielded	-1.3	3.7	6.8	4.4	-3.6	0.2
M	control	0.4	2.3	1.9	1.1	5.2	-6.8
	fielded	8.5	8.3	9.7	-3.8	-8.6	-5.4

While directional tuning changes were the most specific correlate of learning the novel curl field environments, they were not the only evidence of field-induced modulation of cortical activity. Indeed, average movement-related activity of many cells followed the profile of change in applied forces across the three epochs. Two examples are shown in Figure 4-4A, where average firing rate of the cells was resolved both in time relative to movement onset and across trials. In both cases, average movement-related activity was prolonged in duration and increased in magnitude during the force-field epoch relative to both the baseline and washout epochs. Less frequently, cells exhibit a decrease in activity during the force-field epoch (not shown). These changes followed the "off-on-off" profile of force-field application across the three epochs and were therefore termed field-related activity. Though not specific to the type of force field like the directional tuning changes, field-related activity may reflect the need for an overall increased motor output to compensate for the applied forces.

We identified cells with field-related activity using one-tailed t-tests of the activity at the two transitions between epochs (see Methods). The number of cells with such activity for each cortical area is shown in Figure 4-4B (control includes all cells recorded in null-field sessions; CMA includes all three cingulate areas). All cortical areas had a greater number of cells with field-related activity than was expected by chance. The field-related activity occurred mostly during the movement time, although in PMd significant activity was also seen during the delay and reaction periods. Notably, the cingulate motor areas had a significant amount of field-related activity, but proportionally less than the other areas. Field-related activity was, in fact, specific to the force fields since it was only present at chance levels in cells recorded during control (null-field) sessions. Similar results were found when we applied the same analysis to the EMG database (Fig. 4-4C).

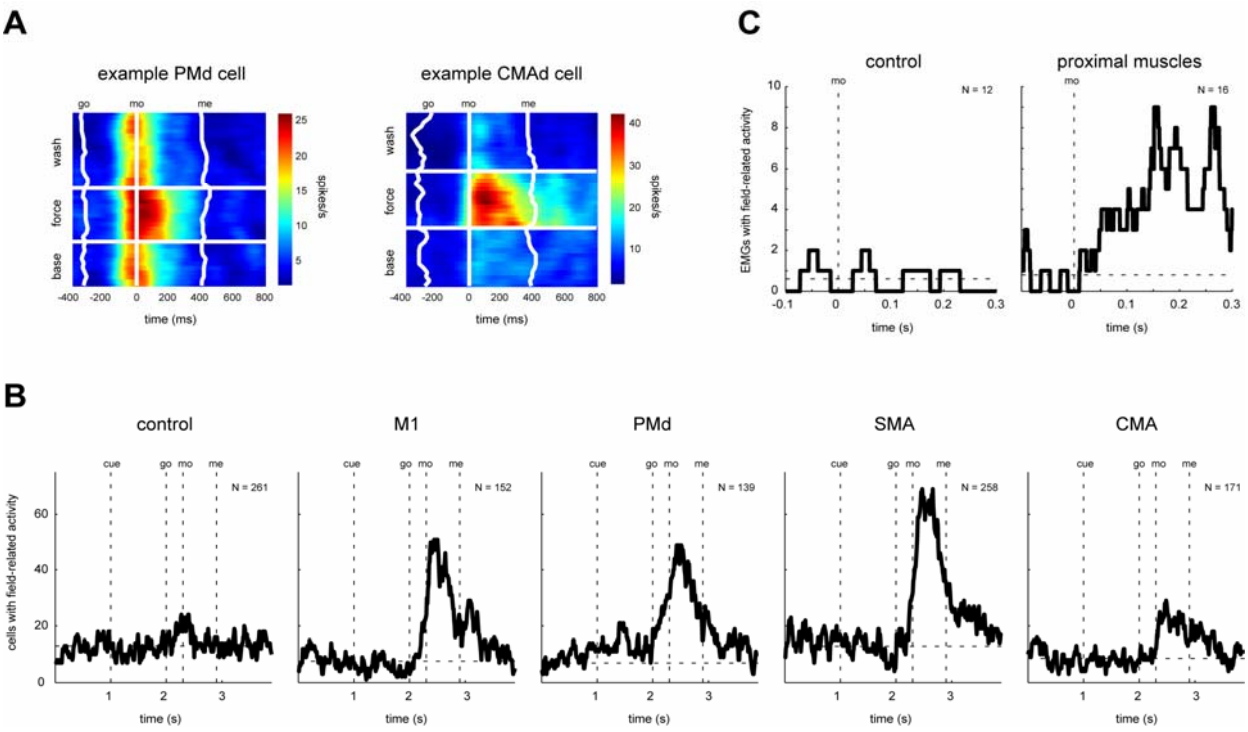

Figure 4-4. Force field-related activity of cortical cells and proximal arm muscles. **A**, Two examples of field-related activity. For each cell, the average firing rate is shown as a function of both time (relative to movement onset) and trial (40 trial moving average across baseline, force-field, and washout epochs, stepping in 8 trial increments, no inter-epoch overlap). **B**, Number of cells in each cortical area with significant field-related activity at a given time. Horizontal dashed line indicates the 0.05*N level of assumed type I errors. **C**, Same as in B, but for EMG activity (includes rhomboid, infraspinatus, biceps, and pectoralis recordings).

In summary, activity changes specific to the presence of an altered mechanical environment were seen in proximal arm muscles and precentral cortical neurons. Directional tuning of the activity, both in movement and in preparation for movement, gradually changed to specifically compensate for the force fields. As with the baseline physiology (Chapter 2), differences between cortical areas during adaptation were subtle. However, there were proportionally less force field-related activity changes in the cingulate motor areas than the other areas and PMd and SMA exhibited preparatory adaptive changes while M1 and CMA did not.

LFP correlates of motor adaptation

Next, we investigated whether correlates of adaptation were also present in the field potentials produced by precentral neuronal populations. In Chapters 2 and 3, we found that both time-domain and frequency-domain features of the LFPs were tuned to movement direction.

Based on the preceding analysis of the present chapter, it was natural to ask whether this directional tuning systematically changed during adaptation and washout. However, these features were generally only tuned in around 25% of LFPs during the baseline epoch and very few of the features, often less than 10%, were significantly tuned in all three epochs. Thus the database was too small to get statistically sound results from a population PD shift analysis similar to that shown above for the muscle and single cell activity.

Rather than look at how the LFP activity's relation to behavior changed during adaptation, we simply analyzed how the LFPs themselves changed across epochs. The most noticeable change in the evoked potentials during the force-field epoch was the presence of extra late peaks in the mEP. For example, in Figure 4-5A, the mEP has an extra negative and positive peak

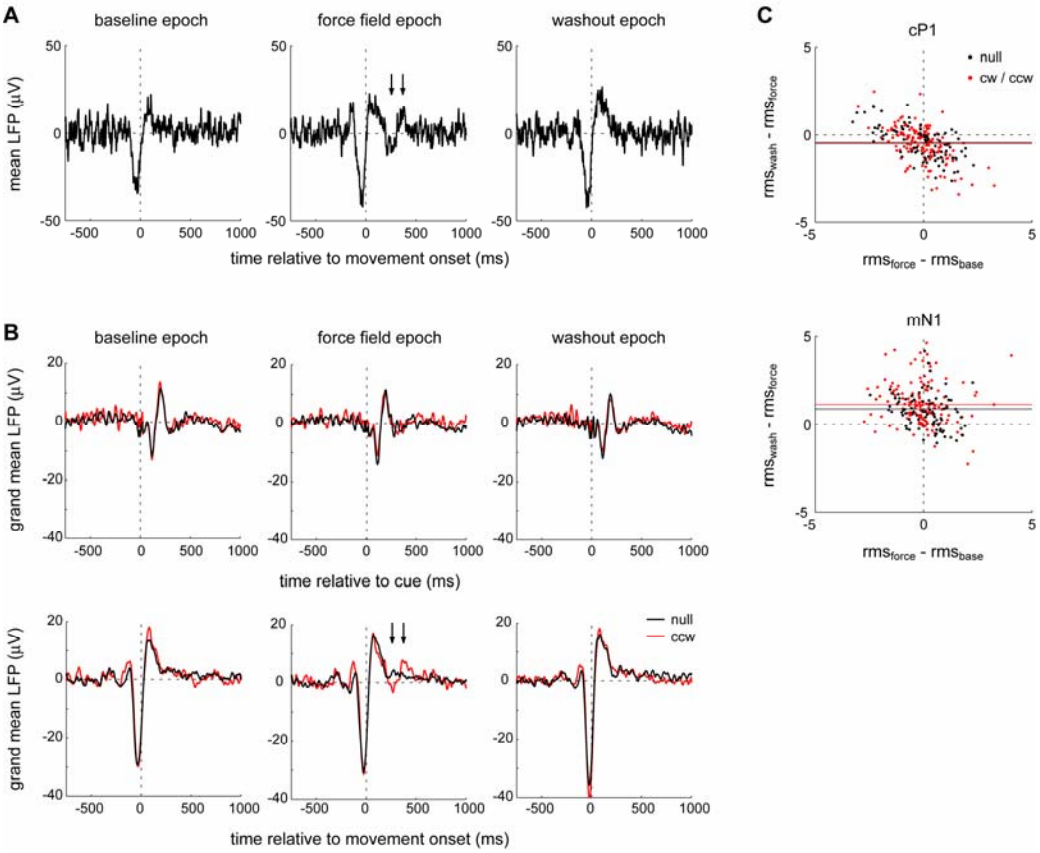

Figure 4-5. Across-epoch changes in evoked potentials of M1 LFPs. **A**, The mEP of an example LFP in each of the three epochs. Arrows point to extra mEP peaks seen only during the force field epoch, during which a counterclockwise field was applied. **B**, The cEP (top row) and mEP (bottom row) of the grand mean across all M1 LFPs (black, mean of all M1 LFPs recorded during null-field sessions; red, mean of all M1 LFPs recorded during counterclockwise sessions). Arrows again point to the extra mEP peaks. **C**, Scatter plots of adaptation changes versus washout changes in cP1 (top) and mN1 (bottom) magnitude (root-mean-square, rms). Lines indicate a significant mean shift in rms (t-test, $p < 0.05$).

following the mP2 peak in the force-field epoch, but not in the baseline or washout epochs. While these extra mEP peaks were not seen in all LFPs, they were present in the population mEP calculated by taking the grand mean across all M1 LFPs (Fig. 4-5B, bottom row, red; for simplicity only the average for counterclockwise-field sessions is shown but similar effects were seen in clockwise-field sessions). To control for the possibility that the late peaks were due to a nonspecific time-related effect, we also computed the population mEP for all null-field sessions. No extra peaks were present in the null-field population mEP (Fig. 4-5B, bottom row, black).

Unlike the mEP, the cEP changed very little across epochs (Fig. 4-5B, top row), aside from slight changes in the magnitude (rms) of the peaks. Across the population, there was a mean decrease in rms of the cP1 peak from the force-field to washout epochs (Fig. 4-5C, top; t-test, $p < 0.05$). This decrease was present both in fielded and null-field sessions and therefore was likely not due to adaptation or deadaptation processes. Shifts in cP1 rms also occurred from baseline to force-field epochs, but the mean shift was not significantly different from zero. Similar magnitude changes were seen for the mEP (Fig. 4-5C, bottom). However, rather than decreasing, the mN1 peak magnitude increased from force-field to washout epochs (t-test, $p < 0.05$). Again, these changes in peak magnitude, unlike the changes in number of peaks, were present in the null-field sessions and thus probably due to time-related effects (e.g. fatigue). Finally, both the changes in number and magnitude of the cEP and mEP peaks were qualitatively similar in the PMd LFPs (data not shown).

Force field-related changes were also apparent in LFP oscillations. In the gamma band, adaptation and deadaptation were associated with a transient increase and decrease, respectively, in oscillation amplitude during movement (Fig. 4-6, bottom row). These movement-time (MT) changes were not seen during null-field sessions, indicating that they were specific to the presence of the forces. However, the changes were not specific for the type of force field since the polarity and magnitude were roughly equivalent in the clockwise and counterclockwise field. Notice that in addition to these transient changes, the overall power in the gamma band tonically increased from baseline to force-field epoch and from force-field to washout epoch (i.e. both adaptation and deadaptation changes were positive; Fig. 4-6, bottom row).

In the beta band, several changes in oscillation amplitude occurred but only two of which were specific to the presence of clockwise or counterclockwise forces. These two field-related changes occurred in the early center hold (CH) time and in the early target hold (TH) time

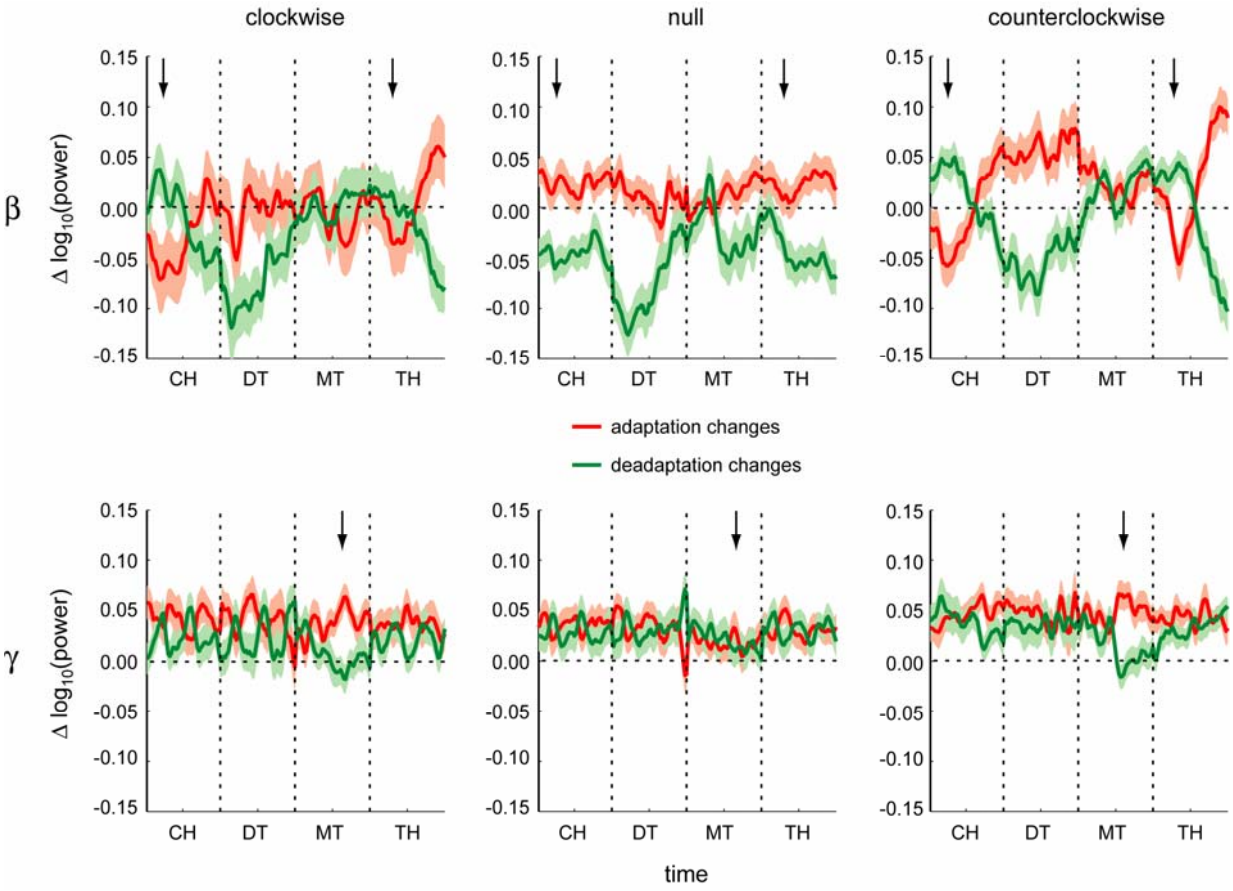

Figure 4-6. Force-field related changes in beta (top row) and gamma (bottom row) oscillation amplitude, averaged over all LFPs. Adaptation changes (red) = force-field epoch power – baseline epoch power. Deadaptation changes (green) = washout epoch power – force-field epoch power. Mean changes ± 95% confidence intervals on the mean are shown. Arrows mark times at which force-field related changes occur (i.e. changes due to clockwise and counterclockwise fields but not due to null field).

(arrows in Fig. 4-6, top row). Both times occur immediately after a movement: either the movement from center to target or the movement from target back to center. At both times, the beta oscillations are transiently decreased for adaptation and transiently increased for deadaptation relative both to zero and to the change seen during the null-field sessions. Again, these changes were essentially the same for clockwise and counterclockwise forces, indicating that they were not specific to the type of force field. There were also relatively large changes that occurred just prior to movement, in the delay time (DT) and the late TH. In particular, pre-movement beta oscillation amplitude was lower in the washout epoch compared to the other epochs (Fig. 4-6, top row). This change was not due to deadaptation since it was also present during null-field sessions. Furthermore, it was likely related to the decrease in cEP magnitude during the washout epoch (Fig. 4-5C).

In summary, activity changes specific to the presence of an altered mechanical environment were seen in the precentral LFP activity. However, these changes were not specific to the type of environment (i.e. clockwise versus counterclockwise curl field). The field-related changes occurred either during movement, in the mEP and gamma-band oscillations, or immediately after movement, in the beta-band oscillations. Adaptation was associated with an increase in power in the gamma band and a decrease in power in the beta band at these times. The opposite was true of deadaptation.

4.4 Discussion

In this chapter, we identified physiological correlates of behavioral adaptation to novel mechanical environments. First, we replicated the finding that adaptation to a velocity-dependent curl field is associated with directional tuning changes in both arm muscles (Thoroughman and Shadmehr, 1999; Shadmehr and Moussavi, 2000) and neurons of M1, SMA, and PMd (Gandolfo et al., 2000; Li et al., 2001; Padoa-Schioppa et al., 2002, 2004; Xiao et al., 2006). These changes often occurred gradually and primarily during movement but also, in some cases, during movement preparation. Second, we found that the cingulate motor areas, while not directionally tuned, do participate in force-field adaptation in a limited way. Third, we identified several correlates of motor adaptation in local field potential activity of the precentral cortex.

The force-field related changes in cingulate neuronal activity were modest but well above chance. To our knowledge, no previous study has looked at perturbation responses in the cingulate. Our work suggests that a minority of these neurons reflect some aspect of the perturbation or compensatory response to applied forces. This is perhaps not surprising given their anatomical connections to M1 and the spinal cord are on par with other cortical premotor areas (Dum and Strick, 2002).

As for the LFP response, the gamma-band oscillation amplitude changes were very similar to the changes seen in motor cortical neurons. In particular, there was an increase in activity during the movement time when the forces were applied. The beta-band oscillation amplitude changes, however, were unique. The post-movement decrease in amplitude during adaptation suggests a prolonged beta desynchronization carrying over into the hold time due to the increased kinetic activity during movements in the force field. When this kinetic load was removed during

washout, the post-movement activity returned to normal. Thus the force field-related effects in beta activity can be interpreted as further demonstrating the antikinetic preference of these oscillations.

The measured changes in both cingulate activity and LFP activity were not specific to the type of force field, but rather specific only to the presence of forces. Therefore, the changes could be interpreted as a correlate of the general increased effort needed to move in the force-field environment instead of a tailored response to the specific forces. However, the latter cannot be ruled out as the specificity of the change is a function of the metric used to quantify the change (i.e. using the absolute value of the preferred direction shift would yield the same conclusion for the direction tuning change analysis).

As we mentioned in Chapter 1, the force field-related changes do not necessarily indicate that movement dynamics are encoded in either the single cell or LFP activity. Much of the behavioral adaptation was incomplete, particularly in the monkey from which the LFP activity was recorded. Thus, there were both dynamic and kinematic differences between the late baseline epoch and late force-field epoch behavior to which the activity changes may relate. The same was true, although to a lesser degree, for the force-field to washout changes.

Finally, several of the previous studies observed changes in activity from the baseline to force field epoch that did not reverse during the washout (Li et al., 2001; Padoa-Schioppa et al., 2004). These residual activity changes were interpreted as a correlate of memory of the learned force-field environment. We did not specifically compare baseline activity to washout activity to look for residual changes in this chapter. We explored this topic, both through data analysis and modeling, in Chapter 5.

5 Motor adaptation with unstable cortical representations[1]

5.1 Introduction

Neural recordings in behaving animals have revealed much about the mechanisms underlying motor learning. Changes in single-unit activity have been correlated with learning sensorimotor associations (Mitz et al., 1991; Ojakangas and Ebner, 1992; Wise et al., 1998; Paz et al., 2003; Paz and Vaadia, 2004), learning movement sequences and skills (Nakamura et al., 1998; Cohen and Nicolelis, 2004), and adapting to novel mechanical environments (Gandolfo et al., 2000; Li et al., 2001; Padoa-Schioppa et al., 2002, 2004; Xiao et al., 2006).

One assumption implicit in many of these studies is that there is an underlying stable neural representation for familiar behavior, and thus changes in the neural representation necessarily reflect motor learning. Empirical support for this assumption is limited to just a few studies (Schmidt et al., 1976; Thompson and Best, 1990; Nicolelis et al., 1997; Williams et al., 1999; Taylor et al., 2002; Greenberg and Wilson, 2004). However, there are several indications that neural representations may, under some circumstances, change even without obvious learning. For example, when exposed to a fixed environment, hippocampal place fields in mice changed over the course of several hours when attentional demands were low (Kentros et al., 2004). Another study, which motivates the present work, showed that when monkeys performed a familiar reaching task the directional tuning of neurons in the supplementary motor area (SMA) changed substantially (Padoa-Schioppa et al., 2004). We refer to such changes in neural representations, which occur without obvious learning, as *background changes*. The cause of background changes and their function are unknown. Background changes may be related to adaptation to slow changes in the environment, e.g. muscle fatigue. Alternatively, background changes may be unrelated to behavior, and the neural representation of familiar tasks may be truly unstable. The main objective of this work is to study what such instability implies for the plasticity mechanisms underlying motor learning.

In the first half of this chapter we characterize background changes by reanalyzing data from the above mentioned recordings in SMA as well as new data from similar experiments in the

[1] This thesis chapter is a revision of a manuscript accepted for publication: Rokni U, Richardson AG, Bizzi E, Seung HS (2007) Motor learning with unstable neural representations. Neuron, in press.

primary motor cortex (MI). We study how the directional tuning changes in a "control" experiment in which the monkey practices a familiar reaching task, and in a “learning” experiment in which the monkey reaches in the presence of novel forces. In the second half of this chapter we explore the theoretical implications of the assumed instability of the motor cortical representation. It has been suggested previously that changes in tuning curves may cancel out at the level of the motor output (Li et al., 2001). Here, we relate this idea to a phenomenon in the theory of neural networks, which we term *redundant networks*. A network is redundant if it uses more neurons than needed to solve its task, such that the neural representation may change without affecting the overall behavior. Using a simple model, we show that noisy learning in a redundant motor cortex produces a background of behaviorally irrelevant changes in tuning curves. Additionally, we examine what further assumptions about the nature of synaptic plasticity are required to explain the observed properties of the background changes.

5.2 Methods

The behavioral (Chapter 1) and electrophysiological (Chapter 2) methods have been described previously. Regarding the electrophysiological methods, recording quality was critical to the arguments advanced in this chapter. To assess how the recording quality impacted our results, some of the analyses described below were repeated on a subset of neurons which were judged subjectively to be: (1) the best-isolated, by having no overlap between their clusters and other clusters or noise spikes in at least one projection of feature space, and (2) the most stable, by having temporally constant waveform features. The results of our analysis were similar whether we included all cells or just the best isolated, most stable cells (Table 5-1). As further evidence that unstable tuning was not due to unstable recordings, we show several examples of tuning curve instabilities in stably recorded cells (Fig. 5-1).

Data analysis

We analyzed 136 cells (93 from M1 and 43 from SMA) recorded during the control (null-field) experiment and 304 cells (105 from M1 and 199 from SMA) recorded during the learning (clockwise- or counterclockwise-field) experiment. Only M1 and SMA were analyzed since they

had the best balance between control and learning data. For each cell and each trial, we computed the average firing rate between 100 ms prior to movement onset and 300 ms after movement onset. We identified movement onset as the last time at which hand speed crossed a 4 cm/s threshold prior to the time of peak speed. For cells recorded during control sessions, we divided the trials into three consecutive blocks of 160 trials. For cells recorded during learning sessions, we divided the data into: entire baseline block, last 80 trials of adaptation (force-field) block and last 80 trials of washout block. The first 80 trials of the adaptation and washout were excluded to focus only on the post-adaptation phase (Li et al., 2001).

We estimated the tuning curve of each cell in each block by 8 mean firing rates corresponding to the different movement directions. We fitted each tuning curve by a sum of an offset, which is the mean of the 8 firing rates, and a cosine function (Eq. 12). To fit the cosine function we defined the two-dimensional AC vector

$$AC = \frac{1}{4}\sum_{k=1}^{8}\begin{pmatrix}\cos\theta_k \\ \sin\theta_k\end{pmatrix} r_k \qquad (1)$$

where θ_k are the movement directions and r_k are the mean firing rates. The amplitude and phase of the cosine were set to the magnitude and direction of AC, respectively. This commonly used method minimizes the squared error between the cosine function and the mean firing rates. We used a t-test to estimate the significance of changes across blocks of mean firing rates at individual movement directions. Because the offsets and cosine components are averages over a large number of trials (160), to test the significance of their changes we used a z-test: a t-statistic with a Gaussian null distribution (Montgomery and Runger, 1999). For testing the changes in the cosine functions we used a bivariate z-test on the two dimensional AC vectors, the large sample analog of Hotteling's t-statistic for multivariate data (Christensen, 2001), thus testing for changes in PD and/or modulation depth. To decide whether a tuning curve has a significant cosine component, we tested whether the AC vector is significantly different from zero by a bivariate z-test with the assumption of isotropic noise. For the analysis of PDs, we chose only cells which had significant cosine components in all three blocks with $p<0.05$, including 93 cells in the control experiment (59 from M1 and 34 from SMA), and 172 cells in the learning experiment (67 from M1 and 105 from SMA).

To test whether PD changes have a non-zero mean we used a z-test. The correlation between PD changes across cells and across time was estimated by Pearson's correlation coefficient. To

estimate the significance of the correlation coefficient, we used a nonparametric permutation test. For example, for data of pairs $(x_1, y_1),\ldots,(x_n, y_n)$, we randomize the *y*-data with respect to the *x*-data 1000 times and recomputed the correlation coefficient for each iteration. The p-value of the correlation coefficient is the fraction of times the simulated correlation coefficient had an absolute value larger than the real correlation coefficient.

In order to estimate the autocorrelation of the population of PDs in the control experiment we binned the data into 12 consecutive blocks of 40 trials. We computed the PD of each cell within each block as described above. We defined the correlation between PDs in two bins numbered *k* and *m* as

$$c(k,m) = \frac{1}{N_{cells}} \sum_{i=1}^{N_{cells}} \cos\left[\psi_i(k) - \psi_i(m)\right] \tag{2}$$

where $\psi_i(k)$ is the PD of cell *i* in bin *k*. This correlation is 1 only when the PDs in the two bins are equal, and -1 only when they are opposite. The autocorrelation function with lag *k* was estimated by

$$ACF(k) = \frac{1}{N_{bins} - k} \sum_{m=1}^{N_{bins}-k} c(m, m+k) \tag{3}$$

where $N_{bins} = 12$.

Model equations

Model of reaching. When presented with a target in direction θ, the two sensory inputs of our model are activated proportionally to the coordinates of the target relative to the initial hand position

$$\begin{aligned} x_1^t &= \cos\theta \\ x_2^t &= \sin\theta \end{aligned} \tag{4}$$

The two sensory inputs activate *N* motor cortical cells according to

$$r_i = \sum_{j=1}^{2} W_{ij} x_j^t \tag{5}$$

where *i* designates the cell number and W_{ij} are the weights of the cortical cells' input connections. r_i is interpreted as firing rate averaged over movement time relative to baseline

firing rate before movement, and therefore may be negative. The motor cortical cells generate an end-point force by

$$f_i = \sum_{j=1}^{N} Z_{ij} r_j \tag{6}$$

where i=1,2 designates the force components and Z_{ij} are the cells' output weights. These weights were fixed to

$$\begin{aligned} Z_{1,j} &= \frac{2}{N}\cos\alpha_j \\ Z_{2,j} &= \frac{2}{N}\sin\alpha_j \end{aligned} \tag{7}$$

where α_j are the direction of force generated by the neurons, which we distributed uniformly. We normalized Z_{ij} by 1/N such that firing rates of order 1 produce force of order 1. The final coordinates of the hand relative to the initial hand position were computed from f_i by

$$x_i = \sum_{j=1}^{2} R_{ij} f_j \tag{8}$$

where R_{ij} is the 2x2 identity matrix in the absence of the perturbation and a rotation of angle φ in the presence of the perturbation.

Model of plasticity. The task of the network is to have $x_i = x_i^t$. We assume that in order to learn this task W_{ij} are incremented after each trial by

$$\Delta W_{ij} = -\frac{W_{ij}}{\tau_{forget}} + \sigma n_{ij} - \frac{N}{\tau_{learn}} \frac{\partial E\left(x, x^t\right)}{\partial W_{ij}} \tag{9}$$

The second term is additive noisy synaptic changes, where n_{ij} are unbiased normalized i.i.d Gaussian noise components and σ is the noise amplitude. The first term is a leak term which prevents W_{ij} from drifting without bound. When only the first two terms are present, the synaptic weights perform a leaky random walk process (Fig. 5-4B), with a time constant τ_{forget} and a variance which scales with σ^2 / τ_{forget}. The third term is a gradient descent learning signal, which is a method commonly used for teaching artificial neural networks (Rumelhart et al., 1986). This method optimizes a cost function E with respect to the network weights W_{ij} by making small

steps of W_{ij} in the direction which decreases E the most. For our model, we use the squared error cost

$$E\left(x, x^t\right) = \frac{1}{2}\sum_{i=1}^{2}\left(x_i - x_i^t\right)^2 \tag{10}$$

The gradient of this cost is related to the error by

$$\frac{\partial E\left(x, x^t\right)}{\partial W_{ij}} = \sum_{k=1}^{2}\left(x_k - x_k^t\right) Z_{ki} x_j^t \tag{11}$$

Because the gradient scales as 1/N, we introduced a pre-factor N in front of the learning signal in Eq. (9). The gradient with respect to a synapse depends on information not local to that synapse (e.g. Z_{ki} in Eq. 11). Previous work has shown that the gradient can be computed by correlating noise in synaptic transmission with a global reward signal (Seung, 2003). Such a learning rule produces a noisy estimate of the gradient, which justifies our noisy gradient learning rule (Eq. 9).

Model parameters. In order to reproduce the experimental results in Figure 6, we used the parameter values $\tau_{learn} = 50, \tau_{forget} = 1500, \sigma = 0.025, \varphi = 60^\circ, N = 10000$. The model performs well already at N = 100 (see Supplemental Data), however to have better statistics we chose $N = 10000$. τ_{learn} was set according to the learning time constants observed in the monkeys' behavior during the learning experiment. We set σ to a value which in the control simulation produced PD changes of a magnitude similar to the observed magnitude. τ_{forget} was set to reproduce the rate of the experimentally observed background changes. φ was fit to reproduce the observed anti-correlation between adaptation and washout changes. All simulations, started with 10000 trials of pre-training, which is considerably longer than the equilibration time of the synapses τ_{forget} (1500 trials). Consequently, our results do not depend on the initial W_{ij} (which was zero).

5.3 Results

The control experiment: background changes were random and slow

In order to characterize background changes, we have analyzed data of a control experiment in which monkeys performed a familiar reaching task on which they had been trained for several months. On each of the 480 trials, performed each day of recording, the monkey had to reach to

one of eight targets arranged on a circle. The hand trajectories showed relatively small changes between different epochs within a practice session (Chapter 1, Fig. 1-2A; see also Supplementary Data). We analyzed the movement-related responses of 136 cells, 43 from SMA of one monkey (from Padoa-Schioppa et al., 2004) and 93 from M1 of a second monkey (new data). Because we found similar results in both brain areas, we pooled all 136 cells in subsequent analyses. We characterized each cell's movement-related activity by the mean firing rate in a time window from 100 ms prior to movement onset to 300 ms after movement onset. Tuning curves were defined by mean firing rate as a function of the eight reach directions of the task. To examine changes in tuning curves we artificially divided the data from the 480 trials into three consecutive blocks of 160 trials and computed tuning curves for each block separately.

Tuning curves changed. The left column in Figure 5-1 shows four example cells whose tuning curves changed between block 1 (crosses) and block 3 (circles). This tuning instability was not due to recording instability, since the spike waveforms did not change from block 1 to block 3 (Fig. 5-1, right columns), and similar changes in tuning curves were observed in a subpopulation of cells judged as best-isolated and most stable (Table 5-1; see also Methods). In 23% of the 8 directions x 136 neurons there was a statistically significant change from block 1 to block 3 in the mean firing rate (t-test, $p<0.01$). Even more significant changes were seen using aggregate measures of the tuning curves. 77% of the variance of the changes in tuning curves was accounted by changes in their offsets, and 16% was accounted by changes in the cosine components (total of 93%, see Supplemental Data). Therefore, to quantify the changes in tuning curves we first fitted the tuning curve of each cell in each block by an offset plus a cosine function (lines in Fig. 5-1, left column)

$$r(\theta) = B + A\cos(\theta - \psi) \qquad (12)$$

where $r(\theta)$ is firing rate as a function of target direction, B is the offset, A is the modulation depth and ψ is the preferred direction (PD). Next, we compared the fitted parameters between different blocks. We found changes in offsets (e.g. Fig. 5-1, row 4), modulation depths (e.g. Fig. 5-1, row 1) and PDs (e.g. Fig. 5-1, row 2). In 73% of the neurons offset changes between blocks 1 and 3 were statistically significant (z-test, $p<0.01$), and in 63% of the neurons changes between blocks 1 and 3 in the cosine function (i.e. changes in PDs and/or modulation depths) were statistically significant (bivariate z-test, $p<0.01$, see Methods). Thus, as observed by Padoa-

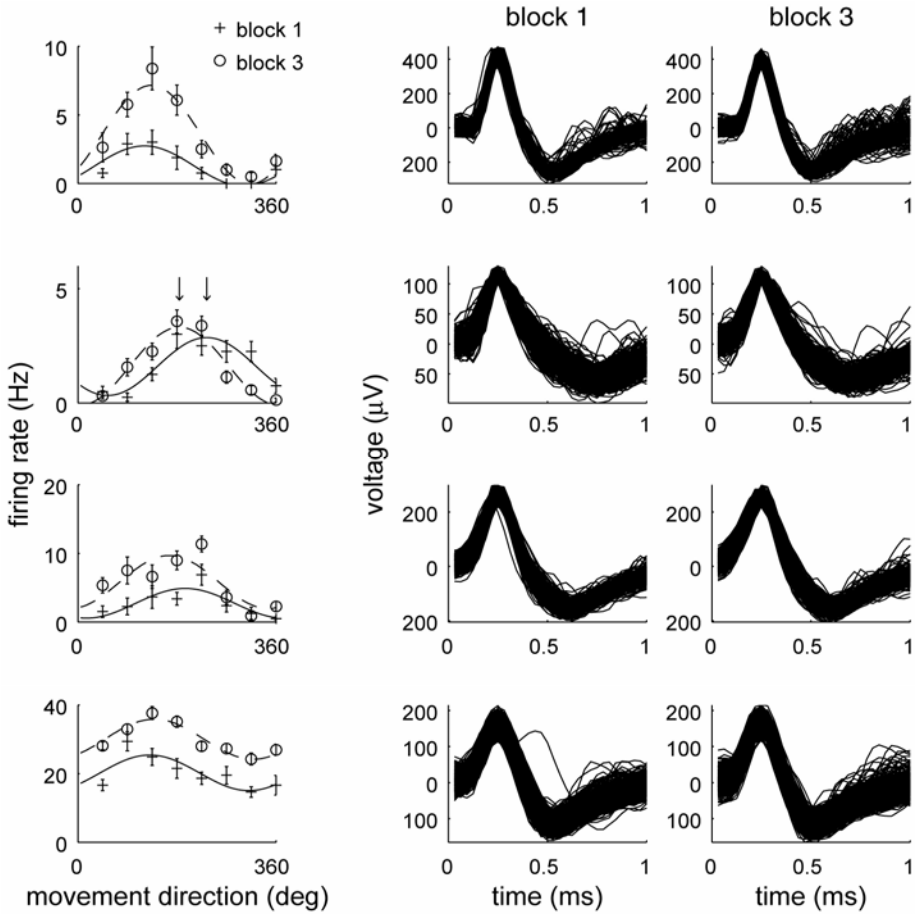

Figure 5-1. Changes in tuning curves in the control experiment. Each row corresponds to a sample cell. *Left*, Mean firing rates in block 1 (crosses) and block 3 (circles) as a function of movement direction, with fitted cosine tuning curves (lines). Error bars correspond to standard errors and arrows in second row designate the PDs. *Middle and right*, Random sample of 1000 spike waveforms in block 1 (middle) and block 3 (right).

Schioppa et al. (2004), motor cortical tuning curves may change even when the monkey is performing a familiar task.

Background changes were random across neurons and time. We found that changes in offsets, modulation depths, and PDs had similar statistical properties. The statistical properties for PD changes of 93 neurons (out of 136) whose tuning curves had a statistically significant cosine component in all blocks (bivariate z-test, $p<0.05$) are shown in Figure 5-2. Figure 5-2A presents the distribution of PD changes from block 1 to block 3. The average PD change was not statistically different from zero (z-test, $p>0.05$). Figure 5-2A averages across different days, and hence it is possible that on a given day different neurons tend to shift their PDs in the same direction. To test this possibility, for all pairs of cells recorded simultaneously, we plotted the PD

Table 5-1. Statistics of tuning curve changes in the learning experiment from baseline to washout and in the control experiment from block 1 to block 3. '±' indicates standard error.

statistics	learning experiment	control experiment	control experiment (best isolated cells)
sig. changes in cosine (%)	63 ± 3	63 ± 4	61 ± 7
Δ PD mean (deg)	-1 ± 2	-2 ± 3	3 ± 3
Δ PD st. dev. (deg)	35 ± 2	29 ± 3	19 ± 3
Δ mod. depth mean (Hz)	0.6 ± 0.2	0.3 ± 0.3	1.1 ± 0.5
Δ mod. depth st. dev. (Hz)	3.7 ± 0.2	3.3 ± 0.3	3.8 ± 0.5
sig. changes in offset (%)	76 ± 2	73 ± 4	69 ± 7
Δ offset mean (Hz)	1.8 ± 0.4	1.5 ± 0.7	3.3 ± 1.4
Δ offset st. dev. (Hz)	7.0 ± 0.4	7.3 ± 0.7	10.0 ± 1.4

change of one neuron against the PD change of the other neuron (Fig. 5-2B). We found no statistically significant correlation among these pairs of PD changes (permutation test, $p>0.05$). In order to test whether PD changes across different times were correlated, for each cell we plotted the PD change from block 1 to 2 versus its PD change from block 2 to 3 (Fig. 5-2C). Here as well, we found no statistically significant correlation (permutation test, $p>0.05$). These results show that tuning curve changes in the control experiment were random across neurons and time.

Background changes were slow. We characterized the correlation time of the randomly changing PDs. For this purpose, we binned the data into 12 consecutive blocks of 40 trials each. For every pair of bins, we computed the correlation between the populations of PDs at the two time bins, and averaged the correlations across all cells and among all pairs of bins separated by the same lag. Figure 5-2D shows the mean correlation as a function of the lag. Notice that within the range of lags that we measured, the correlation decayed linearly (solid line shows linear fit; the *y*-intercept is not 1 because of standard errors of the PDs). The slope of the autocorrelation was roughly 1/3000 trials, indicating a slow correlation time of the PDs, on the order of thousands of trials (notice that the correlation presented in Fig. 5-2D does not contradict the lack of correlation in Fig. 5-2C, because Fig. 5-2C shows that PD *changes* were uncorrelated across time, whereas Fig. 5-2D shows that the PDs themselves were correlated across time). Presently, it is unclear how much the correlation decays over more trials. Additionally, it is unclear whether the time unit relevant for these changes was number of trials or real time.

A similar analysis showed that the offsets and modulation depths also changed slowly and randomly across cells and time (data not shown).

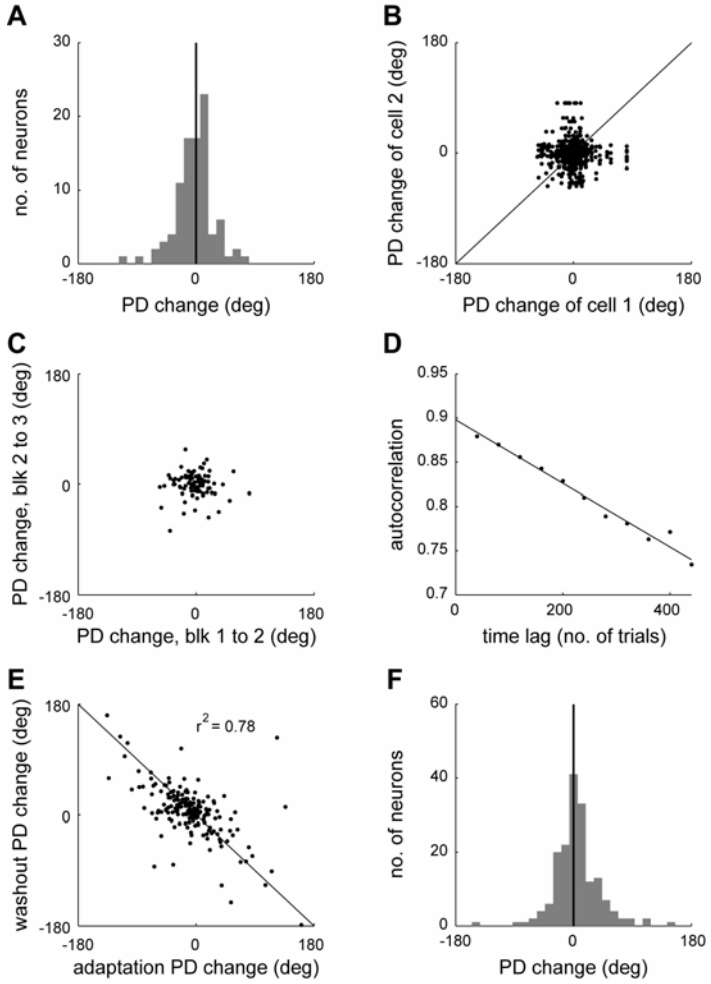

Figure 5-2. Statistics of changes in PDs in control and learning experiments. **A**, Distribution across cells of PD changes from block 1 to 3 in control experiment. **B**, PD change from block 1 to 3 of one cell vs. PD change from block 1 to 3 of another cell recorded simultaneously, across all simultaneously recorded pairs. Each pair is represented by two points symmetrically positioned around the $y = x$ diagonal (solid line). **C**, PD change from block 1 to 2 vs. PD change from block 2 to 3, across cells in control experiment. **D**, Autocorrelation of population of PDs and linear fit (solid line). **E**, Adaptation PD changes vs. washout PD changes across cells in learning experiment. Solid line represents the $y = -x$ diagonal. **F**, Distribution across cells of baseline-to-washout PD changes in learning experiment.

The learning experiment: learning related changes occur on top of background changes

In this section we show that learning adds systematic changes on top of the background of random changes described above. The data for this analysis were recorded while the monkeys performed the same reaching task as above, except that novel forces generated by a robotic manipulandum were applied to the arm during the middle 160 trials of each session. Thus, the

experiment consisted of three consecutive blocks of 160 trials: (1) a *baseline* block in the absence of forces, (2) an *adaptation* block in the presence of forces, and (3) a *washout* block in the absence of forces. The forces applied during the adaptation block were curl velocity force fields, i.e. proportional to the hand speed and orthogonal to its direction of movement. The learning-related behavioral changes have been described previously (Chapter 1, Fig. 1-2B).

We analyzed the responses of 172 neurons (67 from M1 and 105 from SMA) recorded during this novel task that had tuning curves with statistically significant cosine components in all blocks (bivariate z-test, $p<0.05$). We constructed three separate tuning curves for each neuron, respectively from the activity of the baseline block, the late adaptation (last 80 trials) and the late washout (last 80 trials). We designate the changes from baseline to late adaptation as *adaptation changes* and the changes from late adaptation to late washout as *washout changes*.

In contrast with the control experiment, in which PD changes at different times were uncorrelated across cells (Fig. 5-2C), in the learning experiment adaptation and washout changes were anti-correlated and distributed along the $y = -x$ diagonal (Fig. 5-2E; see also Padoa-Schioppa et al., 2004). This indicates that on average adaptation changes were reversed by washout. However, there was also considerable spread indicating that PDs of individual cells did not return to their baseline values after washout. Using similar methods as we used for the control experiment, we found that for many cells differences in tuning curves between baseline and washout were statistically significant (Table 5-1; see also Padoa-Schioppa et al., 2004). It was previously proposed that the baseline-to-washout changes underlie learning of the force task. Additionally, it is possible that these changes are related to the monkeys not fully deadapting in the washout. To challenge these interpretations, we compared the statistics of the baseline-to-washout changes in the learning experiment with changes in the control experiment over a similar number of trials. We found that the distribution of baseline-to-washout PD changes (Fig. 5-2F) was similar to the distribution of PD changes in the control experiment from block 1 to block 3 (Fig. 5-2A). Furthermore, every statistic we have examined— of the changes in PDs, modulation depths, and offsets of the tuning curves— showed no statistically significant difference between the learning and control experiments (z-test, $p>0.05$; Table 5-1). This result suggests that changes from baseline to washout were unrelated to either the force adaptation or deadaptation processes.

As an alternative interpretation, we suggest that changes in tuning curves in the learning experiment were a sum of two components: systematic learning-related changes and random background changes that exist regardless of learning. The learning-related changes reverse at washout and are therefore responsible for the anti-correlation observed between adaptation and washout changes. The changes from baseline to washout are purely random background changes. The fact that the statistics of these background changes were so similar in the control and learning experiments implies that the learning-related and background changes do not interact.

Theory: background changes are due to noisy learning in a redundant network

What is the interpretation of the background changes? Perhaps background changes reflect subtle behavioral changes (although we did not find evidence for this, see Supplemental Data). Alternatively, the background changes may be behaviorally irrelevant. We have constructed a theory which suggests why behaviorally irrelevant changes in the neural representation might occur. The theory is based on three assumptions: (1) motor cortex is redundant in the sense that it uses more neurons than required to produce the desired sensorimotor transformation, (2) when practicing a task, sensory feedback about motor errors is translated to synaptic changes which reduce the errors, and (3) this plasticity mechanism is noisy. We found that under these conditions a background of behaviorally irrelevant changes in tuning curves is produced.

Our assumption that motor cortex is redundant allows it to achieve the same sensorimotor transformation with different neural representations. In terms of synaptic weights, this implies a continuum of configurations which produce the desired sensorimotor transformation, which we term the *optimal manifold*. The synaptic configurations within this manifold are minima of the motor error. Therefore, one way to imagine this optimal manifold is by a flat valley in the landscape of the motor error as a function of synaptic weights (Fig. 5-3A). Synaptic learning can be described as going down the error landscape. If learning is noisy and ongoing, then even after reaching the valley and mastering the task, synaptic strengths continue to wander along the valley. Thus, a background of behaviorally irrelevant changes in the neural representation is produced.

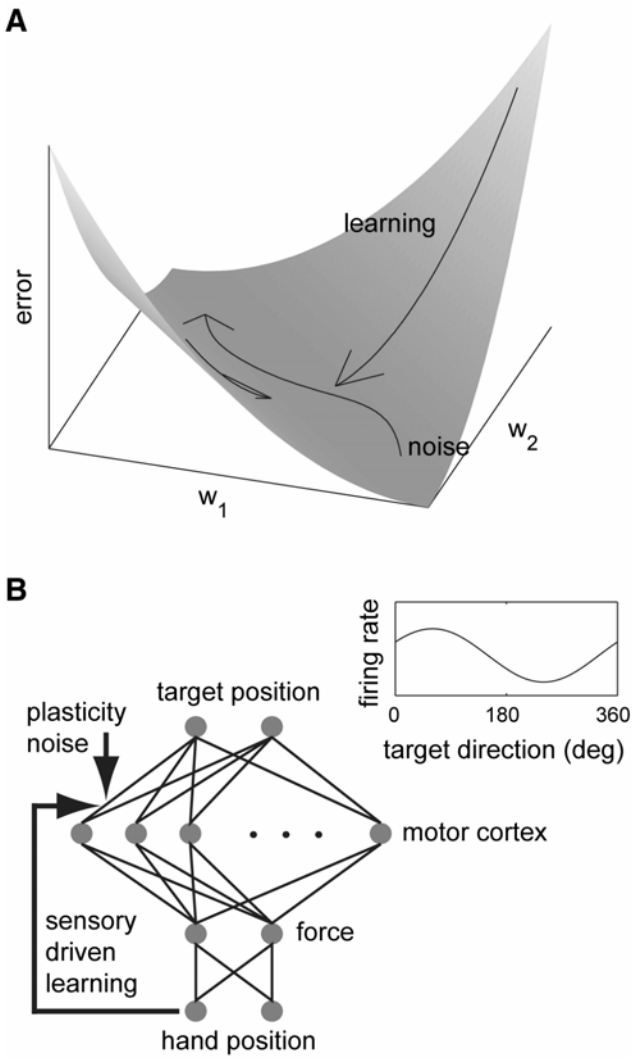

Figure 5-3. Theory for cause of background changes. **A**, The learning signal pushes the synaptic strengths down an error landscape which has a valley of minima at the optimal manifold, and the noise causes the synaptic strengths to drift along this valley. **B**, Model of motor cortical network which generates reaching movements. Tuning curves of model cells are cosine shaped (inset).

A model of the background changes in motor cortical tuning curves

To demonstrate our theory we constructed a simple model of a redundant cortical network that generates reaching movements (Salinas and Abbott, 1995). Our model generated reaching by the following stages (Fig. 5-3B): (a) the appearance of the target activated two sensory units, in proportion to the x-y coordinates of the target in the plane, (b) the sensory units activated a large number of motor cortical neurons, (c) the motor cortical neurons generated a two-dimensional end-point force on the hand and (d) the force moved the hand to a new position in the plane.

Each of these stages was modeled as a linear static mapping. In this static framework we could not represent dynamic force perturbations, so we used a perturbation of a static rotation, which similar to the curl velocity force field required rotation of tuning curves.

The goal of the network was to minimize the error between hand position and target position. For simplicity, we assumed that in order to achieve this task only the input weights of the motor cortical cells could be modified, whereas the cells' output weights were fixed. In this sense, the sensorimotor transformation was stored in the input weights of motor cortex. We assumed that after each trial, i.e. a single run on the network, sensory feedback about the motor error was used to modify the input weights in order to reduce subsequent motor error. Our major assumption regarding this plasticity process was that noise was added to the learning signal, independently at different synapses, and that this plasticity was operative even when the network had already mastered its task. In addition to the noise and learning signal we also added a decay term which limited the degree of wandering of synaptic weights.

We trained the model on eight targets equally spaced along a circle, as done in the experiments. To compute directional tuning curves of the model cells we simulated reaching movements to the different targets and plotted the firing rate as a function of target direction (during these reaching movements we artificially turned off synaptic plasticity). Notice that if the network was wired properly, such that movement direction equals target direction, then these tuning curves also described tuning to movement direction. The tuning curves of our model cells were cosine-shaped (Fig. 5-3B, inset), resembling the broad unimodal tuning curves observed in motor cortex. The cosine-shaped directional tuning stems from our assumption of a linear relation between firing rates and Cartesian position coordinates (Mussa-Ivaldi, 1988; Todorov, 2000). The modulation depths and PDs of the tuning curves were determined by the cells' input connections. When these connections were modified by synaptic plasticity the tuning curves changed. We did not model the offsets of the tuning curves.

Simulation of the control experiment

In order to show how background changes were generated and explain why they were random and slow, we simulated the control experiment. First, we pre-trained the model for many trials to mimic the excessive pre-training the monkeys had experienced. Next, we simulated 480

trials of the task, where at each trial the target was chosen randomly from 8 targets arranged uniformly on a circle.

Model generates background changes. In the simulation of the control experiment the model maintained good performance (Fig. 5-4A, left; there is a small bias because of the weight decay term), and yet the PDs of the model cells changed considerably (inset). Thus, the neural representation wandered in a manifold of configurations which produced the same behavior. To understand this redundancy, we first consider one simple configuration of tuning curves within this manifold, in which the PD of each cell equals the direction of force it generates (and all cells have the same modulation depth). This configuration generates a motor output in the correct

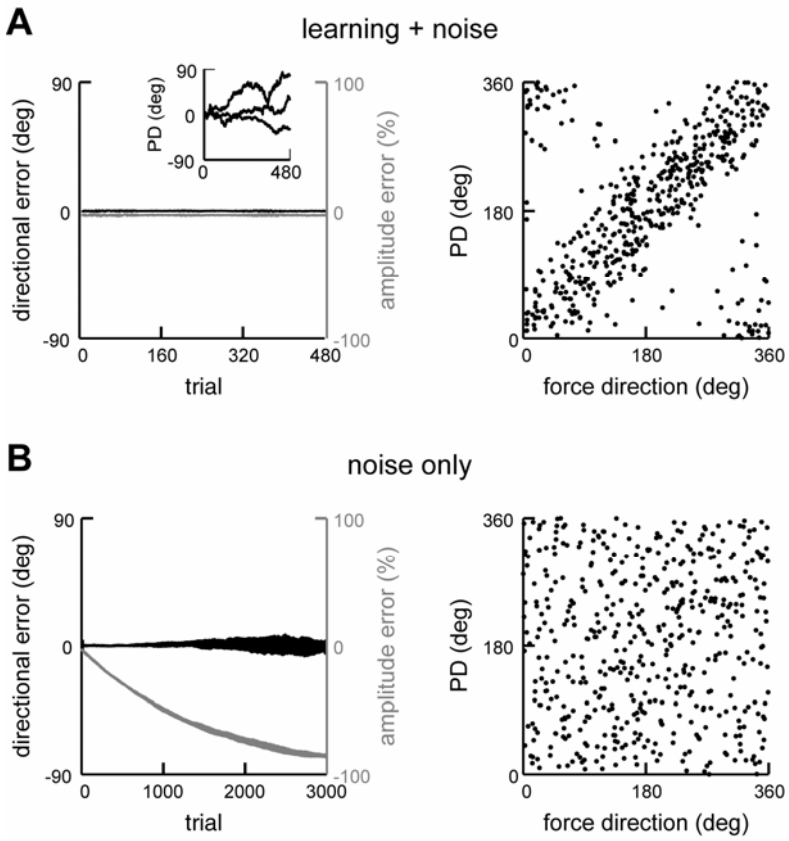

Figure 5-4. Behavior and neural representation in simulations of control experiment. **A**, Simulation with noisy learning rule, $\sigma = 0.025$, $\tau_{forget} = 1500$, $\tau_{learn} = 50$. *Left*, Error in movement direction (black), error in movement amplitude as percentage of desired movement amplitude (gray), and PDs of three sample cells whose PDs started close to zero (inset). *Right*, PD (computed from the firing rate r_i) vs. force direction (denoted α_i in the Methods) from last trial of simulation shown on left. **B**, Same as A but without a learning signal, $\sigma = 0.025$, $\tau_{forget} = 1500$, $\tau_{learn} = 10^6$. In both simulations $N = 10000$, but only 500 randomly sampled cells are shown on right panels.

direction because cells which produce force directions close to the desired direction are preferentially recruited, and the force components orthogonal to the desired direction cancel out. We refer to these tuning curves as the *relevant tuning curves*. Because of the vast convergence from cells to motor outputs, it is possible to add *irrelevant components* to these tuning curves, whose effects on the motor output cancel out. Thus, a generic configuration of tuning curves in the manifold can be decomposed into relevant components which produce the desired output and irrelevant components which do not contribute to the outputs. In such configurations PDs are correlated with, rather than equal to, the force directions (Fig. 5-4A, right). During noisy plasticity, as the neural representation wanders in the manifold, the relevant components remain fixed and the irrelevant components change randomly. The typical size of the irrelevant components is determined by the amplitude of the plasticity noise. The stronger the plasticity noise, the larger the irrelevant components, and therefore the weaker is the correlation between PDs and force directions. In our simulations, the noise amplitude was tuned to reproduce the magnitude of the observed PD changes.

To emphasize the active role of the learning signal in maintaining the performance, we also performed a simulation with the learning signal turned off. In this case, the noise randomized the PDs (Fig. 5-4B, right). Consequently, cells generated forces more or less equally in all directions and the net output diminished (Fig. 5-4B, left). These random changes had relatively little effect on movement direction because they tended to averaged out. The time constant of this forgetting process was set by the time constant τ_{forget} of the decay term in the weight update rule (see more on τ_{forget} below). Notice that these results do not necessarily imply that in the absence of sensory feedback we will be immobilized, because other sources of drive, such as executive control, may take over.

We compared the properties of the model-generated background changes (with the learning signal on) and the experimentally observed background changes. For this purpose, we replicated our analysis of the experimental data on the simulation data. We divided the simulation data into three equal blocks and used the average activity within each block to construct directional tuning curves.

Local noise and high redundancy explain randomness of background changes. Figure 5-5A,B shows that PD changes in the model were random across cells, similar to the randomness observed in the experimental data (compare with Fig. 5-2A,B). The randomness across cells in

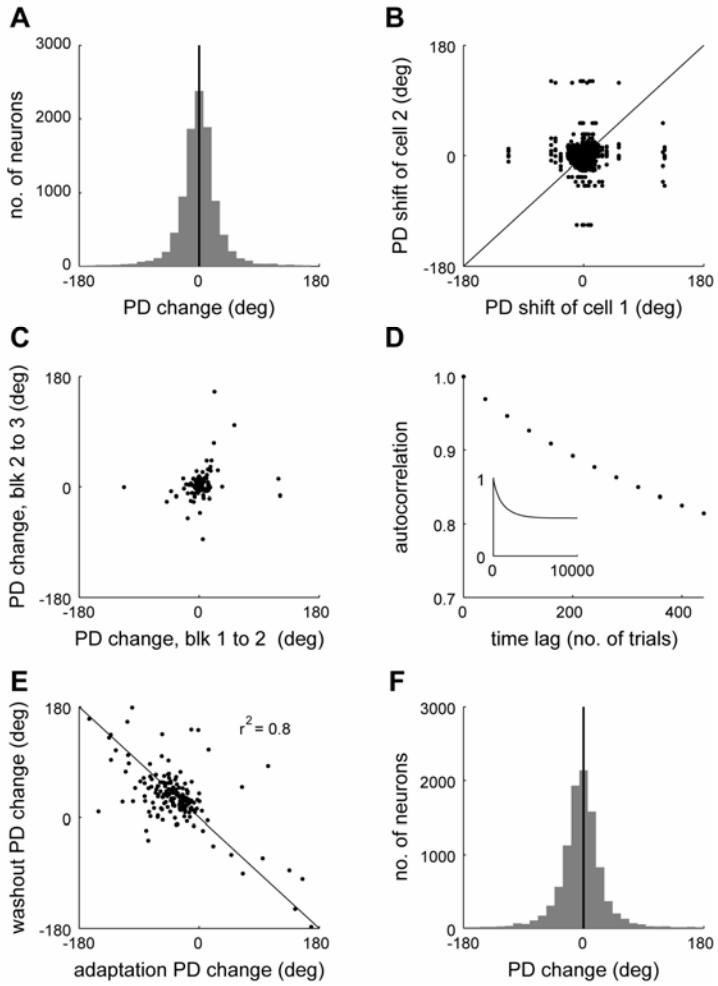

Figure 5-5. Statistics of changes in tuning curves in simulations of control and learning experiments. **A**, Distribution across cells of PD changes from block 1 to 3 in control simulation. **B**, PD changes from block 1 to 3 of pairs of cells. Each pair is represented by two points symmetrically positioned around the $y = x$ diagonal (solid line). **C**, PD change from block 1 to 2 vs. PD change from block 2 to 3, across cells in control simulation. **D**, Autocorrelation of population of PDs. **D inset**, Autocorrelation over long times. **E**, Adaptation PD changes vs. washout PD changes, across cells in learning simulation. Solid line represents the $y = -x$ diagonal. **F**, Distribution across cells of baseline-to-washout PD changes in learning simulation. To facilitate the comparison with the experimental results, we show in B, C and E samples of cells of the same size as in the corresponding subplots in Figure 5-2. Model parameter values are $\sigma = 0.025$, $\tau_{forget} = 1500$, $\tau_{learn} = 50$, $\varphi = 60°$, $N = 10000$.

the model resulted from our assumptions of local synaptic noise sources and a high degree of redundancy. An alternative to local noise sources is noise which comes from the environment, e.g. muscle noise, which through sensory feedback contaminates the learning signal. We found that such environmental noise created changes in tuning curves which were correlated across cells (Supplemental Data). Additionally, if redundancy is not high changes in different cells may

be coupled. When both local noise and high redundancy were assumed, PDs of different cells changed nearly independently. Figure 5-5C shows that PD changes in the model were also random across time, similar to the randomness observed in the experimental data (compare with Fig. 5-2C). The temporal randomness of the changes in the model tuning curves resulted directly from the temporal randomness of the noise in plasticity.

Background changes must be slow to allow learning. The control experiment showed that the background changes are slow, in the sense that PDs have a correlation time on the order of thousands of trials. In our model, the correlation time of the background changes was determined by τ_{forget}. We set $\tau_{forget} = 1500$ trials, so that the autocorrelation of the PDs decayed slowly (Fig. 5-5D), similarly to the experimental autocorrelation (Fig. 5-2D). We found that in order to obtain good performance of the model, τ_{forget} must be much greater than the learning time constant which was set by another parameter, τ_{learn}. There was continual competition between the learning signal which stored motor memories and plasticity noise which erased the memory. When τ_{forget} was much larger than τ_{learn} the erasure caused only a slight bias of the model's output (Fig. 5-4A, left). However, when τ_{forget} was comparable to τ_{learn} this bias increased substantially (not shown).

At long times, PDs were not completely randomized. Even after 10000 trials of the control simulation, the autocorrelation of the PDs did not vanish, but rather decayed to a positive baseline (Fig. 5-5D, inset). This baseline correlation reflects the fixed relevant components of the tuning curves. In other words, the tuning curves did not change completely arbitrarily, but were rather confined to configurations which produced the correct behavior. The value of this baseline correlation depended on the relative magnitude of the relevant and irrelevant components, which in turn depended on the amplitude of plasticity noise.

Simulation of the learning experiment

In order to explain how learning related changes in tuning curves combine with background changes, we simulated the learning experiment. We modeled the effect of the forces as a rotation of the outputs by 60˚. We first pre-trained the model for many trials and then trained the model on: (1) a baseline block of 160 trials without the perturbation, (2) an adaptation block of 160

trials with the rotation perturbation, and (3) a washout block of 160 trials without the perturbation. When the perturbation was turned on or off the model produced a large error which was subsequently reduced by learning (Fig. 5-6).

We repeated the analysis we had performed on the data of the learning experiment on our simulation data. We computed average tuning curves for the baseline, late adaptation (last 80 trials), and late washout (last 80 trials). As in the experiment, we designate changes from baseline to late adaptation as *adaptation changes* and changes from late adaptation to late washout as *washout changes*.

Model generated a combination of learning-related changes and background changes. The learning experiment showed that adaptation and washout changes were anti-correlated, albeit with a considerable spread (Fig. 5-2E). We interpreted this result as indicating that changes in tuning curves were a sum of learning-related changes and background changes. Similarly, in the learning simulation the adaptation changes and washout changes were anti-correlated with considerable spread (Fig. 5-5E). In the model, the learning-related and background changes were caused by the learning signal and plasticity noise, respectively. The learning signal changed synaptic strengths in relevant directions in order to improve performance. At the same time, plasticity noise changed synapses randomly and caused behaviorally-irrelevant changes. Because of these irrelevant changes, after washout synapses were in a configuration which was different from their baseline configuration. Hence, tuning curves changed from baseline to washout (Fig. 5-7A).

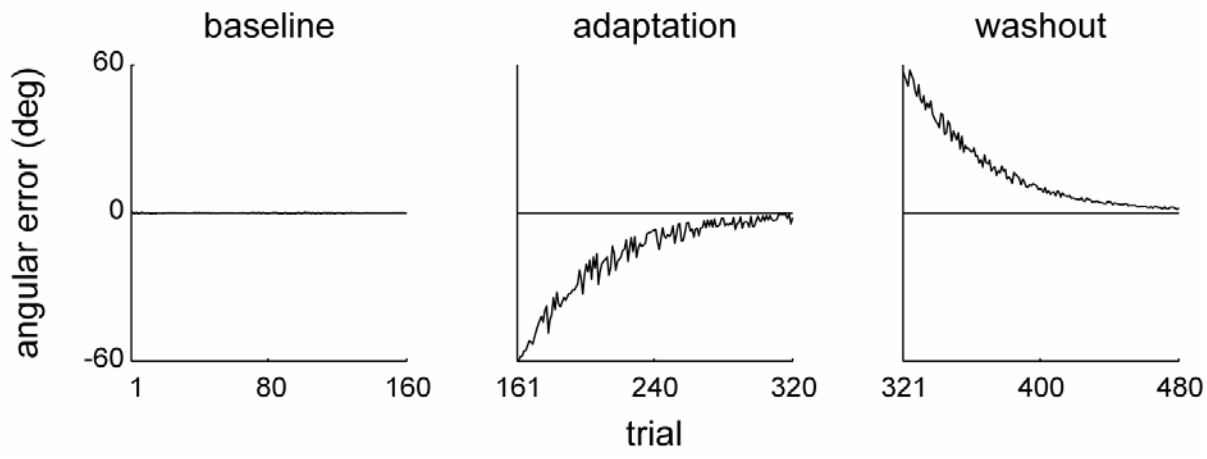

Figure 5-6. Model's error in movement direction in simulation of the learning experiment.

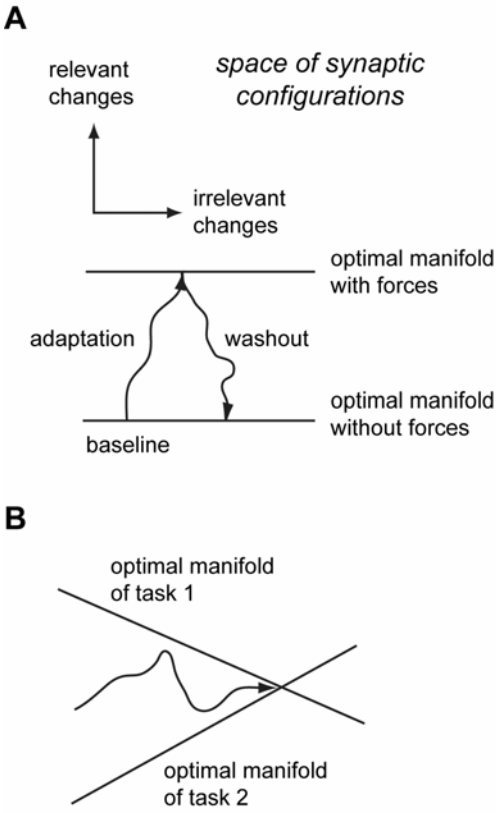

Figure 5-7. Optimal manifolds of multiple tasks. **A**, Changes in tuning curves in the learning experiment are a combination of behaviorally relevant changes created by the learning signal and irrelevant changes created by plasticity noise. After washout synapses return to the manifold optimal for the no-force task at a configuration different from baseline. **B**, Learning several tasks with the same neural circuitry can be described as moving synaptic strengths to a configuration in the intersection of the manifolds optimal for these tasks.

Similarity of baseline-to-washout changes and control changes is explained by additive plasticity noise. Our experiments showed that changes from baseline to washout in the learning experiment had similar statistics as the changes in the control experiment over a similar number of trials. This was also true of our model. The distribution of PD changes from baseline to washout (Fig. 5-5F) was very similar to the distribution of PD changes in the control simulation from block 1 to 3 (Fig. 5-5A; small differences between the two distributions were caused by the fact that learning was not entirely complete at the late washout). This similarity resulted from our assumption of additive plasticity noise. Because the noise was additive, the relevant changes caused by the learning signal and the irrelevant changes caused by the noise did not interact. Thus, learning a new task did not affect the statistics of the irrelevant background changes. If the noise were multiplicative, i.e. scaling with the motor error, learning a novel task would have

increased the background changes. Linearity of neurons is not necessary to make the statistics of background changes independent of learning. Even with nonlinear neurons (and additive noise), if learning does not change the statistics of the gains between synaptic changes and firing rate changes, it does not change the statistics of background changes.

5.4 Discussion

In experiments on motor learning, it is often assumed that there is an underlying neural representation that is stable, and that adaptation takes place on top of this stable background. Our experimental and theoretical results suggest a radically different picture. The experiments show that tuning curves of motor cortical cells are constantly changing even when performing a familiar task. Furthermore, when learning a new task, learning-related changes occur on top of this background of changing tuning curves. To explain these results we proposed a theory which is based on the following assumptions: (1) motor cortex is redundant in the sense that it uses more neurons than required to generate the desired sensorimotor transformation, (2) when practicing a task, sensory feedback is transformed into synaptic changes which reduce the motor error, and (3) this plasticity mechanism is noisy. The basic result of our theory is that under these conditions a background of behaviorally irrelevant changes in tuning curves is generated. The redundancy of the system allows changes in the neural representations that do not affect behavior. The noise changes tuning curves randomly and the learning signal shapes these changes so they do not harm task performance. As a result, tuning curves wander randomly between different configurations which are behaviorally equivalent.

Alternative interpretations. While our theory provides an explanation for why tuning curves changed in the control experiment, there are a number of alternative interpretations which at this point cannot be ruled out. Changes in tuning curves may be related to behavioral changes which we have overlooked, e.g. postural changes that are not reflected in our hand kinematics data. Additionally, it is possible that the recording electrodes injured the cells and consequently affected their tuning curves. Finally, perhaps neuromodulation underlies the changes in tuning curves, rather than synaptic changes.

How does our interpretation of the data differ from previous interpretations? In previous work the significance of background changes was not fully appreciated, and

consequently the data were interpreted differently. Specifically, in previous work cells were classified by how they changed their PDs in the learning experiment. Cells were classified as: *kinematic* cells whose PDs changed very little, *dynamic* cells whose PDs changed during adaptation and changed back during washout, and *memory* cells whose PDs changed without returning to their baseline values (Li et al., 2001; Padoa-Schioppa et al., 2004). This classification suggests a specialization across cells. However, the data do not show clear clusters corresponding to these cell classes, but rather a continuum of response types (e.g. Fig. 5-2E). According to our interpretation, such diversity of response types does not reflect specialized cell classes, but rather the randomness inherent in plasticity. If our interpretation is correct, then recordings across days will show that cells switch randomly between the different classes.

The previous studies proposed that changes from baseline to washout in memory cells reflect memory of the adaptation. In contrast, according to our theory changes in tuning curves from baseline to washout are behaviorally irrelevant changes caused by plasticity noise. This interpretation is supported by our result that the statistics of the changes from baseline to washout are very similar to the statistics of the changes in the control experiment over a similar number of trials. According to our interpretation, recordings across days will show changes that are uncorrelated, whereas if changes are learning related, they are more likely to be consistent across days.

What additional evidence is there for the theory? According to our theory, even when practicing a familiar task, sensory feedback is continually used to learn and prevent noise from erasing motor memories. Thus, our theory predicts that in the absence of sensory feedback familiar tasks are forgotten (Fig. 5-4B). This prediction is confirmed by experiments that show that interfering with auditory feedback in adult finches or adult humans causes their well-learned vocalizations to slowly deteriorate (Brainard and Doupe, 2000). Additionally, our theory predicts that as a task becomes more demanding the neural representations become more stable. This is predicted to occur because when more task constraints are added the dimension of the optimal manifold reduces, thus reducing the drift in synaptic strengths (for this effect to be appreciable redundancy should be low). This prediction is confirmed by an experiment which shows that as the requirements on spatial navigation of mice increases the spatial representation in their hippocampus becomes more stable (Kentros et al., 2004).

How could the theory be further tested? Besides the above mentioned recordings across days, one may use brain computer interface (BCI) experiments, in which a population of cortical cells is used to control a computer device (Schwartz, 2004). The advantage of BCI experiments is that the mapping from neural activity to motor output is fully known. Knowledge of this mapping can be used to test directly our assertion that changes in the neural representation are shaped so they would not affect the motor output.

What have we learned about plasticity underlying motor learning? First, from the existence of background changes we concluded that this plasticity process is considerably variable. Second, from the spatial randomness of background changes we inferred that the source of variability is local, i.e. independent in different synapses, rather than noise from the environment, e.g. muscle noise, which through sensory feedback contaminates the learning signal. Third, from the fact that baseline-to-washout changes in the learning experiment have similar statistics to changes in the control experiment we concluded that plasticity noise is additive. Finally, from the long correlation time of the background changes we concluded that noise changes synapses very slowly. According to our theory this slowness is necessary to prevent the noise from erasing motor memories. Notice that all these conclusions are based on the assumption that the observed changes in tuning curves are caused by synaptic changes.

The meaning of tuning curves. It is commonly assumed that the tuning of a neuron's activity to a movement parameter directly reflects its effect on movement. For example, a cell's PD is thought to represent the direction of force it generates. However, our model shows that the cells' PDs deviate randomly from the force directions (Fig. 5-4A, right). For the parameter values we used, the mean absolute difference between PDs and force directions was about 40˚. We conclude that the tuning of cells to motor parameters does not uniquely specify their effect on movement, but rather specifies how the cells are recruited to produce the movement.

Doesn't the theory imply that neural representations have no spatial order? Recent studies report that nearby motor cortical cells tend to have similar directional tuning, more than expected by a completely random arrangement (Amirikian and Georgopoulos, 2003; Ben-Shaul et al., 2003; Naselaris et al., 2006b). In our model PDs are correlated with the directions of end-point forces generated by the cells (Fig. 5-4A). Therefore, if the force directions are spatially organized within cortex, then PDs should also be spatially organized. In our simulations, PDs of cells which produce similar force directions are on average 55˚ apart, and thus we predict that

PDs of nearby cells differ on average at least by 55˚ (this would be the case if nearby cells produced exactly the same force directions). This is consistent with the finding of Ben-Shaul et al. that during movement time PDs of nearby cells differ on average by 75˚.

What is the function of plasticity noise? One possibility is that plasticity noise is a harmless phenomenon that has not been screened by natural selection. However, it is also possible that plasticity noise is useful for learning. It is well known in learning theory that adding noise to the learning process may prevent settling in local minima of the performance (Kirkpatrick et al., 1983). Additionally, it was proposed that stochastic plasticity is useful for preventing newly formed memories from overriding existing memories (Fusi, 2002). Finally, there is a whole class of learning methods, known as reinforcement learning, which is based on noise. In reinforcement learning, noise is injected into the system in order to probe different possible outputs and evaluate their success (Sutton and Barto, 1998). Recent studies suggest how reinforcement learning algorithms can be implemented in neural circuits (Seung, 2003).

What is the function of redundancy? Redundancy provides robustness to damage and noise. Additionally, motor cortex may be highly redundant with respect to a given task because it needs to store in the same neural circuit motor memories related to other tasks. This scenario can be visualized with the concept of the optimal manifold, which is the continuum of all synaptic configurations appropriate for a given task. For example, teaching a neural circuit two tasks can be described as moving the synaptic strengths to a configuration in the intersection of the two manifolds optimal for these tasks (Fig. 5-7B).

How would our results generalize to more complicated networks? Our linear model network tunes 2N synapses to perform a 2x2 linear transformation. Consequently, it has a linear optimal manifold of dimension 2N-4. Generally, in a linear network the manifold dimension is the difference between the number of synapses and the number of constraints imposed by the task. In a nonlinear network, the optimal manifold is curved and we speculate that its dimension is roughly equal to the difference between the total number of synapses and the number of synapses actually needed to solve the task. At present, there is no theory describing the nature of these manifolds.

Statistics of modulation depths is accounted by assuming plasticity of neuronal excitability. While our model accounts reasonably well for the statistics of the PDs, it does not describe well the statistics of the modulation depths. The model predicts that the distribution of

modulation depths should peak at intermediate values, whereas the empirical distribution is peaked at low values. Additionally, the model underestimates the degree of modulation depth changes. We found that these problems are remedied if we assume that neuronal excitability is also changed plastically by learning. Thus, our data suggests that task-related information is stored in both synapses and intrinsic cellular properties (see Supplemental Data).

What are the limitations of our model? In this work we chose the simplest model that illustrates that the neural representation of a redundant system may be inherently unstable. Because of its simplicity, our model did not capture accurately certain aspects of the data. Firstly, the model readapted to the baseline condition as fast as it learned the novel task (Fig. 5-6), whereas the monkeys usually readapted to the baseline faster and more completely than they adapted to the forces (Chapter 1). Secondly, the distributions of PD changes generated by the model tended to have heavier tails than the empirical distributions (compare Figs. 5-2B and 5-5B). Thirdly, the autocorrelation of the PDs in the model had a slight curvature which was not observed in the data (compare Figs. 5-2C and 5-5C). Fourthly, the distribution of learning related PD changes in the model was more biased than the empirical distribution (compare Figs. 5-2E and 5-5E).

Another limitation of our model is that synapses have a single forgetting time constant on the order of thousands of trials. We chose this time constant to fit the rate of background changes observed in our data. Since some motor tasks are retained over many years without practice, it is more plausible that there are multiple synaptic forgetting time constants, some of which are very long (Fusi, 2002). To address this issue we have extended our model to include several synaptic forgetting time constants. We found that the model can reproduce the observed rate of background changes and yet in the absence of sensory feedback partially retain motor memories for indefinitely long times (see Supplemental Data). Finally, in the future our model should be extended to allow storage of multiple sensorimotor transformations, by including contextual inputs (Salinas, 2004).

5.5 Supplemental Data

Compact description of tuning curves changes

The directional tuning curve of a neuron in our data is described by the set of 8 mean firing rates for the different movement directions. Changes in the mean firing rates across different directions may be correlated. In this case, changes in tuning curves can be compactly described by a few principal components (PCs), rather than the 8 mean firing rates. To examine this issue, for each neuron we computed a "difference tuning curve", i.e. the changes from block 1 to block 3 in mean firing rate for each direction. We then performed principal component analysis (PCA) on the set of difference tuning curves. We found that the first 3 PCs account for 92% of the variance in the changes in tuning curves (Fig. 5-s1A). Figure 5-s1B shows the first three PCs. The first PC (solid line) approximately corresponds to the offset of the tuning curve and the second and third PCs (dashed-dotted and dashed lines, respectively) approximately correspond to the cosine and sine components of the tuning curve. The other PCs have more complicated forms (data not shown). We conclude that changes in tuning curves in the control experiment can be

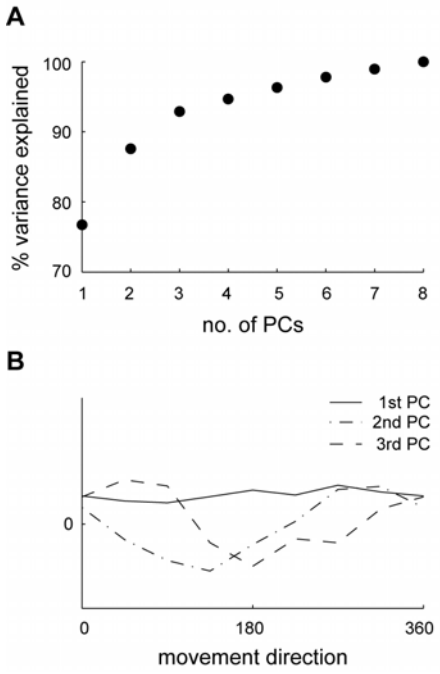

Figure 5-s1. Principal component analysis of changes in tuning curves. **A**, Percentage of explained variance as a function of number of principal components. **B**, First three principal components. The components have been scaled such that they have the same root mean square, and therefore the y-axis has arbitrary units.

reasonably approximated by changes in the tuning curves' offsets and cosine components.

Comparison of changes in tuning curves with behavioral changes

We tested whether the drift in directional tuning curves observed in the control experiment is related to drift in behavior. Overall, we had data from 42 control session, 15 for monkey 1 (monkey with SMA data) and 27 for monkey 2 (monkey with MI data). We searched for correlations between changes in tuning curves and changes in hand trajectories across days. We used three measures to quantify changes in tuning curves in a given session: (1) change in PD, (2) change in modulation depth, and (3) change in offset. For each of these measures we averaged the changes from block 1 to block 3 over the cells recorded in each session. Additionally, we selected measures of behavioral change in two ways: (1) we chose behavioral measures which we judged as likely to be related to the neural measures, and (2) we performed principal component analysis (PCA) of the changes in trajectories within control sessions to find the aspects of movement which changed the most.

We performed a total of 18 comparisons between measures of changes in tuning curves and measures of changes in hand trajectories. Table 5-s1 shows the p-value of the correlation found in each comparison (columns 2-4) and shows for each behavioral measure what fraction of sessions showed a significant change (column 5). Out of the 18 comparisons we have made, only a single comparison had a p-value less than 0.05, which is to be expected by chance. We conclude that we did not find a behavioral correlate of the changes in tuning curves in the control

Table 5-s1. *Columns 2-4*, P-values of comparisons between tuning curve changes (columns) and behavioral changes (rows). *Column 5*, Fraction of control sessions with significant behavioral change from block 1 to 3 (z-test, $p<0.01$).

	PDs	mod. depths	offsets	% sig. changes
deviation area (both monkeys)	0.08			21
monkey 1, tangential PC1	0.31			20
monkey 1, tangential PC2	0.02			27
monkey 2, tangential PC1	0.43			18
monkey 2, tangential PC2	0.35			18
mean speed (both monkeys)		0.86	0.74	62
monkey 1, radial PC1		0.79	0.60	60
monkey 1, radial PC2		0.78	0.55	40
monkey 2, radial PC1		0.56	0.94	86
monkey 2, radial PC2		0.12	0.12	36
hit rates (both monkeys)	0.69	0.36	0.99	14

experiment.

While there are many other comparisons that could be done, it is important to keep in mind that adding more comparisons lowers the statistical power of the overall experiment. Additionally, we emphasize that these results still do not rule out entirely the possibility that the neural changes are related to behavioral changes. First, it is possible that more data is required to detect such correlations. Second, it is possible that the neural changes are related to aspects of the behavior unobservable in the hand kinematics, e.g. changes in arm posture or muscle activity. Next, we explain the different comparisons we have made.

PDs vs. deviation areas. It is natural to assume that changes in the cells' PDs are related to changes in the direction of movement. Because the deviation area measure captured well the

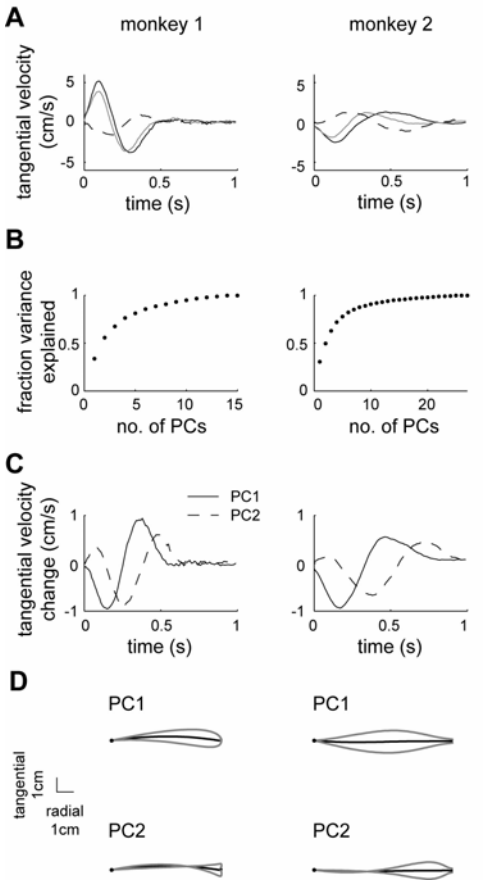

Figure 5-s2. PCA of tangential velocity profiles. **A**, Mean tangential velocity profile averaged over blocks 1 (black) and 3 (grey) of an example session. Difference shown as dashed line. **B**, Explained fraction of variance of block 1 to 3 changes in tangential velocity profile as a function of number of PCs. **C**, Velocity profiles of first two PCs. **D**, Mean trajectories (averaged over block 1 of all sessions; black) and the effect of adding/subtracting each PC (magnified by 4; grey). The dot represents the starting point.

changes in movement direction caused by the forces in the learning experiment (see Chapter 1), we used it also to describe changes in movement direction in the control experiment. We quantified the change in direction of movement on a given session by the change in the mean deviation area from block 1 to block 3. We compared the changes in deviation area with the PD changes, across all control sessions, pooled over both monkeys (Table 5-s1).

PDs vs. principal components of tangential velocity change. Our choice of the deviation area measure for quantifying changes in movement directions is somewhat arbitrary. Another approach for quantifying changes in movement direction is to find the measures that changed the most within the control sessions. For this purpose, we performed the following principal component analysis (PCA). First, we examined the tangential velocity component, i.e. the component of the velocity orthogonal to the axis between the initial hand position and the target (positive tangential velocity corresponds to movement in the counter-clockwise direction). The temporal profile of the tangential velocity is a relatively sensitive gauge of changes in movement direction. Figure 5-s2A shows the tangential velocity profiles averaged over trials in block 1 (black), and averaged over trials in block 3 (grey), in one control session. The change from block 1 to 3 (dashed) reflects changes that occurred in movement direction. We started our analysis by computing the change from block 1 to 3 in the tangential velocity profile for each control sessions.

Next, we performed PCA on the set of profiles of change in tangential velocity, separately for each monkey. In both monkeys we found that the first two principal components (PCs) account for roughly 50% of the variance of these profiles (Fig. 5-s2B), and therefore in subsequent analysis we focused on these two PCs. The profiles of these PCs are shown in Figure 5-s2C. To facilitate the interpretation of these PCs, we computed the mean trajectory of each monkey (Fig. 5-s2D, black), and then perturbed these mean trajectories by adding or subtracting each PC (grey). Because the effects on the trajectories were rather small, we artificially magnified the PCs in Figure 5-s2D by a factor of 4. In both monkeys we found that the 1st PC is related to clockwise/counter-clockwise deviations across the entire trajectory, whereas the 2nd PC is related to deviations mostly at the end of the trajectories.

Subsequently, for each control session we computed the coefficients of the two PCs. These coefficients represent to what extent each PC contributed to the change in the tangential velocity profile. Finally, we used these coefficients as our new measures of change in movement

direction, and compared them with the changes in PDs, across sessions, separately for the two monkeys (2 PCs x 2 monkeys = 4 comparisons; see Table 5-s1). To judge the statistical significance of the coefficient of a given PC on a given session, we computed the coefficients of that PC for all individual trials in blocks 1 and 3 of that session, and used a z-test to test the statistical significance of the difference in the means between blocks 1 and 3.

Modulation depths and offsets vs. movement speed. Because it has been shown that the modulation depths and offsets of directional tuning curves of motor cortical cells scale with speed (Moran and Schwartz, 1999), we compared the changes in modulation depths and offsets to changes in endpoint (hand) speed. To quantify the change in hand speed we first computed the average hand speed for each trial by dividing distance from starting point to target by total movement time. Movement onset was defined as time when speed exceeds 4cm/s, and movement offset was defined as time when speed becomes less than 4cm/s. For each control session, we averaged the mean hand speeds within trials, across trials in block 1 and across trials in block 3, separately in each block. The difference between the mean speeds in blocks 1 and 3 was our new measure of speed change. We compared this measure of speed change with the offset changes and modulation depth changes, across all control sessions, pooled over both monkeys (2 comparisons; see Table 5-s1).

Modulation depths and offsets vs. principal components of radial velocity changes. Above we supplemented the change in deviation area with measures of change in movement direction derived by PCA of the changes in tangential velocity. Following a similar approach, we supplemented the change in hand speed with measures derived by PCA of the changes in radial velocity (the component along the axis from the starting point to the target). While changes in PDs are more likely related to changes in tangential velocity, changes in modulation depths and offsets are more likely related to changes in radial velocity. Figure 5-s3A shows for one example of the mean radial velocity profiles in block 1 (black), block 3 (grey), and the change from block 1 to 3 (dashed). We performed PCA on the set of profiles of radial velocity change across all sessions, separately for each monkey. We found that the first two PCs account for roughly 60% of the variance of the changes in the radial velocity (Fig. 5-s3B). Figure 5-s3C shows the profiles of change in radial velocity which correspond to these PCs. To visualize the effect of these PCs on the movement we computed the mean radial velocity profile of each monkey (Fig. 5-s3D, black), and perturbed this mean profile by adding or subtracting each PC (grey). Because the

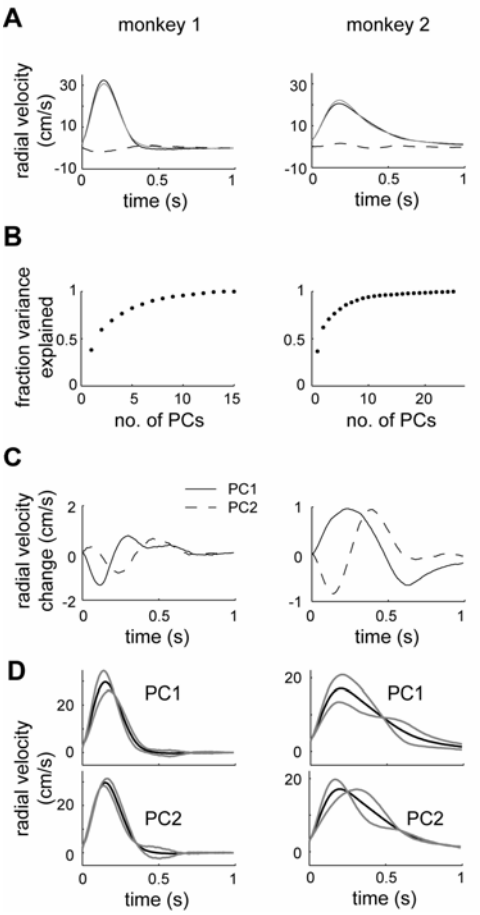

Figure 5-s3. PCA of radial velocity profiles. **A**, Mean radial velocity profile averaged over blocks 1 (black) and 3 (grey) of an example session. Difference shown as dashed line. **B**, Explained fraction of variance of block 1 to 3 changes in radial velocity profile as a function of number of PCs. **C**, Velocity profiles of first two PCs. **D**, Mean trajectories (averaged over block 1 of all sessions; black) and the effect of adding/subtracting each PC (magnified by 4; grey).

effects on the radial velocity profiles were small, we artificially magnified the PCs in Figure 5-s3D by a factor of 4. The two monkeys showed qualitatively different PCs. Monkey 1 showed changes in movement time (PC 1), and increases/decreases in the duration of the acceleration phase coupled with overshooting/undershooting the target (PC 2). Monkey 2 showed changes in the shape of the velocity profile.

We computed the coefficients of these PCs for each session, and used them as our new measures of movement changes. We compared these coefficients with the changes in modulation depths and offsets across sessions, separately for each monkey (2 PCs x 2 neural measures x 2 monkeys = 8 comparisons; see Table 5-s1). The statistical significance of the coefficients was judged by the same method used for the coefficients of the PCs of the tangential velocity (see above).

PDs, modulation depths and offsets vs. hit rates. The above tests included only successful trials. It could be argued that the changes in the neuronal tuning are related to the changes in the probability of success. After all, getting the reward is probably the aspect of the task that is most important to the monkeys. Within each block in each control session we computed the percentage of successful trials, which we term the hit rate. Hit rates across control sessions were 95% ± 3% for monkey 1, and 84% ± 6% for monkey 2 (mean±s.d.). Changes in hit rates from blocks 1 to 3 were 1.5% ± 3.6% for monkey 1 and 0.3 ± 6.9% for monkey 2 (mean±s.d.). We compared the changes in hit rates from blocks 1 to 3 with the changes in PDs, modulation depths and offsets, pooled over both monkeys (3 comparisons; see Table 5-s1).

Global noise from the environment causes correlated changes across cells

In the manuscript, we have shown that the changes in tuning curves in the control experiment are random across cells. Additionally, we have shown that randomness across cells can be reproduced by a model in which the source of variability in plasticity is local, i.e. independent across synapses. Here we examine the effect of global plasticity noise, i.e. noise from the environment which through sensory feedback contaminates the learning signal. For this purpose, we modify the plasticity rule (Eq. 9) to

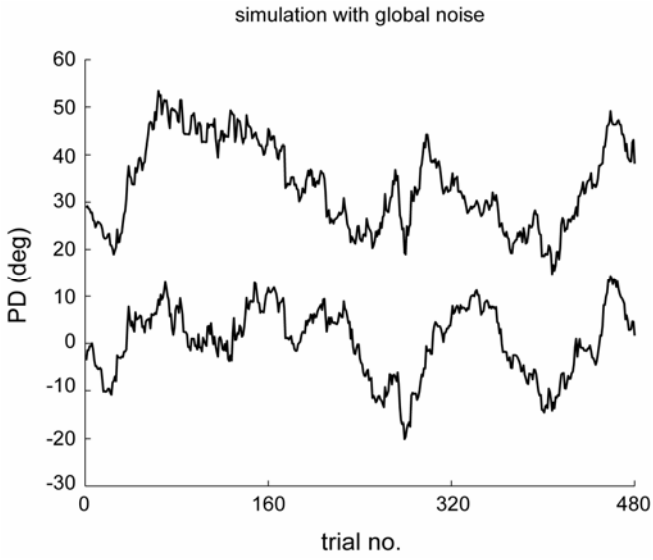

Figure 5-s4. Simulation of model with global noise from the environment. PDs of two model cells as a function of trial number.

.

$$\Delta W_{ij} = -\frac{N}{\tau_{learn}} \frac{\partial E}{\partial W_{ij}} \left(x + \sigma n, x^t \right) \qquad (13)$$

where n is Gaussian noise that is added on top of the model output vector x, and σ is the noise amplitude, which we set to 1. n may be interpreted as either sensory noise, i.e. noise in the estimation of the hand position, or as muscle noise. We simulated the control experiment with this modified plasticity rule. Figure 5-s4 shows that in this simulation the PDs of different cells change in a correlated manner. Thus, global noise from the environment causes changes in tuning curves which are correlated across cells.

Statistics of modulation depths explained by plasticity of neuronal excitability

Problems with original model. The model we have presented in the main text accounts reasonably well for the statistics of the PDs, but does not account well for the statistics of the modulation depths. In order to compare the predicted statistics of the modulation depths to the experimental data, first we scaled the firing rates of the model cells to match the empirical mean modulation depth in the control condition (~5 Hz). Next, we compared the predicted distribution of modulation depths in the control condition to the empirical distribution (Fig. 5-s5A). The model predicted the distribution is peaked around modulation depths of intermediate size, whereas the true distribution is peaked at small modulation depths. Additionally, we examined the distribution of changes in modulation depths from block 1 to 3 in the control experiment (Fig. 5-s5B). We found that the model underestimates the changes in modulation depths. Similarly, we found that the model underestimates the changes in modulation depths during adaptation and washout in the learning experiment, although it does account for the anti-correlation between these changes (Fig. 5-s5C). Finally, in all the distributions shown in Figure 5-s5, the data has much heavier tails than the predicted distribution.

The modified model. We found that the model's discrepancies in the statistics of the modulation depths can be remedied by assuming an additional plasticity mechanism that alters neuronal excitability. In the original model, changes in tuning curves occur by synaptic modifications. The level of noise in these synaptic modifications was tuned to reproduce the degree of PD changes observed experimentally. Under these conditions, the model underestimated the changes in modulation depths. One possible explanation for this discrepancy

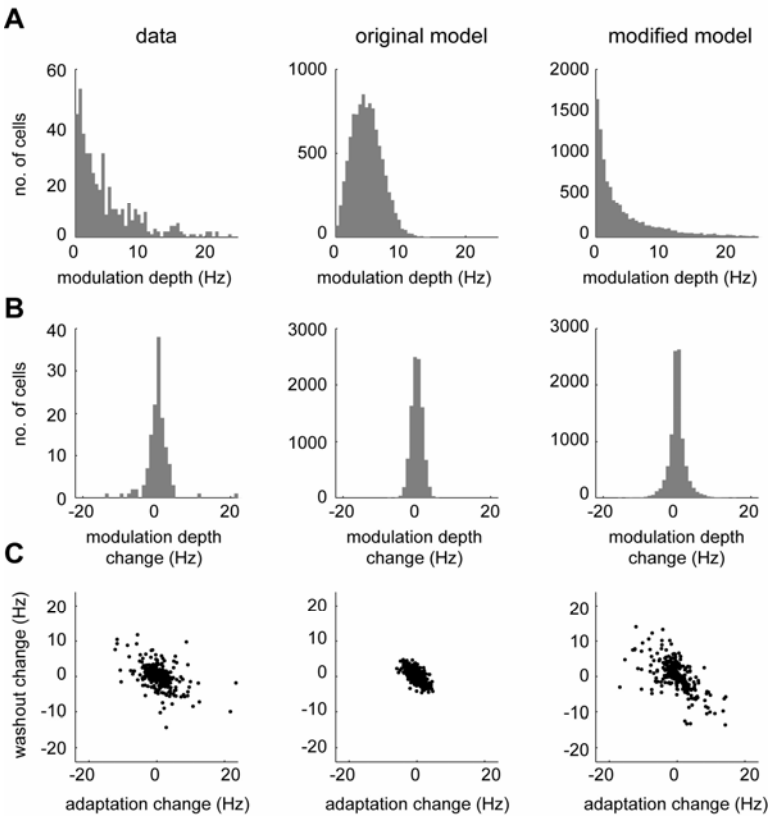

Figure 5-s5. Statistics of modulation depth in experimental data (left), original model (middle), and modified model (right). **A**, Distribution of modulation depths across cells measured from activity in block 1 of control experiment/simulation. **B**, Distribution of changes in modulation depths across cells from block 1 to 3 in control experiment/simulation. **C**, Washout change in modulation depth (last 80 trials of adaptation block to last 80 trials of washout block) vs. adaptation change in modulation depth (baseline block to last 80 trials of adaptation block) across cells in learning experiment/simulation. For the models, we show only a sample of cells of the same size as the experimental sample (172 cells).

is the existence of an additional plasticity mechanism which changes modulation depths but not PDs. In order to modify a cell's modulation depth without altering its PD the cell may change its excitability, and thus modify uniformly the throughput of all its synapses. Persistent changes in neuronal excitability have been reported previously, and were found to be correlated with learning in several experimental preparations (Zhang and Linden, 2003). These experience-dependent excitability changes are a result of the modification of voltage-gated ion channels responsible for action potential generation and propagation. Thus, our modified model may be viewed as storing task-related information through both synaptic and intrinsic modifications.

To test whether noisy learning in both synapses and neuronal excitability can account for the experimental data we extended the original model to include also plasticity of neuronal

excitability. In the original model the gain between the sensory input x_j^t and the firing rate of a cortical cell r_i was determined by the synaptic weight W_{ij} (see Eq. 5 in Methods). In the modified model, we substitute W_{ij} with $g_i W_{ij}$, where g_i is the excitability of neuron *i*

$$r_i = \sum_{j=1}^{2} g_i W_{ij} x_j^t \tag{14}$$

Similar to the original model, we use noisy gradient descent learning to train the model parameters (see Eq. 9 in Methods). However in the modified model we train both W_{ij} and g_i

$$\begin{aligned} \Delta W_{ij} &= -\frac{W_{ij}}{\tau_{forget}} + \sigma n_{ij} - \frac{N}{\tau_{learn}} \frac{\partial E\left(x, x^t\right)}{\partial W_{ij}} \\ \Delta g_i &= -\frac{g_i}{\tau_{forget}^g} + \sigma^g n_i^g - \frac{N}{\tau_{learn}} \frac{\partial E\left(x, x^t\right)}{\partial g_i} \end{aligned} \tag{15}$$

where g_i are constrained to be positive. n_{ij}, n_i^g are independent normalized unbiased Gaussian noise terms. The modified model has the same parameters as the original model and two additional parameters: the amplitude of the noise in plasticity of the excitabilities σ^g, and the decay time of the excitabilities τ_{forget}^g. The learning time constants of the excitabilities and the synapses are assumed the same (denoted τ_{learn}) and equal to the typical learning time observed in the monkeys' behavior (50 trials). As in the original model the cost that is optimized is the squared output error

$$E\left(x, x^t\right) = \frac{1}{2} \sum_{i=1}^{2} \left(x_i - x_i^t\right)^2 \tag{16}$$

The gradients of this cost with respect to W_{ij} and g_i are related to the error by

$$\begin{aligned} \frac{\partial E\left(x, x^t\right)}{\partial W_{ij}} &= \sum_{k=1}^{2} \left(x_k - x_k^t\right) Z_{ki} g_i x_j^t \\ \frac{\partial E\left(x, x^t\right)}{\partial g_i} &= \sum_{k=1}^{2} \left(x_k - x_k^t\right) Z_{ki} \sum_{j=1}^{2} W_{ij} x_j^t \end{aligned} \tag{17}$$

As in the simulations of the original model, before simulating the experiments we trained the model for 10000 trials, thus mimicking the monkeys' previous experience. The performance of the model was as good as that of the original model. Adding the gain changes had a relatively

small effect on the changes in PDs and therefore the parameters of the original model have not been changed much (σ = 0.02, σ^g = 0.018, τ_{forget} = 1500, τ_{learn} = 50, τ^g_{forget} = 500, φ = 60º, N = 10000)[2]. We tuned the parameters σ^g , τ^g_{forget} to match the distributions of changes in modulation depths in the control and learning simulations with the empirical distributions.

Results of modified model. We found that the modified model accounts much better than the original model for the observed statistics of the modulation depths. Remarkably, without fine tuning of parameters the modified model produced a distribution of modulation depths which is peaked at small values and is very similar to the empirical distribution (Fig. 5-s5A). This distribution of modulation depths was established in the pre-training stage of the model, prior to the simulation of the control experiment, and regardless of initial conditions. In the original model cells with weak modulation depths are rare. This property of the original model is related to the structure of the inputs to the cortical cells. Each cortical cell sums sine and cosine functions of direction, weighted by two synaptic weights (see Methods). Under these conditions, a cell's modulation depth is weak when a rare coincidence occurs in which both input synapses are weak simultaneously. More generally, when a cell receives multiple synaptic inputs with different directional tuning, the cell has a weak modulation depth when a rare configuration of synaptic weights occurs, such that the input tuning curves nearly cancel out. In contrast, in the modified model a neuron may have a weak modulation depth whenever its excitability is weak. In other words, in the original model a weak modulation depth requires several (two) variables to be weak simultaneously, whereas in the modified model it is sufficient that one variable, namely excitability, is weak. This occurs often as noise changes excitabilities, and consequently weak modulation depths are abundant.

Additionally, the modified model accounts much better for the distribution of the modulation depth changes in the control experiment (Fig. 5-s5B). As expected, changes in modulation depths became larger than in the original model because of the added contribution of the excitability changes. To account well for the size of the modulation depth changes in the control condition we had to assume that random excitability changes occur on a faster time constant than synaptic

[2] σ has been slightly reduced because the gain changes cause the PD changes to increase a little bit, indirectly. In the original model the random PD changes are slowed down by the learning signal as it makes corrections to the tuning curves in order to preserve the performance. In the modified model with the gain changes, part of these corrections is done by gain changes, thus less corrections are done in the synapses, and the PDs are somewhat more free to change.

changes ($\tau^{g}_{forget} = 500, \tau_{forget} = 1500$). The reason for this difference in time constants is that empirically, modulation depths had larger fractional changes than PDs. Changes in modulation depths had a standard deviation of ~3 Hz, which is roughly 60% of the mean modulation depth (~5 Hz). In contrast, PD changes had a standard deviation of ~30˚, which is roughly 15% of the maximal possible change of 180˚.

Adding the excitability changes also produced heavy tails in the distribution of changes in modulation depths, similar to the heavy tails observed in the experimental data (Fig. 5-s5B). These heavy tails result from the product of synaptic changes and excitability changes. In general, taking the product of two random variables tends to produce heavy tails, because occasionally the two variables simultaneously deviate from the average moderately, which causes the product to deviate from the average strongly. Thus, according to our model the heavy tails in the distribution of modulation depth changes reflect coincidences between excitability changes and synaptic changes. For similar reasons, our model produces heavy tails also in the distribution of the modulation depth changes in the learning experiment (Fig. 5-s5C) and in the distribution of the modulation depths (Fig. 5-s5A).

We found that in order to account for the changes in modulation depths in the learning condition (Fig. 5-s5C) we must assume that the excitabilities are tuned to improve performance. When we simulated the learning experiment without the excitability gradient term in Eq. (15), but still included the random changes in g_i, the model underestimated the size of the changes in modulation depths and the predicted anticorrelation between the adaptation and washout changes was much weaker than the empirical anticorrelation (not shown). Thus, according to our model excitability changes are not purely random, but are in fact tuned to improve the behavior.

The modified model still accounts reasonably well for the statistics of the changes in PDs (Fig. 5-s6). The only aspect in which the modified model is slightly worse than the original model, is that the predicted anticorrelation between the adaptation and washout PD changes is somewhat weaker than the observed anticorrelation and the anticorrelation predicted by the original model (compare Fig. 5-s6E with Figs. 5-2E, 5-5E in Results). Because in the modified model part of the learning is achieved by excitability changes, it has somewhat less learning related changes in PDs, and therefore less anticorrelation between adaptation and washout PD changes.

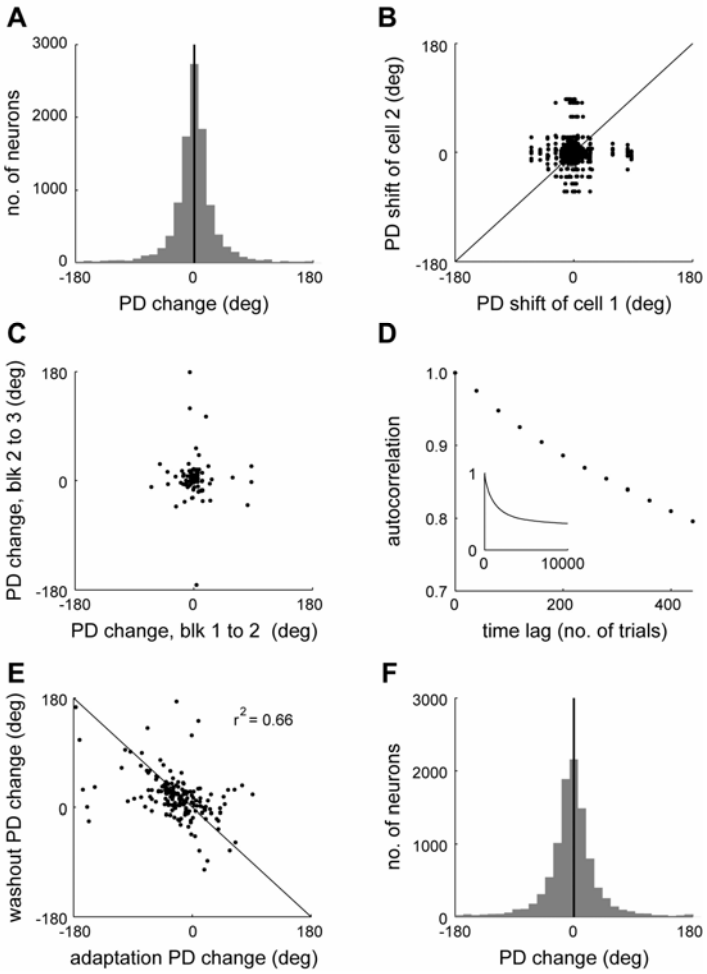

Figure 5-s6. Statistics of changes in tuning curves in simulations of control and learning experiments with the modified model. **A**, Distribution across cells of PD changes from block 1 to 3 in control simulation. **B**, PD changes from block 1 to 3 of pairs of cells. Each pair is represented by two points symmetrically positioned around the $y = x$ diagonal (solid line). **C**, PD change from block 1 to 2 vs. PD change from block 2 to 3, across cells in control simulation. **D**, Autocorrelation of population of PDs. **D inset**, Autocorrelation over long times. **E**, Adaptation PD changes vs. washout PD changes, across cells in learning simulation. Solid line represents the $y = -x$ diagonal. **F**, Distribution across cells of baseline-to-washout PD changes in learning simulation. To facilitate the comparison with the experimental results, we show in B, C and E samples of cells of the same size as in the corresponding subplots in Figure 5-2.

Extension of model to several forgetting time constants

In our model, noise driven changes in tuning curves are shaped by sensory driven learning, so they will not harm performance. In our simulations, the correlation time of the noise driven changes τ_{forget} was set to 1500 trials, in order to reproduce the observed correlation time of the tuning curves. In the absence of sensory feedback, the noise erases the motor memory stored in

the network, within several time constants τ_{forget}, i.e. within several thousands of trials. This consequence of the model seems implausible, since some motor skills are retained, at least partially, over many years without practice.

Here we show that by extending the model, such that it includes several forgetting time constants, it is possible to reproduce the observed correlation time of changes in tuning curves and yet maintain, at least partially, memory of motor skills for very long times. We assume a model with the same architecture as the original model, except that each sensory neuron makes a pair of synapses onto each motor cortical cell, including one unstable synapse and one stable synapse. Thus, instead of Eq. (5) in the Methods, the firing rates of the cortical cells are computed by

$$r_i = \sum_{j=1}^{2} \left(W_{ij}^{U} + W_{ij}^{S} \right) x_j^t \qquad (18)$$

where W_{ij}^{U}, W_{ij}^{S} are the weights of the unstable and stable synapses, respectively. W_{ij}^{U}, W_{ij}^{S} are modified by the same rule as in the original model (see Eqs. 9 and 11 in Methods), except that for W_{ij}^{U} we use τ_{forget}=750 trials, and for W_{ij}^{S} we use τ_{forget}=10^6 trials. Additionally, we set

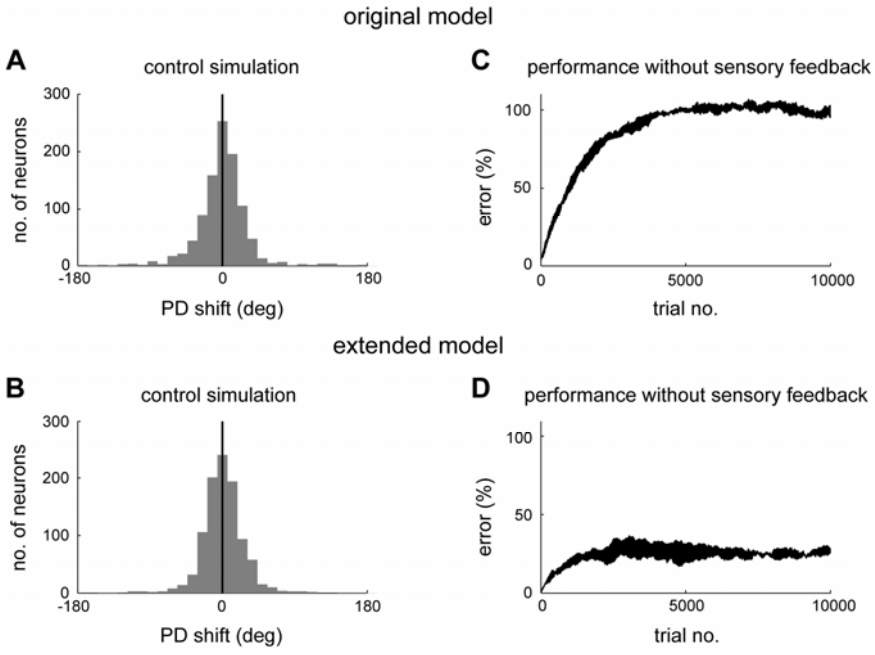

Figure 5-s7. Extension of model to several forgetting time constants. **A**, Distribution of block 1 to 3 PD changes in control simulation of original model. **B**, Same as A for extended model. **C**, Error in hand position, in % of desired movement amplitude, as a function of trial number in simulation of original model without sensory feedback. **D**, Same as C for extended model.

$\sigma = 0.018$ for both types of synapses, and the number of cells N=1000. A similar model with two forgetting and learning time constants has been proposed recently to explain interesting behavioral findings in learning experiments (Smith et al., 2006). Here we are also interested in how multiple time constants affect the changes in the neural representation.

Figure 5-s7 compares the original model with the extended model. In both models, simulation of the control experiment produces a similar amount of change in tuning curves (Fig. 5-s7A,B). On the one hand, in the extended model only half of the synapses are unstable, whereas in the original model all synapses are unstable. On the other hand, the forgetting time constant of the unstable synapses is shorter in the extended model compared with the original model. These two effects cancel out such that tuning curves change a similar amount in both models. However, the performance of the models is very different when simulating without sensory feedback over many trials. The original model completely forgets what it has learned (Fig. 5-s7C), whereas the extended model partially retains what it has learned (Fig. 5-s7D). The extended model maintains its memory through stable synapses. We conclude that by having several time constants, it is possible to account for the observed degree of change in tuning curves and have motor skills remembered over very long times.

Dependence of model performance on number of neurons

In our simulations, the model's output slightly deviated from the desired output. Furthermore, the output for the same target changed over trials, with a typical time constant of the learning time constant τ_{learn}. In terms of the synaptic weights, these errors imply that the system fluctuates around the optimal manifold, i.e. the valley in the error landscape (Fig. 3 in Results). In this section we examine the dependence of these errors on the number of neurons N. To asses the overall performance of the model we computed the mean squared error (MSE) in hand position

$$MSE = \left\langle \left\| x - x^t \right\|^2 \right\rangle \qquad (19)$$

where x is the hand position vector, x^t is the target position vector, and $\langle \ldots \rangle$ denotes averaging over many trials (we used 100000 trials). We estimated the MSE for different values of N, and found that it asymptotes at roughly N~100 (Fig. 5-s8A, dots).

To understand this behavior, it is useful to separate the squared error into the squared bias and variance contributions

$$MSE = bias^2 + variance \tag{20}$$

The bias is the systematic deviation of the hand from the target position

$$bias^2 = \left\langle \left\| \left\langle x \right\rangle_{x|\theta} - x^t(\theta) \right\|^2 \right\rangle_\theta \tag{21}$$

Here $\langle \ldots \rangle_{x|\theta}$ denotes averaging over trials for which the target was in direction θ, $x^t(\theta)$ is the position of the target in direction θ, and $\langle \ldots \rangle_\theta$ denotes averaging over movement directions. The bias is caused by the forgetting term in our synaptic weight update rule (Eq. 9 in Methods), which biases the synaptic weights slightly from the optimal manifold towards zero. This bias is independent of N (Fig. 5-s8A, circles; small changes are caused by sampling noise). The size of the bias depends on the ratio of time constants $\tau_{learn}/\ \tau_{forget}$ which determines the relative sizes of the forgetting and learning terms. When $\tau_{learn}/\ \tau_{forget}$ increases the forgetting term is more effective in biasing the synaptic weights from the optimal manifold, and the bias increase. At the regime where τ_{forget} is much longer than τ_{learn} this relation is approximately linear (Fig. 5-s8B)

$$bias \sim \frac{\tau_{\text{learn}}}{\tau_{\text{forget}}} \tag{22}$$

The second contribution to the MSE is the variance, i.e. the randomness in hand position

$$variance = \left\langle \left\langle \left\| x - \langle x \rangle_{x|\theta} \right\|^2 \right\rangle_{x|\theta} \right\rangle_\theta \tag{23}$$

The variability in hand position is caused by the synaptic plasticity noise which pushes the synaptic weights around the optimal manifold. The size of the variance depends on a number of factors. First, the variance decreases with N (Fig. 5-s8A, crosses), proportionally to $1/N$ (not shown), because there are on the order of N independent noise sources which average out at the output. Second, the variance scales with the variance of the noise σ^2 (Fig. 5-s8C). Lastly, the variance depends on τ_{learn}. When τ_{learn} increases, the learning signal becomes weaker, and thus the force driving the synaptic weights back to the optimal manifold weakens (Eq. 9 in Methods). Consequently, the variance in synaptic weights and the motor output increases, in proportion to τ_{learn} (Fig. 5-s8D). Putting these different factors together, we have approximately

$$variance \sim \frac{\tau_{\text{learn}}\sigma^2}{N} \tag{24}$$

Now we are in a position to explain why the MSE asymptotes at roughly N~100. The MSE asymptotes when the variance term becomes small relative to the bias term, which according to Eqs. (22),(24) implies

$$\left(\frac{\tau_{\text{learn}}}{\tau_{\text{forget}}}\right)^2 \; \square \; \frac{\tau_{\text{learn}}\sigma^2}{N} \tag{25}$$

Rearranging terms we find

$$N \; \square \; \frac{\left(\tau_{\text{forget}}\sigma\right)^2}{\tau_{\text{learn}}} \sim 30 \tag{26}$$

For the parameter values that we used in our simulations (τ_{learn}=50, σ=0.025, τ_{forget}=1500), the right hand side of Eq. (26) is approximately 30. This explains why the error does not decrease much beyond N~100.

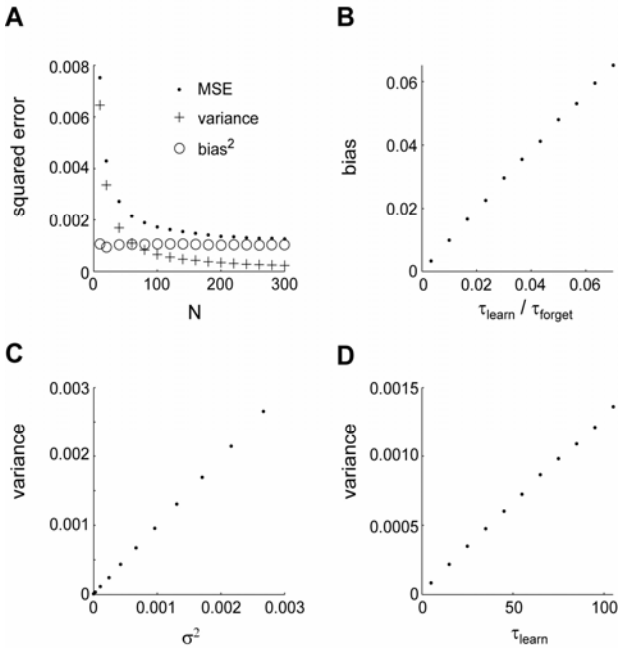

Figure 5-s8. Dependence of model's error in position on parameters. Baseline parameters were σ = 0.025, τ_{forget} =1500, τ_{learn} = 50, and N = 100. **A**, Simulations with different N. **B**, Simulations with different ratios of τ_{forget} and τ_{learn}. **C**, Simulations with different σ. **D**, Simulations with different τ_{learn}.

6 Causal link between motor cortex and adaptation: a rTMS study[3]

6.1 Introduction

The human motor system generally uses acquired knowledge of the mechanical properties of both the arm and the environment in the control of reaching behaviors (Lackner and Dizio, 1994; Shadmehr and Mussa-Ivaldi, 1994; Sainburg et al., 1999). This allows the system to attenuate expected disturbances in an anticipatory manner and improve motor performance. Adapting to a novel dynamic environment involves learning new mechanical properties. Memories of specific environments may over time become resistant to interference from new learning, in a process referred to as motor memory consolidation (Brashers-Krug et al., 1996; Shadmehr and Brashers-Krug, 1997).

Several studies have explored the neural structures underlying adaptation to novel mechanical contexts using functional imaging, transcranial magnetic stimulation (TMS), and neurological populations. A network including the dorsolateral prefrontal cortex, posterior parietal cortex, striatum, and cerebellum is engaged specifically in motor adaptation, and not just motor execution (Shadmehr and Holcomb, 1997; Krebs et al., 1998; Nezafat et al., 2001; Della-Maggiore et al., 2004; Maschke et al., 2004; Smith and Shadmehr, 2005). This network may provide both cognitive responses to movement error (Malfait and Ostry, 2004) and error-driven acquisition of an internal model of the movement dynamics (Kawato, 1999). As the memory of the movement dynamics consolidates, activity partially shifts to a network including premotor cortex, posterior parietal cortex, and cerebellar cortex, which may store the internal model (Shadmehr and Holcomb, 1997; Krebs et al., 1998; Nezafat et al., 2001).

Human primary motor cortex (M1) is involved in several types of motor skill learning (Pascual-Leone et al., 1994; Karni et al., 1995; Ghilardi et al., 2000; Sanes and Donoghue, 2000) but does not appear to be differentially activated when adapting to new movement dynamics, compared to baseline execution (Shadmehr and Holcomb, 1997; Krebs et al., 1998). Single-unit recordings in monkeys, however, suggest that involvement of M1 in motor adaptation may not be apparent in more global measures of activity. In particular, distributed subsets of M1 neurons

[3] This thesis chapter is a revision of a previously published article: Richardson AG, Overduin SA, Valero-Cabre A, Padoa-Schioppa C, Pascual-Leone A, Bizzi E, Press DZ (2006) Disruption of primary motor cortex before learning impairs memory of movement dynamics. J Neurosci 26:12466-12470.

appear to support a memory trace of novel movement dynamics, while the population as a whole reflects only the task execution (Li et al., 2001).

The present study aimed to more directly assess the role of M1 in human adaptation to novel dynamical environments. We used low-frequency, repetitive TMS (rTMS) to interfere with M1 function while subjects performed reaching movements in a velocity-dependent force field. Applying rTMS to M1 prior to the first exposure to the force field, we tested subjects' ability to adapt to the novel dynamics as well as their ability to recall these dynamics 24 hours later. We found that M1 disruption did not affect initial adaptation, but did hinder next-day performance relative to controls. These results suggest that a network including M1 may be critical to the early stages of motor memory development.

6.2 Methods

Paradigm

Sixteen right-handed subjects (mean 25 years old; 6 males) participated in the experiment. Participants were screened for history of seizures, familial epilepsy, and other TMS contraindications. Ethical approval was obtained through the MIT Committee On the Use of Humans as Experimental Subjects. The subjects were randomly assigned to two experimental groups ("control" and "rTMS").

Subjects were instructed to hold onto a robotic manipulandum with their right hand and make reaching movements in the horizontal plane to targets presented on a vertically-oriented monitor (for details, see Shadmehr and Mussa-Ivaldi, 1994). Targets included four peripheral squares spaced around a central square at a distance of 10 cm, such that the movements from either central to peripheral or peripheral to central resulted in eight movement directions, uniformly spanning 360º. The peripheral squares were located at 0º, 45º, 90º, and 135º, according to the direction labels in Figure 6-2C. Subjects were given 0.50 ± 0.05 s to complete each movement. Trials completed in the specified time were indicated to the subject by a brief sound. Trials completed too quickly or too slowly were indicated to the subject by a transition in the target color from white to red or blue, respectively.

Participants performed reaching movements to a pseudorandom sequence of targets in three different epochs, denoted as "baseline" (two subepochs of 253 ± 8 trials and 152 ± 4 trials separated by 15 min), "learning" (400 ± 0 trials), and "retest" (403 ± 10 trials; mean ± standard

deviation). The number of trials in each (sub)epoch for the control group and rTMS group did not significantly differ. The duration of the interval between the baseline and learning epochs was approximately 15 min. The learning and retest epochs were separated by 24 hr.

All subjects experienced a null (0 N·s/m) force field during the baseline epoch, and a velocity-dependent clockwise field generated by the robotic manipulandum in the learning and retest epochs. The curl forces, of magnitude 15 N·s/m, were calculated on-line as $f = \mathbf{B}\dot{x}$, where $\mathrm{B} = \begin{bmatrix} 0 & 15 \\ -15 & 0 \end{bmatrix}$ and $\dot{x}$ was the movement velocity.

TMS was delivered using a Magstim Super Rapid stimulator (Whitland, Wales, UK). Between the two subepochs of the baseline epoch, the location and threshold for stimulation were determined in the rTMS subjects. This involved using single pulses of TMS over the left motor cortex to determine: 1) the scalp location capable of reliably and maximally inducing visible contractions in the right biceps brachii muscle, and 2) the intensity threshold necessary to reliably elicit a motor-evoked potential in the resting right biceps muscle following standard criteria (at least 50 μV, present in 5 out of 10 consecutive attempts). The intensity level of the rTMS used in the experiment was then calculated to be 90% of the resting biceps motor threshold level, an intensity known to induce long-lasting depression of motor cortex excitability (Gangitano et al., 2002; Romero et al., 2002). Between the baseline and learning epochs, rTMS pulses were applied at a frequency of 1 Hz for 15 min. (i.e. 900 pulses) using a hand-held figure-of-eight coil (double 70 mm; Magstim), positioned tangentially relative to the scalp in a 45^{o} posterior-to-anterior and lateral-to-medial orientation, at the same location found to optimally evoke biceps activity during localization.

We did not use sham stimulation in control subjects because the rTMS was delivered "offline", while the subject was at rest prior to force field exposure. Thus it was unlikely that any non-specific attentional or behavioral effects of the TMS were present during the subsequent learning epoch (Robertson et al., 2003). In support of this claim, we found that rTMS and control subjects' performance in the learning epoch (i.e. just after rTMS was applied) did not significantly differ, arguing that rTMS had no immediate, specific or non-specific effect on motor performance (Fig. 6-2A; see Results).

Analysis

We quantified performance on each trial as the signed peak perpendicular deviation relative to a straight line connecting the beginning and end positions of the trial (Shadmehr and Moussavi, 2000). This performance measure was normalized in each epoch and for each group by subtracting the group's average baseline epoch performance. The normalization removed inter-group differences in baseline task performance in order to isolate learning-specific performance changes. Note that without normalization, the pattern of statistically significant results presented in the Results was not altered. Trials in which the subject failed to reach the target within a 0.50 ± 0.25-s time window were excluded from the analysis. Trials were binned by 16 trials in each epoch and group. Statistical results were based on the within-bin-averaged perpendicular deviation. Not all subjects were given exactly 400 trials to complete in each of the learning and retest epochs (see above), hence we only used the first 24 (rather than 25) 16-trial bins in each of these epochs for the statistical tests. Main and interaction effects of rTMS, time (either individual or grouped time bins; see Results), and movement direction were assessed using repeated measures ANOVAs. All significant effects (at the $p < 0.05$ level) are reported.

To assess the robustness of our results, we repeated the analysis using two other measures of performance: signed deviation angle (the angle between the lines connecting beginning and end positions and beginning and maximum speed positions)(Della-Maggiore et al., 2004) and signed deviation area (the area between the hand trajectory and the line connecting beginning and end positions). The results using each of these measures were very similar; for brevity we report only the analysis using deviation angle in the Results (Fig. 6-2B).

6.3 Results

Subjects exhibited a typical pattern of adaptation to the velocity-dependent force field (Fig. 6-1; Shadmehr and Mussa-Ivaldi, 1994). Reaching trajectories produced in the clockwise force field environment were initially deviated in the clockwise direction. With practice, in both the learning and retest epoch, the trajectories returned to a less-deviated form like that exhibited under null-field conditions.

In the baseline epoch, the performance was stable for both rTMS and control groups (i.e. there was no significant effect of Time) and there were no significant differences between the groups (Fig. 6-2A, left panel). Following the baseline epoch, the rTMS subjects received 15 min.

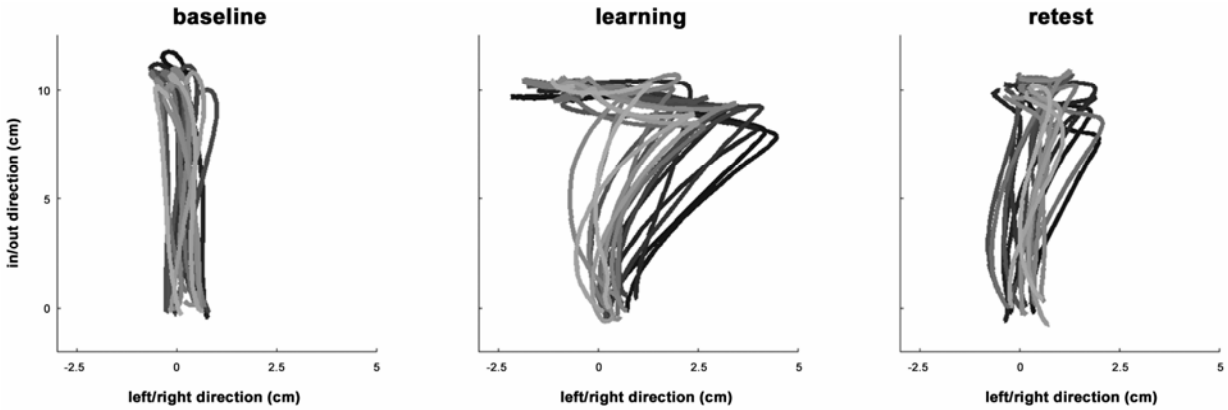

Figure 6-1. Subjects adapted to a velocity-dependent force field introduced in the learning epoch and repeated at retest 24 hr. later. The sample trajectories include all those performed by one control subject in the forward direction of reach, from among the 150 baseline trials and the first 150 trials performed in the two clockwise-field epochs. The temporal order of the trajectories within each epoch is given by the transition from black (early trials) to gray (late trials).

of 1-Hz rTMS centered over M1, while control subjects waited for an equivalent time while seated in the same position. Immediately after this interval, all participants performed a 400-trial learning epoch in a clockwise force field environment generated by the robotic manipulandum. Subjects adapted to the force field (Fig. 6-2A, middle panel), as supported by a significant effect of Time on the peak perpendicular deviation ($F_{(23,322)} = 24.48$, $p < 0.0001$). Notably, there was no significant effect of rTMS on subjects' performance.

An effect of rTMS was, however, apparent when the participants returned 24 hours following learning for the retest epoch. Within the 400-trial retest epoch, subjects again adapted to the clockwise force field (Fig. 6-2A, right panel), captured as before by a significant main effect of Time ($F_{(23,322)} = 8.33$, $p < 0.0001$). But in contrast to the learning epoch, there was also a significant main effect of rTMS ($F_{(1,14)} = 3.15$, $p = 0.0482$), with the rTMS group performing with a higher level of error than the control group. This relative difference in error cannot be attributed to a relative difference in movement speed (to which the forces were proportional), as there was no significant main or interaction effect of rTMS on peak speed in the retest (or any other) epoch.

rTMS did not completely interfere with the memory of the novel dynamics experienced in the learning epoch, as both groups performed with significantly less error at the beginning of the retest epoch than they did at the beginning of the learning epoch, although to different degrees. Indeed, in a comparison of the peak perpendicular deviation in the first third of the learning and

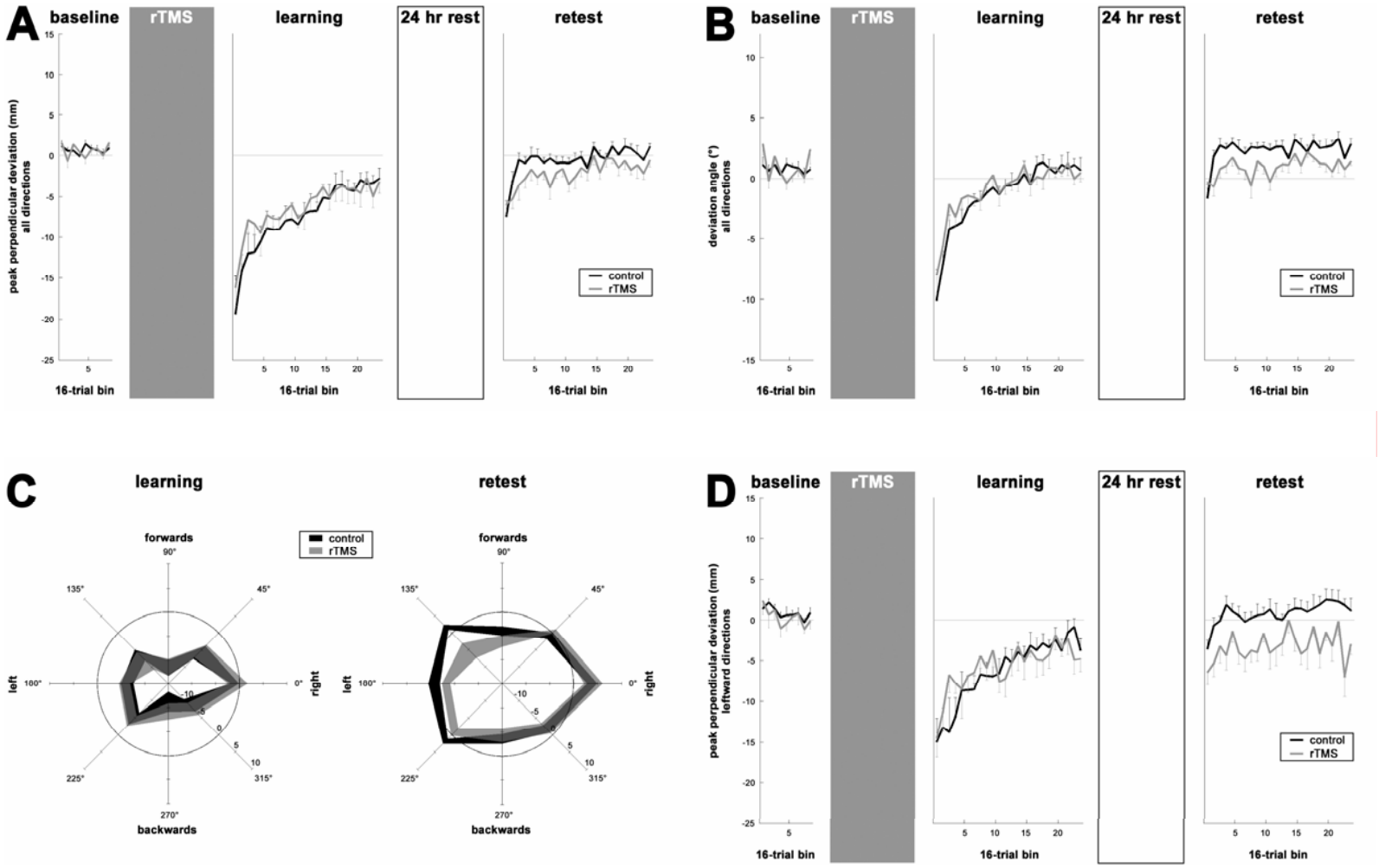

Figure 6-2. rTMS of M1 spares initial motor performance and force field acquisition but impairs retest performance. **A**, The performance (quantified by the baseline-normalized peak perpendicular deviation) of control (black) and rTMS (gray) groups are shown for baseline, learning, and retest trials (mean ± s.e.m. of 16-trial bins; lower error bar for control group and upper error bar for rTMS group are removed for clarity). **B**, Same as A, but using the baseline-normalized deviation angle as the performance measure. **C**, The average learning and retest performance error for control (black) and rTMS (gray) groups is shown for each movement direction (shaded region indicates ± 1 s.e.m. around the mean performance over the entire epoch). The performance (shown on the radial axis) is quantified by the peak perpendicular deviation, where negative errors indicate clockwise deviation, as in A. **D**, Same as A, but restricted to only leftward-directed (135º, 180º, and 225º) movements.

retest epochs (Fig. 6-2A), there were significant effects of both Time and its interaction with rTMS ($F_{(1,14)} = 100.67$, $p < 0.0001$ and $F_{(1,14)} = 6.47$, $p = 0.0089$, respectively). In fact, beyond the first few trials, the initial retest performance error was even less than late learning epoch error, particularly for the control group. Again, significant Time and rTMS × Time effects ($F_{(1,14)} = 8.36$, $p = 0.0040$ and $F_{(1,14)} = 3.54$, $p = 0.0383$, respectively) were evident in a comparison of the last third of the learning epoch with the first third of the retest epoch (Fig. 6-2A).

In addition, the effect of rTMS in the retest epoch was not uniform over all eight movement directions (Fig. 6-2C, right panel). A repeated-measures ANOVA, again using the peak perpendicular deviation measure, revealed significant main effects of rTMS ($F_{(1,14)} = 3.84$, $p = 0.0325$) and direction ($F_{(7,98)} = 13.47$, $p < 0.0001$), as well as a significant rTMS × direction interaction ($F_{(7,98)} = 2.71$, $p = 0.0292$). In particular, the rTMS group performed with relatively more error only in leftward-directed movements (Fig. 6-2C, right panel). In contrast, for the learning epoch (Fig. 6-2C, left panel), the same repeated-measures ANOVA revealed no significant main or interaction effects of rTMS, only a significant main effect of direction ($F_{(7,98)} = 25.52$, $p < 0.0001$). Thus, the movement direction-specific effect of rTMS was only present at retest, not during initial learning.

All of the statistically significant trends reported for the all-direction analysis were seen when restricting the analysis to just the three leftward-directed (135º, 180º, and 225º) movements (Fig. 6-2D). In particular, during the baseline epoch (Fig. 6-2D, left panel), there was no effect of Time or rTMS on performance. During the learning epoch (Fig. 6-2D, middle panel), there was only a significant main effect of Time on the peak perpendicular deviation ($F_{(23,322)} = 11.18$, $p < 0.0001$). During the retest epoch (Fig. 6-2D, right panel), their were significant main effects of both Time and rTMS ($F_{(22,308)} = 2.83$, $p = 0.0002$ and $F_{(1,14)} = 9.69$, $p = 0.0024$, respectively). This analysis again shows that the directionally-specific effect of rTMS during retest performance was not also present during initial acquisition of the motor skill.

Finally, the results presented above were robust in that they could be replicated using other performance measures. For example, using deviation angle as the measure of performance (see Methods), there were again no significant changes in the baseline epoch (Fig. 6-2B, left panel) and only a main effect of Time ($F_{(23,322)} = 25.04$, $p < 0.0001$) in the learning epoch (Fig. 6-2B, middle panel). In the retest epoch (Fig. 6-2B, right panel), there were significant effects of Time and rTMS ($F_{(23,322)} = 3.94$, $p < 0.0001$ and $F_{(1,14)} = 10.57$, $p = 0.0018$, respectively), as reported

previously with the peak perpendicular deviation measure. Note that in the retest epoch, the deviation angle measure indicates that the control group actually overcompensates for the clockwise force field (i.e. has counterclockwise error), while the rTMS group's error is closer to zero (Fig. 6-2B, right panel). It has been previously shown that increasing uninterrupted practice in a force field leads to increasing overcompensation of movement trajectories (Thoroughman and Shadmehr, 2000). Thus, we interpret the greater counterclockwise error as being more adaptive and, consequently, that the rTMS group was impaired relative to the control group, consistent with our previous conclusion.

6.4 Discussion

In this experiment, we studied the role of M1 in the adaptive control of human reaching movements. We used rTMS to disrupt M1 function just prior to subjects' initial exposure to a velocity-dependent force field. rTMS had no effect on initial performance or adaptation to the force field. However, when subjects performed in the same force field 24 hours later, those who had received rTMS the day before performed worse than those who had not.

The use of a 15-min. train of subthreshold 1-Hz rTMS was specifically chosen to depress M1 excitability for the duration of the learning epoch (Chen et al., 1997; Gangitano et al., 2002; Romero et al., 2002). Nevertheless, we found that rTMS subjects and control subjects performed equally in this epoch. Given that changes in M1 excitability are known to be sufficient to measurably affect behavior (Pascual-Leone et al., 1994), the implication is either that M1 is not involved in initial motor adaptation (Diedrichsen et al., 2005; Paz et al., 2005) or that its involvement can be acutely compensated by the recruitment of other brain areas (Lee et al., 2003). Indeed, while changes in M1 neuronal activity mirror those of muscle activity in force field adaptation (Li et al., 2001), other cortical motor areas show similar activity changes (Padoa-Schioppa et al., 2004; Xiao et al., 2006). The non-necessity of M1 in motor performance and early motor learning has been previously documented in both force field tasks and ballistic finger movement tasks (Muellbacher et al., 2002; Baraduc et al., 2004). It is important to note, however, that other motor cortical and even subcortical areas may also have been influenced by the stimulation, either by transynaptic transmission or direct volume conduction of the magnetic field effects (Chouinard et al., 2003), though the latter should have been quite minimal (Fox et al., 1997).

The novel result in our study was the effect of rTMS on retest performance. Both groups exhibited some memory of the force field in the retest epoch, since initial retest errors were not as large as those of the early learning epoch. However, the rTMS subjects exhibited a relative memory impairment. The memory impairment was not compensated by the return of M1 to normal function approximately 10 min. following the end of stimulation, once the effects of the stimulation subsided (Romero et al., 2002). This suggests that M1 plays an important role early in motor memory formation, starting specifically at the time of acquisition. This conclusion is substantiated by recent electrophysiological evidence that M1 supports a short-term memory trace of novel movement dynamics (Li et al., 2001). Our conclusion is also consistent with a recent rTMS study by a different group claiming M1 maintains a persistent representation of previously learned motor skills (Cothros et al., 2006).

The relative impairment in performance of the rTMS group in the retest epoch was manifest only in leftward movement directions. This directional selectivity was an unexpected finding, but the cortical representation of arm muscles as well as their activation in force field learning may offer an explanation. The leftward-directional tuning of the impairment is nearly identical to the directionally-specific recruitment pattern of the biceps brachii muscle in a clockwise velocity-dependent force field (Thoroughman and Shadmehr, 1999). The rTMS protocol employed here targeted the M1 representation of the biceps muscle, but selective stimulation of this representation is unlikely given the close proximity of other muscle representations in motor cortex (Schieber, 2001) and the known spatial resolution of TMS (Siebner and Rothwell, 2003). Rather, the similarity in directional tuning of the impairment and the biceps recruitment may be related to the distribution of corticospinal projections to proximal arm motor neuron pools. In humans and other primates, there are significantly more corticomotoneuronal cells projecting to biceps than triceps motor neurons (Palmer and Ashby, 1992). Furthermore, contrary to traditional clinical assumptions, lesions in human motor cortex lead to a corresponding distribution of proximal arm weakness: elbow flexors are affected to a relatively greater extent than elbow extensors in the paretic limb (Colebatch et al., 1986; Colebatch and Gandevia, 1989; Andrews and Bohannon, 2000). Thus we suggest that the "virtual lesion" created by rTMS had relatively greater effect on directions of movement that involved the greatest biceps activation. This may have preferentially impaired the memory of the dynamics in these directions, assuming the process of early memory formation is sufficiently local and not as robust to M1 disruption as

motor performance.

In some respects, our results are similar to those of Muellbacher et al. (2002) who found, using a ballistic finger movement task, that rTMS to M1 immediately after learning interfered with retention of the motor skill. They concluded M1 is involved in early motor memory consolidation, where consolidation was defined as the stabilization of the memory (i.e., resistance to interference). In our study, we applied rTMS before, rather than after learning, but it similarly interfered with the motor memory. However, unlike the Muellbacher et al. (2002) study, the interference did not bring retest performance in the force field back to a naïve state. This was true even if one considers only leftward-directed movements (Fig. 6-2D). This difference in degree of learning retention after M1 disruption between a ballistic movement task (as in Muellbacher et al., 2002) and a force field adaptation task (as in our study) was noted explicitly by Baraduc et al. (2004). However, unlike Baraduc et al. (2004), our study identified an important role for M1 in motor memory formation of novel dynamics, one which is not related to memory stabilization.

Indeed, the TMS interference in our study resulted in a pattern of retest performance that more closely resembles a second form of consolidation documented in the procedural memory literature—an offline skill improvement that occurs between practice sessions (Robertson et al., 2004). In particular, immediately after the first few trials (during which cognitive systems may dominate the behavior as subjects readjust to the experimental conditions), the control group showed an improved performance relative to their error level late in the learning epoch. In contrast, the rTMS group showed no such improvement. Therefore, disruption of a network including M1 may selectively impair offline skill enhancement, as shown in sequence learning tasks (Robertson et al., 2005). While further work will be needed to specifically address this issue, our present findings are remarkable for their implication that proper M1 function during adaptation to a novel dynamical environment is important for the full development of a memory of these dynamics.

Conclusion

Since about 1870, the precentral cortex has been know to be the primary seat of motor activity in the cerebral cortex (Humphrey, 1986). The work in this thesis follows a long line of investigation since that time concerning the specific nature of cortical motor processing. Using both neural recording in monkeys and neural stimulation in humans, we studied the role of the precentral cortex in planning and controlling reaching movements and in learning to reach in the presence of novel perturbing forces. Our results largely confirm and extend previous anatomical and physiological studies showing that many distinct areas of the precentral cortex are involved in motor control and motor learning. Most of the relevant discussion of these results has been included at the end of each chapter. However, there are several additional points to be made about the local field potential (LFP) results from Chapters 3 and 4. Below, we discuss these LFP results and propose future experiments that might aid their interpretation.

Directional tuning of precentral cortical LFPs

The amplitude of LFP oscillations, both in the beta and gamma frequency bands, was often tuned to movement direction (see Chapter 3). Directional tuning of LFPs recorded during reaching movements has only recently been documented, both in the precentral cortex (Mehring et al., 2003a; Rickert et al., 2005; Heldman et al., 2006; O'Leary and Hatsopoulos, 2006) and in the posterior parietal cortex (Scherberger et al., 2005). These findings potentially have both physiological and engineering implications. First, it has been suggested that the tuned LFP implies that their may be local spatial order to directional representation in the cortex (Mehring et al., 2003b). Second, it has been suggested that the LFP may be a useful neuroprosthetic control signal given its direction informational content and the fact that it is easier than single cells to record stably for long periods of time (Andersen et al., 2004).

However, our data argues against both of these implications. We and others have found that simultaneously recorded LFPs on different electrodes, even when they are many millimeters apart, have very correlated tuning curves resulting in nonuniform, clustered preferred direction distributions (Scherberger et al., 2005; O'Leary and Hatsopoulos, 2006). Furthermore, we found there was almost no correlation between the tuning curves of LFP and single cell activity recorded on the same electrode. These two facts appear to be at odds with the hypothesis that LFP tuning is a result of local neuronal tuning. As an alternative hypothesis, the more global

tuning of the LFP that we observed may be due to anisotropic task demands, as described in the Discussion of Chapter 3. For example if the amplitude of the LFP oscillation reflects the required attention to a cue signal or the amount of isometric contraction needed during a hold period, then any movement direction-related differences in these quantities would result in LFP tuning. If LFP tuning is a function of the task demands, then it would probably be quite limited as a neuroprosthetic control signal without constant recalibration as task demands, and perhaps even attentional states, change.

There are several further studies that could be done to determine whether this alternative hypothesis is correct. With respect to the beta-band target-hold tuning, a biomechanical model of the primate arm could provide insight into whether the static forces required to hold the limb at each of the eight peripheral targets (i.e. the joint torques counteracting gravitational forces at each posture) are tuned similarly. Also, further recordings of muscle activity may reveal more co-contraction in some directions than others. With respect to the beta-band cue-related tuning, we have preliminary evidence that the tuning curves were oriented along movement directions that experienced the most incorrect trials (data not shown). Thus, the tuning could be related to expectation of movement error or reward or an attentional process. To test these possibilities, the reaching task could be modified to get a predetermined directional bias in reaching difficulty or reward, which could then be compared to the directional bias of the LFP oscillation amplitude.

The directional tuning of gamma-band oscillation amplitude during movement brings up a different but related issue. The increase in LFP power during movement is quite a broadband phenomenon, extending from around 70 Hz up to at least 200 Hz (Rickert et al., 2005). We also observed this broadband power increase extending all the way up to 1000 Hz, well into the frequency range of action potential waveforms (data not shown). Action potential waveforms, which are generally thought to have high frequency content, are also associated with slower membrane potential fluctuations (e.g. depolarizing afterpotentials and after-hyperpolarizations) that probably have power in the 70-200 Hz range. Thus it is certainly possible that the gamma-band power increase during movement is merely a reflection of the fact that, over the population, cortical motor areas have the highest fire rates during movement (see Chapter 2). If this is the case then the gamma-band directional tuning, and the nonuniform preferred direction distribution of this tuning, could be caused by the need for globally higher firing rates in some directions due to the need for greater muscular effort, for example. To test this possibility an additional analysis

could look at whether single cell firing rates, averaged across the whole population in each direction separately, have the same overall directional bias as the gamma-band PD distribution. One piece of data that is not obviously consistent with this alternative hypothesis is the phase-locking of spikes to the gamma oscillations. Modeling, both of the frequency content of action potentials and of the phase-locking of spikes to these frequencies, may provide some insight. As an aside, there does seem to be a gamma-band process involved in motor control that may be distinct from global cortical firing rates. In particular, at low gamma-band frequencies (30-70 Hz) there is increased corticomuscular coherence during movement preparation (Schoffelen et al., 2005) and movement execution (Marsden et al., 2000; Omlor et al., 2007).

Precentral cortical LFPs and neuroprosthetic applications

The discussion above suggests that the directional information in the LFP signal may be task-dependent and thus not well suited to control a neurprosthetic device. However, there is one minor engineering application related to the LFP signal that has become apparent in this work. In particular, while the high gamma band power may reflect global spiking activity in the motor cortex as mentioned above, even higher frequency power (600-1000 Hz) seemed to reflect the firing rate of local single cells recorded on the same electrode. This of course makes sense given that multiunit activity is obtained by bandpass filtering the recording at around 300-9000 Hz. In fact, although we did not include this in the thesis, the average power in the 600-1000 Hz band (which we'll call the spike band) was often extremely closely correlated with the firing rate of the cell that had the highest amplitude waveform.

Neuroprosthetic devices will ultimately require that recorded neural control signals be sent to the device wirelessly. But since detecting action potentials requires a sampling rate of around 20000 Hz per channel and many channels (perhaps hundreds) are required for adequate control, the power requirements on the wireless transmission are very high. Although there are many proposed methods of decreasing the bandwidth of the control signal and thus the power requirement (Zumsteg et al., 2005), a novel method would be to simply use the spike-band spectral power as a surrogate for the firing rate. This would allow recording at around 2000 Hz per channel—a ten-fold reduction in bandwidth. This is approximately the bandwidth reduction that could be achieved by transmitting only spike times (Zumsteg et al., 2005). However the advantage of transmitting the continuous signal at about 2000 Hz is that the lower frequency

(e.g. beta-band) LFP signal would also be available to use as a part of the control signal. Aside from neuroprosthetic applications, this approach could also be useful as a low-power alternative for wirelessly recording neural activity from freely moving animals.

References

Akkal D, Bioulac B, Audin J, Burbaud P (2002) Comparison of neuronal activity in the rostral supplementary and cingulate motor areas during a task with cognitive and motor demands. Eur J Neurosci 15:887-904.

Alexander GE, Crutcher MD (1990) Preparation for movement: neural representations of intended direction in three motor areas of the monkey. J Neurophysiol 64:133-150.

Amirikian B, Georgopoulos AP (2003) Modular organization of directionally tuned cells in the motor cortex: is there a short-range order? Proc Natl Acad Sci U S A 100:12474-12479.

Andersen RA, Musallam S, Pesaran B (2004) Selecting the signals for a brain-machine interface. Curr Opin Neurobiol 14:720-726.

Andrews AW, Bohannon RW (2000) Distribution of muscle strength impairments following stroke. Clin Rehabil 14:79-87.

Ariff G, Donchin O, Nanayakkara T, Shadmehr R (2002) A real-time state predictor in motor control: study of saccadic eye movements during unseen reaching movements. J Neurosci 22:7721-7729.

Atkeson CG (1989) Learning arm kinematics and dynamics. Annu Rev Neurosci 12:157-183.

Backus DA, Ye S, Russo GS, Crutcher MD (2001) Neural activity correlated with the preparation and execution of visually guided arm movements in the cingulate motor area of the monkey. Exp Brain Res 140:182-189.

Baker SN, Olivier E, Lemon RN (1997) Coherent oscillations in monkey motor cortex and hand muscle EMG show task-dependent modulation. J Physiol 501 (Pt 1):225-241.

Baker SN, Kilner JM, Pinches EM, Lemon RN (1999) The role of synchrony and oscillations in the motor output. Exp Brain Res 128:109-117.

Baker SN, Spinks R, Jackson A, Lemon RN (2001) Synchronization in monkey motor cortex during a precision grip task. I. Task-dependent modulation in single-unit synchrony. J Neurophysiol 85:869-885.

Baraduc P, Lang N, Rothwell JC, Wolpert DM (2004) Consolidation of dynamic motor learning is not disrupted by rTMS of primary motor cortex. Curr Biol 14:252-256.

Ben-Shaul Y, Stark E, Asher I, Drori R, Nadasdy Z, Abeles M (2003) Dynamical organization of directional tuning in the primate premotor and primary motor cortex. J Neurophysiol 89:1136-1142.

Bhushan N, Shadmehr R (1999) Computational nature of human adaptive control during learning of reaching movements in force fields. Biol Cybern 81:39-60.

Brainard MS, Doupe AJ (2000) Auditory feedback in learning and maintenance of vocal behaviour. Nat Rev Neurosci 1:31-40.

Brashers-Krug T, Shadmehr R, Bizzi E (1996) Consolidation in human motor memory. Nature 382:252-255.

Brunia CH (1999) Neural aspects of anticipatory behavior. Acta Psychol (Amst) 101:213-242.

Burdet E, Osu R, Franklin DW, Milner TE, Kawato M (2001) The central nervous system stabilizes unstable dynamics by learning optimal impedance. Nature 414:446-449.

Cadoret G, Smith AM (1995) Input-output properties of hand-related cells in the ventral cingulate cortex in the monkey. J Neurophysiol 73:2584-2590.

Cadoret G, Smith AM (1997) Comparison of the neuronal activity in the SMA and the ventral cingulate cortex during prehension in the monkey. J Neurophysiol 77:153-166.

Caithness G, Osu R, Bays P, Chase H, Klassen J, Kawato M, Wolpert DM, Flanagan JR (2004) Failure to consolidate the consolidation theory of learning for sensorimotor adaptation tasks. J Neurosci 24:8662-8671.

Cardoso de Oliveira S, Gribova A, Donchin O, Bergman H, Vaadia E (2001) Neural interactions between motor cortical hemispheres during bimanual and unimanual arm movements. Eur J Neurosci 14:1881-1896.

Chan SS, Moran DW (2006) Computational model of a primate arm: from hand position to joint angles, joint torques and muscle forces. J Neural Eng 3:327-337.

Cheah CC, Liu C, Slotine JJE (2006) Adaptive tracking control for robots with unknown kinematic and dynamic properties. International Journal of Robotics Research 25:283-296.

Chen D, Fetz EE (2005) Characteristic membrane potential trajectories in primate sensorimotor cortex neurons recorded in vivo. J Neurophysiol 94:2713-2725.

Chen H, Hua SE, Smith MA, Lenz FA, Shadmehr R (2006) Effects of human cerebellar thalamus disruption on adaptive control of reaching. Cereb Cortex 16:1462-1473.

Chen R, Classen J, Gerloff C, Celnik P, Wassermann EM, Hallett M, Cohen LG (1997) Depression of motor cortex excitability by low-frequency transcranial magnetic stimulation. Neurology 48:1398-1403.

Cheney PD, Fetz EE (1980) Functional classes of primate corticomotoneuronal cells and their relation to active force. J Neurophysiol 44:773-791.

Chouinard PA, Van Der Werf YD, Leonard G, Paus T (2003) Modulating neural networks with transcranial magnetic stimulation applied over the dorsal premotor and primary motor cortices. J Neurophysiol 90:1071-1083.

Christensen R (2001) Multivariate linear models. In: Advanced linear modeling, 2nd Edition, pp 1-73. New York: Springer-Verlag.

Cisek P, Kalaska JF (2004) Neural correlates of mental rehearsal in dorsal premotor cortex. Nature 431:993-996.

Cohen D, Nicolelis MA (2004) Reduction of single-neuron firing uncertainty by cortical ensembles during motor skill learning. J Neurosci 24:3574-3582.

Colebatch JG, Gandevia SC (1989) The distribution of muscular weakness in upper motor neuron lesions affecting the arm. Brain 112 (Pt 3):749-763.

Colebatch JG, Gandevia SC, Spira PJ (1986) Voluntary muscle strength in hemiparesis: distribution of weakness at the elbow. J Neurol Neurosurg Psychiatry 49:1019-1024.

Conditt MA, Mussa-Ivaldi FA (1999) Central representation of time during motor learning. Proc Natl Acad Sci U S A 96:11625-11630.

Conditt MA, Gandolfo F, Mussa-Ivaldi FA (1997) The motor system does not learn the dynamics of the arm by rote memorization of past experience. J Neurophysiol 78:554-560.

Conway BA, Halliday DM, Farmer SF, Shahani U, Maas P, Weir AI, Rosenberg JR (1995) Synchronization between motor cortex and spinal motoneuronal pool during the performance of a maintained motor task in man. J Physiol 489 (Pt 3):917-924.

Cothros N, Kohler S, Dickie EW, Mirsattari SM, Gribble PL (2006) Proactive interference as a result of persisting neural representations of previously learned motor skills in primary motor cortex. J Cogn Neurosci 18:2167-2176.

Courtemanche R, Pellerin JP, Lamarre Y (2002) Local field potential oscillations in primate cerebellar cortex: modulation during active and passive expectancy. J Neurophysiol 88:771-782.

Courtemanche R, Fujii N, Graybiel AM (2003) Synchronous, focally modulated beta-band oscillations characterize local field potential activity in the striatum of awake behaving monkeys. J Neurosci 23:11741-11752.

Crammond DJ, Kalaska JF (1994) Modulation of preparatory neuronal activity in dorsal premotor cortex due to stimulus-response compatibility. J Neurophysiol 71:1281-1284.

Crutcher MD, Russo GS, Ye S, Backus DA (2004) Target-, limb-, and context-dependent neural activity in the cingulate and supplementary motor areas of the monkey. Exp Brain Res 158:278-288.

Davidson PR, Wolpert DM (2004) Scaling down motor memories: de-adaptation after motor learning. Neurosci Lett 370:102-107.

Davidson PR, Wolpert DM (2005) Widespread access to predictive models in the motor system: a short review. J Neural Eng 2:S313-319.

Della-Maggiore V, Malfait N, Ostry DJ, Paus T (2004) Stimulation of the posterior parietal cortex interferes with arm trajectory adjustments during the learning of new dynamics. J Neurosci 24:9971-9976.

di Pellegrino G, Wise SP (1993) Visuospatial versus visuomotor activity in the premotor and prefrontal cortex of a primate. J Neurosci 13:1227-1243.

Diedrichsen J, Hashambhoy Y, Rane T, Shadmehr R (2005) Neural correlates of reach errors. J Neurosci 25:9919-9931.

Dingwell JB, Mah CD, Mussa-Ivaldi FA (2002) Manipulating objects with internal degrees of freedom: evidence for model-based control. J Neurophysiol 88:222-235.

Donchin O, Shadmehr R (2004) Change of desired trajectory caused by training in a novel motor task. In: Proceedings of the 26th Annual International Conference of the IEEE Engineering in Medicine and Biology Society, pp 4495-4498. San Francisco, CA, USA.

Donchin O, Francis JT, Shadmehr R (2003) Quantifying generalization from trial-by-trial behavior of adaptive systems that learn with basis functions: theory and experiments in human motor control. J Neurosci 23:9032-9045.

Donchin O, Gribova A, Steinberg O, Bergman H, Cardoso de Oliveira S, Vaadia E (2001) Local field potentials related to bimanual movements in the primary and supplementary motor cortices. Exp Brain Res 140:46-55.

Donoghue JP, Sanes JN, Hatsopoulos NG, Gaal G (1998) Neural discharge and local field potential oscillations in primate motor cortex during voluntary movements. J Neurophysiol 79:159-173.

Dum RP, Strick PL (1991) The origin of corticospinal projections from the premotor areas in the frontal lobe. J Neurosci 11:667-689.

Dum RP, Strick PL (2002) Motor areas in the frontal lobe of the primate. Physiol Behav 77:677-682.

Evarts EV (1968) Relation of pyramidal tract activity to force exerted during voluntary movement. J Neurophysiol 31:14-27.

Farmer SF (1998) Rhythmicity, synchronization and binding in human and primate motor systems. J Physiol 509 (Pt 1):3-14.

Fisher NI (1993) Statistical Analysis of Circular Data. New York: Cambridge University Press.

Flanagan JR, Wing AM (1997) The role of internal models in motion planning and control: evidence from grip force adjustments during movements of hand-held loads. J Neurosci 17:1519-1528.

Flanagan JR, Vetter P, Johansson RS, Wolpert DM (2003) Prediction precedes control in motor learning. Curr Biol 13:146-150.

Fox P, Ingham R, George MS, Mayberg H, Ingham J, Roby J, Martin C, Jerabek P (1997) Imaging human intra-cerebral connectivity by PET during TMS. Neuroreport 8:2787-2791.

Franklin DW, Osu R, Burdet E, Kawato M, Milner TE (2003) Adaptation to stable and unstable dynamics achieved by combined impedance control and inverse dynamics model. J Neurophysiol 90:3270-3282.

Fusi S (2002) Hebbian spike-driven synaptic plasticity for learning patterns of mean firing rates. Biol Cybern 87:459-470.

Gandolfo F, Mussa-Ivaldi FA, Bizzi E (1996) Motor learning by field approximation. Proc Natl Acad Sci U S A 93:3843-3846.

Gandolfo F, Li C, Benda BJ, Schioppa CP, Bizzi E (2000) Cortical correlates of learning in monkeys adapting to a new dynamical environment. Proc Natl Acad Sci U S A 97:2259-2263.

Gangitano M, Valero-Cabre A, Tormos JM, Mottaghy FM, Romero JR, Pascual-Leone A (2002) Modulation of input-output curves by low and high frequency repetitive transcranial magnetic stimulation of the motor cortex. Clin Neurophysiol 113:1249-1257.

Gemba H, Sasaki K (1984) Distribution of potentials preceding visually initiated and self-paced hand movements in various cortical areas of the monkey. Brain Res 306:207-214.

Georgopoulos AP, Schwartz AB, Kettner RE (1986) Neuronal population coding of movement direction. Science 233:1416-1419.

Georgopoulos AP, Kettner RE, Schwartz AB (1988) Primate motor cortex and free arm movements to visual targets in three-dimensional space. II. Coding of the direction of movement by a neuronal population. J Neurosci 8:2928-2937.

Georgopoulos AP, Kalaska JF, Caminiti R, Massey JT (1982) On the relations between the direction of two-dimensional arm movements and cell discharge in primate motor cortex. J Neurosci 2:1527-1537.

Ghilardi M, Ghez C, Dhawan V, Moeller J, Mentis M, Nakamura T, Antonini A, Eidelberg D (2000) Patterns of regional brain activation associated with different forms of motor learning. Brain Res 871:127-145.

Gray CM, McCormick DA (1996) Chattering cells: superficial pyramidal neurons contributing to the generation of synchronous oscillations in the visual cortex. Science 274:109-113.

Greenberg PA, Wilson FA (2004) Functional stability of dorsolateral prefrontal neurons. J Neurophysiol 92:1042-1055.

Gribble PL, Ostry DJ (2000) Compensation for loads during arm movements using equilibrium-point control. Exp Brain Res 135:474-482.

Gruber WR, Klimesch W, Sauseng P, Doppelmayr M (2005) Alpha phase synchronization predicts P1 and N1 latency and amplitude size. Cereb Cortex 15:371-377.

Hasenstaub A, Shu Y, Haider B, Kraushaar U, Duque A, McCormick DA (2005) Inhibitory postsynaptic potentials carry synchronized frequency information in active cortical networks. Neuron 47:423-435.

Hatsopoulos NG, Ojakangas CL, Paninski L, Donoghue JP (1998) Information about movement direction obtained from synchronous activity of motor cortical neurons. Proc Natl Acad Sci U S A 95:15706-15711.

He SQ, Dum RP, Strick PL (1993) Topographic organization of corticospinal projections from the frontal lobe: motor areas on the lateral surface of the hemisphere. J Neurosci 13:952-980.

He SQ, Dum RP, Strick PL (1995) Topographic organization of corticospinal projections from the frontal lobe: motor areas on the medial surface of the hemisphere. J Neurosci 15:3284-3306.

Held R, Freedman SJ (1963) Plasticity in Human Sensorimotor Control. Science 142:455-462.

Heldman DA, Wang W, Chan SS, Moran DW (2006) Local field potential spectral tuning in motor cortex during reaching. IEEE Trans Neural Syst Rehabil Eng 14:180-183.

Hogan N (1985) Impedance Control - an Approach to Manipulation .1. Theory. J Dyn Syst Meas Control 107:1-7.

Hoshi E, Sawamura H, Tanji J (2005) Neurons in the rostral cingulate motor area monitor multiple phases of visuomotor behavior with modest parametric selectivity. J Neurophysiol 94:640-656.

Humphrey DR (1986) Representation of movements and muscles within the primate precentral motor cortex: historical and current perspectives. Fed Proc 45:2687-2699.

Hutchison WD, Dostrovsky JO, Walters JR, Courtemanche R, Boraud T, Goldberg J, Brown P (2004) Neuronal oscillations in the basal ganglia and movement disorders: evidence from whole animal and human recordings. J Neurosci 24:9240-9243.

Huxter J, Burgess N, O'Keefe J (2003) Independent rate and temporal coding in hippocampal pyramidal cells. Nature 425:828-832.

Hwang EJ, Smith MA, Shadmehr R (2006) Adaptation and generalization in acceleration-dependent force fields. Exp Brain Res 169:496-506.

Ikeda A, Shibasaki H, Kaji R, Terada K, Nagamine T, Honda M, Kimura J (1997) Dissociation between contingent negative variation (CNV) and Bereitschaftspotential (BP) in patients with parkinsonism. Electroencephalogr Clin Neurophysiol 102:142-151.

Jackson A, Gee VJ, Baker SN, Lemon RN (2003) Synchrony between neurons with similar muscle fields in monkey motor cortex. Neuron 38:115-125.

Jacobs J, Kahana MJ, Ekstrom AD, Fried I (2007) Brain oscillations control timing of single-neuron activity in humans. J Neurosci 27:3839-3844.

Jansen BH, Agarwal G, Hegde A, Boutros NN (2003) Phase synchronization of the ongoing EEG and auditory EP generation. Clin Neurophysiol 114:79-85.

Jasper HH, Penfield W (1949) Electrocorticograms in man: effect of the voluntary movement upon the electrical activity in the precentral gyrus. Archiv fur Psychiatrie 183:163-174.

Johnston D, Wu S (1995) Foundations of Cellular Neurophysiology. Cambridge, MA: MIT Press.

Jordan MI, Rumelhart DE (1992) Forward Models - Supervised Learning with a Distal Teacher. Cog Sci 16:307-354.

Kalaska JF, Crammond DJ (1992) Cerebral cortical mechanisms of reaching movements. Science 255:1517-1523.

Kalaska JF, Cohen DA, Hyde ML, Prud'homme M (1989) A comparison of movement direction-related versus load direction-related activity in primate motor cortex, using a two-dimensional reaching task. J Neurosci 9:2080-2102.

Kalaska JF, Scott SH, Cisek P, Sergio LE (1997) Cortical control of reaching movements. Curr Opin Neurobiol 7:849-859.

Karni A, Meyer G, Jezzard P, Adams MM, Turner R, Ungerleider LG (1995) Functional MRI evidence for adult motor cortex plasticity during motor skill learning. Nature 377:155-158.

Kawato M (1999) Internal models for motor control and trajectory planning. Curr Opin Neurobiol 9:718-727.

Kentros CG, Agnihotri NT, Streater S, Hawkins RD, Kandel ER (2004) Increased attention to spatial context increases both place field stability and spatial memory. Neuron 42:183-185.

Kirkpatrick S, Gelatt C, Vecchi M (1983) Optimization by simulated annealing. Science 220:671-680.

Klassen J, Tong C, Flanagan JR (2005) Learning and recall of incremental kinematic and dynamic sensorimotor transformations. Exp Brain Res 164:250-259.

Klee MR, Offenloch K, Tigges J (1965) Cross-Correlation Analysis of Electroencephalographic Potentials and Slow Membrane Transients. Science 147:519-521.

Klimesch W, Schack B, Schabus M, Doppelmayr M, Gruber W, Sauseng P (2004) Phase-locked alpha and theta oscillations generate the P1-N1 complex and are related to memory performance. Brain Res Cogn Brain Res 19:302-316.

Krakauer JW, Ghilardi MF, Ghez C (1999) Independent learning of internal models for kinematic and dynamic control of reaching. Nat Neurosci 2:1026-1031.

Krebs HI, Brashers-Krug T, Rauch SL, Savage CR, Hogan N, Rubin RH, Fischman AJ, Alpert NM (1998) Robot-aided functional imaging: application to a motor learning study. Hum Brain Mapp 6:59-72.

Kubota K, Hamada I (1979) Preparatory activity of monkey pyramidal tract neurons related to quick movement onset during visual tracking performance. Brain Res 168:435-439.

Kurtzer I, Herter TM, Scott SH (2006) Nonuniform distribution of reach-related and torque-related activity in upper arm muscles and neurons of primary motor cortex. J Neurophysiol 96:3220-3230.

Lackner JR, Dizio P (1994) Rapid adaptation to Coriolis force perturbations of arm trajectory. J Neurophysiol 72:299-313.

Lai EJ, Hodgson AJ, Milner TE (2003) Influence of interaction force levels on degree of motor adaptation in a stable dynamic force field. Exp Brain Res 153:76-83.

Le Van Quyen M, Foucher J, Lachaux J, Rodriguez E, Lutz A, Martinerie J, Varela FJ (2001) Comparison of Hilbert transform and wavelet methods for the analysis of neuronal synchrony. J Neurosci Methods 111:83-98.

Lebedev MA, Wise SP (2000) Oscillations in the premotor cortex: single-unit activity from awake, behaving monkeys. Exp Brain Res 130:195-215.

Lecas JC, Requin J, Anger C, Vitton N (1986) Changes in neuronal activity of the monkey precentral cortex during preparation for movement. J Neurophysiol 56:1680-1702.

Lee H, Simpson GV, Logothetis NK, Rainer G (2005) Phase locking of single neuron activity to theta oscillations during working memory in monkey extrastriate visual cortex. Neuron 45:147-156.

Lee L, Siebner HR, Rowe JB, Rizzo V, Rothwell JC, Frackowiak RS, Friston KJ (2003) Acute remapping within the motor system induced by low-frequency repetitive transcranial magnetic stimulation. J Neurosci 23:5308-5318.

Li CS, Padoa-Schioppa C, Bizzi E (2001) Neuronal correlates of motor performance and motor learning in the primary motor cortex of monkeys adapting to an external force field. Neuron 30:593-607.

Luppino G, Matelli M, Camarda RM, Gallese V, Rizzolatti G (1991) Multiple representations of body movements in mesial area 6 and the adjacent cingulate cortex: an intracortical microstimulation study in the macaque monkey. J Comp Neurol 311:463-482.

MacKay WA (1997) Synchronized neuronal oscillations and their role in motor processes. Trends Cogn Sci 1:176-183.

Mah CD, Mussa-Ivaldi FA (2003) Evidence for a specific internal representation of motion-force relationships during object manipulation. Biol Cybern 88:60-72.

Makeig S, Westerfield M, Jung TP, Enghoff S, Townsend J, Courchesne E, Sejnowski TJ (2002) Dynamic brain sources of visual evoked responses. Science 295:690-694.

Malfait N, Ostry DJ (2004) Is interlimb transfer of force-field adaptation a cognitive response to the sudden introduction of load? J Neurosci 24:8084-8089.

Malfait N, Shiller DM, Ostry DJ (2002) Transfer of motor learning across arm configurations. J Neurosci 22:9656-9660.

Malfait N, Gribble PL, Ostry DJ (2005) Generalization of motor learning based on multiple field exposures and local adaptation. J Neurophysiol 93:3327-3338.

Marsden JF, Werhahn KJ, Ashby P, Rothwell J, Noachtar S, Brown P (2000) Organization of cortical activities related to movement in humans. J Neurosci 20:2307-2314.

Maschke M, Gomez CM, Ebner TJ, Konczak J (2004) Hereditary cerebellar ataxia progressively impairs force adaptation during goal-directed arm movements. J Neurophysiol 91:230-238.

Maynard EM, Hatsopoulos NG, Ojakangas CL, Acuna BD, Sanes JN, Normann RA, Donoghue JP (1999) Neuronal interactions improve cortical population coding of movement direction. J Neurosci 19:8083-8093.

McBain CJ, Fisahn A (2001) Interneurons unbound. Nat Rev Neurosci 2:11-23.

McGaugh JL (2000) Memory--a century of consolidation. Science 287:248-251.

Mehring C, Rickert J, Vaadia E, Cardosa de Oliveira S, Aertsen A, Rotter S (2003a) Inference of hand movements from local field potentials in monkey motor cortex. Nat Neurosci 6:1253-1254.

Mehring C, Rickert J, Cardosa de Oliveira S, Vaadia E, Aertsen A, Rotter S (2003b) Hints for a topographic map of tuning properties in primate motor cortex. In: Proceedings of the 1st International IEEE EMBS Conference on Neural Engineering, pp 28-31. Capri Island, Italy.

Mehta B, Schaal S (2002) Forward models in visuomotor control. J Neurophysiol 88:942-953.

Miall RC, Wolpert DM (1996) Forward Models for Physiological Motor Control. Neural Netw 9:1265-1279.

Mitsuda T, Onorati P (2002) Three-dimensional tuning profile of motor cortical activity during arm movements. Neuroreport 13:1477-1480.

Mitz AR, Wise SP (1987) The somatotopic organization of the supplementary motor area: intracortical microstimulation mapping. J Neurosci 7:1010-1021.

Mitz AR, Godschalk M, Wise SP (1991) Learning-dependent neuronal activity in the premotor cortex: activity during the acquisition of conditional motor associations. J Neurosci 11:1855-1872.

Mitzdorf U (1985) Current source-density method and application in cat cerebral cortex: investigation of evoked potentials and EEG phenomena. Physiol Rev 65:37-100.

Montgomery DC, Runger GC (1999) Applied statistics and probability for engineers, 2nd Edition. New York: John Wiley & Sons Inc.

Moore BR (1980) A Modification of the Rayleigh Test for Vector Data. Biometrika 67:175-180.

Moran DW, Schwartz AB (1999) Motor cortical representation of speed and direction during reaching. J Neurophysiol 82:2676-2692.

Muellbacher W, Ziemann U, Wissel J, Dang N, Kofler M, Facchini S, Boroojerdi B, Poewe W, Hallett M (2002) Early consolidation in human primary motor cortex. Nature 415:640-644.

Murthy VN, Fetz EE (1992) Coherent 25- to 35-Hz oscillations in the sensorimotor cortex of awake behaving monkeys. Proc Natl Acad Sci U S A 89:5670-5674.

Murthy VN, Fetz EE (1996a) Oscillatory activity in sensorimotor cortex of awake monkeys: synchronization of local field potentials and relation to behavior. J Neurophysiol 76:3949-3967.

Murthy VN, Fetz EE (1996b) Synchronization of neurons during local field potential oscillations in sensorimotor cortex of awake monkeys. J Neurophysiol 76:3968-3982.

Mussa-Ivaldi FA (1988) Do neurons in the motor cortex encode movement direction? An alternative hypothesis. Neurosci Lett 91:106-111.

Nakamura K, Sakai K, Hikosaka O (1998) Neuronal activity in medial frontal cortex during learning of sequential procedures. J Neurophysiol 80:2671-2687.

Nanayakkara T, Shadmehr R (2003) Saccade adaptation in response to altered arm dynamics. J Neurophysiol 90:4016-4021.

Naselaris T, Merchant H, Amirikian B, Georgopoulos AP (2006a) Large-scale organization of preferred directions in the motor cortex. I. Motor cortical hyperacuity for forward reaching. J Neurophysiol 96:3231-3236.

Naselaris T, Merchant H, Amirikian B, Georgopoulos AP (2006b) Large-scale organization of preferred directions in the motor cortex. II. Analysis of local distributions. J Neurophysiol 96:3237-3247.

Nezafat R, Shadmehr R, Holcomb HH (2001) Long-term adaptation to dynamics of reaching movements: a PET study. Exp Brain Res 140:66-76.

Nicolelis MA, Ghazanfar AA, Faggin BM, Votaw S, Oliveira LM (1997) Reconstructing the engram: simultaneous, multisite, many single neuron recordings. Neuron 18:529-537.

Niemi P, Naatanen R (1981) Foreperiod and Simple Reaction-Time. Psychol Bull 89:133-162.

O'Leary JG, Hatsopoulos NG (2006) Early visuomotor representations revealed from evoked local field potentials in motor and premotor cortical areas. J Neurophysiol 96:1492-1506.

Ojakangas CL, Ebner TJ (1992) Purkinje cell complex and simple spike changes during a voluntary arm movement learning task in the monkey. J Neurophysiol 68:2222-2236.

Omlor W, Patino L, Hepp-Reymond MC, Kristeva R (2007) Gamma-range corticomuscular coherence during dynamic force output. Neuroimage 34:1191-1198.

Oram MW, Hatsopoulos NG, Richmond BJ, Donoghue JP (2001) Excess synchrony in motor cortical neurons provides redundant direction information with that from coarse temporal measures. J Neurophysiol 86:1700-1716.

Ostry DJ, Feldman AG (2003) A critical evaluation of the force control hypothesis in motor control. Exp Brain Res 153:275-288.

Osu R, Burdet E, Franklin DW, Milner TE, Kawato M (2003) Different mechanisms involved in adaptation to stable and unstable dynamics. J Neurophysiol 90:3255-3269.

Osu R, Franklin DW, Kato H, Gomi H, Domen K, Yoshioka T, Kawato M (2002) Short- and long-term changes in joint co-contraction associated with motor learning as revealed from surface EMG. J Neurophysiol 88:991-1004.

Overduin SA, Richardson AG, Lane CE, Bizzi E, Press DZ (2006) Intermittent practice facilitates stable motor memories. J Neurosci 26:11888-11892.

Padoa-Schioppa C, Li CS, Bizzi E (2002) Neuronal correlates of kinematics-to-dynamics transformation in the supplementary motor area. Neuron 36:751-765.

Padoa-Schioppa C, Li CS, Bizzi E (2004) Neuronal activity in the supplementary motor area of monkeys adapting to a new dynamic environment. J Neurophysiol 91:449-473.

Palmer E, Ashby P (1992) Corticospinal projections to upper limb motoneurones in humans. J Physiol 448:397-412.

Paninski L, Fellows MR, Hatsopoulos NG, Donoghue JP (2004) Spatiotemporal tuning of motor cortical neurons for hand position and velocity. J Neurophysiol 91:515-532.

Pascual-Leone A, Grafman J, Hallett M (1994) Modulation of cortical motor output maps during development of implicit and explicit knowledge. Science 263:1287-1289.

Paz R, Vaadia E (2004) Specificity of sensorimotor learning and the neural code: neuronal representations in the primary motor cortex. J Physiol Paris 98:331-348.

Paz R, Boraud T, Natan C, Bergman H, Vaadia E (2003) Preparatory activity in motor cortex reflects learning of local visuomotor skills. Nat Neurosci 6:882-890.

Paz R, Natan C, Boraud T, Bergman H, Vaadia E (2005) Emerging patterns of neuronal responses in supplementary and primary motor areas during sensorimotor adaptation. J Neurosci 25:10941-10951.

Penfield W, Jasper HH (1956) Epilepsy and the Functional Anatomy of the Human Brain. Boston: Little, Brown and Company.

Pfurtscheller G, Graimann B, Huggins JE, Levine SP, Schuh LA (2003) Spatiotemporal patterns of beta desynchronization and gamma synchronization in corticographic data during self-paced movement. Clin Neurophysiol 114:1226-1236.

Prut Y, Fetz EE (1999) Primate spinal interneurons show pre-movement instructed delay activity. Nature 401:590-594.

Rathelot JA, Strick PL (2006) Muscle representation in the macaque motor cortex: an anatomical perspective. Proc Natl Acad Sci U S A 103:8257-8262.

Richardson AG, Overduin SA, Valero-Cabre A, Padoa-Schioppa C, Pascual-Leone A, Bizzi E, Press DZ (2006) Disruption of primary motor cortex before learning impairs memory of movement dynamics. J Neurosci 26:12466-12470.

Rickert J, Oliveira SC, Vaadia E, Aertsen A, Rotter S, Mehring C (2005) Encoding of movement direction in different frequency ranges of motor cortical local field potentials. J Neurosci 25:8815-8824.

Riehle A, Requin J (1993) The predictive value for performance speed of preparatory changes in neuronal activity of the monkey motor and premotor cortex. Behav Brain Res 53:35-49.

Robertson EM, Theoret H, Pascual-Leone A (2003) Studies in cognition: the problems solved and created by transcranial magnetic stimulation. J Cogn Neurosci 15:948-960.

Robertson EM, Pascual-Leone A, Miall RC (2004) Current concepts in procedural consolidation. Nat Rev Neurosci 5:576-582.

Robertson EM, Press DZ, Pascual-Leone A (2005) Off-line learning and the primary motor cortex. J Neurosci 25:6372-6378.

Romero JR, Anschel D, Sparing R, Gangitano M, Pascual-Leone A (2002) Subthreshold low frequency repetitive transcranial magnetic stimulation selectively decreases facilitation in the motor cortex. Clin Neurophysiol 113:101-107.

Roux S, Mackay WA, Riehle A (2006) The pre-movement component of motor cortical local field potentials reflects the level of expectancy. Behav Brain Res 169:335-351.

Rubino D, Robbins KA, Hatsopoulos NG (2006) Propagating waves mediate information transfer in the motor cortex. Nat Neurosci 9:1549-1557.

Rumelhart DE, Hinton GE, Williams RJ (1986) Learning representations by back-propagating errors. Nature 323:533-536.

Russo GS, Backus DA, Ye S, Crutcher MD (2002) Neural activity in monkey dorsal and ventral cingulate motor areas: comparison with the supplementary motor area. J Neurophysiol 88:2612-2629.

Sainburg RL, Ghez C, Kalakanis D (1999) Intersegmental dynamics are controlled by sequential anticipatory, error correction, and postural mechanisms. J Neurophysiol 81:1045-1056.

Salinas E (2004) Fast remapping of sensory stimuli onto motor actions on the basis of contextual modulation. J Neurosci 24:1113-1118.

Salinas E, Abbott LF (1995) Transfer of coded information from sensory to motor networks. J Neurosci 15:6461-6474.

Salinas E, Sejnowski TJ (2001) Correlated neuronal activity and the flow of neural information. Nat Rev Neurosci 2:539-550.

Sanes JN, Donoghue JP (1993) Oscillations in local field potentials of the primate motor cortex during voluntary movement. Proc Natl Acad Sci U S A 90:4470-4474.

Sanes JN, Donoghue JP (2000) Plasticity and primary motor cortex. Annu Rev Neurosci 23:393-415.

Sanger TD (1994) Theoretical Considerations for the Analysis of Population Coding in Motor Cortex. Neural Computation 6:29-37.

Sanner RM, Kosha M (1999) A mathematical model of the adaptive control of human arm motions. Biol Cybern 80:369-382.

Scherberger H, Jarvis MR, Andersen RA (2005) Cortical local field potential encodes movement intentions in the posterior parietal cortex. Neuron 46:347-354.

Schieber MH (2001) Constraints on somatotopic organization in the primary motor cortex. J Neurophysiol 86:2125-2143.

Schmidt EM, Bak MJ, McIntosh JS (1976) Long-term chronic recording from cortical neurons. Exp Neurol 52:496-506.

Schnitzler A, Gross J (2005) Normal and pathological oscillatory communication in the brain. Nat Rev Neurosci 6:285-296.

Schoffelen JM, Oostenveld R, Fries P (2005) Neuronal coherence as a mechanism of effective corticospinal interaction. Science 308:111-113.

Schwartz AB (2004) Cortical neural prosthetics. Annu Rev Neurosci 27:487-507.

Scott SH, Kalaska JF (1997) Reaching movements with similar hand paths but different arm orientations. I. Activity of individual cells in motor cortex. J Neurophysiol 77:826-852.

Scott SH, Gribble PL, Graham KM, Cabel DW (2001) Dissociation between hand motion and population vectors from neural activity in motor cortex. Nature 413:161-165.

Sejnowski TJ, Paulsen O (2006) Network oscillations: emerging computational principles. J Neurosci 26:1673-1676.

Sergio LE, Hamel-Paquet C, Kalaska JF (2005) Motor cortex neural correlates of output kinematics and kinetics during isometric-force and arm-reaching tasks. J Neurophysiol 94:2353-2378.

Seung HS (2003) Learning in spiking neural networks by reinforcement of stochastic synaptic transmission. Neuron 40:1063-1073.

Shadmehr R, Mussa-Ivaldi FA (1994) Adaptive representation of dynamics during learning of a motor task. J Neurosci 14:3208-3224.

Shadmehr R, Brashers-Krug T (1997) Functional stages in the formation of human long-term motor memory. J Neurosci 17:409-419.

Shadmehr R, Holcomb HH (1997) Neural correlates of motor memory consolidation. Science 277:821-825.

Shadmehr R, Moussavi ZM (2000) Spatial generalization from learning dynamics of reaching movements. J Neurosci 20:7807-7815.

Shadmehr R, Wise SP (2005) The Computational Neurobiology of Reaching and Pointing. Cambridge, MA: MIT Press.

Shadmehr R, Brandt J, Corkin S (1998) Time-dependent motor memory processes in amnesic subjects. J Neurophysiol 80:1590-1597.

Shen L, Alexander GE (1997) Preferential representation of instructed target location versus limb trajectory in dorsal premotor area. J Neurophysiol 77:1195-1212.

Shima K, Tanji J (1998) Role for cingulate motor area cells in voluntary movement selection based on reward. Science 282:1335-1338.

Siebner HR, Rothwell J (2003) Transcranial magnetic stimulation: new insights into representational cortical plasticity. Exp Brain Res 148:1-16.

Smith MA, Shadmehr R (2005) Intact ability to learn internal models of arm dynamics in Huntington's disease but not cerebellar degeneration. J Neurophysiol 93:2809-2821.

Smith MA, Ghazizadeh A, Shadmehr R (2006) Interacting adaptive processes with different timescales underlie short-term motor learning. PLoS Biol 4:e179.

Sutton R, Barto G (1998) Reinforcement Learning: An Introduction.: The MIT Press.

Tanji J, Evarts EV (1976) Anticipatory Activity of Motor Cortex Neurons in Relation to Direction of an Intended Movement. J Neurophysiol 39:1062-1068.

Tanji J, Taniguchi K, Saga T (1980) Supplementary motor area: neuronal response to motor instructions. J Neurophysiol 43:60-68.

Taylor DM, Tillery SI, Schwartz AB (2002) Direct cortical control of 3D neuroprosthetic devices. Science 296:1829-1832.

Thach WT (1978) Correlation of neural discharge with pattern and force of muscular activity, joint position, and direction of intended next movement in motor cortex and cerebellum. J Neurophysiol 41:654-676.

Thompson LT, Best PJ (1990) Long-term stability of the place-field activity of single units recorded from the dorsal hippocampus of freely behaving rats. Brain Res 509:299-308.

Thoroughman KA, Shadmehr R (1999) Electromyographic correlates of learning an internal model of reaching movements. J Neurosci 19:8573-8588.

Thoroughman KA, Shadmehr R (2000) Learning of action through adaptive combination of motor primitives. Nature 407:742-747.

Thoroughman KA, Taylor JA (2005) Rapid reshaping of human motor generalization. J Neurosci 25:8948-8953.

Tin C, Poon CS (2005) Internal models in sensorimotor integration: perspectives from adaptive control theory. J Neural Eng 2:S147-163.

Todorov E (2000) Direct cortical control of muscle activation in voluntary arm movements: a model. Nat Neurosci 3:391-398.

Tong C, Wolpert DM, Flanagan JR (2002) Kinematics and dynamics are not represented independently in motor working memory: evidence from an interference study. J Neurosci 22:1108-1113.

Trillenberg P, Verleger R, Wascher E, Wauschkuhn B, Wessel K (2000) CNV and temporal uncertainty with 'ageing' and 'non-ageing' S1-S2 intervals. Clin Neurophysiol 111:1216-1226.

van Elswijk G, Kleine BU, Overeem S, Stegeman DF (2007) Expectancy induces dynamic modulation of corticospinal excitability. J Cogn Neurosci 19:121-131.

Walter WG, Cooper R, Aldridge VJ, McCallum WC, Winter AL (1964) Contingent Negative Variation: an Electric Sign of Sensorimotor Association and Expectancy in the Human Brain. Nature 203:380-384.

Wang T, Dordevic GS, Shadmehr R (2001) Learning the dynamics of reaching movements results in the modification of arm impedance and long-latency perturbation responses. Biol Cybern 85:437-448.

Weinrich M, Wise SP (1982) The premotor cortex of the monkey. J Neurosci 2:1329-1345.

Williams D, Kuhn A, Kupsch A, Tijssen M, van Bruggen G, Speelman H, Hotton G, Loukas C, Brown P (2005) The relationship between oscillatory activity and motor reaction time in the parkinsonian subthalamic nucleus. Eur J Neurosci 21:249-258.

Williams JC, Rennaker RL, Kipke DR (1999) Stability of chronic multichannel neural recordings: implications for a long-term neural interface. Neurocomput 26-27:1069-1076.

Wise SP, Moody SL, Blomstrom KJ, Mitz AR (1998) Changes in motor cortical activity during visuomotor adaptation. Exp Brain Res 121:285-299.

Wolpert DM, Kawato M (1998) Multiple paired forward and inverse models for motor control. Neural Netw 11:1317-1329.

Wolpert DM, Ghahramani Z, Jordan MI (1995) An internal model for sensorimotor integration. Science 269:1880-1882.

Wolpert DM, Doya K, Kawato M (2003) A unifying computational framework for motor control and social interaction. Philos Trans R Soc Lond B Biol Sci 358:593-602.

Xiao J, Padoa-Schioppa C, Bizzi E (2006) Neuronal correlates of movement dynamics in the dorsal and ventral premotor area in the monkey. Exp Brain Res 168:106-119.

Zhang W, Linden DJ (2003) The other side of the engram: experience-driven changes in neuronal intrinsic excitability. Nat Rev Neurosci 4:885-900.

Zumsteg ZS, Kemere C, O'Driscoll S, Santhanam G, Ahmed RE, Shenoy KV, Meng TH (2005) Power feasibility of implantable digital spike sorting circuits for neural prosthetic systems. IEEE Trans Neural Syst Rehabil Eng 13:272-279.